A Practical Guide to Particle Tracking Systems

incorporating *Streams*

1st Edition

Roger Nokes

2021

Table of Contents

Dedication

To my dear children, Mike and Kim.

Acknowledgements

My experiences in the use of particle tracking systems have arisen from laboratory studies at the University of Canterbury over the last two decades. I am indebted to my tireless graduate students, Dave Plew, Caroline Fraser (née Ballard), James McBryde, Langford Sue, Colin Whittaker, Bill Veale, Claire Cohen (née Biggs), Andrew Dark, Alex Meredith, Gustaff Kikkert, Eric Scheepbouwer, Adam Crowe, Adi Ramakanth, Lizzy North, Lisa Ottenhaus, Wenchen Dong, Arsalan Niroomandi, Justin Brown, Mike Parr and Rahman Al-Behadili, and my countless, enthusiastic undergraduate students who have implemented so many of the techniques and ideas described in this book. Your willingness to advance our collective understanding of these techniques through your own trials and successes has benefitted me greatly. Thank you.

I also wish to acknowledge, and thank, the outstanding team of technical staff in the Department of Civil and Natural Resources Engineering at the University of Canterbury, Ian Sheppard, Colin Bliss, Kevin Wines, Russell McConchie, Alan Thirwell, and Mike Weavers, who have brought their expertise to bear on many of the technical issues associated with light source development, particle selection, camera control and the many other challenges that every experimentalist faces. Without your insights and skills our systems simply wouldn't exist.

Finally, I wish to thank my many colleagues, particularly Mark Davidson and Claudia Cenedese, who have encouraged and supported me in the "labour of love" which is *Streams*. Ideas from you have helped me to clarify my thinking and inspired me to take the software in new directions. I suspect the journey is not yet complete.

Preface

Particle tracking systems have been used in experimental mechanics for nigh on 40 years. The technique originated in the domain of fluid mechanics, where it was typically referred to as **particle tracking velocimetry** (PTV), but it has spread to other domains such as structural engineering in the intervening years.

Conceptually the technique is refreshingly simple. Some material, whether solid, fluid or gaseous is "marked" in some way and modern image capture equipment, typically a digital camera of some sort, is employed to record the motion of those marks (particles) through time. Finally, the recorded images are analysed by a suitable software tool to extract physically meaningful quantities such as material displacement or velocity, or some quantity derived from these variables, such as vorticity or strain. One of the attractions of particle tracking systems is that "what you see is what you get". There are no sophisticated electronics behind the scenes processing electrical signals coming from a sensor of some sort. Instead, a set of physical objects – the particles – move through space and their motion not only generates the variables of interest, but provides the experimenter with a highly visual record of the material's actual behaviour.

In choosing particle tracking as a primary technique in the fluid mechanics laboratory at the University of Canterbury we have been determined to ensure that it would be available to all students working in the laboratory. It is not uncommon for laboratories to have one expensive, off-the-shelf, measurement system (typically supporting **particle image velocimetry** (PIV) – a technique closely related to PTV). Such a system is generally dedicated to one experimental project at a time – unless the laboratory is so well endowed with funds that it can afford multiple systems. Thus it was our aim to implement our PTV systems as cheaply as possible, using readily accessible and modestly priced components. In addition, it was our hope that we could develop in-house analysis tools that would enable students to benefit from the power of particle tracking without having to commit to developing their own analysis software. The result of this ambition has been the development, over close to 20 years, of the *Streams* software tool.

I have been involved in the applications of particle tracking in fluid mechanics for the last 20 years, and more recently I have been presumptuous enough to encourage the adoption of this technique by my colleagues in other areas of mechanics – notably structural engineering. During my time at the University of Canterbury dozens of students, both PhD and Masters research students and undergraduate project students, in both fluid mechanics and structural engineering, have been able to utilise the power of particle tracking in their experimental programmes. This book has arisen from a desire to provide a very practical guide to first time users of particle tracking (PT) technology that will enable them to design their own experimental systems and analyse their own data with some level of confidence. While there are monographs on particle image velocimetry, particle tracking is not so well catered for. In addition, these monographs, while erudite, perhaps do not address the many pragmatic details of

implementing a particle tracking system in the laboratory, particularly one based on modestly priced components.

This book has a second objective - to provide the reader with hands on experience of analysing PT image data. From my experience in advising research students on how to analyse their data, true comprehension is really only achieved when they have the opportunity to process and manipulate real image data. For this reason hands on experience of image analysis, and field generation, through a varied set of case studies is also included in this book. The datasets analysed in the case studies are available to the reader in order for them to have the opportunity to undertake their own analysis and hence to build their own experience.

For obvious reasons I will use *Streams* as the analysis tool of choice when presenting these case studies. However, this book does not serve as an extensive introduction to *Streams*. Four comprehensive manuals are provided with the software and the reader should familiarise themselves with at least the core concepts and interface elements (see the System Theory and Design manual) before, or while, progressing through this book. These manuals can be found at the following website:

https://www.canterbury.ac.nz/engineering/schools/cnre/software/streams/

To reflect the twin objectives of the book it has been divided into four parts. Part 1- An Overview of Particle Tracking Systems – describes the essence of a particle tracking system from a broad brush perspective. This section is aimed primarily at researchers considering the adoption of particle tracking in their experimental endeavours. Part 2 – Particle Tracking Systems: Experimental Design – is aimed at the experimenter who wishes to design a particle tracking system and addresses the essential elements of an operational particle tracking system. Part 3 – Particle tracking Systems: Analysis in Practice – assists the data analyst seeking general guidance on the analysis of PT image data. And finally, Part 4 – Case Studies – provides illustrative examples of particle tracking in practice through the presentation of a set of case studies. These case studies are treated in some detail, "warts and all", and the reader is guided through the application of the *Streams* software.

In the same spirit in which *Streams* has been developed to allow wide access to the tools necessary for particle tracking analysis, I offer this book in the hope that it will enable aspiring users of particle tracking technology to quickly, and successfully, achieve their goals in the laboratory, and, perhaps, even have some fun in doing so!

Roger Nokes
Tata Beach
2021

Part 1

An Overview of

Particle Tracking Systems

1. Introduction to Particle Tracking

1.1 Overview

Who hasn't dropped a twig or leaf into a stream and watched it wend its way downstream? In doing so one has performed a crude particle tracking experiment. The twig, or leaf, is the particle and your eye is the recording device that tracks the motion of that particle. The result is qualitative of course, as the actual motion of the object floating downstream isn't recorded in a way that would enable a quantitative analysis to be undertaken. If it were, then the position and velocity of that object could be computed as a function of time.

This simple illustration captures both the intent and one of the key advantages of particle tracking as an experimental technique. The intent is clear. By placing an object onto the surface of the stream and observing its motion, the motion of the stream itself becomes apparent. It tells us whether the water is flowing quickly or slowly, whether it is weakly or highly turbulent, and whether there are significant secondary currents in the stream that move the floating object away from, or towards, the banks as it moves downstream. One can imagine how much more information about the flowing water would be available to us if hundreds, or thousands, of twigs were cast upon the surface of the stream. The result would be a comprehensive description of the surface velocity field.

One of the very specific advantages of this technique is that it not only performs the task of capturing detailed quantitative data regarding the stream flow (provided, of course, that one has some way of recording the actual physical motion of each twig), but it provides the experimenter with a way of visualising the flow at the same time. As alluded to in the Preface – "what you see is what you get". Certainly in the field of fluid mechanics, where the material whose motion interests us is almost transparent, flow visualisation is difficult, and fluid mechanicists have an impressive history of developing innovative ways of overcoming this limitation. For them visualisation is often an important step along the path to understanding.

In many ways particle tracking is a return to the past. Over many years, in the discipline of experimental fluid mechanics, more and more sophisticated techniques have been developed to measure fluid motion. Techniques such as hot-wire and hot film anemometry, and laser Doppler anemometry (LDA) were invented to provide accurate point measurements of turbulent fluid flow based on physical principles quite unrelated to the problem under investigation. Hot-wire and hot-films rely on relating the heat loss from a probe, inserted into the flow, to the speed of the fluid moving past it. An electrical circuit, that measures the thermal properties of the system, yields an output related to the heat loss, and through careful calibration the experimenter can deduce the fluid velocity from the electrical signal. On the other hand a laser Doppler system employs the principle of a Doppler shift in frequency caused by a wave reflected from a moving object (typically fine particles present in the fluid). Again, through careful calibration of the Doppler shift of a laser beam scattered from particles

moving in the flow, the experimenter can determine the velocity of the fluid at an arbitrary point.

There are clear parallels in the discipline of experimental structural mechanics where accelerometers, embedded strain gauges and displacement potentiometers of various types are utilised to measure point, or space-averaged, variables of interest, such as acceleration, strain or displacement.

All of these techniques are technologically impressive, and bear witness to humankind's scientific development and innovation over the last century. So where lies the attraction in returning to such a conceptually simple construct as tracking a particle, or particles, moving in space? There are at least three answers to this question.

The first lies in the dramatic advances in imaging and computer technology that have occurred in the last half century. Today we have access to a dazzling array of digital cameras – both still and video. These cameras enable highly resolved images of experimental systems to be recorded due to their pixel-rich sensors In addition, the sensitivity of these sensors has improved such that cameras, albeit not cheap ones, capable of high frame rates – kilohertz – are available. Such digital cameras have the capacity to generate extremely large datasets, but without the astounding advancement in computer technology the experimenter would simply not be able to store and process these datasets. Therefore these twin advances in technology, which, by the way, continue, have enabled, in the modern era, this new/old technique to sit firmly at the forefront of experimental measurement techniques.

The second answer lies in the expanded measurement capability that particle tracking based systems provide the experimenter. As the reader will have noticed in the previous discussion of experimental methods, in both the structural and fluid mechanics domains, the vast majority of other methods only yield point, or perhaps spatially averaged quantities – the velocity or strain at a point, or the average displacement over some region of a structural specimen. Particle tracking technology, through the very simple possibility of deploying many particles, enables two, or even three-dimensional, field measurements to be made routinely. Take a structural panel, cover it with particles, and your particle tracking system will enable you to measure the displacement and strain fields across the entire panel. This capability of two, or three, dimensional field measurement delivers an enlarged measurement record, rich with possibilities, not previously available to the experimenter.

The third answer lies in the fact that particle tracking systems are non-intrusive. By this it is meant that the measurement technique one employs does not interfere (significantly) with the system that one is attempting to measure. Whenever you place a probe in a fluid flow, or mount a potentiometer on a structural specimen, the very act of installing your measurement device has, to some degree, modified the fluid flow, or structural element, whose behaviour you are attempting to measure. The particles used in both experimental fluid and structural mechanics are, in most cases, dynamically inert. Very fine particles, roughly tens to hundreds of microns in diameter, and accounting for a tiny fraction of the fluid domain of interest, are

distributed within the fluid. Small dots are either drawn on, or stuck onto, the surface of a structural element. In both cases these particles do not affect how the fluid or structural element behaves.

Despite these very significant arguments for the adoption of particle tracking as an experimental technique it should be noted that the technique has its limitations. These are most obvious in the domain of experimental structural mechanics. Until we develop techniques for routinely visualising the inside of a solid material, particle tracking will be unable to provide internal displacement and strain measurements. Such measurements are currently possible in the case of reinforced concrete through the embedment of strain gauges during the casting process. While this technique has its own set of technical challenges, particle tracking cannot, at this time, mimic this capability. In structural mechanics only surface displacement and strain fields are currently possible. While in many circumstances such measurements provide robust evidence of the system dynamics, there will be cases where such measurements are inadequate. It lies with the experimenter to decide whether surface measurements indeed provide insights into the key behaviour of the material.

It is worth adding at this point that this book will focus primarily on applications of particle tracking to experimental fluid mechanics and structural testing. The reason for this is simply because of our experience in these two domains – primarily the first. However, particle tracking is an intrinsically generic technique that can be applied to any physical system where particle motion, and its measurement, can lead to insights into the system. Certainly the extension of particle tracking to disciplines such as geomechanics and materials engineering are obvious. However potential applications lie elsewhere in the general area of engineering. Two come readily to mind. The first is traffic engineering where the aerial recording of street networks could be transformed into a particle tracking problem with the vehicles in the network playing the role of particles. The second is human behaviour during building evacuations – a problem encountered in fire engineering. In this case the particles correspond to the people exiting the building. All of these applications have their own special set of technical challenges. Unfortunately, there is insufficient space in this volume for us to explore these examples further.

1.2 Essence of a particle tracking system

Up until this point the specifics of a particle tracking system (PTS) have been glossed over to some extent. The experimental characteristics have been hinted at but now let us be more explicit. Whilst the features and components of such an experimental system, and the resulting data analysis, will be discussed in considerable detail in later chapters, here we provide a succinct description of the experimental and analytical processes.

Experimental Process:

1. **Particles**. A material body, whose movement is of interest, is "marked" with particles in such a way as to ensure that the motion of the particles mimics that of the material.

2. **Lighting**. Appropriate lighting is employed to illuminate the particles and ensure that they are readily identifiable.

3. **Camera**s. One or more digital cameras are used to record the motion of the particles.

4. **Calibration**. Before an experiment begins each camera captures a number of images that enable the system to be calibrated – i.e. to map image pixel coordinates to physical coordinates.

5. **Image capture**. Once an experiment commences the camera captures a sequence of images at a known frame rate. The images record the movement of the particles, and hence the material.

Analysis Process:

1. **Particle identification**. Particles are identified in the captured images using a particle identification algorithm. This algorithm interrogates each image, identifies particles, and records their location, size and colour.

2. **Particle tracking**. Particles are tracked from frame to frame. This tracking, or matching, process works with pairs of frames. Its task is to determine which particle in the first frame of each pair corresponds to which particle in the second. This process is non-trivial when large numbers of particles are present. The output of the tracking process is a set of particle tracks wherein each track comprises a list of particles (all corresponding to the same physical particle) linked from frame to frame.

3. **Field creation**. The physically important field, displacement or velocity, is computed from the raw particle tracks. Typically this field is generated through the interpolation of the particle displacement/velocity data onto a regular spatial grid, although in some circumstances the particle tracks themselves ultimately comprise the field of interest.

The three analysis steps described above form the framework for all particle tracking analyses. However, auxiliary processes may occur within these steps depending on the application. Here we provide a non-exhaustive list of these optional sub-steps.

- **Pre-processing of images**: The particle identification process may be significantly enhanced if the images are pre-processed in some way. Typically

image processing algorithms are applied to the images in order to boost the performance of the particle identification algorithm.

- **Elimination of spurious particles**: It is not uncommon for particle identification routines to identify invalid or spurious particles due to ambiguous elements in the images. Once particles have been identified tools may need to be applied in order to eliminate these spurious particles.

- **Transformation of particle sets**: To complete the particle identification process the particle data may require a transformation of some kind. The most common would be a transformation that converts particle pixel-based coordinates to physical coordinates.

- **Transformation of field data**: The field computed in step 3 may not be in its most convenient form and a final transformation of the field might be desirable. A simple example from the field of fluid mechanics would be the transformation of all variables into a dimensionless framework.

In later sections typical examples of these auxiliary steps will be described in greater detail, and illustrative examples will be provided in the case studies.

Particle identification and particle tracking, steps 1 and 2 in the analysis process, lie at the heart of a particle tracking system. The reader will notice that much of the discussion in subsequent chapters focusses on how good experimental design can support the effectiveness of these two crucial steps in the analysis pipeline. Because of their importance the following two subsections provide an expanded introduction to their essential characteristics.

1.2.1 Particle identification

High quality particle tracking systems are fundamentally dependent on the ability of the experimenter to record and identify the particles used to track the motion of the material of interest. Sophisticated tracking algorithms are unable to compensate for poor particle identification that may result in particles being missed or incorrectly identified.

Particle identification relies solely on the ability to accurately differentiate between the particles and extraneous background elements within the experimental images. The stronger the contrast between the particles and their surroundings the better, and much thought should be given to how to enhance this contrast. The choice of particles, the choice of lighting source and even the choice of camera can all play a role.

Generally, particle identification relies upon utilising the information stored in a digital image to identify pixels within the image that constitute a particle, and to discard those that do not. For standard colour images this information is comprised of the intensities of three recorded colours – red, green and blue (this is discussed in greater detail in chapter 4). Therefore all particle identification routines will utilise differences in

intensities between the particle pixels and the background pixels. To illustrate, consider the case of a fluid mechanics experiment, undertaken within a darkened room, where fine particles are seeded into a fluid flow and illuminated by a sheet of light. The reason for undertaking such an experiment in a darkened room is to ensure that the background image pixels are effectively black, while the pixels that capture the light reflected from the particles will be grey or white. A typical particle identification algorithm will search the image for clusters of pixels whose intensities exceed some user-defined threshold. Such clusters will be identified as particles.

In chapters 3 and 5 various factors that can impact on robust particle identification are discussed in greater detail. For now it is important to recognise that careful experimental design, that ensures high quality particle identification, is of prime importance.

1.2.2 Particle tracking

Particle tracking follows particle identification. It is this step that transforms the observation of moving particles to the generation of quantitative measurements of particle displacement or velocity. All subsequent calculations of physical fields, such as vorticity or strain, are wholly dependent on the particle tracking process, and the validity of the former is reliant on the accuracy of the latter.

Let us be precise regarding how particle tracking is achieved. The particles identified in two subsequent frames in a video record are analysed together. The tracking algorithm attempts to match particles in the first frame with those in the second, where a match is an assertion that the two matched particles are, indeed, the same physical particle. With a correct match a particle displacement can be computed. It should be clear that an erroneous match, whereby a particle in the first frame is matched to a physically different particle in the second frame, will lead to spurious, though sometimes plausible, estimates for particle displacement and velocity.

So, how might a tracking algorithm determine whether a particle in the first frame should be matched to a particle in the second, particularly when each frame might conceivably contain thousands of particles? Later chapters will provide specific examples of the tracking algorithms that might be successfully employed, but at this point we will discuss the process in a simplistic fashion. In order to determine which two particles should be matched the tracking algorithm needs some characteristic of the two particles that uniquely identifies them as the same particle. In other words, this characteristic would indicate that particle A should be matched to particle B but not to particles, C or D etc.

This idea is most easily understood with a few concrete examples. Imagine a situation where each frame contains only two particles. If one of the particles was red and the other blue then the characteristic of colour would uniquely guide the tracking algorithm to match the correct particles with each other. On the other hand, the particles might be the same colour, but one might be twice the size of the other. In this case the radius, or diameter, would be the unique identifier. Unfortunately these two

characteristics are rarely sufficient in most practical applications. Take the example of the fluid mechanics experiment described above. Here all particles are likely be similar in size and colour, and therefore these two attributes will be insufficient to differentiate between different particles. In such circumstances it is likely that the particle location will guide the tracking algorithm, or, to extend this further, the pattern of particles in the vicinity of the particle under consideration will guide the algorithm. For randomly distributed particles the particle pattern formed by a particle's neighbouring particles will be unique, and this pattern might be the characteristic that enables correct matches to be deduced.

There are other characteristics that might be used to facilitate the tracking algorithm and some of these will be discussed in later chapters. For now it is sufficient to recognise that particle tracking is based on the concept that there is some property of the particles that will enable the tracking algorithm to identify particle matches correctly.

Before leaving this topic it is pertinent to mention that particle tracking for complex physical systems that boast large numbers of particles is unlikely to yield perfect results – where every particle is matched correctly. Therefore, every experimenter should develop two indispensable analysis skills:

- adoption of a conservative approach to particle tracking, whereby they choose to accept fewer matches with high levels of confidence in preference to a greater number of matches with lower confidence levels, and
- a habit of performing detailed quality control checks to provide themselves, and others, with confidence that their results are reliable.

1.3 System Components

1.3.1 Overview

A particle tracking system comprises a number of components, most of which have been alluded to in the discussion up until this point. In this section we provide a brief introduction to each of these components and the role they play in a robust and effective PTS. Each will be discussed in much greater detail in chapters 3 to 7.

It is worth mentioning that we will only consider particle tracking systems that rely on visible light for their illumination. There is no doubt that other technologies, for example systems based on infra-red radiation, are possible, but we have no experience with such systems and are not aware of others who have employed them.

1.3.2 Particle selection

Not surprisingly particles lie at the heart of a PTS. In an abstract sense a particle is any visually identifiable element of, or in, the material being observed. Thus particles might exist naturally. Two examples will illustrate the point. When testing structural timber

elements, knots in the wood could be viewed as particles, and in air, natural specks of dust suspended in the air could play the role.

The difficulty with these naturally occurring particles is that the experimenter has little or no control over, amongst other things, their number, their size, their colour, their shape, or their distribution. All of these are generally important in the design of a PTS.

Therefore the preference is almost invariably for the experimenter to carefully select his or her own artificial particles that will meet the needs of their experimental objectives. Many of these needs will be discussed in chapter 2, and other particular technical requirements will be discussed in chapter 3.

Particle selection is based on two over-riding principles. Firstly, the particles must be clearly identifiable against the background in the images captured by the system's camera(s). Without this characteristic extracting particle information becomes impossible. The second is that the particles must act as surrogates for the material that they are intended to track. In other words, when the material moves in a particular region the particles in that region must exhibit the same behaviour.

Particle behaviour, and hence particle selection, is markedly different for fluid mechanics and structural applications. In fluid mechanics particles are introduced into the fluid and, once present in the flow, are moved about by the fluid. In many fluid experiments particles are observed only for a short period of time before exiting the viewing window of the camera. Consider the case of recording the fluid motion in a flow-through flume. Particles will enter the observation window from its upstream end, spend some time within the window, and then exit at its downstream end. This dynamic nature of the particle behaviour in fluid experiments contributes to the complexity of analysing fluid flow data.

On the other hand, in structural engineering the particles are "attached" to the structural specimen in some way. These particles typically remain visible for the entire length of the experiment, unless the specimen undergoes some catastrophic failure, and, while the particles will move during the experiment, their distribution often will not alter dramatically. Therefore in structural engineering applications particle control is largely in the hands of the experimenter, with the result that the data analysis is generally simpler than that in fluid mechanics.

1.3.3 Cameras

The second key physical component of a particle tracking system is the device used to capture the motion of the particles. Generally this is a digital camera – either still or video. In chapter 2 we will come to understand how certain characteristics of the camera play a crucial role in designing a PTS that meets specific experimental objectives.

For fluid dynamical applications digital video cameras are essential. This includes still cameras with a video mode. But in structural engineering experiments using a quasi-

static loading protocol still cameras are preferable due to their high pixel resolution – particularly if the cameras can be readily synchronised with the application of each load increment.

One issue that is not obvious at first glance is the camera mounting. The simple answer of "mount it on a tripod" is sometimes unsatisfactory, particularly in structural engineering applications. An implicit assumption in particle tracking is that the camera records the motion of particles in a fixed spatial reference frame. Thus particle displacement, velocity and so on are computed in a straightforward fashion relative to this frame of reference. Unfortunately this assumption is not always valid in a large scale laboratory facility, typical of civil engineering laboratories. In a structural laboratory heavy equipment such as cranes, pumps and vehicles can cause vibrations of the camera system such that the particle motion recorded by the camera may include a component of camera motion due to outside influences. This may not appear to be a likely problem in fluid mechanics applications but that is not necessarily so. We have undertaken experiments where the camera has been mounted on a moving trolley where the trolley motion induced unavoidable camera vibration. This issue will be discussed further in chapter 4.

1.3.4 Lighting sources

Easy visualisation, and identification, of the particles is often reliant on employing specialised light sources to illuminate the material under observation. This is particularly true in fluid mechanics.

The role of a light source is to enhance the optical contrast between the particles and the image background, and to do this in such a way as to ease the burden of identifying individual particles in an image. Ensuring that the light intensity is uniform across the entire image is generally an important objective for any light source. Non-uniform lighting and shadows significantly complicate the particle identification process. In structural mechanics the primary challenge is often eliminating shadows, sometimes caused by the experimental rig itself.

In fluid mechanics the lighting challenge is quite different. Because fluid flows are three-dimensional (unless free-surface velocities only are required) the light source is typically responsible for creating a two-dimensional slice through the flow. This is achieved through the use of a light-sheet generator of some sort. Such generators will be discussed in chapter 5.

1.3.5 Analysis tools

The previous three sections have provided a brief overview of the three hardware components of a PTS – particles, lights and cameras. The final component is the analysis tool used to process the images at the completion of the experiments. This analysis tool will pass the experimentally acquired images through the analysis pipeline described in section 1.1.1.

The experimenter can take a number of approaches to accessing an analysis tool.

Firstly, they may choose to develop and code their own tool, dedicated to their particular system. Every PTS is unique in some way and there may be good arguments for developing one's own analysis tool. Examples include:

- the characteristics of the PTS preclude the use of any standard tools,
- the data requirements may require the analysis to be performed on specialised computing hardware, such as a large cluster, and other tools are either not optimised for, or cannot run on, such hardware, or
- no general analysis tools are available.

A second option is to access a third party, general, analysis tool. In many circumstances such a tool will provide all of the processing capabilities required.

A third option is to take a hybrid approach. The general tool may be employed to undertake parts of the analysis pipeline, such as particle identification and particle tracking, while specialist software may be required to post-process the particle track data.

Which option is appropriate will depend on the experimental objectives, the characteristics of the PTS, and volume and complexity of the data it produces.

Streams is a general analysis tool, developed by the author at the University of Canterbury, that provides support for particle tracking (both 2D and 3D) along with a range of other optical experimental techniques typically used in experimental fluid mechanics, such as laser-induced fluorescence and light attenuation. It has been developed over a number of years with a number of core objectives. In brief these are:

- To develop a tool that is rapidly learnt and readily accessible to research students at all levels.
- To provide an analysis tool that provides the necessary support for a broad range of particle tracking applications and their associated experimental needs.
- To provide on-going development so that as new requirements arise in the laboratory the tool is relatively rapidly enhanced to provide support for these new requirements. In some cases these requirements are foreshadowed and the necessary tools are implemented before they are needed.
- To include powerful data manipulation and visualisation tools that enable rapid production of highly processed data and sophisticated figures without the need to export data to other tools.

Streams is freely available and can be downloaded from the following website.

https://www.canterbury.ac.nz/engineering/schools/cnre/software/streams/

The manuals for the software can be downloaded from this site and a perusal of these would provide a prospective user with a good insight into the capability of the software and whether it will satisfy their needs.

Streams has been successfully employed, over many years, by dozens of undergraduate and postgraduate students at the University of Canterbury in both the domains of fluid mechanics and structural engineering. It has also been used at a number of other institutions around the globe.

In order to be able to provide concrete examples of the processing and analysis of particle tracking data *Streams* will be used extensively in this book. While Part 2 of this book may be read with no reference, or access, to *Streams*, Parts 3 and 4 are based entirely upon it.

1.4 Roadmap for this Book

Before proceeding, let us provide a quick overview of the path this book will follow.

In Part 2 the experimental design of particle tracking systems is described in detail. It includes the following chapters.

Chapter 2 explores the experimental objectives that guide the design of the experimental measurement system.

Chapter 3 discusses the role of the particles themselves and how their characteristics can impact on system performance. Specific advice regarding the choice of particles suitable for different fluid and structural mechanics applications is provided.

Chapter 4 familiarises the reader with the fundamental properties of digital cameras that are critical to the design of an experimental system. Practical advice is given with regard to camera selection, operation and mounting.

Chapter 5 addresses the issue of lighting system design. As for the previous chapters general considerations are first discussed followed by specific commentaries on lighting systems for fluid and structural mechanics experiments.

Chapter 6 draws together the central ideas from chapters 2-5 and poses a series of questions, the answers to which will guide the experimentalist in their system design.

In Part 3 the focus is on the analysis of particle tracking datasets, and it will rely heavily on the *Streams* software for illustrative purposes. The following chapters are included.

Chapter 7 provides a general overview of the analysis process. The *Streams* analysis tool is briefly introduction and the manner in which the generic analysis pipeline maps to *Streams* objects and processes is explained.

Chapter 8 covers the first step in the analysis process, the primary objective of which is to accurately identify particles in a set of experimental images. The *Streams* tools available to achieve this are explained in some detail

Chapter 9 discusses the critical second step of the analysis process – namely the tracking of particles from frame to frame. Again, the tools, in *Streams*, that support this activity are described.

Chapter 10 addresses the final step of generating the physical fields sought by the experimenter.

Finally, Part 4 presents a diverse collection of case studies. These are drawn from both the fluid and structural mechanics domains. Datasets are made available to the reader so that they can undertake the analysis process themselves using *Streams*. While these case studies illustrate the analysis process it is hoped that the reader will use them as a springboard for their own exploration of the analysis tools available.

Chapter 11 presents a simple example of particle tracking being used to measure the motion of a floor in a model building, subject to simulated earthquake excitation of the building's foundations.

Chapter 12 explores the application of particle tracking to the measurement of velocities in a gravity current – a current of dense fluid propagating along the bottom of a flume filled with less dense fluid. Considerable time is spent "looking under the hood" of the analysis process in order to gain a robust understanding of how various analysis parameters impact on the results.

Finally, chapter 13 investigates a complex structural engineering application involving multiple cameras with a generalised calibration system. A number of the challenges faced in such an experimental system are discussed, and, as for all of the case studies, illustrative experimental results are provided.

1.5 Summary

This chapter has provided an overview of a particle tracking system. The essential experimental and analytical components have been described with a particular emphasis on the two key steps in the analysis pipeline – namely particle identification and particle tracking. The experimental design of a particle tracking system should focus on ensuring that these two steps yield robust outputs.

Part 2

Particle Tracking Systems:

Experimental Design

2. Experimental Objectives

2.1 Introduction

As with most human activities, forward planning of an experimental programme is vital to its success. Part of that planning involves articulating a clear statement of the objectives that the activity hopes to achieve. The design of an experimental particle tracking system is no exception. Early in the design of the experiments thought should be given to a number of issues associated with the particle tracking system. These include:

- the variables that are to be measured,
- the spatial and temporal resolution of these variables,
- the domain over which these variables are to be measured, and
- the accuracy to which these variables need to be measured.

Each of these is covered in the subsequent sections.

2.2 Variables of interest

Particle tracking systems measure particle displacement. So, in many ways, the variables of interest are largely pre-determined. The system will provide particle displacements and, potentially, quantities derived from displacements such as velocities, accelerations, kinetic energy and the like. In the domain of fluid mechanics interest might lie in variables extracted from the velocity field such as vorticity, turbulent kinetic energy and so on. In structural mechanics the ultimate variable of importance may be the strain field. But in all cases it is the raw particle displacements that allow these higher order variables to be computed.

However, this simplistic view hides the potentially significant differences between the objectives of various experimental programmes, and these differences must be borne firmly in mind in the design of both the experiments and the PTS.

Let us consider a simple example from the area of structural mechanics to illustrate the point. Case study 1 describes an experimental programme whose objective was to capture the motion of the floors of a model multi-storey building under different excitation conditions. The PTS was required to measure the displacement, and hence velocity and acceleration, of one of the building floors, and thence to compare these results with the measurements made with an accelerometer mounted on that floor. As the floor of the building was to be treated as a monolithic mass with no internal variability in displacement (i.e. it was assumed to suffer no internal deformation) the PTS could be designed in a relatively simple way. In theory, a single particle attached to the floor and tracked through time would be sufficient to capture the floor motion. This is in marked contrast to the PTS design that would have been appropriate if internal deformations of the floor were to be expected. In that case a full displacement

(and hence strain) field of the floor mass would have been required, and this would have been achieved by covering the floor mass with an array of particles that enabled the gradients of displacement within the floor to be captured. Such an example is illustrated in case study 3.

In fluid mechanics, significant variation is also possible. Consider the following possible uses for a particle tracking system:

- measure the two-dimensional velocity field along the centre-line of a flume,
- measure the surface velocity field in a shallow channel flow,
- measure the three-dimensional velocity field in the wake of an obstacle, or
- measure the motion of sediment particles along the bottom of a flume with a mobile bed.

Each of these experiments requires different considerations when designing the particle tracking system.

2.2.1 Measured Variables

The vast majority of particle tracking applications focus on the measurement of field variables – displacement fields, velocity fields, strain fields, vorticity fields and so on. In addition, while three-dimensional particle tracking is available, and, in some circumstances essential to achieving the experimental objectives, most applications are still two-dimensional in nature. Therefore, for the remainder of this book our attention will be wholly focussed on two-dimensional particle tracking. Many of the concepts discussed here are relevant to three-dimensional particle tracking, but the higher dimensional system comes with other significant complexities – in particular the need for multiple cameras and their calibration.

So what exactly does the measurement of a field variable entail? Perhaps more importantly, what is the output that is expected from a PTS when a field variable is sought? In practice there are three possible field types that might arise. The first two are most easily conceptualised using the terminology of fluid mechanics.

An **Eulerian** field is a variable whose value is known as a function of x, y and t, where x and y are the two spatial dimensions and t is time. The critical defining feature of an Eulerian field is that x and y are associated with a specific reference frame. This reference frame need not be fixed relative to the laboratory – for example a fluid mechanics experiment on a rotating table simulating geophysical fluid flows will have a rotating coordinate system – but it should be clearly defined and exclude spurious motion such as that due to random camera vibration. Mathematically an Eulerian field would be expressed as

$$u = u\left(x, y, t\right) \tag{2.1}$$

where u is the field variable.

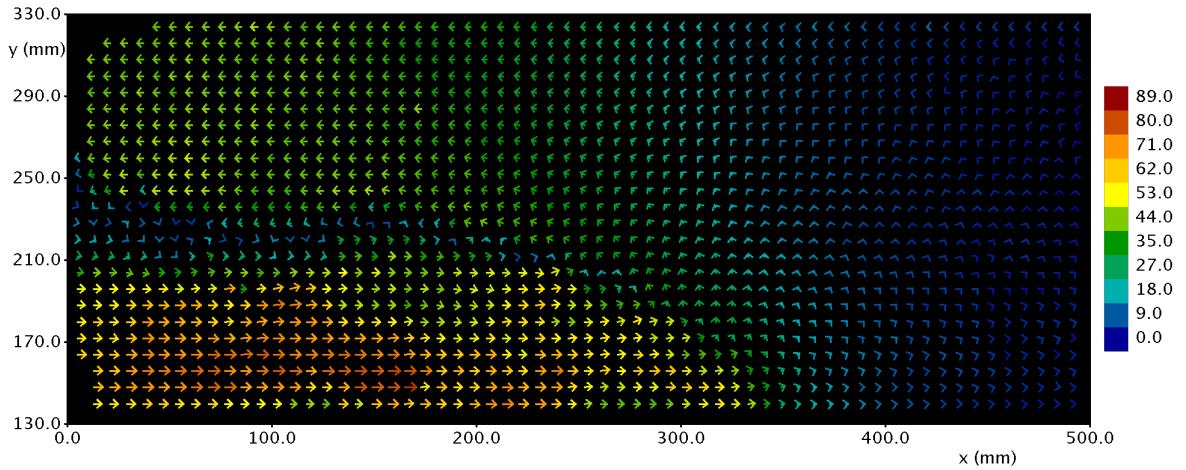

Figure 2.1. An example of an Eulerian field. The figure plots the instantaneous velocity vector field of a gravity current travelling from left to right at a specific time. The velocity field is defined on a rectangular grid. The legend relates the colour of the velocity vectors to their magnitude (in mm/s).

An Eulerian field is readily visualised. Consider a fluid mechanics experiment where particle motions are being recorded along the centre-line of a closed flume. At one end of the flume is a compartment containing salt water, while the remainder of the flume contains fresh water. When the partition between the two fluids is removed a dense current of salt water, known as a gravity current, propagates along the bottom of the flume and the particles within the fluid enable the velocity field of the flow to be recorded – note that this flow is analysed in detail in case study 2 (chapter12). Imagine overlaying a rectangular grid of points on the flow region being observed and computing the fluid velocity at each of the grid points based on the surrounding particle motion. The resulting field on that grid would be an Eulerian field. Each point on the grid has a different (x, y) coordinate, and at each grid point the velocity is known as a function of time. Thus it is clear that the velocity field is of the form expressed in equation 2.1. Figure 2.1 provides an example of such a field.

A **Lagrangian** field is a variable whose value is known for a material particle as a function of time. Thus a Lagrangian field is associated with particular material particles as they move through space and time. Mathematically this can be expressed as

$$u = u\left(n,t\right) \qquad (2.2)$$

where n is a unique identifier for each particular particle, typically conceptualised as a number. Figure 2.2 provides an illustration of a Lagrangian field. The vertical position of ten particles on a structural specimen are tracked as a function of time.

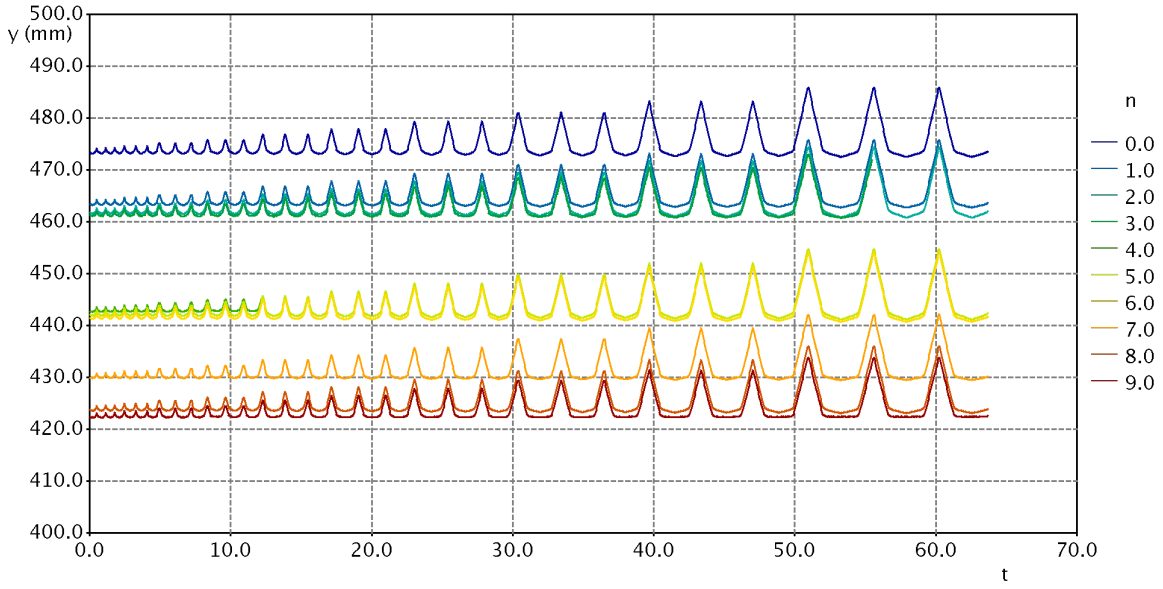

Figure 2.2. An example of a Lagrangian field. The figure plots the vertical position of ten particles (labelled n = 0 – 9) on the surface of a structural timber specimen - the actual experimental setup is shown in figure 3.4. The specimen undergoes a series of increasing cyclic loads – with three cycles at each loading level. In this case the loading is quasi-static. Thus the time axis is not time per se, but is, instead, related to the point within the loading schedule. The legend labels the individual particles.

The third possible field can be viewed as a hybrid of the Eulerian and Lagrangian fields and arises most commonly in material applications such as structural mechanics.

A **material-based** field is similar to an Eulerian field in that the field value is specified as a function of x, y and t. Now, however, the spatial coordinates x and y are not fixed in space. Instead they are fixed to the material, in a similar way to a Lagrangian field. This may be expressed mathematically as

$$u = u\left(x', y', t\right) \tag{2.3}$$

where x' and y' stand for the spatial coordinates relative to the material.

Consider a structural test whereby a beam, simply supported at both ends, is loaded at its centre and deformed as the load is increased. If the strain field were expressed as an Eulerian field, a grid would be laid over the physical domain and the strain field would be computed at each grid point. As the load was increased different parts of the beam would move past different grid points. Some grid points, those below the beam for example, would commence with no defined strain field, but as time passed and the loading increased, some of these grid points would have measured strains as the beam deformed to lie over those grid points. This is not a very informative way in which to visualise how the strains within the beam develop over time. A material-based field is computed by mapping the deformed beam back to its original form. Thus the strain is known at each point within the undeformed beam as the load increases. The result is a field that can be expressed in the form of equation 2.3, and the field is material-based. An example of a material-based field is provided in figure 2.3.

One final remark regarding the measurement of fields in structural testing is worthy of mention. This has already been alluded to in the caption to figure 2.2. If a structural test is dynamic, in other words it operates in real time, such as the testing of a specimen on a shake table, then the time variable in equations 2.1, 2.2 and 2.3 is physically meaningful. On the other hand if the testing is undertaken in a quasi-static way in which the loading of a specimen is not undertaken in real time, but is instead applied incrementally at the experimenter's discretion, then time in these equations is typically a surrogate for the point within the loading cycle.

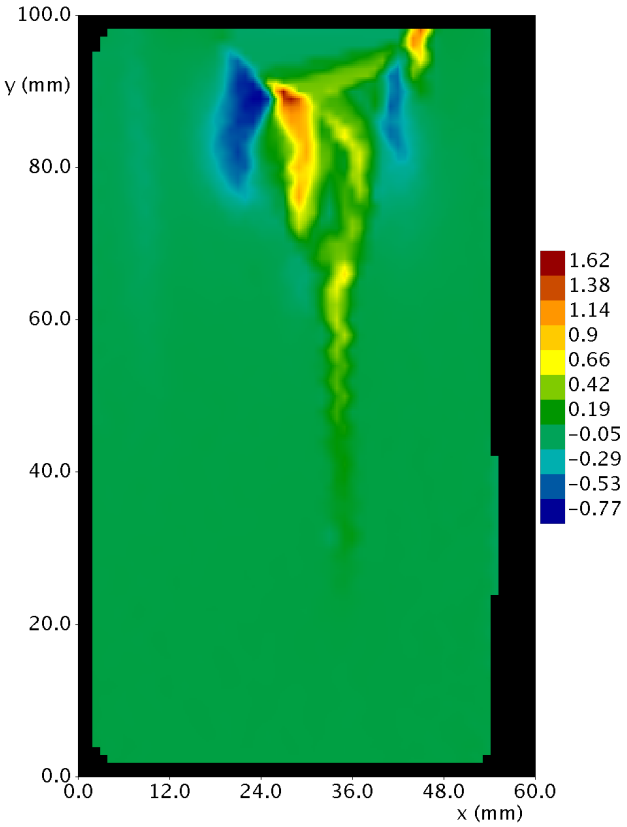

Figure 2.3. An example of a material based field. The figure plots the lateral strain measured at a particular time in a small timber specimen being vertically loaded through an embedded steel dowel located at the centre of the top of the specimen. The actual experimental setup is shown in figure 3.2b. A rectangular grid is conceptually overlaid on the pre-loaded specimen. As the specimen is deformed by the loaded dowel, this grid can be thought of as being deformed as if each grid point were fixed to the timber material. For a material-based field the field at each deformed grid point is mapped back to that grid point's original position on the undeformed specimen. Thus the strain field displayed in the figure appears on the original rectangular grid.

2.3 Resolution

Spatial and temporal resolution are important considerations in any PTS. Before exploring each of these in turn, and providing guidance to the experimental designer, let us first define exactly what we mean by resolution.

Definition:

Resolution is the scale over which changes in a variable can be deduced.

2.3.1 Temporal resolution

All dynamic physical systems possess some characteristic time scale, or, perhaps more likely, a range of timescales, over which changes to the system occur. Two examples may help to illustrate the concept.

Turbulent fluid flows with generally have a timescale that characterises the changes to the mean flow as well as a spectrum of timescales that characterises the turbulent motions in the flow. A shake table test of a structural assembly will typically use a synthetic, or recorded, earthquake excitation record to control the shake table motion. This earthquake record will contain a spectrum of frequencies, or timescales.

When designing a PTS the experimenter must decide the shortest timescale that must be resolved by their measurement system – note this might not equate to the smallest time scale present in the physical system. This choice will dictate the temporal characteristics of the camera(s) that they choose to deploy. Chapter 4 will provide more detailed information regarding digital cameras. For now it is sufficient to understand that all cameras have a characteristic known as the **frame rate** – measured in Hz or frames per second (fps) – that determines how many images the camera can capture each second. Camera selection for a PTS will be partly based on the temporal resolution required of the system.

Rule of thumb:

In choosing a camera the frame rate should be selected so that it is substantially larger (typically by an order of magnitude) than the highest frequency that you wish to resolve in your experiments.

The implications of this rule of thumb can be understood by a simple example. Imagine that your system is characterised by a single time scale T, or frequency $1/T$. The frame rate of your camera ideally should be at least $10/T$, such that the time between frames is no more than $T/10$. Therefore, if a system variable, such as

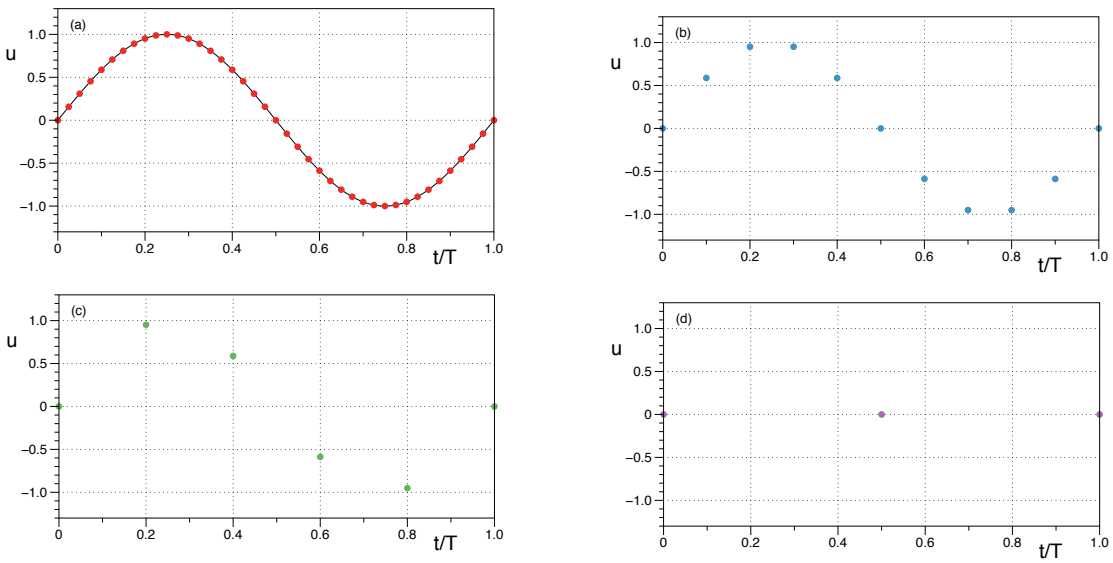

Figure 2.4 Illustration of the effect of time resolution of a signal, assumed to have a single frequency of 1/T. (a). The frame rate is 50 times the frequency of the signal, or the time between frames is T/50. (b) Time between frames is T/10 (recommended). (c) Time between frames is T/5. (d) Time between frames is T/2.

displacement, is measured by the PTS it should be able to resolve each temporal cycle of the displacement with at least 10 data points. A faster frame rate will provide even better resolution of the temporal variation of the displacement while a slower frame rate will provide poorer resolution. The impact of the frame rate on signal resolution is illustrated in figure 2.4.

This issue can also be considered in a reciprocal sense. It is possible that the experimenter has only a limited choice of cameras for their measurement system. For example the frame rate may be a trade off with another of the camera's characteristics – typically the pixel resolution. Thus, if the frame rate of the camera is fixed, the above rule of thumb provides as estimate of the timescales of the system that the PTS will be able to resolve.

2.3.2. Spatial resolution

Spatial resolution, unlike temporal resolution, is unrelated to the characteristics of the camera. Instead it is dependent upon the layout of the particles used to represent the motion of the material of interest. Spatial resolution is directly related to the inter-particle spacing. The closer together the particles, the more highly resolved will be the spatial variations in particle displacement, and vice versa. While it would appear that a camera with a larger number of pixels would provide greater spatial resolution, this is not the case. The pixels themselves do not provide measurements of displacement, the particles play this role, and therefore spatial gradients in displacement are determined by the particles not the pixels. The pixel resolution of a camera does play an important role, however, as we will see in section 2.4.

The rule of thumb for spatial resolution mimics that for temporal resolution.

Rule of thumb:

Choose a particle density such that the smallest spatial scale of interest is substantially larger than the typical inter-particle spacing.

Particle layout is something over which the experimenter has considerable control in structural testing. As the particles are typically applied manually the experimenter can choose both the arrangement and the spacing of the particles on the specimen. These concepts will be discussed in more depth in chapter 3. However it is worth noting here that the experimenter is free to vary the density of particles across the specimen. In regions where strong gradients of strain, or displacement, are likely to occur, high particle densities can be chosen, while in regions where the specimen may be expected to suffer very little deformation larger particle spacings may be sufficient to capture all of the important material behaviour (see case study 3 in chapter 13 for an example). These decisions are completely at the experimenter's discretion.

One issue of particular interest in some areas of structural mechanics is the identification of cracking, and the propagation of cracks over time. The spatial resolution of a PTS determines how accurately cracking can be measured. If one considers a strain field where a crack occurs within an otherwise non-deforming material, this field will be everywhere zero, except along the narrow region containing the crack. A PTS will only be able to locate the crack to within a region that lies between particles. The closer the particles the more accurately the crack location will be determined.

On the other hand, particle layout is largely beyond the control of an experimental fluid mechanicist. Particles are typically mixed into the fluid being observed and this process is implicitly random in nature. The best that the experimenter can achieve is to mix in the appropriate number of particles such that, if they were uniformly distributed throughout the fluid, the inter-particle spacing would be as desired. Of course, under these circumstances there is no capacity to be able to vary the particle density in different regions of the flow.

A naïve approach to the issue of spatial resolution, with the aim of achieving very high spatial resolution, would be to use an extremely high particle density. Such an approach typically is inefficient with computing resources with little ultimate benefit.

2.4 Accuracy

Accuracy is not the same as resolution. Different factors determine the accuracy of a PTS so it is quite possible to design a PTS system with a particular resolution while at the same time being able to adjust its accuracy. The reverse is also true – a fixed accuracy system can have variable resolution.

Definition:

Accuracy is the uncertainty, or error, associated with the measurement of particular quantity. As accuracy increases the uncertainty, or error, decreases.

The accuracy of a PTS is always related to the accuracy with which the particle displacement can be computed. As the time step between frames, set by the camera, is highly accurate, the error, or uncertainty, associated with the particle velocity is essentially the same as that of the particle displacement.

A number of factors contribute to the determination of the particle displacement accuracy and these will be discussed in the following sub-sections. Note, however, that the assumption made throughout this discussion is that all particle matches are correct. If this is not the case then the displacement error is likely to be primarily due to the matching error. We refer the reader back to the advice provided at the end of section 1.2.2.

2.4.1. Location error

The first factor is the accuracy of determining the location of a particle in an image. As discussed in section 1.2.1, the algorithms that identify particles in an image utilise pixel intensity information to determine the pixels that comprise a particle. These pixels are physically distributed in the pixel map of the image and the particle's pixel location can be computed in a number of ways from this distribution. For example, the particle location could be computed as a weighted average of the centre of mass of the pixels comprising the particle, where the weight is related to the intensity of each pixel. All PTSs require a camera calibration that can relate pixel locations to physical locations (see section 4.5). Thus the particle's pixel location can be mapped to a physical location.

The accuracy of this location is determined by the spatial resolution of a pixel. Typically the error in determining the centre of mass of the particle pixels is less than $\pm\frac{1}{2}$ pixel, and often better than this. We generally use $\pm\frac{1}{4}$ pixel as an estimate for the uncertainty in this measurement.

It should be clear that the uncertainty in the particle's physical location is directly related to the size of the physical region recorded by each pixel. For example, imagine an experimental setup where a 6000 x 4000 pixel camera is used to record particle movement in a region measuring 600mm x 400mm. Each pixel in an image covers a physical domain of 0.1mm x 0.1mm. Therefore the estimate of the uncertainty in particle location is $\pm 25\mu m$.

One of the particularly attractive features of a particle tracking system is that its accuracy is readily increased either by using a camera with a greater pixel density, or simply decreasing the size of each pixel – for example by moving the camera closer to the subject, or by using a zoom lens. It is very easy to get highly accurate micro-

measurements by reducing the size of the region captured by the camera. With a suitable lens a camera of 6000 x 4000 pixel resolution, observing a 60mm x 40mm domain, will have an uncertainty in particle location of only $\pm 2.5\mu m$.

2.4.2. Particle displacement

Knowing the accuracy of the particle location is not sufficient. The measurement of the particle displacement is obtained by computing the difference between the particle location in one image and its location in a subsequent image. Based on the rules for calculating uncertainties the uncertainty in particle displacement is the sum of the two absolute errors and is, therefore, approximately $\pm \frac{1}{2}$ pixel. What is of particular interest to the experimenter generally is not this absolute error, but the percentage error, and clearly this depends on how far a particle moves between frames. A particle with a small displacement, say 2 pixels, carries a weighty uncertainty of $\pm 25\%$ in its computed displacement, while a particle moving 20 pixels has an uncertainty in its displacement of only one tenth of this.

2.4.3. Displacement calculation

This simple calculation of a displacement based on the difference between the particle location in two sequential frames is rather simplistic. In mathematical terms this calculation would be termed a forward difference if the displacement estimate was used for the first frame in the sequence, while it would be termed a backward difference if the displacement was used for the second frame in the sequence. In practice a particle track may extend for many frames and therefore it is possible to use a more accurate central difference calculation involving the particle location in the previous and subsequent frames. Such a calculation is known to be more accurate than either of the forward or backward differences, and is likely to at least halve the error.

In addition, when fields are computed on regular grids, interpolation algorithms compute the displacements at grid points using the displacements of neighbouring particles. There are numerous ways to implement this interpolation, but in all cases it is expected that the displacement uncertainty, provided the error is random at each of the points contributing to the interpolation, will decrease due to the use of multiple displacement estimates.

2.4.4. Summary

The accuracy of displacement calculation relies on a number of factors, primarily the size of the physical domain captured by a single pixel, the magnitude of particle displacement between frames, and the method used to compute the displacement at the particle location, and/or on a grid point. All three of these factors are, to some extent, at the discretion of the experimenter. A definitive estimate of the uncertainty associated with the displacement calculation is hard to furnish, but provided central

difference calculations are used it can be expected that the uncertainty will be less than $\pm 1/4$ pixel.

2.5 Coverage

The final issue that must be considered by the PTS designer is the coverage of their system.

Definition:

Coverage is the extent of the physical domain recorded by the PTS.

In a single camera PTS coverage is inextricably linked to accuracy. As described in the previous section, as the pixel size decreases the uncertainty in the particle location decreases. Almost invariably this is a good thing. However, the result of decreasing pixel size, assuming the camera pixel resolution is fixed, is that the physical domain observed by the camera, or the coverage, also decreases. These two characteristics of the system are potentially in tension.

Consider a fluid dynamics experiment of a turbulent jet discharged into a tank of fixed dimensions. The experimenter wishes to capture the fluid motion in the entire tank, and therefore he or she must configure their camera so that the entire tank is captured in an image. However they would also like to increase the accuracy of their system by moving the camera closer to the tank and reducing the size of the domain captured by each pixel. Clearly both of these two objectives cannot be met with a single camera of fixed pixel resolution.

There are a number of ways to unlink the system accuracy from its coverage. We list two below.

- Select a different camera with an increased number of pixels. This may not be easy to achieve if you are already using a top end camera for your experiments, but if you have chosen a cheap camera, or have an older model, upgrading your camera may be a feasible option.
- Use multiple cameras. This option is by far the most flexible and in many cases the only option. It is not unusual in structural engineering to wish to measure displacement fields on multiple surfaces – for example the front and rear of a panel. In this case a single camera is never a realistic option. The use of multiple cameras, whether they are recording adjacent areas on the same surface (see case study 3) or different surfaces altogether, brings with it additional complexity. First and foremost, the cameras need to be synchronised in time. Secondly, each camera must be calibrated and this may involve ensuring that the physical coordinates in one camera's images can be mapped into a global coordinate system in which all camera images can be placed (again see case study 3).

2.6 Summary

This chapter has focussed on the experimental objectives that need to be considered by an experimenter when designing a particle tracking system. Before particle and camera selection can take place, or a lighting system designed, the experimenter must be able to provide clear answers to a number of questions:

- What fields are to be measured by the PTS?
- What spatial and temporal resolution are demanded by the measurements?
- What level of accuracy is required of the measured field?
- What region of the experimental system must be covered by the measurement system?

The answers to these questions will guide the design of the particle tracking system.

3. Particle Selection

3.1 General Considerations

Particle selection is a decision that needs to be made early in the design of a particle tracking system. While naturally occurring particles are possible, and may in fact be the only choice in a field application where the object being observed is inaccessible to the observer, generally an experimenter will make deliberate choices regarding the particles that they will employ.

There are a number of questions that must be answered as part of this selection process, and many of these are important regardless of the application area involved. In each of the following subsections we will discuss, in a general way, the various issues that the experimenter is likely to consider. In sections 3.2 and 3.3 specific examples of particles in fluid mechanics and structural mechanics applications will be discussed and their advantages and disadvantages will be presented in the light of the general issues.

3.1.1 Contrast with image background

Particle identification is one of the two primary concerns in particle selection. Particle identification algorithms generally rely on discernible changes in pixel intensity in an image to be able to discover particles within that image (see section 1.2.1). A change, or contrast, in intensity is generally achieved through one of two pixel characteristics:

Pixel intensity:

Particles that are brighter or darker than the surrounding pixels are readily identified, and thus pixel intensity is a common way of differentiating particles from their surroundings. This differing intensity may be achieved by ensuring that the particles are more or less effective at reflecting light than the other elements in an image. Or it may be achieved by simply choosing particles that are of a darker or lighter hue when compared to their surroundings.

Pixel colour:

Most digital cameras have the ability to capture colour images. If colour information is available then overall pixel intensity variations are not requisite for particle identification. Simply variations in colour can perform the same task. For example, in a structural application, if a specimen were painted blue then red particles, no matter what their relative intensity, could be readily identified.

3.1.2 Material surrogacy

Particle identification, in and of itself, is not sufficient for a robust PTS. It is also vitally important that the experimenter is confident that the motion of the particles recorded by the camera actually represents the motion of the material itself. In other words, the particles are true surrogates for the material. Consider a poorly designed structural testing PTS where small pins with colourful heads – to be used as the particles – are loosely stuck into the surface of a timber panel. As that panel is shaken through the action of dynamic rams the loose connections of the pins result in the pins changing orientation relative to the material on which they are mounted. While the motion of the timber panel will impact on the particle motion, so will the independent motion of the pins as their angle of insertion changes with the motion of the panel. This PTS would provide plausible, yet spurious, results for the displacement and strain fields of the timber panel.

This example is perhaps extreme and hopefully easily identified by the system designer as problematic. However sometimes this issue is more subtle and requires careful thought.

3.1.3 Particle size

Particle size is important for a number of reasons. We summarise these below.

Visibility:

The first is probably the most obvious. Particles needs to be large enough to be seen by the camera. Generally a particle needs to be larger than a single pixel or there is the possibility that it will be lost in the video record, or, perhaps worse, the particle occasionally appears in the image and at other times not. In the latter case the particle flickers in and out of the video record and this can compromise the particle tracking algorithms.

Accuracy of particle location:

The accuracy of a PTS was discussed in some detail in section 2.4. The most important factor in determining the accuracy is the ability to accurately determine the location of a particle. Generally this accuracy is approximately $\pm \frac{1}{4}$ pixel. However in certain circumstances, if the intensity of the pixels within a particle varies smoothly from a maximum at the centre of the particle to a minimum near its edge, more sophisticated algorithms can be used to determine the location of the particle centre that take advantage of this intensity variation. Clearly a particle that occupies only a single pixel or perhaps two pixels will not have a spatial intensity distribution to enable the use of these more sophisticated algorithms.

It is important to note that the accuracy of a standard algorithm for determining the location of the centre of a particle – one that simply averages the x and y coordinates of

the pixels that comprise the particle – is unaffected by the particle size. Thus particle size does not impact system accuracy in this case.

Spatial resolution:

The spatial resolution of a PTS was introduced in section 2.3. To recap, the spatial resolution determines the spatial scale over which variations, or gradients, in particle displacement can be discerned. Spatial resolution is determined by the inter-particle spacing. While spatial resolution is not directly related to particle size, it is perhaps clear that the larger the particles, the further apart must be their centres in order to ensure that the particles do not overlap. Therefore in an indirect sense particle size is constrained by the system's desired spatial resolution, or conversely, the particle size places limits upon the system's spatial resolution.

3.1.4 Particle size uniformity

In the previous section we discussed how particle size can impact on the performance of a PTS. Here we broaden this discussion to consider whether all particles should have the same size.

A variety of particle sizes can enhance the performance of a particle tracking system. To understand this we return to some of the basic concepts of particle tracking reviewed in section 1.2.2. In order to accurately track a particle from one frame to the next the tracking algorithm needs some particle characteristic that helps to uniquely identify it in each frame. As discussed in section 1.2.2 the particle radius or diameter could be such a characteristic. If all particles are effectively the same size then size cannot assist the tracking algorithm. However, if the particle size has some discernible range then it is possible that the particle size could be used to enhance the tracking algorithm's ability to identify the correct particle in the next frame.

When hundreds or thousands of particles are present in a PTS the particle radius or diameter becomes a continuous variable, lying within a constrained range, that is not well suited to assisting the tracking algorithms.

3.1.5 Particle optical uniformity

Particle optical uniformity refers to the range of pixel intensities, or colours, present in the recorded images. As the particle identification algorithms rely on pixel intensity or colour to be able to identify the pixels that comprise a particle, variations in these properties may lead to the algorithms not including the correct pixels in a particle.

The best outcome of such variability is that the particle size and location are incorrectly calculated. The worst possible outcome is that the variability is so large that the identification algorithm identifies multiple particles where only one exists.

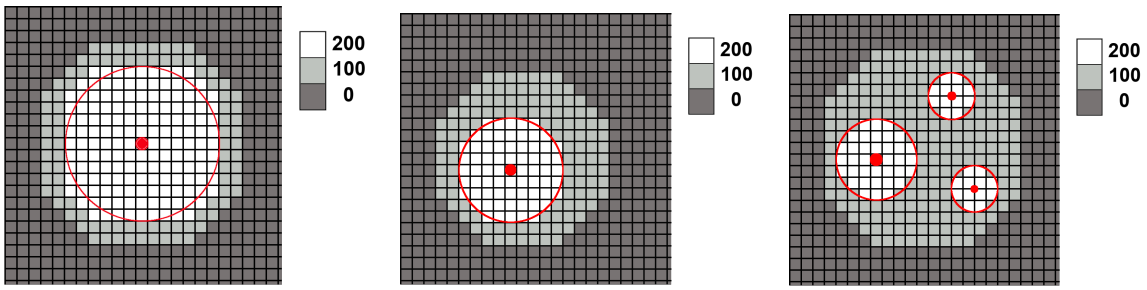

(a) (b) (c)

Figure 3.1 Illustration of the impact of optical non-uniformity. Each figure depicts an idealised pixel map where pixels intensities take one of three values – 0, 100 or 200. The particle identification algorithm identifies any pixel with an intensity above 150 as part of a particle. A red dot locates the centre of an identified particle while a red circle shows its size. (a) The light intensity is uniform across the whole image. (b) The light intensity is non-uniform but varies smoothly from stronger in the bottom left to weaker in the upper right. (c) The light intensity varies unevenly across the image. Optical non-uniformity results in particles with incorrect size and location, or spurious particles being identified.

Figure 3.1 provides an illustration of these effects. In figure 3.1a a particle of high optical uniformity is identifiable in the pixel map through an appropriate choice of intensity threshold – in this case 150. The result is that its size and location are correctly computed – to within the accuracy of the system. In figure 3.1b some of the pixels within the particle have reduced intensity and the system predicts a smaller particle with an incorrect centre. Finally in figure 3.1c the non-uniformity of the intensity of the particle's pixels is such that different, disconnected, regions within the particle are identified as separate particles, thus leading the algorithm to find many particles instead of one, and all of these particles are incorrectly sized and located.

High levels of optical uniformity are important if accurate particle identification is to be achieved, and without it the PTS will be of limited quantitative value to the experimenter. This uniformity can be degraded in a number of ways, particularly in the structural domain where the particles are typically artificially created on the surface of the specimen. This issue will be revisited in sections 3.3 and 3.4.

It is worth noting that the advantage of using particles with a range of sizes, as proposed in section 3.1.4, is potentially equally valid for particles with a range of intensities or colours. Provided all particles, no matter what their intensity or colour, are clearly and accurately identifiable the use of a variety of intensities, or colours, can enhance the accuracy of the particle tracking algorithms. A simple example was provided in section 1.2.2.

3.1.6 Particle spatial distribution

In some particle tracking systems, notably in structural engineering applications, the experimenter has control over the spatial distribution of particles. We will consider two reasons why one might choose to avoid spatial uniformity.

Variable spatial resolution:

By varying the spatial density of particles across the observation window the system resolution can be adapted to the specific requirements of different parts of the domain. In some regions small scale phenomena might be expected, and to capture these a high particle density is required. In other parts of the domain the system might experience only large scale behaviour, and a much lower particle density is adequate to capture the key physics. While one could choose to adopt the higher particle density across the whole domain (certainly a higher particle density will give as much, and more, information than a lower particle density) there are a number of reasons for not doing so:

- depending on how the particles are applied to the domain the additional particles might involve considerable extra work,
- the much larger number of particles will require extra storage and extra processing time for no real additional benefit, and,
- higher density particle distributions place higher demands on the particle tracking algorithms.

Irregular particle distribution:

As has been discussed in section 1.2.2 particle tracking algorithms benefit from being able to use particle characteristics, or traits, that enable each particle to be uniquely identified amongst the other particles in an image. One of the most useful characteristics is the pattern of particles surrounding a particular particle. As that particle moves, the surrounding particle pattern should stay approximately the same for continuous media, in the short term at least. Therefore, there are significant advantages in distributing particles in a pseudo-random fashion so that this pattern is effectively unique for each particle. The corollary is that regular particle configurations should be avoided, as these fail to provide differentiable particle patterns.

Figure 3.2 illustrates two structural applications, one of which has used a pseudo-random particle layout and the other a regular particle array. In both cases particle tracking was successful, but the regular particle layout presented more significant challenges to the tracking algorithms.

3.1.7 Seeding method

The manner in which particles are "attached" to the material under observation is referred to here as the **seeding** method. This method varies substantially between fluid and structural applications and is normally highly dependent on the particle choice. Therefore a detailed discussion of particular seeding methods will be left until sections 3.2 and 3.3 where they can be addressed in context.

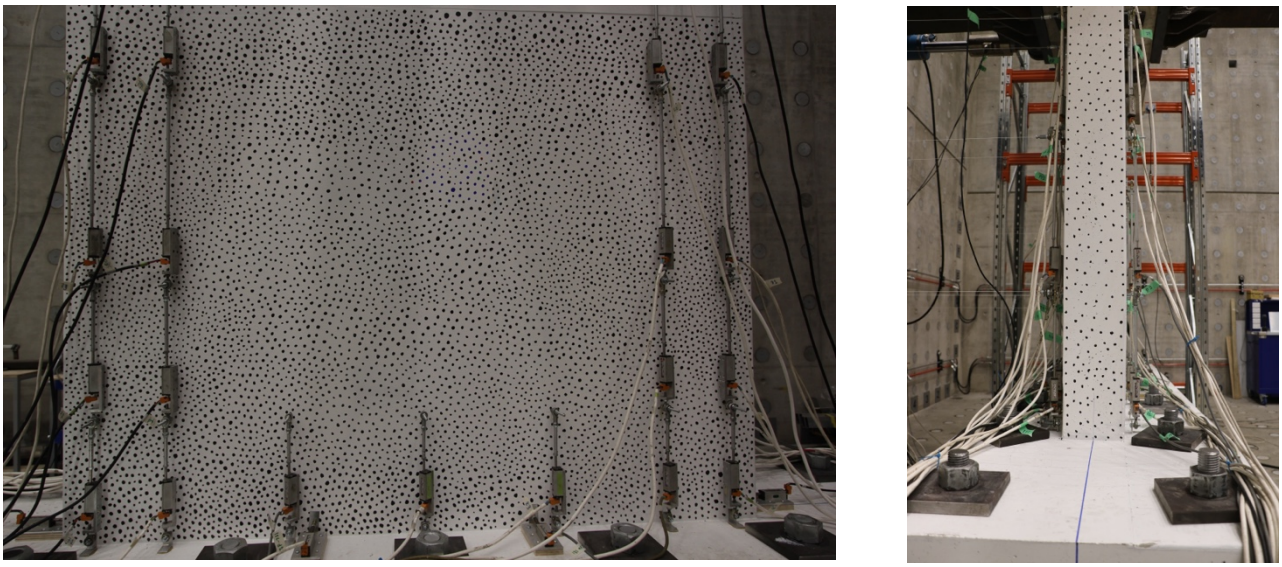

(a)

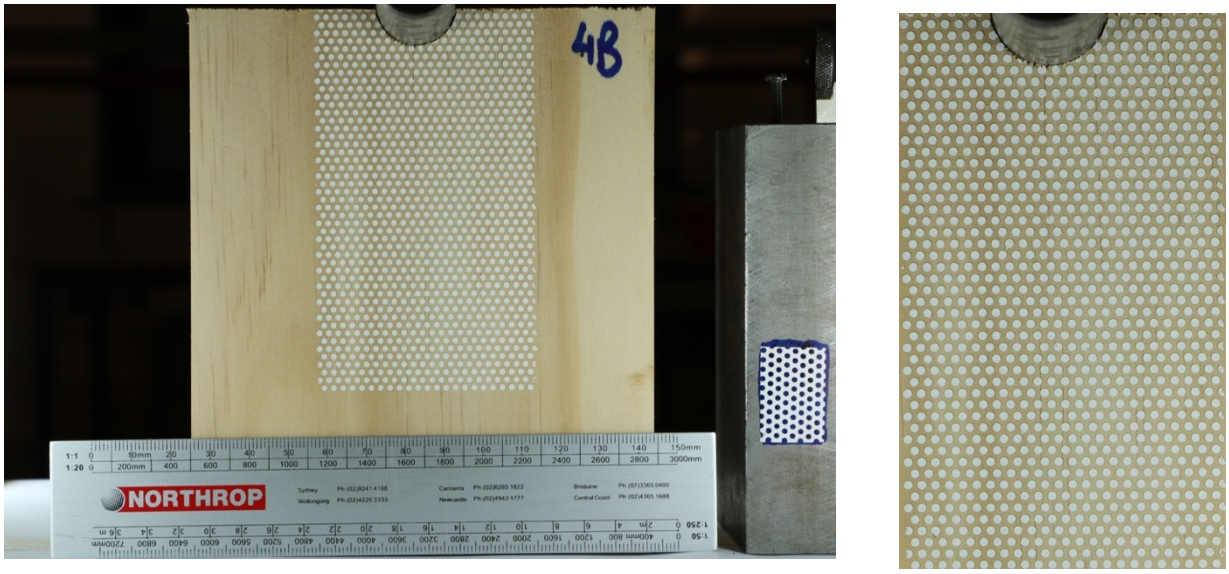

(b)

Figure 3.2 Illustration of different particle distributions. (a) A large scale structural test of a reinforced concrete shear wall. Both the main wall (left image) and the end wall (right image) have been covered in dots to enable particle tracking. The particles have been hand-drawn in a pseudo-random pattern. Courtesy of A. Niroomandi. (b). A small scale timber test measuring the resistance to crushing due to a loaded steel dowel (top of the image). The particles were applied in a regular pattern using the method described in section 3.3.3. The left image shows the full test specimen while the right is an enlarged image of the instrumented region. Courtesy of L. Ottenhaus, P. Cammock and B. McInnes.

3.1.8 Particle availability and expense

A final issue that may play a role in particle selection is the availability and/or expense of the particles. Our approach has been to seek readily available particles, or particle materials, but sometimes "more expensive is better". As an example, hollow glass

spheres, as discussed in section 3.2.2, are an ideal particle choice for internal fluid flow measurements, but they are expensive.

The key point is that you should check on availability and price before making final decisions about particle choice.

3.2 Fluid Mechanics Applications

In this discussion of particle selection in fluid mechanics applications we will focus on liquid systems, and in particular water systems, as these are the systems with which we have most experience.

Water-based particle tracking systems generally have one of three possible objectives:

- measurement of internal fluid velocities, or
- measurement of free surface fluid velocities, or
- measurement of the velocities of objects within the fluid.

Particle selection will depend on which particular objective is relevant, and each type of measurement is discussed in the following sections.

3.2.1 Internal velocities

The measurement of fluid velocities within a fluid domain is by far the most common experimental objective (Crowe et al. 2016). In two-dimensional particle tracking a two-dimensional slice of the fluid is illuminated in some fashion, and particles suspended in the fluid are used to track its motion.

It is a fair question to ask whether, in fact, small particles suspended in a fluid accurately mimic the motion of the fluid around them. In other words are the particles true surrogates for the fluid particles. The answer to this question involves two considerations:

- particle density, and,
- particle response time.

These are discussed below.

3.2.1.1 Particle density

It is technically challenging to exactly match the density of the particles with the density of the fluid – here the density that we are referring to is the mass per unit volume of the particle material. This is even more difficult if the fluid doesn't have a uniform density due to temperature variations or dissolved solute gradients. If the two densities are not the same the particles will experience either a negative or positive buoyancy force, and will move downwards or upwards relative to the fluid

surrounding them. Clearly this motion will contaminate the velocity field obtained by tracking the particles.

Provided the particles in question are very small, and the density differences are not too great, it can be assumed that the terminal velocity of such particles in the fluid is well approximated by the **Stokes' velocity**, v_s, given by

$$v_s = \frac{2}{9}\frac{\Delta\rho g R^2}{\mu} \qquad (3.1)$$

where R is the particle radius, μ is the dynamic viscosity of the fluid, g is the acceleration due to gravity and $\Delta\rho$ is the density difference between the fluid and the particles. This approximation is based on the assumption of viscous, laminar flow around a spherical particle.

An estimate of the Stokes' velocity can provide the experimenter with two important pieces of information that will assist them in determining whether a particular particle choice is appropriate.

Firstly, the Stokes' velocity allows the experimenter to estimate the time period over which the particles suspended in the fluid will settle to the bottom, or rise to the top, of the flow domain. This time period needs to be very much greater than the period of time in which the particles are under observation. That time period may not necessarily be the length of the experiment. Consider the case of an experiment in a flow-through flume where particles enter the flume fully mixed throughout the fluid depth, and stay within the camera observation window for approximately 10 seconds. A settling time of 10 minutes, say, would be satisfactory as it is long compared to the observation time of 10 seconds, even if the duration of the experiment is much longer than the settling time.

Secondly, ideally the Stokes' velocity should be orders of magnitude smaller than the typical fluid velocities. If this criterion is met the measured velocities should be an accurate representation of the fluid motion.

3.2.1.2 Particle response time

A more subtle issue is associated with how the suspended particles respond to changes in fluid motion. Unlike structural applications where the particles are literally attached to the material that they are tracking, in fluid mechanics the suspended particles move due to the forces acting upon them due to the surrounding fluid. Typically this is a drag force, generated when the fluid and the suspended particle have different velocities. Once the drag force arises the particle gradually accelerates to "catch up" with the fluid until, if the drag force acts for long enough without changing direction, the fluid and particle will have matching velocities (assuming the Stokes' velocity is negligible). But in most fluid flows, particularly turbulent ones, the fluid velocity is continually changing on some turbulent timescale. If the suspended particle cannot

adjust its motion rapidly enough it will find that it continually lags behind the fluid and the measured velocities, while plausible, will not be an accurate representation of the fluid motion.

Raffel et al. (1998) provide a crude estimate of the response time, τ_s, of a small spherical particle subject to fluid accelerations given by

$$\tau_s = \frac{2}{9}\frac{\rho R^2}{\mu} \qquad (3.2)$$

where ρ is the density of the particle and the other symbols correspond to those in equation 3.1.

3.2.1.3 Particle seeding

Internal fluid measurements generally involve the suspension of fine particles within the fluid. Introducing these particles into the fluid requires more than simply scattering the particles onto the free surface. Such an approach will result in the particles being caught in the surface film. A relatively straightforward technique is to take a small sample of the liquid, mix it with a very small amount of surfactant, and add the desired volume of particles to this mixture. Through physical stirring the majority of these particles can be mixed into the fluid, providing a highly concentrated slurry that then can be reintroduced and mixed into the experimental fluid system.

This approach works well for an experimental system that involves a fixed volume of experimental fluid, in a tank for example, or one that uses a recirculating system so that particles introduced to the system are not lost over time. If the system is open such that new liquid is continually flowing through the system – for example a flume connected to an external water supply – then a more sophisticated method for seeding the flow is required. While we have no specific experience of such systems, as even our flow-through flumes have a recirculating water supply, our experience would suggest that ideally particles would be introduced into a feeder pipe, if possible, so that they can become uniformly mixed before entering the larger system. As each system is likely to be unique it is hard to provide more specific advice.

3.2.1.4 Particle types

There are very limited options available when selecting particles for the measurement of internal fluid velocities. The reason for this lies in the constraints placed on the particles expressed in equations 3.1 and 3.2.

Particle size, light intensity and camera sensitivity play interconnected roles in determining the ease with which particles can be identified in experimental images. An ideal system will have extremely small particles, so that their Stokes' velocity and response time are both negligible, coupled with very powerful lights and a very sensitive camera. Unfortunately such systems are either very expensive or simply not achievable. For a modestly priced system, using readily available components, some

compromise is required, and almost invariably this compromise is with regard to the particle size. As the particle size increases lower light intensities are acceptable and less sensitive cameras are adequate to capture images that are susceptible to analysis. However, the choice of particle size still must consider the need for relatively small terminal velocities and relatively short response times.

We will discuss two options below.

Pliolite© resin particles:

Pliolite© resin is a rubber-like material used in a number of industrial manufacturing processes. It has a number of properties that make it ideal for particle tracking applications involving internal fluid velocities.

Firstly, the material is almost white and so reflects light effectively. Secondly the material can be ground and sieved in order to produce particle sets that have a reasonably uniform particle size – this is advantageous if the experimenter wishes to retain tight control over the Stokes' velocity and response time. Thirdly, it has a density that is only 3% greater than water. And finally it is relatively cheap.

Resin particles of this sort have been our choice for all internal velocity measurement systems, and we store a selection of particle size ranges for different experimental applications. Figure 3.3 is a typical image obtained using pliolite particles.

Table 3.1 provides a short list of Stokes' velocities and response times for resin particles of different diameter. We rarely use particles smaller than 100μm, because they are difficult to identify, or greater than 400μm, because the Stokes' velocity is too large.

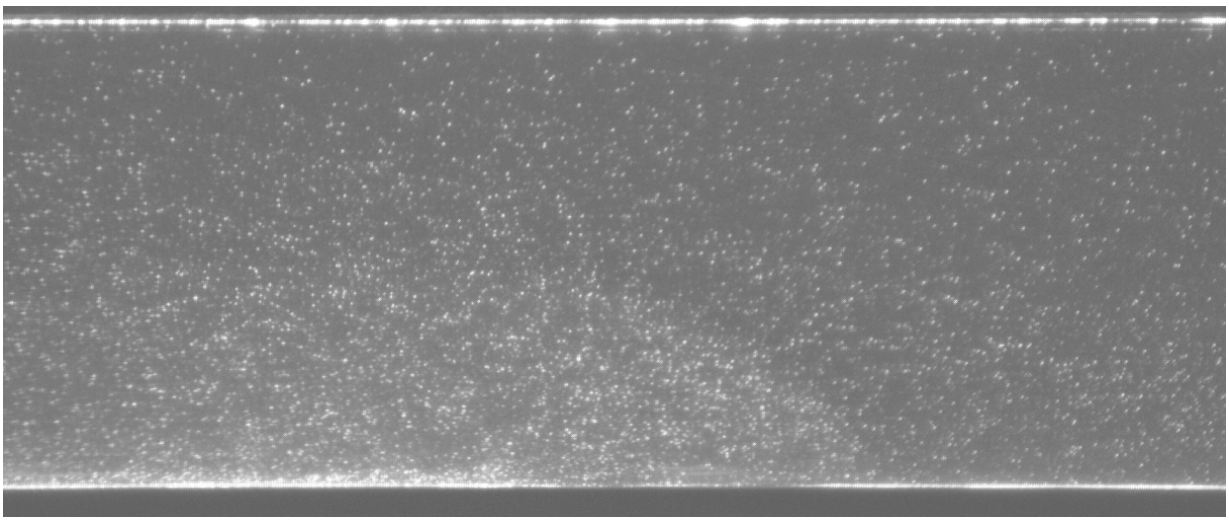

Figure 3.3. An image of Pliolite resin particles suspended in a laboratory flume in which a dense gravity current is propagating from left to right. The bright line at the top of the image is the free-surface. In this experiment the fluid depth was 20cm. The image has been artificially enhanced (all intensities have been doubled) in order to highlight the particles. In practice, due to the small particle size, the intensity of light reflected from the particles is weak and the images appear relatively dark to the naked eye.

Table 3.1 The Stokes' velocity and response time for Pliolite© resin particles of various diameters.

Particle diameter (μm)	Stokes' velocity (mm/s)	Response time (s)
50	4.1×10^{-5}	1.4×10^{-4}
100	1.6×10^{-4}	5.6×10^{-4}
150	3.7×10^{-4}	1.3×10^{-3}
200	6.5×10^{-4}	2.2×10^{-3}
250	1.0×10^{-3}	3.5×10^{-3}
300	1.5×10^{-3}	5.0×10^{-3}
350	2.0×10^{-3}	6.8×10^{-3}
400	2.6×10^{-3}	8.9×10^{-3}

Glass microspheres:

Glass microspheres are a commercial product available in a range of sizes – typically 1 to 300 microns. They have a range of industrial uses and are available in either solid or hollow versions – the latter being termed micro-balloons. The solid spheres have a density roughly 2.5 times that of water, while the density of the micro-balloons is half that of water.

Glass microspheres possess a number of advantages over resin particles. In particular, they are more uniform in size and they are very good light reflectors. However they also have the disadvantage of possessing much larger density differences with water than resin particles. While the solid spheres are reasonably priced, the micro-balloons are considerably more expensive than resin.

3.2.1.5 Refractive index matching

While not strictly a particle-related issue it is convenient at this juncture to raise the thorny issue of refractive index matching for internal fluid velocity measurement. In experimental fluid mechanics, where variations in fluid density play an important dynamical role, problems can arise due to variations in refractive index. When solutes are added to water, or water is heated or cooled, the refractive index of the water changes. If the variations in refractive index are significant enough the integrity of the measurement system can be compromised through the irregular refraction of light rays passing through the fluid. At best this leads to blurred particles. At worst it causes the apparent particle locations to be distorted.

A common solution to this problem is achieved through the introduction of another fluid component that can be employed to balance the refractive indices without compromising the difference in density. For water systems where a solute is added to increase the density – and the refractive index – an alcohol, typically ethanol, is used to increase the refractive index of the less dense fluid so that the two refractive indices match. While ethanol increases the refractive index, it decreases the density. An example of this technique is provided in case study 2 discussed in chapter 12.

3.2.2 Free surface velocities

Free surface velocities are measured by distributing buoyant particles on the free surface of the fluid. The particle density is largely irrelevant in these applications provided the particles do not sink. Likewise the response time is generally less important than it is for internal velocities as the surface tension acting on the particles located in the surface film acts in addition to any drag force exerted by the fluid, and for small particles, tends to dominate this force.

Particles that float on the free surface are sometimes referred to as **drogues**. Generally, because the water is transparent the drogues need to contrast with the tank boundaries – for example, if the internal surfaces of the tank are painted in a light colour then the drogues must be dark to ensure that that are identifiable by the particle identification algorithms.

One issue that is particularly important in particle tracking systems that use surface drogues is the effect surface tension can have on particles in close proximity. Particles at a significant distance from one another behave in an independent manner. However particles that are close together find that they are slowly drawn towards one another, even in the absence of fluid motion. The result is a clustering of particles into groups that then act as single entities and move together.

This effect may or may not have a dramatic impact on the interpretation of the particle tracking results. If the attraction velocities between particles are very small compared to the bulk fluid motion then it is likely that they can be ignored. Provided the particle clusters remain smaller than the scale of motion being measured then the presence of clusters may not be problematic. However, problems can arise if the particle clusters become so large as to affect the surface flow dynamics, or if the clusters, through the action of surface tension, become attached to flow boundaries – potentially blocking the motion of other clusters.

It must be remembered that because the motion on a free surface is entirely two dimensional – unless there are extreme conditions such as wave breaking – clusters of particles, once formed, are very difficult to break up.

In designing free surface drogue experiments the particle spatial density on the free surface is an important factor, as is the timescale of the experiments compared to the timescale of particle clustering. It is advisable to undertake preliminary experiments that explore the rate of clustering for different particle densities and to adjust the number of drogues employed based on the results of these tests. Through careful experimentation good quality data can be obtained by drogue tracking (see Nikora et al 2007), but we do advise caution.

It is probably worth mentioning here that drogue tracking is one of the few applications of particle tracking that can be used straightforwardly in the field. With the increasing use of drones it is possible to distribute floating objects on a pond, or stream, and use the camera on a drone to record the motion of the drogues. Surface tension effects tend

to be substantially reduced in these circumstances because of the increased scale in the field, including the scale of the drogues themselves. There are certainly technical challenges with such measurement systems – particularly the steadiness of the drone's recording location and orientation – but they can still provide valuable data for difficult to access field-scale flows.

3.2.2.1 Particle seeding

The introduction of drogues to a free surface is typically achieved by scattering the particles onto the free surface, much as a farmer may scatter seeds on a field. The aim is to ensure a relatively even distribution of particles and to ensure that the particles are not too close together – for the reason discussed above. The scattering process may be manual or it could be automated – the latter having the potential of achieving more even distributions of particles.

For a system where the particles remain in the system for the duration of the experiment the particle seeding is relatively straightforward and the sort of tests suggested above to determine particle clustering times and speeds are readily undertaken.

If, on the other hand, the system has a "flow through" supply of water, the scattering of the particles on the surface needs to be undertaken in a continuous fashion at, or before, the flow inlet. Again this can be done manually or through an automatic dispenser. One potential difficulty associated with this type of seeding is that the inlet may have significantly smaller spatial dimensions than the measurement region itself. For example, we have undertaken experiments in a large pond where the inlet was a relatively narrow channel. Introducing the particles in the inlet required that the particles were closer together than they were likely to be once they were distributed within the pond. Thus, for a short period of time, there was increased likelihood of clustering.

It is difficult to provide specific advice due to the variety of possible experimental configurations and differing objectives. We can only suggest that these surface measurement systems require more thought and care than systems where internal velocities are the focus. Trial experiments to test the system performance are crucial in our view.

3.2.2.2 Drogues

There are seemingly endless possibilities for the choice of a suitable surface drogue. This book started with an example of a surface flow measurement system whereby a twig or leaf was cast into a stream and its motion was observed. In this case, of course, the twig or leaf was the drogue. The only strict requirement is that the drogue must float, and that generally means the drogue is less dense than water.

Drogues can be split into two main categories.

Surface drogues:

A surface drogue is a particle, or object, that lies almost entirely in the surface layer of the fluid. Therefore its motion will provide an estimate of the surface velocity. Examples of such drogues are small polystyrene pellets (Al-Behadili et al. 2018) – although care must be taken with these considering how sensitive they can be to air movement – or small plastic beads of different sizes (Nikora et al. 2007). These objects are chosen so that their physical dimension is very much smaller than the depth of the fluid, and therefore the extent to which they penetrate the water surface is negligible compared to the water depth.

Sub-surface drogues:

Sub-surface drogues still float in the water column but they differ from surface drogues in the extent to which they penetrate the water column. For sub-surface drogues this penetration depth is not negligible compared to the water depth and therefore the drogue will sample a distribution of velocities below the surface. How it samples this velocity distribution, and therefore how the drogue velocity represents the fluid velocity, is not easily determined. Perhaps the only thing that is certain is that, if the fluid velocity is maximum at the surface, the drogue velocity will be somewhat less than that velocity due to the drag caused by the fluid below.

Sub-surface drogues must be less dense than water and have a physical shape that enables them to take a vertical orientation in the water. We have used plastic golf-tees for this purpose with the cup portion of the tee floating on the surface and the shaft of the tee pointing downwards. However these tees, if filled with water, can sink, and, if not seeded carefully, can end up lying horizontally on the surface.

3.2.3 Foreign object velocities

There are applications in which it is not the velocity of the fluid itself, but the velocity of other objects within the fluid that is of prime interest. Such applications arise in the area of sediment transport, but not exclusively so.

In sediment transport applications the sediment load is often split into two separate parts:

suspended load – particles that are within the water column and primarily move with the fluid, and,

bedload – particles that move along the bed of the channel/tank and that may spend significant portions of their time at rest within the bed.

3.2.3.1 Suspended sediment load

The measurement of the velocities of particles suspended in the water column differs little from the measurement of internal velocities described in section 3.2.1. Provided the sediment particles can be seen by light reflected from their surface, the sediment particles can be treated in the same way as artificially seeded particles with the difference that they may not possess a negligible Stokes' velocity and a negligible response time – neither of which is important in this context.

One consideration that may be important in the measurement of suspended particle motion is the volume of sediment involved. We have all seen a murky stream after a period of intense rainfall. The sediment washed into the stream is of such large volume that the water becomes opaque. Such high concentrations of sediment will preclude effective particle tracking as the light-sheet will be unable to penetrate through the water column and illumine the particles. Even if this weren't the case, in such circumstances the number of particles present would likely render the particle identification and tracking processes intractable.

3.2.3.2 Bedload

Tracking bedload sediment particles presents its own set of challenges (Campagnol et al. 2013). The first is how the sediment motion is to be recorded. Generally in these applications the sediment is viewed from above, through the free surface. Because small disturbances to the free surface can cause serious optical problems for the particle tracking system normally a lid – constructed from Perspex or glass and suspended from above - will be placed on the free surface to ensure a planar, transparent viewing window. While the presence of this lid will disturb the stream flow in the vicinity of the free surface, through the imposition of a no-slip boundary condition, it is assumed that this disturbance will not have a measurable impact on the bedload transport characteristics of the stream.

The second issue is particle identification. If the water channel has a bed lined with naturally occurring sediment, and it is the motion of this sediment that is of interest, then the identification of individual sediment particles is extremely challenging. Some mechanism is required to separate individual particles from those around them. This can be done in a number of ways. A small subset of the particles within the system can be painted a distinctive colour that contrasts with the natural colour of the particles around them. An alternative is to have the bed itself artificially constructed – perhaps through taking a mould of a naturally occurring bed and casting a new bed from plaster or cement, or through 3D printing – and painting it a uniform colour that will contrast with the sediment particles moving along the bed.

The third issue is the difficulty in tracking sediment particles from frame to frame. Unlike the velocity field of a fluid that possesses the characteristics of strong spatial and temporal continuity, the velocities of bed load particles possess neither of these attributes. Sediment particles can move and then suddenly stop for an arbitrary length of time, or, conversely, suddenly be set in motion from rest. In addition two sediment

particles very close to one another are not obliged to move in a similar way. One could be stationary while the other moves rapidly downstream. The lack of continuity in space and time severely affects the viability of the particle tracking algorithms. Therefore the more information that can help to identify individual particles the greater chance the particle tracking algorithms have in successfully tracking particles from frame to frame. Sediment particles rarely possess a regular geometry. Therefore in these applications the particle shape and orientation can provide additional particle attributes that can support the tracking algorithms.

3.3 Structural Engineering Applications

Particle selection and seeding in structural engineering applications involve completely different constraints and challenges to those faced by the experimenter in fluid mechanics. Currently all structural applications involve the measurement of surface displacement or strain fields as transparent structural materials are extremely rare. Therefore the prime focus in particle selection and seeding is ensuring that the particles faithfully replicate the motion of the material itself.

3.3.1 Stick-on particles

Stick-on particles are objects that possess an adhesive that enables them to be attached to a surface, typically through manual application. Common examples are coloured, circular, dots made of paper or plastic, with a sticky surface on one side. These can be purchased in sheets from a stationery store, and they are available in a range of sizes and colours. These dots have a number of attractive properties.

Firstly, they are completely uniform in colour and size. Therefore they will reflect light in a consistent way provided the surface is flat and the lighting system well-designed.

Secondly, they are easily attached to the surface, and, from our experience, remain robustly attached during experimental testing. However, there can be difficulties if the material fractures beneath a particle. Generally the structural integrity of the dot material is significantly greater than the strength of the adhesive. Therefore in this case the particle may either detach from the surface, or it may stay attached to one side of the fracture. Neither of these behaviours invalidates the particle tracking system but the experimenter needs to be aware that they may occur, and how they might influence their results.

Finally, the dots are readily available, cheap, require no fabrication on the part of the experimenter, and, through their range of colours and sizes, can satisfy a range of experimental needs.

Figure 3.4 illustrates the use of stick on particles in an experimental programme aimed at understanding the behaviour of post-tensioned cross-laminated timber (CLT) core walls.

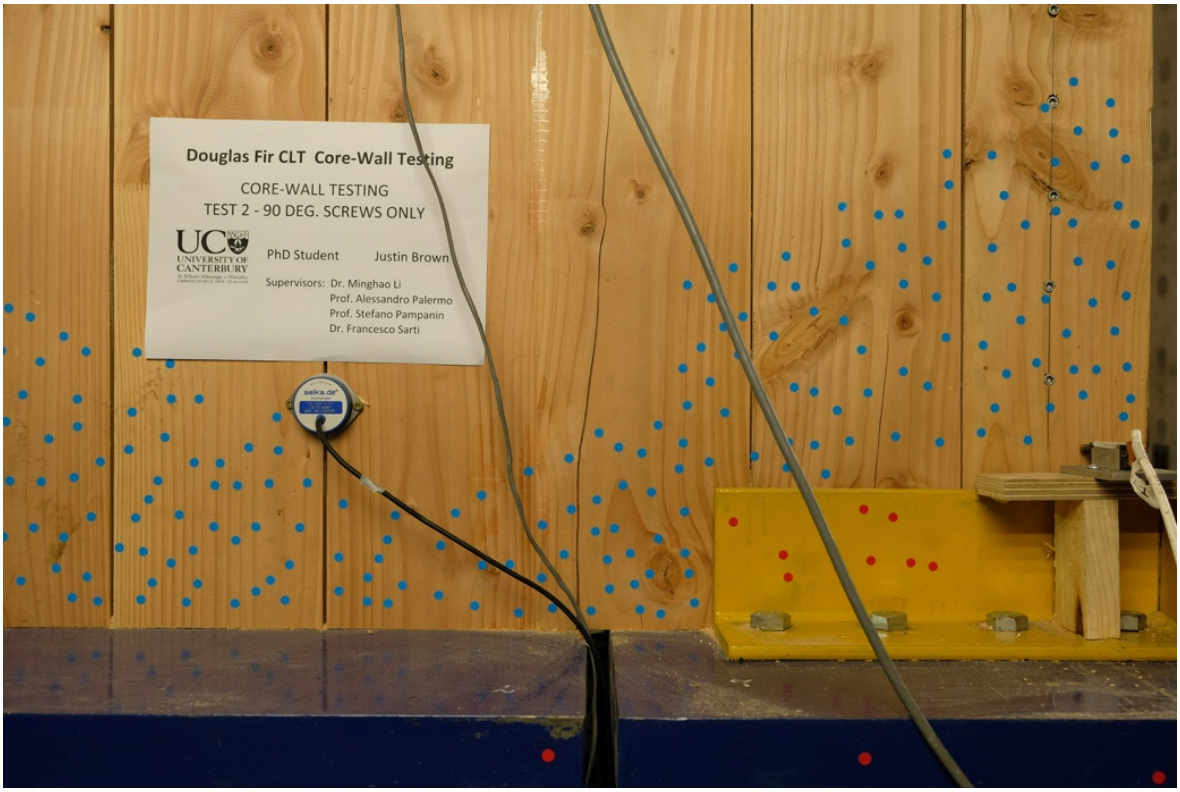

Figure 3.4. An illustration of the use of stick-on particles in the testing of a CLT core wall. The blue colour was chosen as it provided the strongest contrast to the colour of the timber – composed primarily of red and green components. The particles have been randomly located and they have been placed in regions where the most significant deformations are expected. Courtesy of J. Brown.

3.3.2 Hand-drawn particles

An alternative to the stick-on particle is the hand-drawn particle (see figure 3.2a for an example of these in practice). This is certainly the least technical solution as it requires no more than a pen, or a pot of paint and a paint brush. While this approach can lead to equivalent outcomes to the stick-on particles, there are pitfalls. Firstly, the time involved in drawing hundreds, or perhaps thousands, of particles on a surface can be significant. Secondly, it is vitally important that the hand-drawn particles possess a high degree of optical uniformity. Roughly drawn particles, perhaps caused by a desire to speed up the application process, are likely to lead to the problems described in section 3.1.5. Thus, particular care must be taken. The particles employed in case study 3 are hand-drawn and required an "army" of willing postgraduate students to speed up their application.

However, while there are certainly disadvantages in using hand-drawn particles there are also advantages.

Firstly, as has been discussed in section 3.1.4 there are advantages to the particle tracking process in having particles that possess unique characteristics, such as size. In addition different particle shapes can also enhance the tracking process by helping to

identify individual particles. Hand-drawn particles provide the experimenter with a high degree of flexibility in particle shape, particle size and, of course, particle distribution.

Secondly, the occurrence of material fracture may be handled rather more consistently with drawn particles than with stick-on particles. In the case of fracture the particle will not detach, but instead will typically split, with one part of the particle remaining on either side of the fracture line. These two particles provide very strong evidence of the crack location.

Whether the ability to produce "custom" particles through individual application outweighs the time cost, and the need for careful application that they entail, is something the experimenter must decide for themselves. Our experiences have suggested that stick-on particles are preferable for most applications.

3.3.3 Mass-drawn particles

An interesting alternative to hand-drawn particles are mass-drawn particles. These are produced through the use of a stencil or template. The stencil is a sheet of thin material with holes punched through it. Particles are applied to the material surface by placing the template on the surface and painting over the template. This process can produce a large number of particles in a short-time. We have successfully used this technique but there are a number of issues that must be considered.

Particle quality

This technique can lead to poor particle quality if not carefully implemented. This can arise in a number of ways. Firstly, if the stencil is removed before the paint is dry, or close to dry, this action can smear the paint and degrade the particle integrity. Secondly, if the stencil and surface are not in contact the paint can seep through the gap between them and cause particles to blur into one another. And, thirdly, the paint must be applied evenly to avoid the problems associated with spatial non-uniformity discussed in section 3.1.5.

Particle spatial distribution

Most commercially available stencils – we have used as a stencil the adhesive plastic sheet that can be applied to a car window to provide some level of light filtering – have holes in regular patterns. Thus the particle sets produced by this process are likely to be highly regular (see figure 3.2b for an illustration of particles generated by this method and also Ottenhaus et al. 2018). This can adversely affect the particle tracking algorithms as discussed in section 3.1.6.

One solution to this drawback is to manufacture a custom stencil that provides a pseudo-random particle distribution, and even, if desired, a range of particles sizes and shapes – although the latter is likely to make manufacturing of the template rather more challenging. The custom template would seem to offer some of the advantages of the

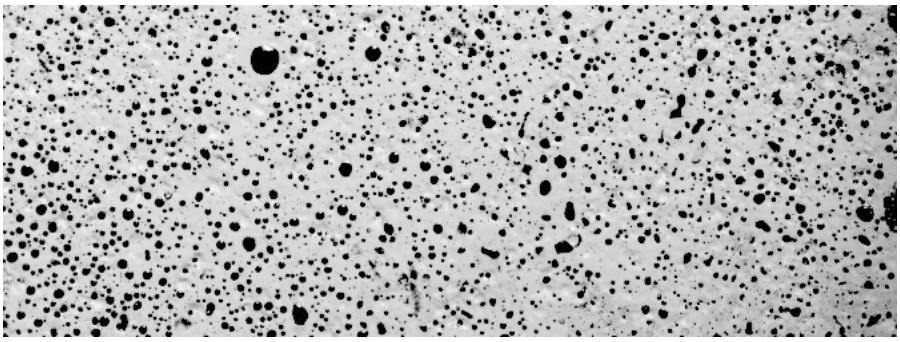

Figure 3.5. An illustration of a particle field generated by a spray technique. The high variability in particle size is worth noting along with the large variation in particle density across the sample. This image comes from an experimental study of concrete behaviour under loading courtesy of M. Serati.

hand-drawn particles without suffering the same time expense. Optical uniformity would remain an issue to be addressed.

3.3.4 Sprayed particles

Paint, or ink, sprays provide another technique that allows the economical application of a large number of particles. A very broad range of applicators can be imagined, and there is certainly scope for the development of bespoke devices. The primary challenge with using a spray is the limited control over particle size and distribution. We have very little experience with using this technique but it is likely that some degree of practice would be required by the experimenter before they were able to achieve consistent particle characteristics such as size and spatial distribution. Figure 3.5 provides an example of particles generated in this way.

3.4 Other Applications

Particle selection is highly application dependent. As has been seen in sections 3.2 and 3.3 the considerations in fluid mechanics and structural mechanics applications are very different. However, the general principles discussed in section 3.1 are applicable to all particle tracking systems and, therefore, no matter what the application area, these principles can help to guide the particle selection process.

3.5 Summary

This chapter has focussed on particle selection. A set of general considerations have been presented that can be applied to any particle tracking system. These are:

- contrast with the image background,
- material surrogacy,
- particle size,
- particle size uniformity,
- spatial optical uniformity,

- particle spatial distribution,
- seeding method, and
- availability and expense.

Specific considerations for fluid mechanics and structural engineering experiments have been discussed in some detail, and particular options for particles in these contexts are discussed within the framework of the general considerations.

4. Image Capture

4.1 Camera fundamentals

The rapid development of digital camera technology over the last few decades has opened up exciting possibilities in the domain of optical experimental systems. Particle tracking is no exception. The range of digital still and video cameras is bewildering. In addition to the cameras available in retail stores from well-known manufacturers such as Sony©, Nikon©, and Canon©, there are catalogues of specialised cameras designed for applications in science, surveillance, security, video communication and many more. Manufacturers of specialised cameras include National instruments (NI©), JAI© and Basler©. No matter what the need, there is likely to be a camera that will provide the solution.

While this book does not pretend to be a textbook on digital photography and videography, there are a number of basic concepts relevant to all cameras that need to be well understood if one is to design a successful particle tracking system. We will provide a brief summary of these concepts in this section.

4.1.1 Image sensor characteristics

A digital camera relies on a light-sensitive chip, or sensor, to record images. This sensor is generally one of two types. In the early development of digital cameras sensors were typically charge-coupled devices (**CCD**), but in recent years for many applications, such as consumer digital still and video cameras, and many specialised video cameras, these sensors have been replaced by active-pixel sensors (**CMOS**). CMOS sensors are generally cheaper to produce and require less power. To the user the sensor type is almost irrelevant, except perhaps in how it impacts on price. Certainly the development of camera technology over the last decade, including the switch from CCD to CMOS sensors, has seen a substantial decrease in camera price for cameras with similar specifications.

Whether the sensor is a CCD or CMOS chip, it can be conceived of as comprising a rectangular matrix of tiny light-sensitive elements known as **pixels**. When an image is captured, the intensity of the light incident on each pixel is recorded and stored in the image. The majority of still and video cameras, certainly those available as consumer products, record the intensities of three **colour channels** or **guns** – red, green and blue – and these colours are stored in the recorded image (how this is done is discussed below). Through the combination of these three colour intensities an enormous range of visible colours can be accurately represented. Such images are referred to as **RGB** images. Some specialised cameras, on the other hand, are designed to capture only a **monochrome**, or grayscale, image. Here the colour information is lost and only an average light intensity is recorded at each pixel.

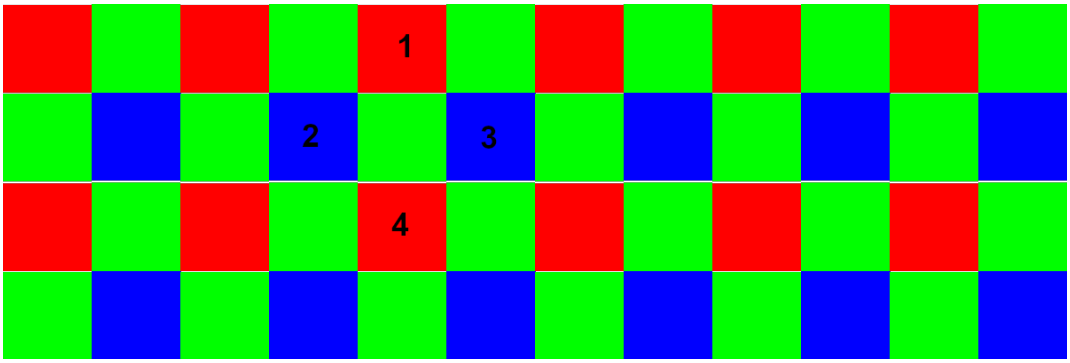

Figure 4.1. An illustration of the Bayer filter used with most single sensor, colour cameras. Each square corresponds to a pixel on the sensor. The sensor pixels are overlaid with the optical filter illustrated. The 2x2 pixel pattern is repeated across the entire sensor. Colour information that is missing at a particular pixel is interpolated using the colour information at surrounding pixels. For example, the green pixel adjacent to the pixels labelled 1-4, will record only the green intensity. The red and blue intensities at this pixel will be computed from the averages of the red intensities at pixels 1 and 4, and the average of the blue intensities at pixels 2 and 3, respectively.

A single pixel cannot record the intensity of all three colour channels simultaneously. A pixel simply counts photons incident on its surface. Therefore, to record colour images with a single sensor a more sophisticated camera design is required. An optical filter, known as a **Bayer filter**, is placed over the face of the sensor. The filter has a separate colour panel for each pixel, arranged in a repeating 2x2 matrix, as illustrated in figure 4.1. One in every four pixels records the red intensity, two in every four pixels records the green intensity, and one in every four pixels records the blue intensity. To generate a full colour image, the colour information missing at each pixel is interpolated using the colour information at surrounding pixels, as illustrated in the figure. Consumer product cameras perform this interpolation automatically so that the captured images have full colour information at each pixel. On the other hand specialised colour cameras tend to generate images that are in their raw Bayer format state, with only one colour intensity recorded at each pixel. It is the responsibility of the experimenter to undertake the colour interpolation.

A related sensor attribute is the **bit depth**. This parameter specifies the resolution of the recorded light intensity. The majority of cameras have a bit depth of 8, but specialised cameras with bit depths of 10, 12 and 16 are not uncommon. The bit depth refers to the number of bits used to represent the colour intensity as a binary number. Therefore the number of possible colour intensities that can be recorded by a colour gun is given by

$$N_{\text{col}} = 2^d \qquad (4.1)$$

where N_{col} is the number of possible colours and d is the bit depth. Thus an 8 bit colour camera can record 256 different values for each of the red, green and blue guns, resulting in a total number of different colours of 256 x 256 x 256 = 16.8 million colours. An 8 bit monochrome camera can record just 256 different light intensities.

In particle tracking applications the bit depth is generally not an important design parameter. Cameras with a bit depth of 8 are more than adequate to allow particles to be distinguished from the surrounding image background.

Perhaps the most important attribute of a camera sensor is the **pixel resolution**. This parameter specifies the number of pixels in each column and row of the pixel matrix. The resolution is stated as W x H where W is the number of pixels in each row (i.e. the number of columns) and H is the number of pixel rows. To be clear, a row of pixels is assumed to be horizontal when the camera is in its upright position.

The pixels in most sensors are square. Therefore the pixel resolution provides a direct measure of the **aspect ratio** (width : height) of the captured image.

Tables 4.1 and 4.2 provide non-exhaustive lists of pixel resolutions currently supported by consumer video cameras.

Still cameras also come in a range of pixel resolutions. At the time of writing, cameras with 24 megapixels, corresponding to a pixel resolution of 6000 x 4000, are common.

Pixel resolution has an impact on the accuracy of a PTS, as described in section 2.4, and therefore is a major consideration in any PTS design.

Table 4.1. High definition (HD) video modes. The scan type is discussed in section 4.1.2. Source https://en.wikipedia.org/wiki/High-definition_video

Video mode	Resolution (W x H)	Pixels per image	W : H	Scan type
720p	1280 x 720	921,600	16:9	Progressive
1080i	1920 x 1080	2,073,600	16:9	Interlaced
1080p	1920 x 1080	2,073,600	16:9	Progressive
1440p	2560 x 1440	3,686,400	16:9	Progressive

Table 4.2. Ultra high definition video modes. The scan type is discussed in section 4.1.2. Source https://en.wikipedia.org/wiki/High-definition_video

Video mode	Resolution (W x H)	Pixels per image	Aspect ratio	Scan type
2000	2048 x 1536	3,145,728	4:3	Progressive
2160p	3840 x 2160	8,294,400	16:9	Progressive
2540p	4520 x 2540	11,480,800	16:9	Progressive
4000p	4096 x 3072	12,583,912	4:3	Progressive
4320p	7680 x 4320	33,177,600	16:9	Progressive

4.1.2 Frame rate

Digital video cameras, and digital still cameras with a video capture capability, record images at a specified rate. This rate is known as the **frame rate** and is measured in Hz, or frames per second (fps). An internal clock on the camera manages the timing of the image capture and this timing is very accurate.

Video cameras available in retail stores will generally conform to one of two standards – phase alternate line (PAL) or national television system committee (NTSC). The first supports a frame rate of 25Hz while the second a frame rate of very close to 30Hz. Specialised video cameras support a range of frame rates that generally are not consistent with the PAL or NTSC standards. The frame rate will generally depend on the price of the camera and may involve a trade off against other camera attributes. For example, an increase in camera pixel resolution will generally lead to a decrease in frame rate, all other things being equal.

In many cases the trade-off between frame rate and pixel resolution is present on a single camera. For example, most digital still cameras provide a video capture mode that will capture high definition (HD) video, 1080p (see table 4.1), at a standard frame rate – PAL or NTSC. Sometimes this frame rate can be doubled if the user is prepared to accept a lower resolution HD format such as 720p.

Specialised cameras may offer a number of options that trade-off frame rate for pixel resolution. A concrete example will illustrate the point. The JAI BM141GE is a specialised video camera produce by JAI© Ltd. The pixel resolution is 1392 x 1040 and the frame rate is 30.12 fps. It provides a variety of "read-out modes" – image formats – as summarised in table 4.3.

Tables 4.1 and 4.2 refer to a video mode attribute called **scan type**. Two scan types exist – **progressive scan** and **interlaced scan**. The difference between the two is important. A camera operating in progressive scan mode will capture all of the pixel rows in an image at once. Thus, for a PAL camera, every 1/25th of a second all pixels will be recorded. On the other hand, a camera operating in interlaced mode will only capture every second row of pixels at one time, and it undertakes this capture at twice the frame rate. To be explicit, pixel rows 1, 3, 5 … will be captured and, for a PAL camera, 1/50th of a second later, rows 2, 4, 6 … will be captured. These two sets of pixel rows are merged and the process repeated. Thus a complete frame of pixels is still captured every 1/25th of a second.

Table 4.3. Read-out modes available for the JAI BM-141GE. Source https://www.1stvision.com/cameras/JAI/dataman/Datasheet_BM-141GE_BB-141GE.pdf

Read-out mode	Pixel resolution (W x H)	Frame rate (fps)
Full	1392 x 1040	30.12
2/3 partial scan	1392 x 694	41.05
1/2 partial scan	1392 x 520	50.06
1/4 partial scan	1392 x 260	74.57
1/8 partial scan	1392 x 130	98.73

Interlaced scanning has implications for a particle tracking system. Imagine a particle that extends vertically over 2 or more rows of pixels. Some of the pixels of this particle will be recorded at one time while the rest will be recorded at a slightly later time. If the particle is moving quite rapidly it is possible for the two sets of pixels to no longer be contiguous in the pixel map. Thus the particle identification algorithms will produce spurious particles, or miss the particle altogether. Cameras operating in interlaced mode should be avoided in any application where particle motion could lead to significant particle distortion in the image. Structural applications, that employ quasi-static loading protocols, generally do not suffer from the use of an interlaced scan camera, as they are not concerned with the dynamic movement of particles.

4.1.3 Focus

Light enters a camera, and impinges on the camera sensor, after passing through an optical device known as a **lens**. The lens comprises a set of inter-related optical components, typically made of high quality glass, that enable the light to be focussed onto the sensor. An adjustment ring on the lens allows the user to change the lens configuration until the image that appears on the sensor is sharp and without blur. This process is known as **focussing**.

Modern day still and video cameras often provide automatic focussing. Thus the camera itself adjusts the lens to ensure that the object in the centre of the image is in focus. As we will note later in this chapter, relying on automatic focussing can potentially generate errors in an experimental PTS, and should be avoided.

Consumer cameras generally come with a lens, either permanently fixed to the camera body, or potentially interchangeable with other lenses offered by the manufacturer. Specialist cameras typically only provide the camera body – a housing that contains the sensor and a number of electrical connections for external computer control. For these cameras third party lenses must be purchased to produce an operational camera. Many of these cameras support a standard lens connector known as a C-mount.

4.1.4 Aperture and shutter speed

All cameras provide the user with some level of control over the amount of light that impinges on the camera sensor. This is known as the **exposure**. It enables the user to ensure that the pixel intensities in the captured image are within a satisfactory range. If too little light hits the sensor the image will appear "under-exposed" and will likely look dark or, under extreme conditions, black. If too much light hits the sensor the image will be "over-exposed" and portions of the image will be saturated, possessing maximum intensity values, and detail within the image will be lost. Neither of these two situations are conducive to successful particle tracking as they can make particle identification difficult through poor contrast.

Two camera attributes provide control over the exposure. The first is the **iris** in the camera lens. The iris is a mechanical screen that allows the portion of the lens that admits light to the camera to be opened or closed. The size of the iris opening is

called the lens **aperture**. The aperture setting is specified by the *f* number of the lens. A small aperture corresponds to a high *f* number and a large aperture to a small *f* number. A typical lens may have an *f* number that varies between 2 and 30. It is important to note that the *f* number does not represent a linear range. The *f* number can also be used to classify the transmission capability of the optical components of the lens. A lens with a very low f number is a **high transmission lens**, letting through large amounts of light when the iris is fully open.

The second attribute that controls the light level is the **shutter speed**. The shutter is a mechanical device that opens and closes to allow light to reach the sensor. The length of time that the shutter is open, typically measured in seconds, is inversely related to the shutter speed. The longer the shutter is open the more light reaches the sensor and vice versa. Most modern day digital cameras do not actually possess a **shutter**, but instead simulate its function electronically. The shutter speed has a lower limit placed upon it by the frame rate of the camera. If a camera captures an image every T seconds, then the shutter can be open for no more than T seconds, or an image will not be complete before the next image capture is initiated.

The shutter speed and aperture, together, provide the user with two tools to control the exposure of an image. For example, the user could select a small *f* number and a fast shutter – corresponding to high levels of light being recorded for a short period of time – or, equivalently, they could select a high *f* number and a slow shutter speed – corresponding to low light levels recorded for a long period of time. Which of these, or some other combination of shutter speed and *f* number, is most suitable for a particular experiment will depend on the characteristics of the experiment itself, but generally for 2D particle tracking a small *f* number and fast shutter speed is preferable.

Both small *f* number and slow shutter speed can cause problems in a PTS. The difficulties that can arise with a slow shutter speed are readily understood. While the shutter is open light enters the camera and is recorded by the sensor. If an object is moving relatively rapidly the result of a long exposure time, or slow shutter speed, is a blurred image of the object as it moves across the image while the shutter is open. The faster the shutter speed the easier it is to "freeze" the object in the image.

The difficulty with a small *f* number is generally of less concern, hence the recommendation above that a small *f* number and fast shutter speed is preferable. To understand the impact of a small *f* number, or wide open iris, one needs to understand the concept of **depth of field**. When a camera is focussed on an object the object is said to lie in the **focal plane**. The question might be asked as to whether objects that do not lie in the focal plane will also be in focus in the image. The region in front and behind the focal plane in which objects also appear to be in focus is known as the depth of field. When the iris of the lens is wide open, in other words the *f* number is very small, this depth of field is very shallow. Objects don't need to be far from the focal plane to be out of focus. On the other hand, if the iris is reduced to almost a pin hole, the depth of field is very large and almost every object in the image is in focus.

In many two-dimensional particle tracking applications all of the particles lie in a plane that is normal to the projection direction of the camera (a line that passes along the centreline of the lens to the sensor). Thus all particles will lie in the focal plane of the camera and the impact of a small *f* number is generally not important. However it is possible to have an experimental configuration where the projection direction of the camera is not normal to the plane of the particles. This might occur in structural applications where viewing of the material surface is hindered by experimental infrastructure such as frames or rams. In this case a shallow depth of field will lead to some particles being out of focus in the captured images.

Two other factors play a key role in this balance between aperture and shutter speed. The first is the intensity of light reflected from the particles onto the sensor. The stronger the light the easier it is to have both a high *f* number and a fast shutter speed. Such high intensity light systems are typical in structural testing. However in fluid mechanics experiments, where the particles might be only tens or hundreds of microns in diameter, the light level is almost invariably very low and this juggling act takes on real significance.

The second factor is the characteristics of the sensor itself. Different sensors possess different light sensitivities, with more sensitive devices invariably costing more. Very high speed cameras are available with frame rates in the kilohertz range. In order to capture images at this frequency the sensor must be highly sensitive – or the light sources extremely bright – and this is one of the primary reasons for the high cost of such cameras. One measure of sensor sensitivity is simply the sensor's physical size. The larger the sensor, the larger is each pixel (for a given resolution), and hence the more light that is captured by each pixel. However this measure of sensitivity must be treated with caution as other factors also impact on the sensor's light sensitivity.

4.1.5 Angle of view

Most cameras today, both still and video, possess lenses that allow the user to seemingly move the objects being observed closer to, or further from, the camera. This is known as **zooming**, and the lens is referred to as a **zoom lens**. While not exactly equivalent, the effect of zooming is very similar to moving the camera closer to, or further from, its target. By zooming in the target appears larger in the recorded image, and the physical domain observed by the camera diminishes in size. Conversely zooming out results in a target with a smaller appearance in the recorded image and a physical domain that increases in size.

Figure 4.2 illustrates a camera with two different zoom settings. The **angle of view** is defined as the angle between the line of projection of the camera and the line that traces to the maximum extent of the physical domain. It is clear from the figure that the angle of view is smaller when the camera is zoomed in than when it is zoomed out. This can have important implications for a PTS.

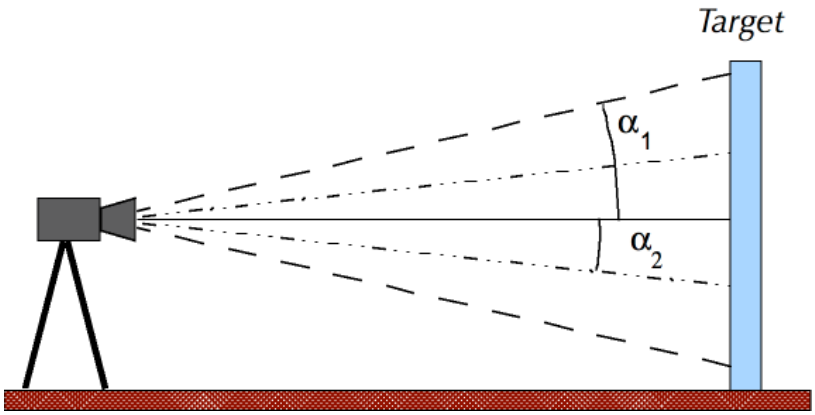

Figure 4.2. A video camera with two different zoom settings and hence different angles of view. Zoom setting 1, corresponding to an angle of view of α_1, observes more of the target with the result that the target looks smaller in the recorded images. Zoom setting 2, corresponding to an angle of view of α_2, observes less of the target with the result that the target looks larger in the recorded images.

Firstly, a wider angle of view can potentially lead to distorted images. For example, fish-eye lenses, common on cameras used for adventure photography or videography, present a highly distorted view while at the same time recording a large physical domain. This distortion is undesirable in a PTS because it makes the mapping of pixel coordinates to physical coordinates strongly non-linear. A solution to this problem is presented in the section describing camera calibration – section 4.5.

The second implication is that the focal plane referred to in the previous section is not in fact a plane. It comprises points that are equidistant from the sensor/lens. For small angles of view these points almost lie on a plane, but for large angles of view the curvature of the focal plane becomes important. Thus if the camera is recording the motion of particles on a flat surface, portions of that surface may be out of focus for large view angles if the *f* number of the lens is small.

This discussion leads to the conclusion that smaller angles of view are generally preferable and this is captured in the following rule of thumb.

Rule of thumb:

Place the camera as far from the particles as possible and use a zoom lens to define the extent of the physical domain that is to be recorded.

A related concept can also have significance for particle tracking applications. **Parallax** refers to the effect we observe when viewing two objects from different positions. Imagine two people viewed by a camera. If the camera and the two people are aligned then the camera will perceive one person standing behind the other. If the camera is now moved, while still looking towards the people, it will appear that the person at the rear has moved in the same direction as the camera. This effect, known as parallax, will cause errors if the particles being observed do not lie in a plane and it is exaggerated the larger the angle of view of the camera.

4.2 Digital still cameras

It is not our intention to describe the range of digital still cameras available on the market today. The number of manufacturers and models is extensive and modestly priced cameras with impressive specifications are readily available. All of the issues discussed in section 4.1 are relevant to still cameras and should be carefully considered both in purchasing the camera and configuring it for an experimental PTS.

However, there are additional issues that need to be considered when employing a still camera. The vast majority of these cameras are intended for non-technical applications – holiday snaps, home videos, family photographs and so on. They are also intended for use by photographers with a broad range of experience and skills. Therefore, while they provide sophisticated tools and features that will satisfy the needs of professional photographers, their default settings are generally geared towards the amateur photographer who is often most happy if they can "point and click". In other words the amateur photographer is not particularly interested in managing the balance between *f* number and shutter speed, or even in focussing the lens. Therefore these elements are typically adjusted automatically by the camera to provide the "best shot".

Such a situation is unacceptable for an experimenter wishing to obtain quantitative data from their recorded images. For example, if the camera identifies a need to adjust the focus during an experiment then the relationship between pixel coordinates and physical coordinates will change, and the crispness of the particles will be compromised. In addition, the experimenter needs to make conscious choices regarding the shutter speed and aperture settings as these can have an impact on particle blur in dynamic experiments.

Fortunately most commercially available cameras enable the user to select a manual mode where all camera settings are selected by the user and remain fixed until the user deems it necessary to adjust them. Therefore in experimental particle tracking systems manual mode should always be selected.

> *Rule of thumb:*
>
> When using a digital still camera in a PTS, ensure that the camera is set to manual mode so that all camera settings are selected by the experimenter and remain fixed throughout an experiment.

A second consideration is the power supply for the camera. Most cameras use a rechargeable battery so that the user is able to roam freely without needing access to a plug-in power supply. The battery can be recharged when the camera is not in use. The problem with a battery power supply is that the camera may choose to shut-down in order to save battery power, and, in doing so, some camera settings may be lost. Both the powering down, and the loss of camera settings, is unacceptable for an experimental system. Therefore it is essential that the camera is always powered from a mains supply in order to prevent these events from occurring. A camera that cannot

be powered from a plug-in source is unlikely to be suitable for use in an experimental PTS unless the experiment lasts for only a short period of time.

This consideration is particularly important for structural testing when the loading is quasi-static. In these cases an experiment may last for hours, or days, and shut-down is almost certain to occur if a mains power supply is not connected.

Rule of thumb:

When using a digital still camera in a PTS ensure that the camera is powered from a mains supply, and not from its battery pack, in order to prevent unexpected shut-downs.

4.3 Digital video cameras

The consumer and specialised digital video cameras discussed in section 4.1 present significantly different operational characteristics that the experimenter needs to weigh carefully when deciding on a suitable camera for their experimental needs. The most important of these is the method used for camera control. For consumer products, camera control is an integral part of the camera, provided to the user through buttons, dials and switches on the camera body and through on-screen menu options. The control of the camera is powerful, relatively intuitive, and is an intrinsic part of the camera.

On the other hand the vast majority of specialised cameras take the form of a sensor housed within a casing that boasts a number of connectors and a screw fitting in which to mount a lens. There are no buttons, dials, switches, nor on-screen menus. All camera control is orchestrated by a computer, connected to the camera by a cable attached to one of the casing connectors, and through manually adjusted focus, zoom and aperture rings on a third party lens mounted on the camera. The computer must run specialised, often bespoke, software to control the camera, and it may be necessary for the experimenter to develop this software themselves if the offerings of the camera manufacturer (typically very limited), or any third parties, are inadequate. Figure 4.3 shows a typical camera of this type.

While there have been moves to standardise the communication protocols for cameras of this sort (for example, CameraLink, GigE etc.) there are still a number of different communication standards, and even within a single standard there can be incompatibility between the implementations of the standard by different manufacturers. Therefore, the choice to adopt the use of specialised cameras, while probably desirable for many applications, needs to be made with a clear appreciation of the technical requirements involved.

Figure 4.3. An example of a specialised digital video camera. The camera comprises a plain casing, without dials and buttons. At the front a screw fitting allows a third party lens to be mounted on the camera, while a power cable and control cable plug into the rear of the casing. Source https://commons.wikimedia.org/wiki/File:Digital_video_camera.jpg.

It is worth noting that consumer video cameras can suffer the same issues regarding default/automatic settings as highlighted in the previous section. The advice furnished in that section should be followed if using video cameras of this sort.

4.4 Camera mounts

Camera mounts can be an important issue where camera vibration is a potential problem. In the majority of fluid mechanics applications the camera can be screwed to a floor-mounted tripod and, provided the tripod is not knocked or disturbed in any way, this form of mounting is entirely adequate.

However, in structural testing the physical environment itself can be prone to external vibrations. Heavy equipment, such as cranes or rams, operating during the experimental programme may generate vibrations that cause the camera mount to move. This will contaminate the measurement of particle motion as some component of that motion will be due to the camera movement. In these circumstances a tripod is wholly inadequate. Instead some type of mount, firmly fixed to the floor, and exhibiting high structural strength is a good alternative. We have fabricated mounting frames from square-section steel tubing and bolted these frames to the strong floor in our structural testing laboratory. These frames have worked well.

If the possibility of camera vibration is a concern, undertaking a simple calibration experiment is worthwhile. The camera can be mounted in an appropriate way, perhaps with custom frames as described above, and focussed on the particles on the structural specimen. The specimen can remain undisturbed while other equipment in the laboratory is activated and the camera records the particles. An analysis of the video record will provide a quantitative measure of the likely impact of camera

vibration on the measured particle motion, and the experimenter can either go forward with their experimental programme, confident that errors due to camera vibration are less than some acceptable threshold, or they can revisit and improve the design of their camera mounting system.

Another technique can be helpful in these circumstances. Particles can be attached to some surface in the laboratory which is known to undergo negligible movement even when heavy equipment is operating. If the movement of these reference particles can be recorded by the camera, along with that of the particles on the specimen itself, then that motion is due entirely to camera movement, and it can be subtracted from the motion of the particles on the specimen. Sometimes this technique is not possible because of the particular experimental arrangement, but when it is, it provides a robust mechanism for eliminating camera vibration from the record of particle motion.

The image in the left hand panel of figure 3.2 illustrates an example of such a setup. The small patch of blue dots to the right of the image are attached to a component of the testing rig. All motion of the particles attached to the timber specimen was relative to the rig. Thus any gross motion of the rig was recorded by the motion of the blue particles and this motion was subtracted from the motion of the particles painted on the timber specimen.

4.5 Camera calibration

In order to analyse experimental images the analyst must be able to convert pixel coordinates to physical coordinates. We refer to this as **camera calibration**. In the majority of cases this involves no more than recording the image of a physical scale, such as a ruler, captured by the same camera, with the same settings, used in the recording of the particle motion. A straightforward interrogation of this image enables the analyst to determine a conversion scale factor, in mm/pixel for example, that converts particle information, such as location and size, from pixel to physical units. It is worth noting that a single scale factor is sufficient if the sensor pixels are square. In some cameras this may not be the case and two scale factors, one in the horizontal, and one in the vertical, direction, are required.

Not all experimental systems can be calibrated in such a simple fashion. There are two primary reasons for why this might be the case.

- The camera lens suffers significant distortion because of its quality, or because the camera is placed close to the particles. This was discussed in section 4.1.5.
- The camera could not be positioned so that the projection direction of the camera was normal to the two-dimensional region being observed. This is most likely due to physical constraints that restrict the positioning of the camera.

A suitable calibration process for this more complex case is available. Its aim is to deduce mapping functions that will map the (x_p,y_p) pixel coordinates to (x,y) physical coordinates. To do this the experimenter overlays the measurement surface with a **calibration template**. The template consists of an array of points with accurately

known physical coordinates, and that cover the entire extent of the measurement region. The number of points depends on the accuracy of the mapping required, and the degree of non-linearity of the mapping functions. Thirty or forty calibration points would be adequate in most circumstances. An image of the template is recorded by the camera and the pixel coordinates of each calibration point are found by interrogating the image. Using an appropriate analysis tool (this can be done in *Streams*) two mapping functions are computed. These are given by

$$x = x\left(x_p, y_p\right) \tag{4.2}$$

$$y = y\left(x_p, y_p\right) \tag{4.3}$$

where x and y are the physical coordinates and x_p and y_p are pixel coordinates. The functions used in equations 4.2 and 4.3 are at the discretion of the experimenter – we typically use two dimensional polynomials of modest order, deduced from a least squares best fit based on the calibration points.

The form of calibration template employed is also at the discretion of the experimenter. We find a particularly simple, yet effective, template is a rectangular grid of lines, with accurately known spacings. The calibration points correspond to the intersection of the grid lines. An example of this approach is provided in case study 3.

4.6 Summary

A brief review of the key principles of digital photography/videography has been provided in this chapter. When designing an experimental PTS the following camera characteristics will play central roles in defining the system performance:

- sensor characteristics, and in particular, pixel resolution,
- frame rate,
- focus,
- exposure due to the lens aperture and shutter speed settings, and
- angle of view and the use of zoom lenses.

In addition, the reader has been alerted to some of the potential pitfalls that can arise through the adoption of off-the-shelf cameras or specialised video cameras.

Camera choice will be driven by the specific experimental objectives, as discussed in chapter 2, but in all cases camera operation should be guided by the recommendations furnished in this chapter.

5. Lighting Systems

5.1 General considerations

All particle tracking systems require illumination in order for the camera(s) to be able to record the particle field. A range of lighting types are available and a suitable lighting configuration will depend on the particular requirements of the measurement system being used. Even so, all lighting systems have a number of things in common and these are discussed below.

5.1.1 Light intensity

The primary requirement of any lighting system is the generation of sufficiently intense light to illuminate the particles under observation. However, it is important to recognise that this characteristic of the lighting system is intrinsically related to the choice of camera and the particles themselves. A light intensity that is insufficient for one camera may be more than sufficient for another that has a larger, or more sensitive, sensor, or for one that possesses a very high transmission lens. A light that is too weak when 100μm particles are used in a fluid mechanics experiment may be strong enough if the particle diameter is doubled. Therefore the lighting system design must go hand in hand with camera selection and the choice of particles.

It is worth noting that digital cameras are, in some ways, more sensitive than the naked eye. While a human may struggle to identify particles in a poorly lit image when it is displayed on a computer screen, image processing on the computer may still be able differentiate particles from the image background provided there is a small, yet consistent, difference in intensity. This is not a recommendation to rely on very dim particle images in experimental design, but simply an observation that the image analysis may be more successful than one might expect with apparently less than ideal images.

5.1.2 Temporal variations

Lighting systems must be able to deliver temporally invariant illumination in order for the particle identification algorithms to perform satisfactorily. Variations of light intensity can arise from a number of sources and all of these should be checked and evaluated for a new experimental setup.

It is recommended that a set of performance tests is undertaken before experiments are initiated in order to understand the temporal behaviour of the chosen lighting system. Such performance tests should involve recording the intensity of a fixed target, perhaps the particle field itself or even a simple sheet of paper, over a period of time that is at least as long as a typical experiment. The results of these tests will provide the experimenter with explicit information about the three types of temporal variation discussed in the following subsections, and once in possession of that information they

will be able to evaluate, and, if necessary, mitigate, the impact of these variations on their experimental plans.

5.1.2.1 Warm up period

Some lighting types require a warm up period during which the light intensity gradually rises until it achieves its final steady state value. This period varies with the type of lights employed and can range from seconds to minutes. Old-fashioned fluorescent light bulbs have a significant warm up period for example. A long warm up period is not, in itself, a major issue provided it is recognised and catered for in the experiment plan. Simply activating the lights well before the experimental testing starts is normally an adequate strategy for handling this matter. However, if experimental measurements are taken during the warm up period the particle identification process may be compromised because the threshold required to differentiate between background and particle pixels may be time dependent.

5.1.2.2 Lighting stability

All light sources will exhibit some temporal variability. It is intrinsic in the technology involved in the manufacture of the lights and, perhaps, in the way that they are powered. For example, lights powered by a 50Hz AC mains power supply may exhibit temporal variations associated with the varying input voltage or current. It is likely that lights will exhibit thermal noise, that manifests itself as a random intensity variation atop a steady mean signal. Measuring and isolating this noise is difficult because all camera sensors also exhibit random noise in their output signal. However, by undertaking a simple performance test whereby the light intensity at a number of fixed pixel locations is recorded and analysed, the experimenter can gain a good appreciation of the level of the combined noise generated by the camera and the lights. From an experimental design perspective the noise level must not interfere with, or degrade, the performance of the particle identification algorithms.

5.1.2.3 Long term variability

In theory, once a light source has warmed up and achieved its steady state intensity, the experimenter can rely on an unvarying mean light intensity. In practice, however, the operating characteristics of the light source may undergo long term variations. These can arise in a number of ways but most typically they are associated with a changing operating environment. As most light sources dissipate power as heat, as well as utilise the power to generate electromagnetic radiation, the light source may heat up during its operation. This temperature change may lead to slow changes in performance, and hence light intensity, with time.

5.1.3 Spatial variations

Spatial variations in light intensity can also cause serious problems in a particle tracking system. We have already commented on the impact of poor particle optical uniformity in section 3.1.5. That non-uniformity may arise from the characteristics of

the particles themselves, but it might also arise because of spatial variations in the light intensity experienced in the experimental target region. While some level of spatial non-uniformity may be mitigated by appropriate image processing techniques, such techniques may not be viable in all cases and ideally the experimenter would prefer to avoid this complication.

Spatial variations in light intensity can arise from a number of sources. These are discussed in the following sub-sections.

5.1.3.1 Shadows

Spatial variations in structural testing commonly arise from shadows cast across the test specimen by objects present within the testing environment. If the experimenter chooses to rely solely on ceiling lights to illuminate their specimen it is likely that elements of the rig, or even the specimen itself, might block direct light from the source. For example, rams or reaction frames may cause interference.

For this reason it is almost invariably wise to construct a lighting system that is specifically designed to meet the needs of a particular experimental arrangement. Such a system may include a number of light sources placed to ensure that all shadows are eliminated and the resulting light intensity is, by and large, uniform on the measurement surface.

5.1.3.2 Light source variability

The light emitted from the source itself may exhibit significant spatial variations. An extreme example is a spotlight which typically possesses a strong central core of light surrounded by a halo of rapidly decreasing intensity. Such a light source would normally be inappropriate for particle tracking applications. But this characteristic of a spotlight is inherent in all light sources even if not to the same extent. No light source is available that will distribute an entirely uniform radiance.

A typical solution to this difficulty is to construct a light source from multiple individual lights such that the combined output of this amalgamation is essentially uniform over the region in which particles are to be tracked. The design of this multi-element light source will depend on a number of factors – the size of the region being illuminated, the distance between the light source and the measurement region, and the intensity of light required in order for the tracking system to function correctly. In most practical circumstances preliminary trials with a range of lighting configurations is likely to guide the experimenter to a workable lighting solution.

5.2 Lighting types

A wide range of lighting types is currently available. Most are modestly priced and many are suitable for different particle tracking applications. We cannot provide an exhaustive survey of all lighting options, so in this section we will simply list some of the lighting types that we have successfully employed in our particle tracking systems.

The specific uses of these lights will be discussed in more detail in sections 5.3 and 5.4 where particular fluid and structural mechanics applications are presented.

We have utilised the following lighting types:

- LED lights, typically in linear arrays (see section 5.3),
- linear halogen bulbs (see section 5.3),
- fluorescent tubes or LED equivalents (see sections 5.3 and 5.4), and
- spotlights (see section 5.4).

5.3 Fluid mechanics applications

The lighting requirements for internal velocity measurements and surface velocity measurements are significantly different. We will discuss them separately in the following sections.

5.3.1 Internal velocity measurements

Internal velocity measurements present the biggest challenge for lighting design. In experiments of this nature the experimenter must generate a narrow light-sheet that enables a roughly two-dimensional slice of the flow to be isolated and interrogated. These experiments are normally undertaken in a darkroom where the only light reaching the camera originates from the light reflected from the invariably small particles suspended in the flow (see section 3.2.1). Therefore, in these experiments high intensity light sources are essential.

The requirement that the light is restricted to a narrow sheet presents certain technical challenges when considered in conjunction with the need for high intensity. We discuss a number of the issues that the experimenter will need to consider in their design.

5.3.1.1 Sheet generation

The first issue to be addressed is how to generate a sheet of light. To achieve this a beam of light that is "long" in one dimension and "short" in the normal direction must be created. We discuss each of these technical challenges in turn.

A long beam of light, of relatively uniform intensity, can be created in at least two ways. The first utilises a "long" light bulb. We have employed linear halogen bulbs for this purpose. These bulbs are very high intensity and can be tens of centimetres in length. The second approach uses a string of individual light bulbs. If these bulbs are positioned close together, and the distance between the bulbs and measurement region is very much greater than the inter-bulb separation, the light generated from such a linear array will appear approximately continuous due to the overlapping nature of the individual light beams. LED lights seem particularly well suited to this type of linear array. They are physically small and high intensity lights are available. Of course,

based on the same principle, linear halogen bulbs could also be mounted in a line to create a longer light sheet.

All lights, except lasers, generate light beams that spread significantly from their source. Therefore, with the exception of lasers, no light sources are able to generate a sheet of light with a strongly constrained width. To achieve this constraint, at least to some reasonable approximation, some type of light guide is required. Two options could be considered. In the first the light is passed through two long slits spaced some distance apart. Only light rays that pass through both slits illuminate the experimental apparatus. The greater the separation of the slots the more tightly constrained is the light-sheet. To generate a light-sheet that is approximately 1cm wide we have employed two 5mm wide slits – the first located close to a linear halogen bulb acting as the light source, and the second located approximately 30cm from the first.

The second option involves guiding the light between two parallel planes fabricated from matt black material, designed to absorb, not reflect, the light incident upon them. Thus only light rays that travel from the source without impinging upon the constraining planes will exit the space between the two planes. The longer the planes the more accurately a two-dimensional light-sheet will be produced. To generate a 1cm wide light sheet we used two planes that are 5mm apart and 50cm long.

The reader will have noted that in the examples above we have designed our light-sheet generators to produce light sheets that are approximately 1cm wide, although it is important to recognise that this light-sheet is still somewhat divergent. This width has been selected based on the requirements of our experiments. Each experimental programme will have its own characteristics that will guide the design of the light source. Two concerns need to be considered in this design. While seemingly highly desirable, for most particle tracking applications, particularly those involving turbulent flow, a very narrow light-sheet is not suitable. The reason for this is that turbulent fluctuations normal to the light-sheet, which is generally parallel to the primary direction of flow, will cause particles to move normal to the light sheet. The narrower the sheet the less time particles will spend within the sheet and therefore the less time they will be visible. The result is very short, or non-existent, particle tracks and less robust velocity data. Conversely wide sheets are also generally undesirable. A two-dimensional PTS implicitly assumes that the measurements are being taken within a region where the flow is two-dimensional. The broader the light-sheet the more this assumption is likely to be compromised. Take for example, an experiment designed to measure the centre-line velocities of a turbulent jet or plume. A broad light-sheet will ensure that, close to the source, velocities significantly off the centre-line contribute to the measured particle motion and the resulting velocity field will be contaminated by these extraneous velocities. The take-away message is that the light-sheet width needs to be carefully considered based on the peculiar requirements of each experimental programme.

An observant reader will have noticed that we have not recommended lasers as a suitable light source, despite the fact that they are commonly used in particle image

velocimetry systems. While the use of lasers is possible there are a number of reasons for our decision not to include them in this guide.

Firstly, a high-powered laser is a serious health and safety hazard. Typically experimental facilities that use such lasers are required to install elaborate safety mechanisms, such as automatic cut-out switches, to ensure the safety of the laboratory users. These requirements can be onerous.

Secondly, lasers produce a narrow beam of light that must be converted into a sheet in order to be suitable for particle tracking applications. Beam production is generally achieved via a sequence of optical elements. For example, the beam can be directed onto a rapidly rotating, multi-faceted, mirror that directs the reflected beam towards a parabolic mirror that, in turn, outputs a narrow, light-sheet. The difficulties that a narrow light-sheet poses for particle tracking have been described above. This narrowness is not a concern in PIV applications due to the different nature of the image capture. Instead of capturing single images at a fixed frame rate, PIV typically employs a camera that captures two images, temporally very close together, at each time step. These image pairs are analysed together, and particle displacements between the frames in the pair are very much shorter than those between frames from a camera capturing only single images. Thus, the issues relating to motion perpendicular to the sheet are of less importance. Supplementary optical elements would be required to produce wider light sheets, adding to an already complex, and potentially costly, optical system.

Lastly, high quality lasers are generally very expensive, and they do not fit comfortably with our philosophy of designing PT systems that are modest in price and widely available within our laboratory.

5.3.1.2 Light security

Internal velocity measurement systems are normally undertaken in a darkened room so that the only light entering the camera is that reflected from the particles. Therefore the light-sheet generator must create a light-sheet and nothing else. While the methods for creating a light-sheet discussed in the previous section do indeed use some of the light rays emanating from the light source to create a sheet of light, all other light rays must be suppressed in order not to contaminate the camera recordings. Generally this requires the light source to be encased in some housing that is entirely lightproof except for the sheet itself. In this regard the LED approach to light-sheet generation has definite advantages. These lighting elements dissipate very little power as heat and enclosing them does not present any particular challenges. On the other hand, linear halogen bulbs are high wattage and generate a great deal of heat. The housing we have used to encase these bulbs has been, of necessity, constructed from fire-proof material, and two cooling fans, designed to circulate air through the internal cavity, have been built into the sides of the housing. Even with these measures in place we try to limit the time these boxes are operating due to safety concerns.

5.3.1.3 Optical elements

The light guides discussed in section 5.3.1.1 may not be the only components required in a light-box design. Optical elements such as mirrors or lenses can also play a role, particularly with the LED arrays already described. The overwhelming demand on any light-sheet generator is to generate high intensity light. Therefore, the greater proportion of the light generated by the light source that passes through the light guide, the greater the light intensity. Some LED bulbs come mounted on an optically shaped mirror, or located behind a specifically designed lens, that causes the light emitted from the LED to exhibit a limited angle of spread. One can conceive of this as a cone of light emanating from each lighting element. The narrower the angle of spread, the narrowed the cone, and the greater the proportion of the light directed along the guide. The LED based light-sheets in our laboratory all incorporate LEDs mounted with purpose-built lenses.

5.3.1.4 Uniformity

The issue of light uniformity has been raised a number of times in the discussion of light sources. It is worth mentioning again in this context. Variability in cross-sheet light intensity will be an inherent property of all light-sheet generators. The light tends to be most intense along the centre-line of the sheet with decreasing intensity towards the edges. In general this is not particularly problematic. Particles will be harder to identify as they move towards the edges of the light-sheet until they finally disappear from view. This amounts to a rather milder form of the tracking problem, characteristic of very narrow sheets, discussed towards the conclusion of section 5.3.1.1.

Variability in along-sheet light intensity is rather more challenging. In this case particle data will vary along the measurement domain so that particle identification will not be consistent throughout the particle field, unless pre-processing of the images is undertaken. One method for mitigating this problem is to ensure that the longitudinal extent of the light-sheet is substantially greater than the actual measurement region. Thus the measurements are taken in a region where light intensity is largely uniform.

5.3.2 Surface velocity measurements

The design of light sources for drogue tracking on the free surface of water bodies is typically less complex than for internal velocity measurements. However, even here some innovation can lead to improved performance.

Drogue tracking can be undertaken in undarkened rooms using standard lights - ceiling lights for example. Provided the drogues can be clearly distinguished from the background then particle identification should be relatively straightforward. However uncontrolled lighting, such as ceiling lights, can lead to unexpected difficulties. For example, if the bottom of the tank, in which the experiments are taking place, is visible and light in colour, ceiling lights may generate drogue shadows on the tank bottom and these shadows will likely lead to the identification of bogus particles, seriously contaminating the particle record.

In the most extensive drogue study undertaken in our laboratory racks of fluorescent bulbs were mounted beneath a tank constructed from Perspex, or Plexi-glass. The experiments were conducted in a darkroom, and the small plastic drogues were backlit by the lighting arrangement such that they appeared as black shapes moving across a bright background. This configuration eliminated all stray light and precluded the presence of shadows.

Preliminary experiments should be conducted to test the lighting system before the experimental programme is started in earnest. We have frequently found unexpected optical artefacts through this process, and that has led to the modification and improvement of our lighting system.

5.4 Structural engineering applications

Lighting is often a minor part of the experimental design for structural testing. Frequently ceiling lights are adequate provided shadowing is inconsequential or manageable. The underlying considerations remain those elucidated in section 5.1.

However, the use of specialised lighting systems does carry with it some advantages. It enables more control of the light intensity and, in particular, the light uniformity. Light banks are useful in this context. These light banks are comprised of light bulbs laid out in a two-dimensional array. The result is a high intensity distributed light source that dominates diffuse natural light, or light from ceiling mounted bulbs, and enables the experimenter to fine tune the illumination of the particles on their specimen. We have commonly used racks of fluorescent bulbs, or their LED equivalents, for this purpose. It can be beneficial to use some optical material, mounted in front of the bulbs, to diffuse the light and improve its uniformity. Figure 5.1 shows an example of these racks in a structural test setting.

One problem that may arise with stick-on particles is worth mentioning in the context of lighting design. Commercially available stick-on dots are generally quite reflective. This may appear to be an advantage, but it can lead to undesirable consequences. If light from the lighting system reflects directly from the particle to the camera the reflective surface can lead to the dot appearing extremely bright in the recorded image. An analogy might be useful. Imagine the sun shining on a steel roof on a summer's day. The naked eye sees the roof clearly from the light scattered from the surface. But if the orientation of the sun and roof are such that the sun reflects directly off the roof into the eye then the intensity of light can be blinding. The situation in the laboratory is not quite so dramatic, but even so, instead of seeing a set of dots of a particular colour, some dots appear white and very bright. The experimental system illustrated in figure 3.4 suffered from this problem until the lighting system was realigned to avoid direct reflections entering the camera.

Figure 5.1. An example of light banks used for illumination in structural testing. The light banks are comprised of 8 horizontally aligned fluorescent bulbs. In some cases a diffuser screen made of 3mm thick translucent white Perspex, or Plexi-glass, is mounted in front of the bulbs to enhance the uniformity of the generated light.

5.5 Summary

A lighting system is the third key hardware component of a PTS. In this chapter we have discussed general considerations of importance in lighting system design, namely

- light intensity,
- temporal variability, and
- spatial variability

The particular attributes of lighting systems for specific experimental programmes in fluid and structural mechanics have been discussed. The light-sheets required for internal velocity field measurements pose the greatest technical challenge due to the constrained nature of the light-sheet and the need for high intensity output.

In all cases it is recommended that preliminary tests of the lighting system, in conjunction with the selected camera and particles, is undertaken to evaluate system performance. Such tests can highlight deficiencies that must be rectified before robust particle identification and tracking can be assured.

6. Experimental Design Synopsis

6.1 Key design questions

The preceding four chapters have presented detailed coverage of the primary design considerations for an operational particle tracking system. We do not intend to repeat the content of those chapters here. Instead we pose a number of questions that the designer of a particle tracking system would need to answer during the design process. The responses to these questions should guide the selection of particles, cameras and lighting, and provide confidence that all components of the system will deliver the desired performance.

Experimental objectives:

- What output fields are expected from the PTS?
- What temporal resolution is adequate for these fields?
- What demands do the experimental objectives place on the spatial resolution?
- What measurement accuracy is desired?
- What portion of the experimental domain needs to be covered by the measurement system?

Particle selection:

- How many particles must be visible in order to meet the experimental objectives?
- How should they be distributed?
- Should all particles have similar characteristics – colour, size and shape – or would variations be advantageous?
- What specific particle types will satisfy the above considerations?
- Will these particles act as surrogates for the material being observed?
- How will these particles be seeded or applied?
- Are there any special considerations that must be taken into account – matching refractive indices for example?
- Are the particles readily available and affordable?

Camera selection:

- What camera pixel resolution and viewing window size are required to meet the accuracy demands of the system?
- Given the coverage requirements and viewing window size, how many cameras must be deployed?
- If multiple cameras are to be deployed how will they be synchronised?
- Does the system require video capability?

- If video capability is required, what frame rate is needed to satisfy the temporal resolution?
- How will the camera(s) be calibrated?
- Where will the camera(s) be positioned and what implications will that have for the zoom capability of the camera lens(es)?
- Is the camera selected able to be controlled completely by the experimenter, including being permanently powered from an external power supply?
- How will the camera(s) be mounted?
- Will vibrations in the environment impact on camera performance?

Lighting selection:

- What type of lighting will be required to satisfy the experimental objectives – for example, is a light sheet required and, if so, what sheet width is suitable?
- Will the lighting system ensure clearly identifiable particles?
- Does the lighting system provide sufficiently uniform light intensity across the measurement domain?
- Are shadows of concern?
- Are the operating characteristics of the lighting system – warm up requirements, long term variability, stability – understood and suitable for the experimental requirements?

Testing

- Has the performance of the entire PTS been tested in advance of the experimental programme?
- Have the test images been analysed with the chosen software tool to ensure that particle identification is robust?

The last two questions regarding testing cannot be over-emphasised. Before any proper experimentation is undertaken the system performance must be checked, and its suitability verified. In our experience, despite the very best efforts of the system designer to consider all possible eventualities, it is only through preliminary testing that they can be confident that the system will deliver the desired results.

As a final comment it is worth reiterating that the choices of particles, camera(s) and lighting are inextricably linked. The choice of one will impact on the choice of the others, generally, by restricting the options available to the experimenter. Thus it is important to adopt a holistic approach to the system design that considers all elements concurrently.

Part 3

Particle Tracking Systems:

Analysis in Practice

7. Analysis Overview

7.1 The analysis pipeline

A general introduction to the hardware components, and experimental objectives, that underpin the implementation of a successful particle tracking system have been provided in the preceding chapters. Once suitable choices have been made regarding particles, camera(s) and a lighting system, and these various components have been successfully deployed, experimental measurements can begin.

The output of a particle tracking experiment is a sequence of images that capture the particle motion. It is the analysis of those images, the extraction of meaningful physical quantities from them, and the manipulation of those quantities, that is the focus of this chapter and the three that follow.

Let us briefly recapitulate the steps involved in a typical particle tracking analysis as previously presented in chapter 1.

1. Particles are identified in the images using a suitable particle identification algorithm (PID). Pre-processing of the images may be required in order to enhance the contrast between the particle pixels and the image background thereby assisting the effectiveness of the particle identification algorithm. Some degree of post-processing may be required if spurious particles have been incorrectly identified by the PID.
2. Particles are tracked from frame to frame, or image to image, using particle tracking algorithms. These algorithms are selected by the analyst, and generally the performance of each algorithm is determined by a set of user-defined parameters. The result is a set of particle tracks. Unless a simple scale factor that converts pixel coordinates to physical coordinates is available mapping functions, deduced from the calibration images captured in advance of an experiment, must be computed and applied to the particle pixel coordinates.
3. The field of interest is computed from the particle tracks generated in step 2. The specific process will depend on the field of interest. Eulerian and material-based fields are either directly, or indirectly, interpolated onto a regular, rectangular grid, using appropriate interpolation techniques. Lagrangian fields are extracted directly from the particle tracks. It is not uncommon to perform some type of transformation on the field data in order to convert it to a more useful form.

The subsequent chapters in Part 3 are dedicated to providing detailed, practical, guidance on how to approach the analysis of a typical particle tracking dataset. In order to do this it is most helpful if reference can be made to a specific analysis tool, and, unsurprisingly, *Streams* is chosen for this purpose. It is assumed that the reader is conversant with the key concepts of the *Streams* system, and understands the framework upon which its user interface is founded. If the user does not possess this knowledge they should take time to read the *Streams*: *System Theory and Design*

manual before embarking on the remainder of Part 3 and the case studies that follow in Part 4. While this book is most certainly not a textbook for the *Streams* software, section 7.2 does provide a brief glossary of some of the rudimental elements found within the software – elements that will be referred to extensively in the following material.

7.2 *Streams*

7.2.1 Key concepts

The *Streams* environment comprises a set of interacting **objects**, each of which corresponds to an entity, or process, that naturally arises in the analysis of particle tracking data. All of these objects are defined, or generated, by the user or through the functionality within the software. Objects provide the user with two mechanisms for interaction. Firstly, the data stored within an object is observable through one of the object's **views** – of which there may be many. Views display some aspect of the object's data and may allow the user to edit that data. Secondly, the user can access these views, and other functionality of an object, through the object's pop-up menu.

The majority of the primary entities in *Streams* support a set of **processes** – objects that act on the entity in some way through the execution of an algorithm. Processes can be strung together to create **process pipelines**, allowing multiple algorithms to act on an entity in a well-defined sequence. Processes, independent of any particular entity, known as **free processes**, are also available.

In the following sections we list a number of the core entities and processes and describe their purpose. Note that the names of all objects, views and processes that are peculiar to *Streams* will be highlighted using `courier` font.

7.2.2 Image sequence

An `image sequence` is the starting point for all particle tracking analyses. It encapsulates a sequence of frames, or images, captured by a digital camera of some sort. The creation of an `image sequence` is generally the first step that must be undertaken before the analysis process can begin.

7.2.3 Image filter

An `image filter` is an image processing algorithm that operates on an image to produce a modified image of the same size. `Filters` can be combined into pipelines in much the same way as processes, and an `image filter pipeline` is a process that can act on an `image sequence` to produce another `image sequence` containing the transformed, or filtered, images.

7.2.4 Particle identifier

A `particle identifier` (`PID`) is a process that produces a set of particles by analysing the images in an `image sequence`. It produces a `particle 2D record`.

7.2.5 Particle 2D record

A `particle 2D record` is an abstract representation of the particles identified by a `particle identifier`. It stores only their defining attributes, such as location, size and colour, not the original pixel maps from which the particles were extracted.

7.2.6 Particle filter 2D

A `particle filter` 2D is an algorithm that can be utilised to eliminate spurious particles from a `particle 2D record`. `Particle filters` are organised into pipelines that operate on `particle 2D records`.

7.2.7 Particle 2D record transform

A `particle 2D record transform` is an algorithm, applied to a `particle 2D record`, that changes the record's particle data in some way. For example a `map coordinates` transform can be used to convert pixel based particle coordinates to physical coordinates using mapping functions. `Particle 2D record transforms` are organised into pipelines.

7.2.8 PTV 2D analysis

A `PTV 2D analysis` object implements an optimisation algorithm, based on a suite of user-defined parameters, that matches particles in one frame to particles in the next in a `particle 2D record`. `PTV 2D analysis` objects are combined in pipelines.

7.2.9 Costing

A `costing` is an algorithm that computes a cost associated with matching a particular pair of particles. A cost of 0 indicates a perfect match, while an increasing cost indicates a less desirable match. Most, but not all, `costings` are designed so that the cost they compute is a non-dimensional measure that lies between 0 and 1. A `PTV analysis` object will include at least one `costing` in order for it to be able to execute its optimisation algorithm.

7.2.10 Lagrangian 2D path fields

`Lagrangian 2D path fields` are Lagrangian fields that comprise a set of particle paths derived from a `particle 2D record`. Each path corresponds to a single particle tracked for a certain period of time.

7.2.11 Lagrangian 2D path field transform

`Lagrangian 2D path field transforms` operate on `Lagrangian 2D path fields`. The effect is to transform the particle track data in some way. As for `particle 2D record transforms` `Lagrangian path field transforms` are organised into pipelines.

7.2.12 Velocity 2D field time series

A `velocity 2D field time series` encapsulates an Eulerian velocity field. Flow velocities are defined at nodes on a user-defined, rectangular grid, where the grid possesses two spatial dimensions corresponding to *x*, *y* and a temporal dimension corresponding to *t*. It is produced from a `particle 2D record`.

7.2.13 Displacement 2D field time series

A `displacement 2D field time series` is analogous to a `velocity 2D field times series` except that, in this case, the particle displacement, not the particle velocity, is interpolated onto a rectangular grid. In addition, at the discretion of the analyst, the displacement field can be Eulerian in nature or material-based – the latter being the most common. A `displacement 2D field time series` can be computed from a `particle 2D record`, or, more usually, from a `Lagrangian 2D path field`.

7.2.14 Calculators

A `calculator` is an agent that computes specific variables from a `velocity 2D field time series`, a `displacement` 2D field time series, or `Lagrangian 2D path field` – for example the `calculators` defined for a `velocity 2D field time series` include the vorticity and the turbulent kinetic energy.

7.2.15 Velocity 2D field transform

A `velocity 2D field transform` transforms the data in a `velocity 2D field time series`. These transforms are organised into pipelines.

7.2.16 Displacement 2D field transform

A `displacement 2D field transform` transforms the data in a `displacement 2D field time series`. These transforms are also organised into pipelines.

7.2.17 Fields

A `field` is an object representing a mathematical scalar or vector field having 0, 1, 2, or 3 dimensions. `Fields` are computed by `calculators`, and they correspond to the physical fields sought by the analyst. Figures 2.1, 2.2 and 2.3 provide three examples of such fields.

7.2.18 Tablets

A `tablet` is an internal analysis tool that supports a scripting language for manipulating `fields`. It also acts as a convenient repository where related `fields` can be stored together. The non-linear mapping functions that might be required to map pixel coordinates to physical coordinates (see section 4.5) can be computed within a `tablet`.

A number of the objects described in the previous sections possess the "2D" qualifier to differentiate them from their 3D equivalent. As there is no ambiguity as to which of these objects we are referring to in the text from henceforth the qualifier "2D" will be omitted.

7.3 Analysis process using *Streams*

It is worthwhile revisiting the particle tracking analysis process, and viewing its various steps through a *Streams* lens. In this way the generic steps outlined in section 7.1 can be associated with concrete *Streams'* objects and processes. Figures 7.1 and 7.2 provide diagrammatic representations of the analysis pipeline for two typical examples – a fluid mechanics experiment where the velocity field is sought (figure 7.1), and a structural test were the displacement field is sought (figure 7.2). In each case a number of sub-steps have been included to illustrate their possible appearance in the pipeline.

As always a set of image files provides the input to the analysis pipeline. Initially an `image sequence` is created from these image files.

Step 1: Particle identification

In both cases an `image filter pipeline` pre-processes the images to create a new `image sequence` that contains the filtered images. From this `image sequence` a `particle identifier` extracts the particles from each image, producing a `particle record`. In the fluid mechanical example manual tools or a `particle filter pipeline` are used to eliminate spurious particles from the `particle record,` while it is assumed that no such spurious particles are identified in the structural example. The final sub-step in the structural example applies a `mapping transform` to convert from pixel to physical coordinates. In the fluid mechanical example a simple scale factor, defined in the original image sequence, achieves the same outcome.

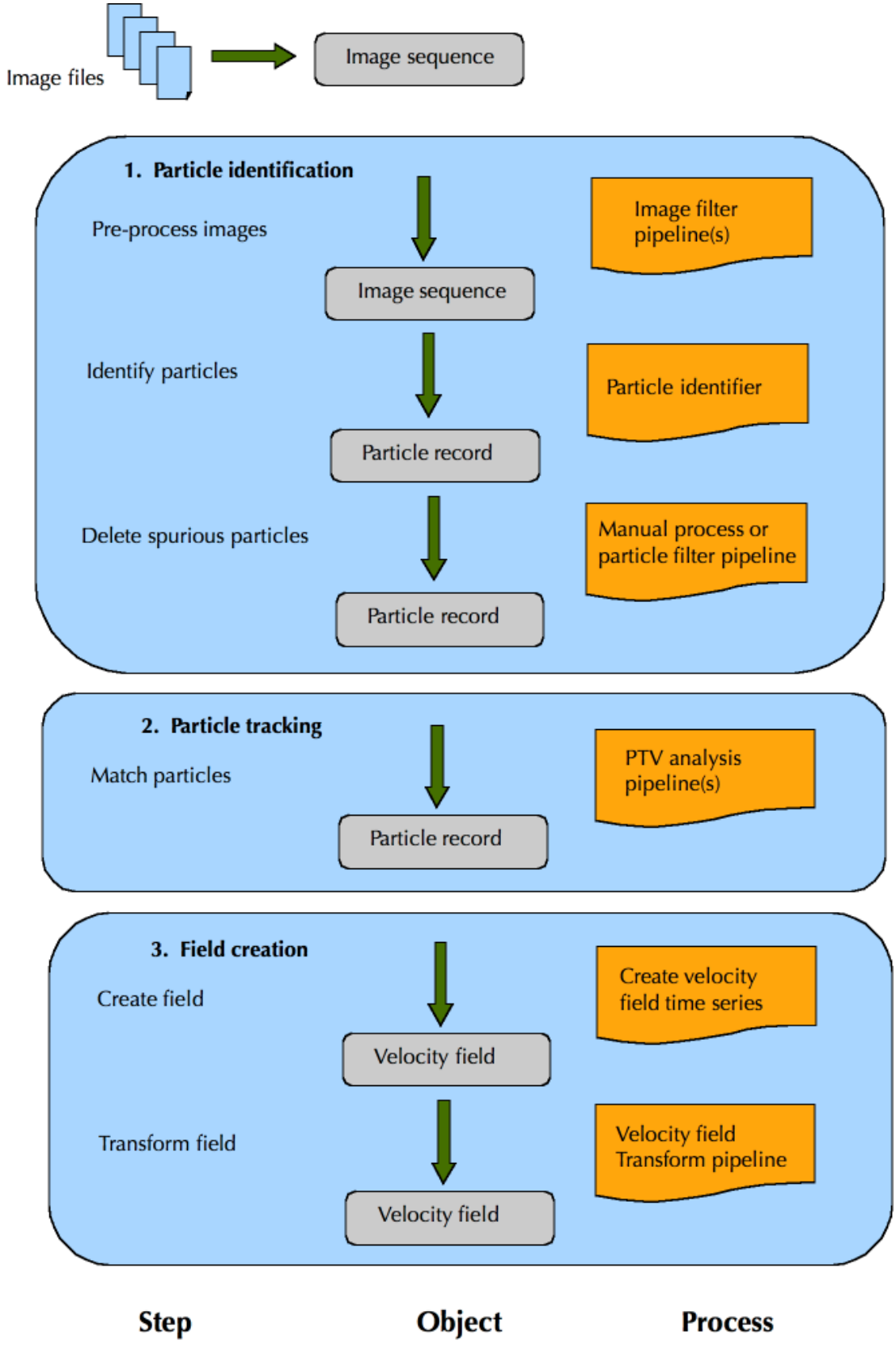

Figure 7.1. A schematic representation of the analysis process implemented in Streams. The generic sub-steps appear in the left hand column with their equivalent Streams processes appearing in the right hand column. The Streams objects that are manipulated in each step and result from the various processes appear in the centre column. The diagram illustrates the processing of a typical fluid dynamics experiment in which a `velocity field time series` *is sought.*

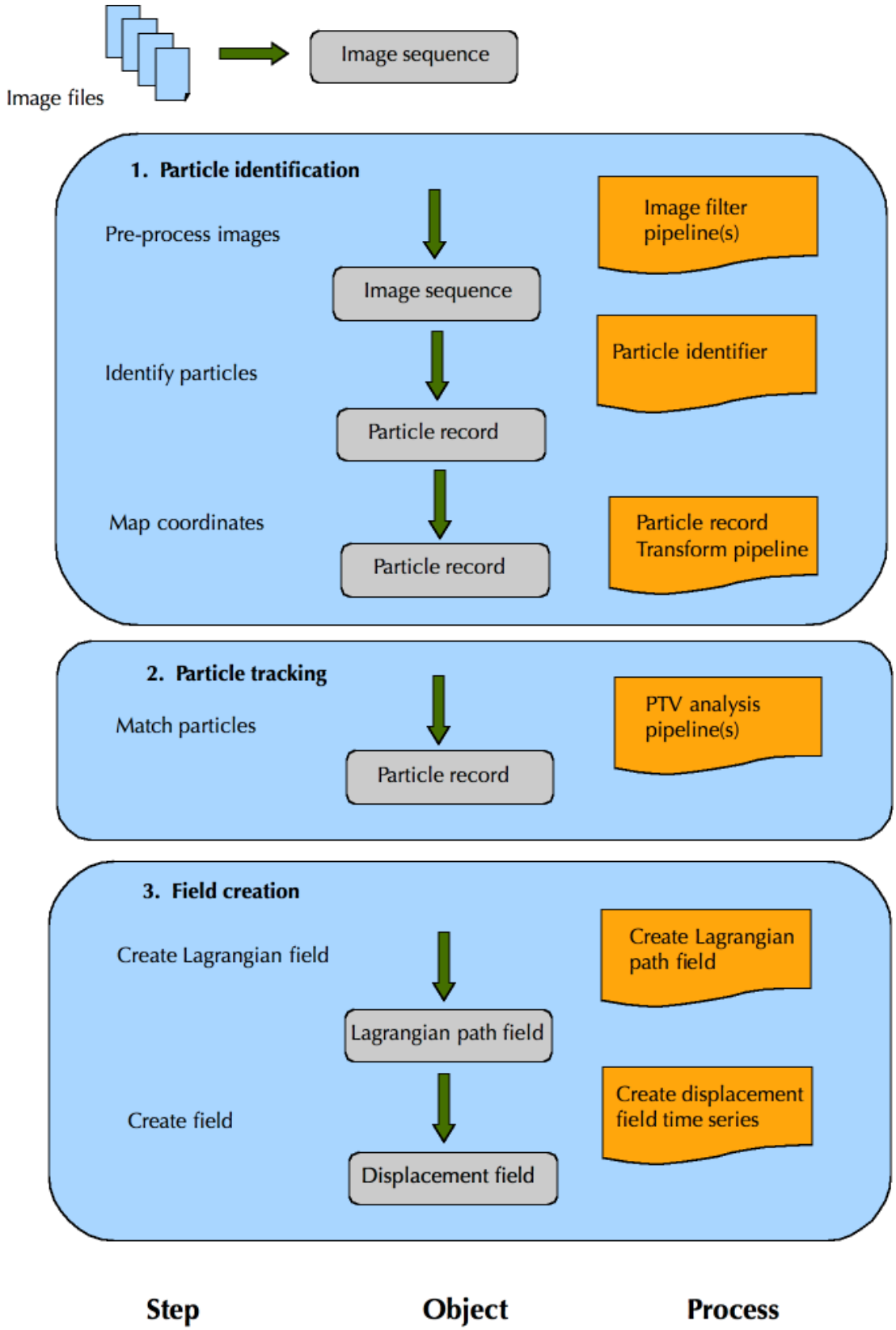

Figure 7.2. A schematic representation of the analysis process implemented in Streams. The generic sub-steps appear in the left hand column with their equivalent Streams processes appearing in the right hand column. The Streams objects that are manipulated in each step and result from the various processes appear in the centre column. The diagram illustrates the processing of a typical structural test in which a `displacement field time series` *is sought.*

Step 2: Particle tracking

A `PTV analysis pipeline` (or perhaps more than one) processes the `particle record`, output from step 1, matching particles from frame to frame. The resulting `particle record` is identical to the original except that particle matches are now stored within the record.

Step 3: Field creation

At this point the two processes slightly diverge. In the case of the fluid mechanics experiment a `create velocity field time series` process interpolates the particle velocity data in the `particle record` onto a regular, rectangular grid. The output is a `velocity field time series`. Finally, the analyst transforms the `velocity field time series` into a more convenient form, perhaps so that all variables are dimensionless, using a `velocity field transform pipeline`. The result is a new `velocity field time series` containing the transformed field information.

In the case of the structural test the desired `displacement field time series` is best computed from a `Lagrangian path field` instead of the `particle record` itself. The reason for this is that the `displacement field time series` will most likely be material-based and hence cumulative displacement information is sought. This information comes most naturally from a `Lagrangian path field` as it implicitly tracks the cumulative displacement of material particles through time. Thus a `Lagrangian path field` is generated from the `particle record` before a `create displacement field time series` process interpolates the particle displacement data from the `Lagrangian path field` onto a regular, rectangular grid. The output is a `displacement field time series`.

While this sequence of processes completes the formal analysis pipeline, in practice, this is unlikely to be the end of the analysis phase. As each experimental programme will possess its own specific set of objectives it is not possible to provide a generic statement of the activities that are likely to follow the final steps in figures 7.1 or 7.2. However, some comments may be useful. Firstly, the `velocity field time series`, or `displacement field time series`, is unlikely to be the most convenient final form of the data. The analyst will generally prefer to explore the behaviour of specific physical fields derived from the velocity, or displacement, fields – vorticity or strain for example – and then, most likely, some derived field – for example their temporal or spatial average. These physical fields can be extracted from the `velocity` or `displacement field time series` via the use of their `calculators`.

Secondly, even the `fields` computed by the `calculators` may not be the final word. The analyst may have more sophisticated manipulation of these `fields` in mind. This manipulation can be accomplished by exporting the `fields` from *Streams* for analysis in another tool, such as MATLAB©, or by utilising the in-built tools provided within a `tablet`.

7.4 Guidance roadmap

In the next three chapters we will delve into the practical details of each analysis step, and provide some general guidance on how one might approach, in a consistent manner, the analysis of an `image sequence` utilising *Streams*. This guidance will act as a framework for the analysis presented for each of the case studies. There is nothing mysterious about the advice offered here. It has been garnered through years of experience analysing image sets captured in different experimental contexts. At the core of this advice is the commitment to **quality assurance**. Whilst a number of the suggestions provided to the reader are, in some ways, superfluous to the analysis process itself, they are included to assist the analyst in gaining a more profound understanding of the data with which they are confronted. It is through this deeper knowledge of the dataset that the best analysis tools can be selected, and the greatest confidence in the reliability of the final results can be gained.

To provide some structure to this guidance we dedicate a separate chapter to each of the three analysis steps, including the sub-steps referred to previously. Thus chapter 8 explores the particle identification phase, chapter 9 the particle matching phase, and chapter 10 the field creation phase.

7.5 Summary

This chapter has provided a high level view of the particle tracking analysis pipeline, and related the steps in that pipeline to specific processes and entities within the *Streams* environment.

8. Particle identification

8.1 Overview

The purpose of the first step of the analysis pipeline is the identification of an accurate set of particles derived from the images captured by the particle tracking system. The identification process involves the interrogation of the image pixel data with the aim of detecting clusters of pixels that correspond to the images of physical particles.

Three support processes may be required to achieve this goal. The first, preceding the identification step, pre-processes the images using carefully selected image-processing algorithms. The purpose of this step is to enhance the contrast between the background and particle pixels, thus increasing the reliability of the identification algorithms. The second, subsequent to the identification step, parses the identified particles and eliminates bogus particles that have been incorrectly identified. And finally, the third transforms the particle data into a more useful form. A typical example is the application of a mapping transform that converts pixel to physical coordinates. The outcome of these steps is a set of high quality particles, a **particle record** in *Streams*, that is suitable for particle tracking.

We will describe each of these sub-steps in the order in which they are applied in the analysis pipeline, while remembering that the first, third and fourth steps may be redundant.

8.2 Pre-processing images

The first, optional, step involves pre-processing the images through the application of one or more image-processing algorithms. In *Streams*, such an algorithm is encapsulated in an `image filter`, and the entire pre-processing is implemented with one or more `image filter pipelines`. The purpose of this step is to enable the user to more clearly differentiate between the pixels that comprise the particles, and those that lie in the image background, thus facilitating the particle identification that occurs in the following step.

Streams provides a convenient tool for exploring the impact of various `image filters` on the experimental images. The `image view` of an `image sequence` displays the images through a video-player like interface. In this view the analyst can select an `image filter pipeline`, defined for that `image sequence`, in order to visualise the images that result from the application of that pipeline. Changes can be made to the `filters` within the pipeline with the effects immediately displayed on screen. It is common for the analyst to spend some time experimenting with different `filters`, and adjusting their particular parameters, in order to understand the best way to enhance their images.

Streams provides many different `filters` for manipulating images, but there are a small number specifically designed to assist the pre-processing of images obtained from a particle tracking system. We will discuss the three most useful filters below.

8.2.1 Invert filter

All of the *Streams* particle identification algorithms assume that the pixels comprising a particle have a greater "intensity" – whether that is an average intensity of all colour components or the intensity of a specific colour channel – than the surrounding pixels. Thus, if a PTS involves dark particles on a bright background (see section 5.3.2 for an example) the pixel colour intensities first must be inverted (subtracted from 255 for 8 bit RGB images) before the particle identification process can proceed. The `invert filter` performs this task.

8.2.2 Remove background filter

Even in a well-designed PTS the uniformity of light intensity can vary across the image. Consider a PTS designed to measure internal fluid velocities using a light-sheet. The images captured in such a system will show bright spots on a dark background, but the intensity of the dark background could well vary across the image. This could make the selection of a single intensity threshold for the particle identification algorithm problematic.

Ideally, the analyst would like to normalise the intensities in some way so that the pixel intensities of the background across the image are consistent. The `remove background filter` provides one mechanism for achieving this. For each pixel in the image an average background intensity is computed. A number of methods are provided to calculate this average but let us refer to just one of these in this discussion. The user specifies the size of a square region, with the pixel at its centre, that is used to compute an average pixel intensity. This intensity is then subtracted from the intensity of the pixel itself. This process works most effectively when the cluster of pixels comprising the particle is small compared to the size of the square region. In this case, while the particle pixels will contribute to the computation of the average intensity, their contribution will be small.

The effect of applying this `filter` is to reduce the intensity of the background pixels, throughout the image, to close to zero, while maintaining a measurable difference in intensity between the particle pixels and the background pixels.

8.2.3 Mathematical formula filter

The `mathematical formula filter` supports a simple mathematical script that enables the analyst to construct a mathematical expression for computing the intensity at each pixel. This mathematical expression can include not only the intensity of the three colour channels, but also the physical location of the pixel within the pixel map, and the time associated with the image in the image sequence. Therefore, in theory,

this `filter` could be utilised to adjust non-uniformity in pixel intensity in both time and space.

However, let us highlight one particular use for this `filter` that is especially valuable in structural testing where a complex image background is not uncommon. Imagine a PTS where blue stick-on particles are used to track a timber specimen. The specimen does not fill the entire image and regions incorporating a variety of colours, including white, but purposely not blue, are also present. Trying to identify particles through the use of a blue threshold intensity will produce spurious particles because white regions, and perhaps others such as those that include shades of purple, also have a high blue content. An effective mechanism for isolating the blue particles is to construct a `mathematical formula filter` that computes the difference between the blue and red intensities for each pixel. White pixels, or those exhibiting a shade of grey, for which all three colour channels have similar intensities, will appear very dark after the application of this filter, and other regions which combine all three colours will also have a significantly reduced intensity compared to the blue pixels comprising the particles. The analysis of the system illustrated in figure 3.4 used this approach, and the reader will see it employed in case study 1 and case study 3.

Another example from the structural domain will aid in underlining the flexibility of this `filter`. Consider the PTS illustrated in figure 3.2b. Here, white dots have been painted onto a timber specimen. Initial analysis of these images using the average intensity (i.e. an average of the three colour channels) in the particle identification process proved to be ineffectual because the intensity of the timber pixels was not substantially different from the intensity of some of the particle pixels. Instead a `mathematical formula filter` was employed. The natural colour of timber comprises mostly red and green – hence its yellow hue. Therefore a formula that computed the difference between the intensity of the red gun and the blue gun generated a value close to zero for the particle pixels, but a measurably non-zero value for the timber pixels. Creating a `filter pipeline` that included this `mathematical formula filter`, followed by an `invert filter`, resulted in an image with bright particles superimposed on a darker background, and this approach led to reliable particle identification.

8.3 Particle Identification

Particle identification is charged with the task of accurately extracting particle information from the experimental images. It is intrinsically linked to the image pre-processing, if used, and for that reason the two steps are often explored in tandem. The `image view` of an `image sequence` allows the user to not only observe the effect of applying a particular `image filter pipeline` to each image in the sequence, but also provides a mechanism whereby a `particle identifier` can be applied to the filtered image, with the identified particles displayed atop the filtered image. In practice, before settling on their final choice of pre-processing and particle identification algorithms, the analyst is likely to expend some effort using the tools available in this view to explore the impact on particle identification of adjusting the

`image filter pipeline` parameters together with those of the chosen `particle identifier`.

It is strongly recommended that, once the analyst has settled on what appears to be a suitable `image filter pipeline`, and a reliable `particle identifier`, they apply these to a subset of the images in the `image sequence`, thus generating a truncated `particle record`. This truncated `particle record` allows the analyst to undertake a critical quality assurance analysis before generating the complete `particle record`. The reason for working with a truncated `particle record` is perhaps not clear. Some `image filters` are computationally demanding – the `remove background filter` is a good example – and therefore, for an `image sequence` of potentially thousands of images, the processing time to identify the particles in all of the frames may be significant. As the analyst needs to be able to repeat the pre-processing and particle identification steps a number of times while they refine their analysis parameters, it is most desirable that the time required for each iteration is kept as short as possible. We would recommend 100 frames as a good compromise between efficiency and thoroughness.

8.3.1 Quality assurance measures

Before describing the particle identification process in greater detail it is worthwhile discussing some of the rules of thumb that should be applied when undertaking the quality assurance analysis referred to in section 7.4.

8.3.1.1 Variability in particle numbers:

It is generally better to identify fewer particles in an image if those particles are judged to be more reliable. This is particularly relevant to the images obtained in fluid mechanics applications where internal velocities are being measured. Figure 3.3 provides an excellent example of an image that might be recorded in an experiment of this nature. The reader will notice that the intensity of the particles varies significantly, due primarily to variations in the particle diameter, and to the fact that the light-sheet strength decays away from its centre-line. By adjusting the settings of the `particle identifier` so that the larger, clearer particles are identified, while the smaller, less clear particles are not, will result in a smaller set of particles, but a set whose particles are likely to be easier to track. A tell-tale sign that the analyst has attempted to extract too many particles from an `image sequence` is a high degree of variability in the number of particles identified in each frame. A small degree of variability is expected as particles exit and enter the camera's observation window and disappear from the light-sheet, but a variation greater than a few percent should be a cause for concern. This statistic is easily assessed in the `match summary view` of the `particle record`. This view lists the number of particles identified in each frame together with the number of matches (we will return to this second statistic in the next chapter).

This variability tends not to be a major issue for structural mechanics applications as the particles tend to remain under observation for the entire duration of the experiment. The nature of the particles, and the manner in which they are illuminated,

should ensure that the particles can be seen, and identified, in every frame. The only exceptions to this will occur if particles leave the observation window because deformations of the material become very large – perhaps indicating inappropriate camera settings – or because the material has suffered catastrophic failure.

8.3.1.2 Poor temporal coherence:

It is possible that the variability of particle numbers between frames is small and yet the quality of the particle sets is low. This can occur due to what we term poor **temporal coherence**. In order to track particles they must be observed and identified through a contiguous set of frames. For example, a particle may enter the observation window in frame 35 and exit in frame 78. Ideally this particle will be identified, and tracked, in every frame between when it enters and when it exits the field of view. However, poorly chosen particle identification parameters may result in the particle appearing and disappearing multiple times between frames 35 and 78. This will most likely occur when the particle barely satisfies the particle identification criteria. For example, if the intensity of the particle is very close to the threshold intensity, then slight variations in light intensity as the particle moves within a light-sheet, could cause the particle intensity to drop below the threshold.

In fluid mechanics applications this problem often occurs if one is careless in the selection of image pre-processing and particle identification algorithms and, if not discovered, will lead to poor particle tracking performance. However, it is relatively easily identified. The `particle view` of the `particle record` allows the analyst to display the particles from multiple frames simultaneously, somewhat like a long exposure photograph. By displaying 5-10 frames at once, and observing the particle motion through time, poor temporal coherence exhibits itself as a continual flickering of particles as they appear and disappear from the record. Ideally no such flickering will be observed, and, instead, long coherent particle tracks will be seen to move smoothly through time.

As the reader may surmise, this difficulty is primarily a concern for an experimenter undertaking internal velocity field measurements. Only through very poor analysis choices would a structural engineer discover poor temporal coherence in their `particle record`.

8.3.1.3 Spurious particles:

In most applications it is difficult to avoid the identification of bogus particles. These bogus particles can be identified as their motion (if they move at all) is not consistent with the movement of the particles surrounding them. The question is whether the presence of bogus particles degrades the quality of the `particle record` to the extent that the results from particle tracking will be untrustworthy. Tools are available within the `particle identifier` to help minimise the number of these particles that are identified in the first place, and additional tools, discussed in section 8.4, can be utilised to eliminate them once the `particle record` has been created.

In many cases spurious particles occur either outside the actual measurement domain, or on one of its boundaries. False particles of this nature are normally relatively easy to expunge from the `particle record`, and this process will be discussed in section 8.4. Consider the reinforced concrete panel experiment shown in figure 3.2a. In the right hand image it is highly likely that some portions of the image background will be evaluated by the `particle identifier` as very similar to the black dots being used as the particles. Or consider the image from the fluid mechanics experiment in figure 3.3. In this case stray reflections from the flume bed and the free surface will lead to the identification of false particles along these two surfaces. In the first example spurious particles, external to the measurement area, will be found, while in the second, these particles will appear on the boundary of the measurement region. In both cases remedial action can be taken.

The real difficulty arises when the bogus particles appear within the measurement domain itself. In this case the identification and removal of these particles becomes extremely challenging. *Streams* provides some tools to assist in this, but generally a more robust approach is to return to the image pre-processing and particle identification algorithms in order to find means by which the particles are not identified in the first place. Our general advice would be that the design of the particle tracking system may need to be revisited if the elimination of these particles cannot be achieved through the software tools available. To undertake a particle tracking analysis with randomly located, bogus particles present in the record, will almost certainly lead to invalid particle tracks, albeit potentially plausible ones.

8.3.2 Particle identification algorithms

Streams implements a number of particle identification algorithms, or `particle identifiers`. We will focus on the most generic, and commonly used, of these, while briefly mentioning the other variants at the end of this section.

8.3.2.1 Single threshold monochrome PID:

The `single threshold monochrome PID` is a generic particle identification algorithm that is suitable for almost all particle tracking applications. It is founded on the simple principle, referred to in previous sections, that pixels that comprise a particle can be identified by an intensity that exceeds some user-defined threshold. Thus the intensity threshold is a demarcation between background pixels and particle pixels. The intensity used in this calculation can be based on any of the individual colour channels, or on an average of all three.

The algorithm searches for clusters of adjacent pixels whose intensities exceed the threshold. Such clusters are identified as particles, and the particle characteristics – location, size and colour – are deduced from the properties of each pixel cluster. The aggregation of all such clusters comprises the particle set identified for one frame.

It is important to clarify how adjacency is defined in this context. Two pixels in the same row or column of a pixel map, that stand next to each other, are termed adjacent.

Two pixels whose row and column numbers both differ by one (like two touching white squares on a chessboard) are not. Thus two pixels, arranged in that manner, whose intensity exceed the threshold, would correspond to two particles.

The location, the most important of the particle's attributes, is computed from a weighted centre of mass of the pixels within the cluster, where the weighting is the intensity of the pixel. As discussed in chapter 2 this algorithm will provide particle locations accurate to better than $\pm \frac{1}{4}$ pixel. The size is computed on the assumption that the particle is circular in nature. Thus the area covered by the pixel cluster is converted into an equivalent circle with the same area, and the radius of this circle is recorded for each particle. The colour of each particle is obtained by averaging the intensity of each colour channel for all of the pixels in the cluster.

An algorithm, based purely on an intensity threshold, generally does not provide sufficient control over the particle identification process to produce reliable `particle records`. Thus, a number of additional tools are available that can be employed to identify, and eliminate, particles that are judged to be spurious. Two criteria can be used to make this judgement. Firstly, the analyst can place a lower limit and/or an upper limit on the permissible particle diameter. Any particle that does not meet these criteria will be eliminated. In the majority of particle tracking systems the particles are either the same size (for example, stick-on particles in structural mechanics) or exhibit a narrow range of sizes (for example, pliolite particles in fluid mechanics experiments, or hand-drawn particles in structural mechanics). Thus the expected range of particle diameters is constrained and the user can take advantage of this knowledge to eliminate spurious particles from the record. The specification of a lower limit on the diameter is particularly useful in excluding very small regions, sometimes comprising just a single pixel, that meet the threshold criteria, but that are clearly not valid particles.

The second criteria is based on the particle shape. The `particle identifier`, while ultimately converting each particle into an equivalent circle, actually approximates each particle as an equivalent ellipse and computes the various geometric parameters of this ellipse. From these parameters an aspect ratio – the ratio of the major and minor axes of the ellipse – is computed. The analyst may place a constraint on the upper limit of this aspect ratio to determine whether a particle is valid or not. The assumption is that all particles are circular, or close to circular, and so that a particle with an aspect ratio exceeding a particular value can be assumed to not correspond to a particle deployed in the PTS. A re-examination of figure 3.3 will identify opportunities for the utilisation of this criterion. Along the base of the flume is a long, narrow region of intense light. This cluster of pixels would meet the threshold criterion, but fail the aspect ratio criterion, if it were suitably imposed.

An additional tool is available for excluding pixel clusters from the analysis process. A set of two-dimensional regions can be specified for the `particle identifier`. Any pixel lying within one of these regions is automatically excluded from the analysis so that pixel clusters lying completely within one of these regions will not lead to an identifiable particle. The *Streams* manuals explain how these regions can be created.

Three other PIDs are available. All are variations on the **single threshold monochrome identifier** discussed above, and include the tools available for the exclusion of particles based on their diameter and aspect ratio, and their presence within excluded regions. The key difference between these identifiers is the manner in which the threshold is imposed and, perhaps, how the particle location is computed. The three PIDs are summarised briefly below.

8.3.2.2 Single threshold colour PID:

For this PID the user can specify the threshold for each of the three colour guns separately. In addition, they can specify the rule for applying these thresholds. Either a pixel must exceed all three colour thresholds, or only one of them, in order to be identified as lying within a particle.

8.3.2.3 Dual relative threshold PID:

The user specifies a peak threshold (again this can be based on any of the colour channels or an average of all three) that must be met before a particle pixel is identified. However, the pixels that comprise the particle are determined by a separate threshold, computed as a user-defined fraction of the maximum pixel intensity found. Thus, the peak threshold can be viewed as the test for the existence of a particle, while the fraction of the maximum intensity determines the extent of the pixel cluster comprising the particle. For this PID the location is simply the centre of mass of the pixels – no weights are used.

8.3.2.4 Dual threshold Gaussian PID:

This algorithm is specifically intended for use in internal fluid mechanics experiments where the particles are assumed to be small and spherical. Based on this assumption the pixel intensity near the centre of the particle is assumed to be approximately Gaussian in both the *x* and *y* directions. This PID fits Gaussian curves to the intensities of the pixels around the maximum. From these curve fits the location of the maximum of each Gaussian can be computed and the location of these maxima determine the location of the particle. The pixel cluster comprising a particle is determined in a similar way to the **dual relative threshold** PID, except in this case the second threshold is an absolute value, not a fraction of the maximum intensity. If pixels on both sides of the pixel with maximum intensity do not meet the second threshold criterion then a Gaussian curve fit is not possible, and a simple centre of mass calculation is used instead to determine the location of the particle.

8.4 Removal of spurious particles

The presence of spurious particles in a **particle record** invariably degrades the quality of the outcomes of the particle tracking process. These particles have a proclivity to cause the optimisation process to favour incorrect particle matches.

Ideally all spurious particles are eliminated from a `particle record` before particle matching is undertaken.

The `particle identifiers`, described in the previous section, provide a number of tools that can prevent the identification of invalid particles. By restricting the particle size, aspect ratio, and location the analyst has considerable control over the integrity of the identification process. However, in some circumstances spurious particles still appear in the **particle record** and *Streams* provides additional manual and automated tools that can be used to eliminate particles incorrectly identified.

The manual tools are provided within the `particle view` of a `particle record`. Within this view the analyst can create two-dimensional regions that can be used to select portions of the particle domain upon which the analyst can execute a variety of particle editing commands. The simplest command deletes all particles present within a region. If a single frame is displayed, this command will eliminate particles from that frame. If a number of frames (perhaps all of those contained in the `particle record`) are displayed then this command deletes particles within the region from all of the frames displayed. This simple command is a very effective and efficient mechanism for removing spurious particles that lie outside, or on the boundary of, the domain of interest. It is of less use when trying to edit the particles within that domain. A second command can be used to delete particles based on their defining attributes – position, size, and colour. The analyst can specify ranges for some, or all, of these attributes, and particles matching these criteria will be eliminated from the specified region.

An automated process for eliminating certain particles, utilising `particle filter pipelines`, is also provided. `Particle filters` provide an algorithmic approach to identifying erroneous particles. Currently only one `particle filter` is available. It eliminates particles that lie within user defined regions that move through space as time progresses. Details can be found in the *Streams* manuals.

As a general guide, it is preferable for spurious particles to never appear in the `particle record` through the judicious choice of parameters in the `particle identifier`. However, if such particles do appear in the record the analyst should make every effort, using the tools provided, to eliminate them before particle tracking is attempted.

8.5 Transform of particle record

A number of reasons might exist that require the transformation of a `particle record` before particle tracking commences. Such a transformation is contained within a `particle record transform pipeline` that, by definition, could contain more than one transform if so desired.

The most likely transformation to be applied is one that maps the particle coordinates from pixel to physical space. This transformation can be achieved in two ways, only one of which requires the heavy machinery of a specific transform. Often the

conversion between pixel and physical space is performed by a simple scale factor (in mm/pixel for example) extracted from a calibration image captured by the camera before experimentation is initiated. In this case this scale factor, or scale factors if the camera pixels are not square, can be specified when the original `image sequence` is created. However, in some circumstances, due to characteristics of the experimental design, this transform is not linear and a more sophisticated mapping process is required (see section 4.5). A formal transformation, based on the mapping functions described in section 4.5, is computed from camera calibration data and then applied to the `particle record` through a `map coordinates` transform contained within a `particle record transform pipeline`.

A range of other transforms are available including ones that rotate the particle field (perhaps due to a misaligned camera) or allow for, and remove, unwanted camera movement such a camera vibration. Further details can be found in the *Streams* manuals.

8.6 Summary

The *Streams*-specific tools provided for particle identification, and the supporting processes of image pre-processing, spurious particle elimination, and particle record transformation, have been revealed in this chapter. Throughout, there has been an emphasis on quality assurance, whereby the analyst seeks opportunities to check the robustness of the particle identification process, and if need be, to take steps to improve it.

On the completion of this step of the analysis pipeline the analyst should have generated a `particle record` that is free of extraneous, or erroneous, particles, and in a form ready for particle tracking to be undertaken.

9. Particle tracking

9.1 Overview

Particle tracking is the most challenging step in the analysis pipeline, and it is certainly the one that relies most profoundly on both experience of the process, and an understanding of the data being analysed. Our aim, in this chapter, and through the case studies, is to fast-track somewhat this experience for the reader by providing them with advice on how to approach the particle tracking process, and allowing them to apply that advice to the datasets offered in the case studies.

Before we begin our discussion, let us be explicit regarding what constitutes the tracking process. It is most easily described if we consider just two consecutive frames in a `particle record`. Each frame consists of a set of particles – although the number in those two sets need not be the same. The particle tracking process attempts to match particles in the first frame to those in the second, where a match between two particles is an assertion that the two particles are the same physical particle. Therefore, a perfect tracking process will correctly match every particle in the first frame that also appears in the second, will leave every particle in the first frame, that does not appear in the second, unmatched, and, similarly, will leave every particle in the second frame, that does not have an equivalent particle in the first, unmatched. Such a set of matches will provide valid estimates for the particle displacements between frames.

In general, this matching procedure amounts to an optimisation process, and *Streams* provides a number of algorithms to undertake this optimisation. At the core of these algorithms is the concept of a **cost**. As briefly described in chapter 7, a cost is a numerical value assigned to a particular match that signifies its desirability, with a cost of zero indicating a highly desirable match. The cost for a particular match is computed by one or more `costings` defined by the analyst. It should be understood that the effectiveness of the matching algorithm will be strongly dependent on wise `costing` choices.

In this chapter we will introduce a number of the important parameters that the analyst can manipulate to control the optimisation process, and describe a number of the most useful and versatile `costings` that they are likely to employ. By the conclusion of the chapter the reader should have a clear understanding of how they would confront the tracking problem when they first begin their data analysis, and how they might ultimately refine and improve that process.

9.2 Optimisation control

9.2.1 Global optimisation

The default particle tracking process implemented in *Streams*, known as global optimisation, is a variant of the well-known optimisation problem referred to as the **assignment problem** – a more complete discussion of which can be found in the *Streams: System Theory and Design* manual. In this problem the objective function, that is to be minimised through the optimisation process, is the sum of all costs associated with a particular set of matches. Thus, the algorithm iterates through different combinations of matches until an optimal set, corresponding to the least total cost, is discovered.

Unfortunately, for typical particle tracking applications involving thousands of frames, each containing thousands of particles, this algorithm can become unmanageable due to its computational demands. There are two primary reasons for this. Firstly, the simple task of computing the cost of matching every particle in the first frame to every particle in the second can lead to millions of cost calculations. Secondly, some of the cost calculations are processor intensive. The result is that the matching process for thousands of frames can take a prohibitive amount of computer time. Tools for significantly accelerating this process are required.

To ease this burden the analyst can define a `search window` that limits the particles considered as potential matches for each particle in the first frame. It is clear that a particle on one side of the measurement region is unlikely to match one on the opposite side, at least in most continuum mechanics applications, and therefore calculating the cost of such a match is a waste of computational resource. The `search window` defines a specific rectangular region within the domain, relative to the particle to be matched, in which all potential matches must lie. Particles outside this window are never considered as potential matches. With an astute use of the `search window` the number of potential matches might be reduced from thousands to just a handful, and the optimisation process significantly accelerated. The user must estimate the largest displacement any particle will likely undergo between frames, and use this estimate to deduce the appropriate size for the `search window`. It needs to be remembered that the direction of particle motion is relevant in this definition. Consider the case of a fluid mechanics experiment in a flume where the mean flow is unidirectional. In this case the `search window` will probably not include the location of the particle itself, but, instead, will be defined as a region downstream of the particle in which the particle is sure to lie in the next frame due to its motion downstream.

This search process also can be optimised. In its crudest form the optimisation process will search through the entire list of particles in the second frame looking for particles that lie within the `search window`. This search can be substantially accelerated if the particles in each frame are initially segmented. `Segmentation` divides each frame into a rectangular grid of cells and particles are allocated to the cell in which they reside. The search process need only consider a small number of cells in the

neighbourhood of a particle for which a match is being sought. `Segmentation` carries a modest demand on storage, corresponding to perhaps 20% of the memory used by the `particle record` itself, but the optimisation process may run up to two orders of magnitude more quickly depending on the number of cells in the grid and the `costings` used.

While the calculation of the cost for each particle match consumes computational resources, so does the optimisation process itself. The optimisation will be faster if the number of particles considered in the optimisation is reduced. The `search window` is one tool available to dramatically reduced the number of potential matches considered by the optimisation. A second tool is known as the `maximum matching cost` (`MMC`). As described in section 7.2.7 a cost of zero is viewed as optimal, while increasing costs are regarded as less and less desirable. The `maximum matching cost` places an upper limit on the cost of a potential match before that match is deemed unacceptable. In this way particles that lie within the `search window` may still be excluded from the optimisation process because the cost associated with their match is too high. It is important to understand the effect of manipulating the `MMC`. By reducing this parameter the analyst is putting stronger and stronger constraints on the particles in the second frame that are considered as possible matches for a particle in the first. As the cost of the correct match is rarely zero, at some point a further reduction in the `MMC` will exclude the correct particle from consideration. The following rule of thumb might be helpful:

Rule of thumb:

A reduction in the `MMC` generally causes the optimisation process to generate more accurate matches, while at the same time reducing the total number of matches produced. The analyst should aim to identify the optimal value of `MMC` whereby all, or close to all, matches are correct and the number of matches is maximised.

The optimisation algorithm, by default, begins with frames 1 and 2, generates the matches between these two frames, and then proceeds to frames 2 and 3. This continues until all frames have been included in the analysis. Under certain circumstances the optimisation process, if executed again would generate a different, hopefully improved, set of matches. The analyst has the option to demand that the optimisation process repeats a specified number of times, and, if seen as desirable, to alternate the direction in which the frames are analysed. Thus the optimisation could traverse the frames twice, once from frame 1 to frame N, and a second time from frame N to frame 1. The circumstances under which this approach might be valuable will be discussed in a later section.

Now let us consider a number of variants of the optimisation process employed by the particle tracking algorithm that could be employed as a substitute for the global optimisation.

9.2.2 Local optimisation

In the global optimisation particle matches are chosen such that the total cost of all particle matches is minimised. This optimisation by no means guarantees that each individual particle is matched to its own preferred partner in the next frame. The **local optimisation** does not consider all particles together. Instead each particle in the first frame is allocated the particle in the second frame for which the associated cost is least, provided no other particle in the first frame will generate a lower cost when matched to the same particle. Thus the particles in the two frames must see the other as its optimal match. This optimisation may lead to more robust matches but with reduced numbers when compared to the global optimisation.

9.2.3 Residual optimisation

A particle matching process will generally match some proportion of the particles whilst leaving others unmatched. The **residual optimisation** attempts to match only those particles that have been left unmatched, the residuals, while leaving the current matches untouched. This process is particularly valuable in that it allows the analyst to freeze a set of matches that they view as robust, while attempting to add to those matches.

9.2.4 Clean-up

A **clean-up** is often used as the final process in a `PTV analysis pipeline`. It can be viewed as a post-processing step that eliminates matches judged to be unsatisfactory. This process is not strictly an optimisation. Instead the costs associated with the current set of particle matches are computed, and if the cost of a particular match exceeds the `MMC` then the match is removed. No new matches are created.

As `PTV analysis` objects are typically strung together in a pipeline, it is quite possible that different `PTV analysis` objects will employ different optimisation strategies.

9.3 Costing selection and performance

The performance of each of the processes described in the previous section is heavily reliant on the analyst's choice of `costings`. The optimisation processes are generic in nature, while it is the `costings`, through their computation of the costs of particle matches, that ultimately guide the final set of particle matches. Therefore it is the choice of `costings` that is primary in determining the performance of the particle tracking process.

Streams provides an extensive set of `costings`, and it is this array of choices that can be bewildering to the novice. In this section, and those following, we will focus on the `costings` that are most effective in the majority of experimental settings, and provide insights into how these `costings` work and why they are useful.

All `costings` fall into one of two categories. The difference between these categories is important in `costing` selection. The two categories are referred to as **state-based** and **matching-based** `costings`. `Costings` in the first category rely solely on the information gathered during the particle identification phase to compute the cost. Thus, the particle's position, its size and its colour may contribute. `Costings` in the second category use current matching information in order to compute the cost. It should be clear that as no matching information is initially available, all particle tracking processes must begin with at least one state-based `costing`. Subsequent analyses in a `PTV analysis pipeline`, or in separate pipelines, can incorporate matching-based `costings`.

In the previous section the reader was alerted to the possibility that a `PTV analysis` could be instructed to execute multiple times. This option can be valuable when matching-based `costings` are used. As the cost calculations are dependent on the current particle matches, each iteration of the optimisation process will lead to changes in the matches. Thus, the final particle matches rendered after a single iteration will differ from those resulting from multiple iterations. The same is not true of analyses based solely on state-based `costings`. As the particle matches, in this case, do not influence the cost calculations the final particle matches will be independent of the number of iterations.

Each `PTV analysis` object can contain one or more `costings`. Our preference is normally to utilise only one `costing` in each analysis and to include multiple analysis objects, each with different `costings`, in the `PTV analysis pipeline`. This allows a more precise strategy to be devised for each analysis. However, if multiple `costings` are incorporated into one `PTV analysis` object the analyst can select weighting factors that specify the contribution each `costing` makes to the total cost of a match.

The analyst needs a set of versatile and powerful `costings` at their disposal when constructing an effective particle tracking algorithm. We will now introduce four `costings`, that, from our experience, perform well in nearly every particle tracking application. There are other `costings` within *Streams* that have occasional usefulness, but we will leave it to the reader to discover those for themselves by studying the manuals. Note that not every parameter that is at the analyst's disposal for each of these `costings` will be described here. We will focus on the parameters that are of primary importance and will leave the purpose of the other parameters to be gleaned from the manuals.

Two of these `costings` are state-based and two are matching-based. Three of them are based on a similar principle that is worth elucidating before the specific `costing` details are introduced. Ideally the analyst would like to be able to predict where a particle will be in the next frame, and then search for the particle that is closest to that predicted location. Imagine a laminar fluid flow where the flow velocity is everywhere 10 mm/s in the positive *x* direction. If frames are captured at 10Hz, then each particle will move 1mm to the right in each frame. Therefore the best match would be the

particle in the second frame that is closest to this 1mm offset. In a perfect PTS, where particle locations are perfectly computed, and where particles are always present in the `particle record`, there will always be a particle located exactly where it is predicted to be. Therefore the logical algorithm for computing the cost for each match is to first compute the predicted position of the particle in the next frame, and then use the distance from a prospective match to that position as the cost. This approach, that we term **predict and test**, is common to the `distance costing`, the `local velocity costing` and the `recent velocity costing`. Where they differ is in the method used to predict the particle's location in the following frame.

If p_1 in frame 1 is matched to p_2 in frame 2, then the cost for a `costing` based on the predict and test strategy is given by

$$C = \frac{\left|\mathbf{r}_{pred} - \mathbf{r}_{p2}\right|}{l_{norm}} \tag{9.1}$$

where

C – the cost of matching particles p_1 and p_2.
$\mathbf{r}_{\text{pred}}$ – the predicted position of p_1 in frame 2.
$\mathbf{r}_{\text{p2}}$ – the position of p_2.
l_{norm} – a normalisation length, used to ensure that the cost is dimensionless.

9.3.1 Distance costing

The `distance costing` is one of the simplest state-based `costings`, but one that is remarkedly effective under certain conditions. It adopts the predict and test strategy in its crudest form. It predicts that a particle doesn't move between frames. For this costing the predicted position in equation 9.1 is given by

$$\mathbf{r}_{pred} = \mathbf{r}_{p1} \tag{9.2}$$

where

$\mathbf{r}_{\text{p1}}$ – the position of p_1.

The normalisation length in equation 9.1 is set by the analyst. It is typically related to the size of the `search window`, such that a match to a particle at the extreme limits of the `search window` yields a cost of 1.

For a stationary fluid, or a non-deforming solid, the cost for each correct match will be zero, or close to it, and the `costing` will perform extremely well. While this might seem rather restrictive the `distance costing` also performs well in less constrained circumstances. Its performance is well predicted by a simple ratio of two length scales – the particle displacement and the inter-particle separation. When this ratio is very much less than one, the `distance costing` works well. As the ratio approaches one and exceeds it, its performance degrades badly and it becomes a poor choice. The rational for this performance trait is straightforward. When a particle

moves a distance that is much smaller than the distance to the next particle, the particle in the second frame closest to a particle's original location will be the particle itself. Other particles are, by definition, more distant. In this case the calculated cost for the correct match will not be zero, but it will be the smallest value, and hence this match will be selected by the optimisation algorithm.

Streams actually provides a simple extension to this algorithm by enabling the user to specify a theoretical velocity field that can be used to predict the particle's location in the next frame (this is couched in terms of velocity because of the fluid mechanical origins of *Streams*). The theoretical velocity is expressed through two mathematical formulae, one for each velocity component. In practice, this extension is of limited use unless the analyst already has clear insights into the nature of the fluid motion.

9.3.2 Pseudo-correlation costing

The `pseudo-correlation costing` is the only `costing` discussed here that does not adopt the predict and test scheme. It is a state-based `costing` that utilises particle patterns to predict correct particle matches – in other words it uses particles other than those being matched in its cost calculations. The `pseudo-correlation costing` is closely related to two other costings provided within *Streams*, the `correlation costing` and the `adjacency costing`. All three are based on the same general principle, and they have much in common with the correlation-based analysis used in particle image velocimetry (PIV).

Let us return to our initial description of particle tracking given in chapter 1. Particle tracking requires some characteristic of a particle that uniquely identifies it from amongst its peers. Colour, size and location are all examples of characteristics that can be used for this purpose, and the `distance costing` can be viewed in that way – it uses the particle location as the distinguishing characteristic. Two particles at the same location are deemed to be the same particle. Unfortunately none of these simple characteristics is a universally reliable predictor of particle identity. One of the most powerful characteristics available to the analyst goes beyond the individual particle and involves the pattern of particles surrounding it. If the particles have been distributed in a random fashion (which is almost always the case for fluid mechanics experiments) then the pattern of particles in any rectangular region of the flow should be unique. As these particles move, provided the assumed continuum nature of the material is valid, this particle pattern should retain its structure, at least for short periods of time, and its degradation should be smooth not abrupt. Therefore, it can be argued that two particles in consecutive frames are the same particle if the patterns of particles surrounding them are the same or, at least, very similar.

The computation of a cost based on such a premise is most easily explained using the `correlation costing`. The pattern of particles in a rectangular window, centred on the particle of interest, is overlaid with the pattern surrounding a particle in the next frame. Imagine this as a pixel map, as in the original image, where pixels comprising a particle have the intensity of the particle and all other pixels have an intensity of zero. The correlation is computed by multiplying together the intensities in the two overlain

pixel maps - pixel by pixel – and summing them. The resulting correlation calculation is then normalised by the square root of the product of the two self-correlations. If the two particle patterns are identical the result of this calculation is one, while if the two particle patterns are totally uncorrelated – in other words no particles in the two patterns overlap – the result is zero. This correlation is converted to a cost by subtracting it from one, in order to ensure a perfect match has a cost of zero.

This pure correlation computation is computationally rather expensive. In order to mimic this behaviour at significantly less computational cost, the `pseudo-correlation costing` has been developed. While this `costing` is somewhat different in its mechanics its ultimate purpose is the same.

The `pseudo-correlation costing` proceeds as follows: The particles present in a rectangular window surrounding particle p_1 in the first frame, and particle p_2 in the second frame, are found. For each particle in the set of particles surrounding p_1 the particle closest to it – its **adjacent** particle – in the set surrounding p_2 is found. This adjacent particle is assumed to be the corresponding particle in the pattern in the neighbourhood of p_2. Figure 9.1 illustrates this idea. The cost is then computed as follows

$$C = \frac{1}{W}\sum_{i=1}^{n} w_i \frac{\min\left\{d_i, r_i + r^a{}_i\right\}}{r_i + r^a{}_i} \qquad \text{where} \quad W = \sum_{i=1}^{n} w_i \qquad (9.3)$$

where

- C – the cost of matching particles p_1 and p_2.
- n – the number of particles in the window surrounding p_1.
- r_i – the radius of the i^{th} particle in the set of particles surrounding p_1.
- $r^a{}_i$ – the radius of the adjacent particle to the i^{th} particle.
- d_i – the distance between the centre of the i^{th} particle in the set of particles surrounding p_1 and the centre of its adjacent particle. This distance is computed based on the premise that all frame 1 particles have been translated so that p_1 lies atop p_2 in the second frame.
- w_i – the weight of the i^{th} particle's contribution to the cost based on its distance from p_1.
- W – the sum of the weights.

It is important to note that the two particle sets may not contain the same number of particles. Therefore, under certain conditions, two particles in the window surrounding p1 may have the same adjacent particle in the second frame. The analyst is at liberty to decide whether this duplication is allowed. If not then some particles in the first frame window may not have adjacent particles, and therefore they do not contribute to the computation of the cost.

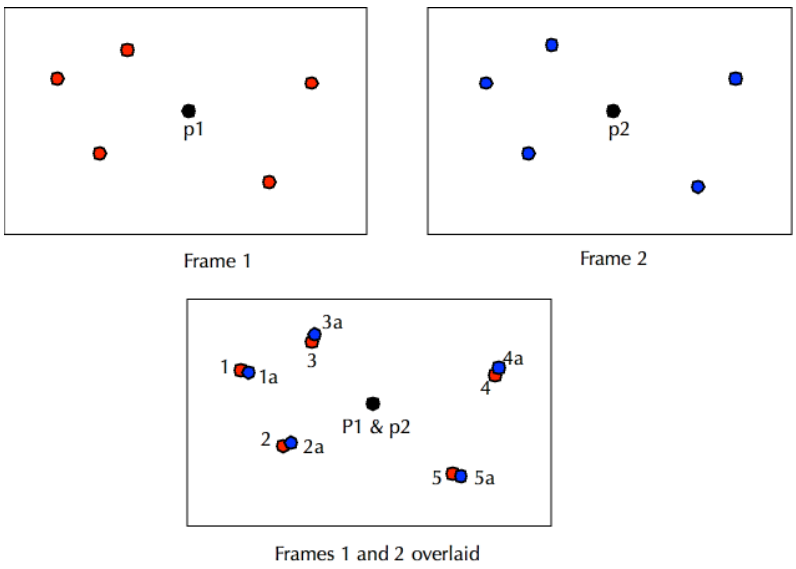

Figure 9.1. A schematic illustrating the pseudo-correlation costing algorithm. The match between particle p_1 in frame 1 (top left panel) and particle p_2 in frame 2 (top right panel) is being computed. A rectangular window is drawn around each particle with the particle at its centre. All particles within the windows are identified. The two windows are overlaid (bottom panel) such that p_1 lies atop p_2. For each particle in frame 1 (labelled 1, 2, 3 etc.) the nearest particle in frame 2 (labelled 1a, 2a, 3a etc.) is identified. The cost depends of the distance between the centres of each pair of particles according to equation 9.3. The closer the centres the lower the cost, thus indicating a strong correlation in the particle patterns in the two frames.

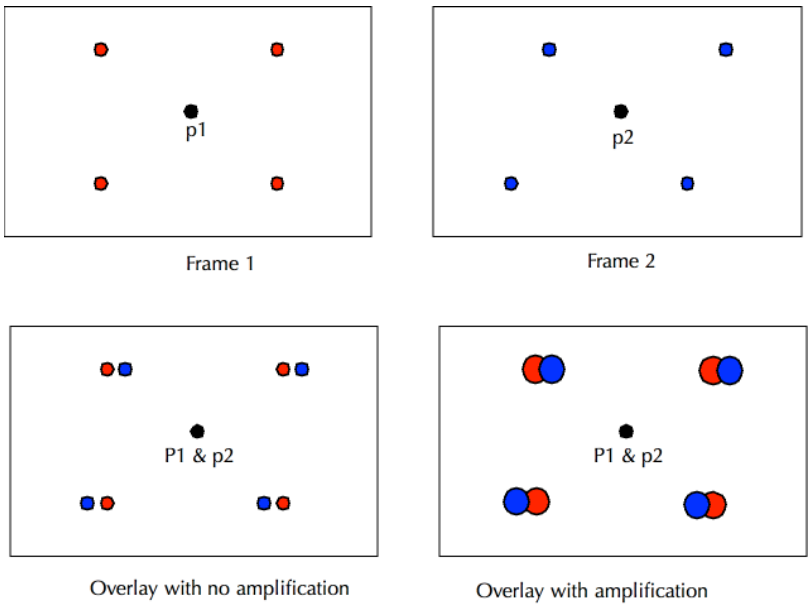

Figure 9.2. A schematic illustrating the impact of employing radii amplification in the pseudo-correlation costing algorithm. The material is suffering vertical shear such that particles above p_1 in frame 1 move further than p_1 while those below move less far. For fine particles this shear causes the correlation between the two particle patterns to disappear, as illustrated in the bottom left panel, even though p_1 and p_2 are, in fact, the same particle. If the particle radii are amplified, as illustrated in the bottom right panel, the correlation between the two patterns is recovered to some extent.

In this `costing` the distance between the centres of adjacent particles is used as a surrogate for the correlation between the two particles. If the particles lie atop one another their contribution to the cost will be zero. As they get further apart their contribution to the cost increases, until finally, when they are separated by the sum of their radii– in other words they are just touching – their contribution is 1.

The performance of this `costing` can be enhanced through an artificial amplification of the particle radii. Imagine the use of fine particles, as typically encountered in an internal fluid mechanics PTS. In a region of vertical shear a particle above or below p_1 will move a different distance than p_1 itself, as the particle pattern will be sheared by the fluid motion. If this shear is strong enough it is possible that many of particles surrounding p_1 will contribute the maximum amount to the cost calculation as they do not overlap with their adjacent particles in the second frame. By amplifying the radii the impact of this shear is reduced and the correlation between the patterns is somewhat re-established. This effect is illustrated in figure 9.2.

9.3.3 Local velocity costing

The `local velocity costing` is a matching-based `costing` that also employs the predict and test strategy. The reason that this `costing` is so effective, and it is one that is almost invariably employed in our work, is that it takes a sophisticated and robust approach to the prediction step. It is based on the following assumptions:

- particle matches have been generated using previous analysis objects,
- the matches are, in general, of good quality, and
- the particle motion in the vicinity of each particle is consistent with the continuum assumption such that gradients in displacement and velocity are smooth.

Under these assumptions, as for the correlation-based `costings`, it can be anticipated that the motions of particles in a small region will be similar to one another. Thus, if particles in the same locality as the particle under consideration have matches, and these matches are generally correct, then these matches can be used to predict where the particle itself should be located in the next frame. See figure 9.3.

The `local velocity costing` uses the matches of particles located within a rectangular window, centred on a particle, to predict the location of that particle in the next frame. The calculation of the particle's predicted position is weighted by the distance between the particle and the particle whose match is being incorporated into the calculation. Thus the motion of particles that are closer to the particle of interest are weighted more heavily than those further away.

For this costing the normalisation length in equation 9.1 is given by

$$l_{norm} = \max\left\{\left|\mathbf{r}_{pred} - \mathbf{r}_{p1}\right|, l_{def}\right\} \tag{9.4}$$

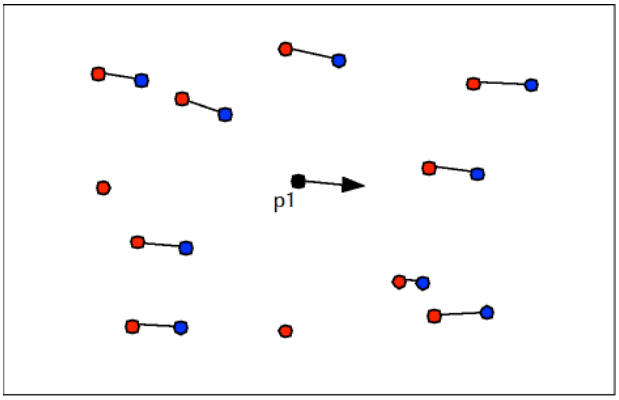

Figure 9.3. An illustration of the local velocity costing prediction step. Particle p_1 in frame 1 is to be matched. The cost to match any particle, p_2, in frame 2, to p_1 is based on the distance from p_2 to the predicted location of p_1 in the next frame. This predicted location, indicated by the arrow in the figure, is computed from a weighted average of the displacements of the particles in frame 1 that lie within a rectangular window centred on p_1. These displacements are determined from the current matches for these particles – indicated by the black lines connecting the red, frame 1, particles to the matched blue, frame 2, particles. Note that two frame 1 particles are not matched to frame 2 particles and therefore they do not contribute to the prediction calculation. In addition, although one of the frame 1 particles appears to be incorrectly matched (the short black line in the bottom right corner), its contribution to the calculation of the predicted position of p_1 is small.

where

l_{def} – is a default length that is used in the normalisation if the distance p_1 is predicted to move between frames is less than this value.

The strength of this `costing` lies in two areas. Firstly, the `costing` uses the data from a number of particles in the prediction step – we typically aim to choose a window that includes at least 10 other particles. Thus the averaging over the matches of many particles leads to a robust prediction of the particle's new location, even if some of these matches are not perfect. Secondly, even when the particle motion includes significant shear the prediction is quite accurate because the impact of the shear is significantly lessened due to the estimates of the particle's location coming from particles surrounding the particle of interest.

This `costing` often benefits from multiple iteration of the optimisation process. During the first iteration often the number of matches decreases as invalid or inconsistent matches are eliminated. The result is a smaller set of matches that are more likely to be accurate. During subsequent iterations the number of matches increases again and the new matches are likely to be highly reliable.

The `local velocity costing` performs best in regions of high particle density. Here, many closely located particles can contribute to the prediction calculation.

Conversely, where particle densities are low, the `local velocity costing` performs less well. In order to have sufficient particles contributing to the prediction calculation under these circumstances the window must be large, and the assumption that the particles within the window possess a similar velocity to the particle itself becomes tenuous.

9.3.4 Recent velocity costing

The `recent velocity costing` is the second matching-based `costing` that we will describe. It is not as reliable as the `local velocity costing` but, nevertheless, it can play a role in a carefully designed analysis. It, too, adopts the predict and test strategy. In this case it uses a particle's past history, and, potentially, the future history of the particle to which it is being matched, to predict its future location – as illustrated in figure 9.4. The normalisation length in equation 9.1 for this `costing` mirrors that for the `local velocity costing` in equation 9.4.

This approach appears, at first glance, to be the ideal way to predict the particle's location in the next frame. If a particle has been matched through a series of previous, or future, frames then a very good estimate of its future, or past, location can be computed. Under ideal circumstances this reasoning is valid, and under these conditions the `costing` will perform very well. However, it suffers two drawbacks compared to the `local velocity costing`.

- If the two particles have no past or future matches no prediction can be made as to their future or past location. In contrast, because many particles are involved in the prediction calculation in the `local velocity costing`, a prediction is almost always available.
- Even when previous and/or future matches are available, if one or other of these matches is incorrect, the prediction will be faulty and the resulting match probably invalid. The presence of incorrect matches has considerably less impact on the `local velocity costing` because, again, many particles are involved in the calculation of the cost.

We have found that the `recent velocity costing` is an effective tool at completing, or filling in, particle tracks, when all current matches have already been judged to be highly accurate. It is less effective at improving a set of matches that are contaminated by invalid matches, or where many particles are unmatched.

9.4 General guidance on particle tracking

The previous sections have provided a detailed explanation of the particle tracking process and the various objects that contribute to it. In this final section on particle tracking we offer some general guidance on how to approach particle tracking in practice.

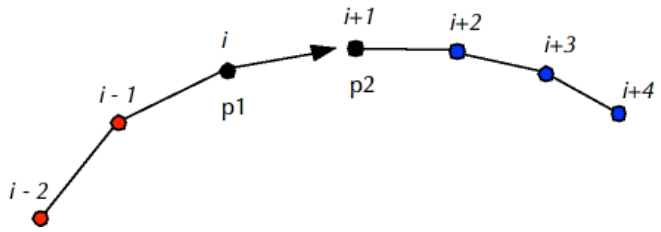

Figure 9.4. An illustration of the recent velocity costing prediction step. Particle p_1 in frame i is to be matched to particle, p_2, in frame i+1.The cost is based on the distance of p_2 from the predicted location of p_1 in the next frame according to equation 9.1. This predicted location, indicated by the arrow in the figure, is computed from the past history of p_1, indicated by the matches to the red particles in frames i - 2, and i – 1, and the future trajectory of p_2, indicated by the matches to the blue particles in frames i + 2, i + 3 and i + 4. A cost cannot be computed if both p_1 and p_2 are unmatched in the previous and next frames respectively.

Before embarking on the creation of a `PTV analysis pipeline`, and its associated analysis and `costing` objects, the analyst should spend some time familiarising themselves with the `particle record` they are about to analyse. This is most easily achieved by displaying 5-10 frames simultaneously in the `particle view` of the `particle record`, and observing the record through time. This will provide an invaluable overview of the particle motion – identifying regions, or times, of large displacement or velocity, regions/times of minimal displacement, and regions/times that might exhibit particular complexity. One statistic that should be extracted from the record at this point is an estimate of the maximum displacement experienced by a particle between frames. This information is important when specifying a `search window` for the optimisation process.

One should begin the analysis by constructing a `PTV analysis pipeline` containing a `PTV analysis` object that includes a single state-based `costing`. From a perusal of the `particle record` it should be possible to deduce whether a `distance costing` is likely to be successful. If not, then resort should be made to a more sophisticated `costing` such as the `pseudo-correlation costing`. Sensible parameters should be chosen for both the `PTV analysis` object and the `costing`, and it is recommended that they are tested on a subset of the frames in the `particle record` – the `PTV analysis` object allows the user to specify a range of frames to analyse. A group of frames that appear to be the simplest to analyse would be a good starting point – typically those with small displacements, or velocities, and exhibiting limited complexity. If the analysis is not effective for these frames it will not work for a more demanding portion of the record. Once the analysis is proven to be successful for this initial subset of the frames the analyst can expand the analysis to check its performance on the entire record, or at least sections of the record that are likely to be the most challenging. This may require the analyst to revise their parameter choices for both the `costing` and the analysis objects.

After each step of the analysis process the analyst should undertake a quality assurance exercise. An understanding of the quality of the matches produced by the analysis can be obtained in a number of ways. We recommend the following. The `particle record match summary view` yields two different perspectives of the match data. In the `matches` tab the number of particles, and the number of particle matches, in each frame are listed. We have already made reference to how the number of particles can provide a measure of the quality of the outputs from the particle identification process. The number of matches can provide insights into the quality of the particle tracking process. Very low numbers of matches, or a high degree of variability in the number of matches between frames, both point to a poorly performing analysis and/or `costing(s)`.

A further perspective can be found on the `paths` tab of the `match summary view`. Here an analysis of the path lengths of the particle tracks generated by the analysis is presented. All paths are identified and categorised by the number of particles that comprise them. A path with a length of 1 indicates a single particle that has been left unmatched by the optimisation process. There is no general path length target that indicates that the analysis has been successful, as different applications have their own peculiarities. Take, for example, a structural test where catastrophic failure does not occur, and all particles are present throughout the `particle record`. In this case one would realistically expect that the majority, if not all, of the path lengths to equate to the length of the record itself. On the other hand, in a fluids experiment where particles flow through the measurement window such that they are only present within that window for, say, 20-30 frames, the analyst could not expect path lengths to exceed 30 because of the physical constraints. Thus the analyst's judgment will be based on their understanding of the physics of the problem together with the characteristics of the measurement system. However, it is a general rule that relatively long paths are indicative of a sound matching process.

The information provided in the `match summary view`, while providing hints as to whether the particle tracking has been more or less successful, does not provide direct feedback on the quality of the matches themselves. It is relatively easy to perform an analysis resulting in almost 100% matches, only to find that many of those matches are invalid. The quality of the matches is best viewed in the `particle view` of the `particle record`. In addition to displaying the particles in a number of frames simultaneously, this view can display the current matches – drawn as lines between particles in two consecutive frames. If the particle matches are correct, the particle tracks, visible when the particles in multiple frames are viewed concurrently, should overlay the lines corresponding to the matches. Observing these data, the particles and the match lines, moving through time, provides the analyst with a strong sense of the quality of the matches. By identifying particular regions, or times, where the matching process has failed, the analyst can work to discover which parameters within the optimisation process and/or `costing(s)` need to be adjusted to improve their performance.

It is important to note that after a single analysis, based on one state-based `costing`, perfect matches should not be expected. Instead, the objective of this initial analysis is

to lay the foundations for later analyses based on matching-based `costings`. Therefore, the analyst should experiment with a range of parameter settings in this initial analysis in order to produce the most robust set of matches possible. We strongly recommend that it is worth the time exploring a number of different optimisation configurations so that the analyst gains a sense of the range of outcomes the analysis can produce. Perhaps some settings provide a high percentage of particle matches with many invalid matches, while other settings provide much lower matching levels but with the compensation that those matches are more accurate. The analyst may wish to try both `distance` and `pseudo-correlation costings` separately in order to compare their performance. Limiting this experimentation to say 100 frames is a way of ensuring rapid testing can occur. However, before proceeding to the next stage all frames do need to be analysed to ensure that the chosen settings are suitable for the entire `particle record`.

Once an initial set of matches, that satisfies the analyst's critical eye, has been produced, the analysis can be extended by the inclusion of additional `PTV analysis` objects. The user can approach this in a number of ways. The simplest, but least efficient, is to add each new `PTV analysis` object to the original `PTV analysis pipeline`. When this pipeline is executed the entire pipeline will execute from the beginning, repeating the analysis that has already been given the stamp of approval. We prefer to save the `particle record` in its partially analysed state, and to use that as the basis for all future experimentation. In this way the original matching process does not get repeated every time. A new `PTV analysis pipeline` is created for each new step in the analysis process, and only this pipeline is executed. Of course, this procedure can be repeated as many times as the analyst wishes. Once a new set of matches, hopefully better than the matches resulting from the previous analysis, has been generated, the `particle record` can be saved, and a subsequent analysis, using a new `PTV analysis pipeline`, can be applied to this `particle record`.

The second `PTV analysis` object to be applied to the analysis is likely to include a matching-based `costing` such as the `local velocity costing`. As with the previous analysis the analyst should feel empowered to experiment with the analysis and `costing` parameters in order to understand their impact on the number, and quality, of the matches. After each attempt, resort should be made to the `match summary` and `particle views`, as described above, in order to make some judgement on the success, or otherwise, of the latest parameter choices. After some level of iteration the matches produced from this analysis should be significantly better than those attained after the first analysis, and the analyst is either ready to move onto the next iteration with a new analysis object and `costing`, or to finish the analysis, satisfied that the matches obtained are optimal, and, most importantly, correct.

A simple illustration of this entire procedure is provided in figure 9.5. Here the analysis uses two different PTV analysis pipelines, the first using a state-based (SB) costing and the second a matching-based (MB) costing. The iterative process at each step in the analysis is indicated, as is the act of saving each particle record along the way.

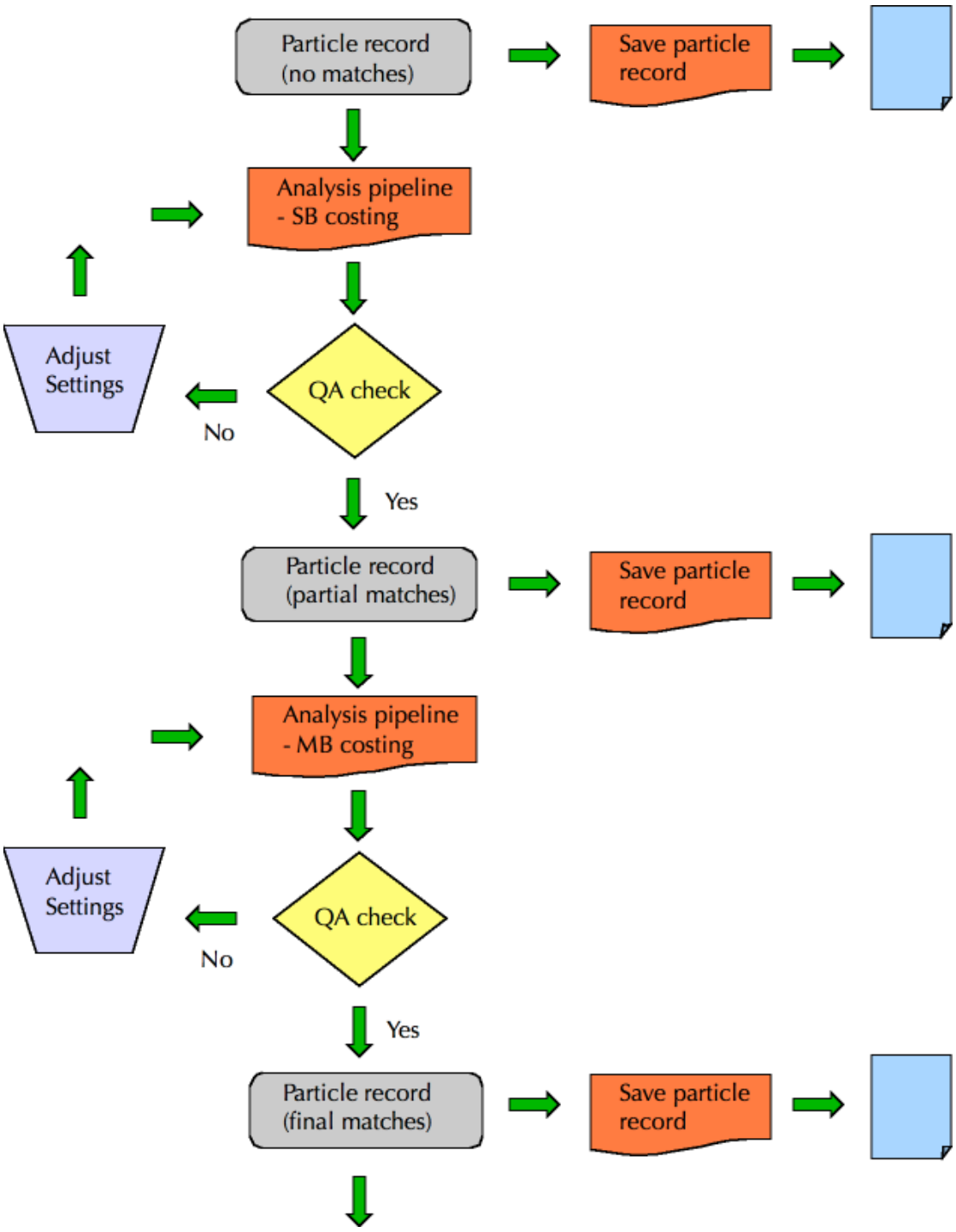

Figure 9.5. A schematic illustrating a systematic approach to the particle matching process. A ***`particle record`*** *with no matches is first analysed using a single state-based (SB)* ***`costing`****. The matches produced are checked for their quality, and, if unsatisfactory, adjustments are made to the parameters in both the* ***`PTV analysis`*** *object and the* ***`costing`****, and the analysis is repeated. A second* ***`PTV analysis`*** *utilises a matching-based (MB) costing. Again, an iterative approach, involving a quality check and parameter adjustments, is taken before a final set of matches is confirmed. The* ***`particle records`*** *are saved at each step so the analyst can return to any of the intermediate states of the* ***`particle record`****. This sequence of steps could continue with further* ***`PTV analyses`****.*

9.5 Summary

In conclusion, it is important to reiterate that the reliability of the outputs from all subsequent steps in the analysis process are directly correlated to the quality of the particle matches generated in the particle tracking process. Therefore, this step is, in many ways, the most critical and the most time consuming, particularly early in an experimental programme. The analyst must focus on quality throughout their endeavours and attempt to profit from the range of tools available to them to generate high quality particle matches. In judging the outcomes of the particle tracking step the following rule of thumb is worth remembering.

Rule of thumb:

It is better to have fewer correct matches, than more matches of variable quality.

10. Field creation

10.1 Overview

The final step in the analysis pipeline computes the time varying field of interest – typically a `displacement field time series` or a `velocity field time series` – from the particle tracks generated in step 2. This step, and the optional sub-step of field transformation, are the focus of this chapter.

10.2 Field generation

The creation of Eulerian and material-based fields requires a transformation of the particle-based data onto a regular, rectangular grid of nodes. For an Eulerian field this grid is fixed in space, while for the material-based field it is fixed to the material as it deforms. The application domain also has an impact on the data that is recorded at the grid nodes, and thus the process for computing the field. For fluid mechanics applications the Eulerian field of interest is invariably the velocity field. This field is computed from the particle displacements between frames in the `particle record`. On the other hand, in the area of material dynamics or structural testing a material-based field is generally required and it is the cumulative displacement of the material over time that is of interest. For example, the strain field is based on the cumulative displacement of the material not the incremental displacement between frames. This difference between the incremental displacements required for velocity field creation, and the cumulative displacements required for displacement field creation, leads to two slightly different variants of the third step in the analysis pipeline. These variants are reflected in figures 7.1 and 7.2 and discussed in the following two subsections.

10.2.1 Velocity field creation

Velocity field data are interpolated directly onto a grid from the **particle record**. *Streams* offers a range of schemes for interpolating both the field itself and its derivatives. The most common scheme, and the one that serves as the default, is based on a **Delauney** or **Thessian triangulation** of the particle data. Such a triangulation computes a mesh, comprising triangular elements, where the nodes in the mesh are the particles for which velocity estimates are available from the particle matching process. This triangulation changes from frame to frame as the particles move and the set of matched particles alters with time.

The Delauney triangulation has the attractive property that long, narrow, triangles are minimised within the mesh. The interpolation interrogates the triangular mesh to determine the triangle in which a grid node lies, and then estimates the velocity at that node using the velocities of the three particles located at the corners of the triangle.

An alternative scheme, commonly used, employs a set of nearest neighbour particles to each grid point to generate a two-dimensional polynomial least squares fit to the

velocity in the vicinity of the grid point and bases the velocity estimate at the grid point on this fitted polynomial.

A number of schemes are available for computing the field derivatives at the grid nodes and, as the choice of this scheme is largely independent of the scheme used for the field interpolation itself, the analyst has considerable flexibility in their overall interpolation strategy. Details of all of these schemes are best garnered from the *Streams* manuals.

It is not unusual to have regions within the measurement domain that contain no particles and are not physically part of the material being observed. Imagine a fluid flow where an obstacle is present in the flow and the experimenter is interested in how the obstacle affects the fluid motion. Interpolating the fluid velocity data onto the space occupied by the obstacle is clearly meaningless. It is possible for the analyst to define regions that are excluded from the interpolation process. If a grid node lies in one of these regions the field is recorded as undefined at that node, and when the field is viewed through any of the available visualisation tools such regions will appear blank.

Finally, the manner in which the velocity is actually computed is worthy of mention. The interpolation scheme will typically use the velocity of particles surrounding a grid node to estimate the velocity at the node – for example the particles at the corners of a triangle in a triangulation mesh. For some particles matches to particles in the previous and next frames are available. In other situations only one of these matches may exist. In the first case the particle's velocity can be computed using a central difference estimate in time, while in the second only a forward or backward difference can be employed. Clearly the first of these is preferable and the analyst is at liberty to demand that only particles with both matches can be used in the interpolation process. Depending on the length of typical particle paths this imposition may have a greater or lesser impact on the interpolated field. If large numbers of particles possess only a single match then these particles are excluded from the interpolation and the particles, whose data are to be used to interpolate onto a particular grid point, may be more distant from the grid point than if the central difference requirement was relaxed. When a Delauney triangulation scheme is used this equates to larger triangles in the mesh. Therefore, under these circumstances, the increase in accuracy that is gained by the central difference estimate may be offset by the greater distance between the grid node and the particles participating in the interpolation. If the vast majority of particles are members of particle paths with lengths greater than two, and this is generally the case, then the central difference requirement will have little impact on the set of particles employed in the interpolation, and the resulting field will be somewhat more accurate. The analyst can gain a sense of the typical path length through the `paths` tab in the `match summary view` of the `particle record`.

The selection of the grid's spatial dimensions is entirely at the analyst's discretion. However, it is worth remarking that the node spacing does not determine the resolution of the field. As discussed in chapter 2 the spatial resolution of the measurements is determined by the inter-particle spacing. Therefore, there is no

advantage in specifying grid node spacings that are significantly smaller than the typical inter-particle spacing.

Once this interpolation process has been completed for each frame in the particle record a full three-dimensional (x, y and t) grid of velocity data is produced and this forms the core of the required `velocity field time series`.

10.2.2 Displacement field creation

It is possible to generate a displacement field following exactly the same process as that described in the previous section, and *Streams* provides this capability. However there are disadvantages in doing so. The primary weakness to this approach is accuracy. As discussed at the beginning of this chapter it is the cumulative displacement that is of prime importance when considering displacement field applications. By interpolating the incremental displacement – which is effectively what is done when interpolating the displacement from one frame to the next in a particle record – significant noise may appear in the cumulative displacement field due to interpolation errors being aggregated when the incremental displacements are summed.

For this reason it is preferable to work directly with cumulative displacements. As these are inherently stored in `Lagrangian path fields` through the particle tracks themselves, it is recommended that displacement fields are generated from a `Lagrangian path field` derived from the `particle record` of interest. The result is that reductions in noise can be achieved. This intermediate step of creating a `Lagrangian path field` is illustrated in figure 7.2. A number of observations regarding this modified process are worthy of mention.

- The interpolation process used to generate the displacement field mirrors that described for the velocity field in section 10.2.1 with the fundamental difference that the particle data comes from the `Lagrangian path field`, not the `particle record`. In other words the interpolation schemes are the same.
- It is the cumulative displacements of the particles that are interpolated not the incremental displacements.
- Only particle tracks that start in the first frame of the `Lagrangian path field` participate in the interpolation process. The reason for this restriction is perhaps obvious. Only particle tracks starting in the first frame can provide the cumulative displacement through time.

10.3 Field transformation

The last step, although not always required, transforms the computed field into a more convenient form. For example, in the fluid mechanics arena non-dimensional frameworks are almost always preferred, and so this transformation could correspond to a transformation that non-dimensionalises the independent coordinates, *x*, *y* and *t*, as well as the field itself.

Transformations are supported through the transform pipelines for the `displacement field time series` and `velocity field time series`. Both types of pipeline support a range of standard transformations, including a linear transformation that would perform the non-dimensional conversion alluded to above.

10.4 Summary

This chapter concludes our detailed consideration of the analysis process. Chapters 8-10 have presented comprehensive guidance on a practical approach to particle tracking analysis. In order to place this advice on firm, practical, foundations all three chapters have referenced the *Streams* analysis tool. In this way very specific guidance has been possible. All three steps, together with the optional sub-steps, have been discussed in detail. It is intended that the advice offered is general enough in nature to enable particle tracking data, arising from a range of contexts, to be confidently tackled by the analyst.

Emphasis has been placed on three key aspects of a successful particle tracking analysis:

1. The analyst should spend time familiarising themselves with the nature of their data. This familiarity will expedite the wise selection of appropriate analysis processes and their associated parameters.
2. A number of steps in the process require manual iteration. Analyses utilising different analysis procedures and different parameter selections can help the analyst find the optimal approach to processing their image data. This iterative approach should not be overlooked.
3. Throughout the process the analyst must embrace a strong commitment to quality assurance testing. A number of tools that facilitate this have been suggested. These tests provide the analyst with confidence that their final results are reliable and accurate.

It is worth mentioning that the time invested in determining the most appropriate analysis tools is of particular importance in the early stages of an experimental programme. If the nature of the experiments changes little during the programme, then it is likely that the analyst can reuse their initially determined analysis scheme with minimal modification. In certain circumstances, in particular when the manual elimination of erroneous particles is not required, the analysis process may be entirely automated. A process pipeline that acts on an image sequence and produces a final transformed `velocity` or `displacement field time` series may be possible under these circumstances.

Part 4

Case Studies

11. Case Study 1: Floor Motion in a Model Building

11.1 Introduction

The first case study offers an ideal vehicle for introducing the analyst to the practicalities of particle tracking for the first time. It is a simple problem that aims to deduce the motion of a floor in a multi-storey model building, where the building is mounted on a small shake table driven by a scaled earthquake record. Its primary objective is to be able to compare floor displacements, measured using a PTS, with those deduced from a floor-mounted accelerometer, although that comparison will not be included here.

No internal deformation of the floor is expected. Thus, the floor can be treated as a point mass undergoing complex motion due to the movement of the building's foundations. Such measurements are normally very straightforward in a particle tracking system as very few particles are required, and the tracking process is largely trivial. However, the analysis still requires a number of the optional sub-steps discussed in chapters 8-10, and the simplicity of the problem enables the analyst to focus on the tools rather than the complexity of the physics.

The author acknowledges C Hendrickson and W Roper who kindly provided their data for this case study. A brief report of their work can be found in Hendrickson and Roper 2019.

11.2 Analysis overview

In this section we provide a concise overview of the tools that will be illustrated in the analysis of this case study. This overview provides the reader with a quick reference to the *Streams* objects and processes that are to be covered in section 11.4.

In this case study the following *Streams* tools are employed:

1. *Image pre-processing*: The `mathematical formula` and `convert type filters` will be used in the pre-processing of the images. The `extract filter` is also mentioned.
2. *Particle identification*: The `single threshold monochrome PID` will be employed for particle identification.
3. *Particle tracking*: Particles will be tracked using a `PTV analysis` based on the `distance costing`. The `pseudo-correlation costing` will also be referred to briefly.
4. *Field generation*: The motion of the building floor will be captured with a `Lagrangian path field`. A number of `fields` will be computed that yield specific measurements of interest.

5. *Field transformation*: Simple manipulation of the `fields` within a `tablet` will be demonstrated.

11.3 Experimental setup

The experimental setup is illustrated in figure 11.1. A simple timber frame was used to emulate the structural elements of a building comprising three floors. The floors and columns were constructed from lightweight medium density fibreboard (MDF), connected with L-shaped steel fittings. Steel blocks were placed on the second and third floors to provide additional mass to the structure, thus ensuring more realistic natural mode frequencies.

The entire structure was mounted on a miniature shake-table, driven by a computer-controlled electric motor. A scaled version of the time history of an earthquake record retrieved from the NGA (Next Generation Attenuation) strong-motion database (Chiou et al. 2008), and recorded at station El Centro Array #6 in California, USA, was used to drive the shake-table motion. The pseudo acceleration spectrum for this time series is plotted in figure 11.2.

11.3.1 Particle tracking system

The experimental particle tracking system comprised the following components:

- Blue stick-on dots (24 in total) were employed as particles and attached to the front faces of each of the three floors (8 per floor). Figure 11.3 provides a raw image of these particles attached to the top floor.
- Three Fujifilm X-T2 digital cameras, with a pixel resolution of 1280 x 720 (720p), operating in video mode, captured the particle motion for each floor at a frame rate of 50Hz. The aperture, shutter speed and focus were all set manually. The camera location and lens zoom setting resulted in an observation window of approximately 579 x 326 mm.
- Ambient laboratory lighting was sufficient to illuminate the particles uniformly.

A separate camera recorded the motion of each floor in response to the simulated earthquake excitation. On completion of an experiment individual images were extracted from each video record in preparation for analysis in *Streams*.

Before continuing with the particle tracking analysis itself, it is worth reflecting on the issues of resolution and accuracy. The time step between frames is 0.02s based on the camera frame rate of 50Hz. Following the guidance in chapter 2 this will enable behaviour at timescales greater than 0.2s to be well resolved. From figure 11.2 it is clear that there is a modest portion of the spectral energy present in timescales shorter than 0.2s, and therefore the resolution of those time scales will not be ideal.

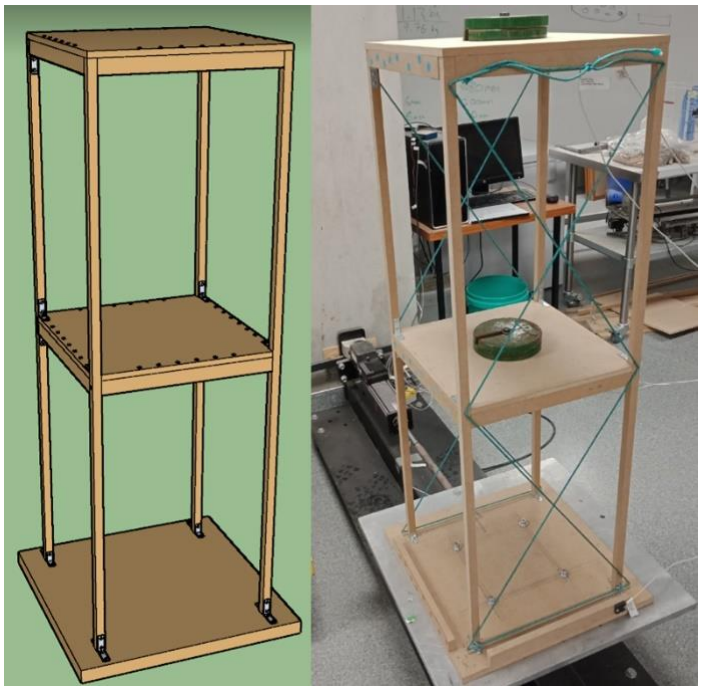

Figure 11.1. A schematic, and photograph, of the experimental testing system. The model building comprised three floors for which the floors and columns were constructed from lightweight medium density fibreboard (MDF) connected with L-shaped steel fittings. Floor masses were increased by steel blocks being placed on the second and third floors. The building was placed on a mini shake-table driven by an electric motor, and controlled by a computer.

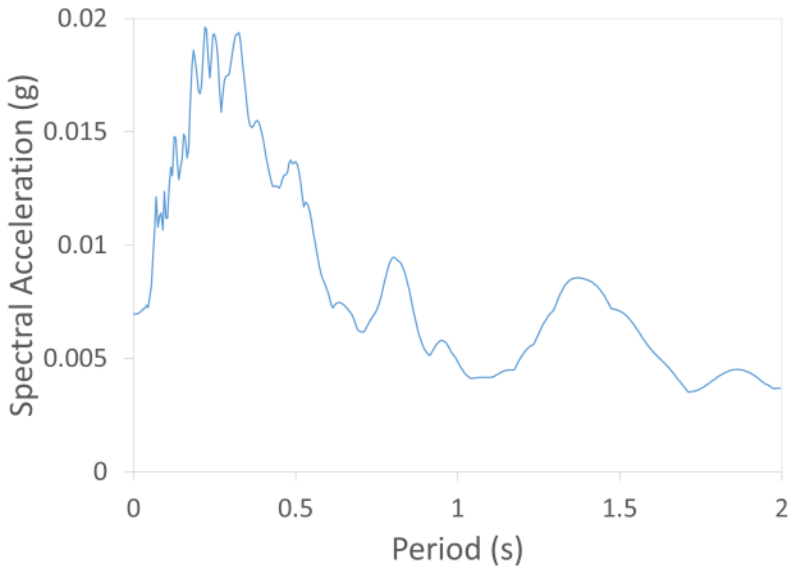

Figure 11.2. The pseudo acceleration spectrum for the scaled earthquake record.

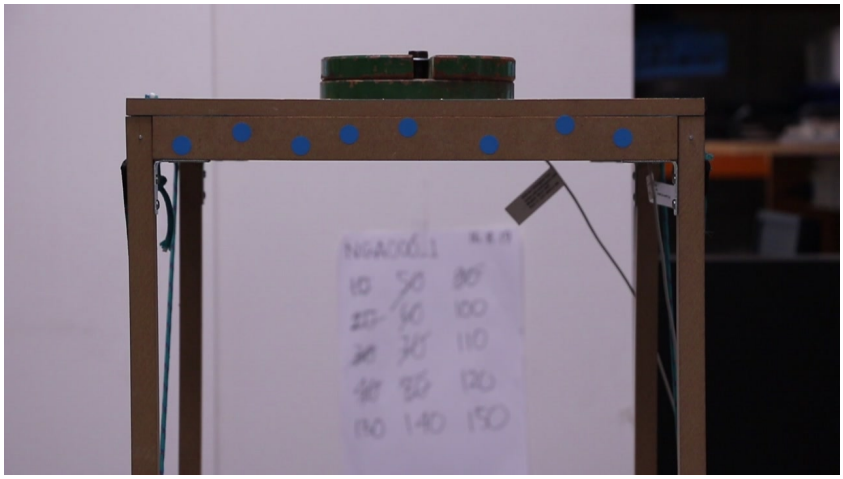

Figure 11.3. A sample image of the 3rd floor. The blue stick-on dots are clearly visible on the front face of the floor.

Spatial resolution is not an issue for this measurement system as only the bulk motion of the floor is sought. Spatial gradients are not relevant to the analysis.

Finally, the accuracy of the displacement measurement is expected to be no worse than $\pm\frac{1}{4}$ pixel, according to the analysis in chapter 2. Given the domain coverage and camera resolution this estimate corresponds to a physical uncertainty of ±0.11mm.

11.4 Analysis guide

This section takes the reader through the various steps in the analysis pipeline, explaining issues that need to be addressed at each stage, and recommending viable analysis strategies. The experimental images are available (see link below) and the reader is strongly encouraged to undertake the analysis themselves. By doing so they will gain invaluable experience with both the analysis process and the operation of the software. Through their own experimentation – choosing different analysis options, picking alternative parameters, observing the impacts of these changes, and even exploring different tools – they will rapidly gain confidence in their ability to tackle their own datasets.

To begin, the reader should download the experimental images from figshare© using the DOI below. The files are contained in a single zip file. Using these images the reader can create an `image sequence` in *Streams*. A scale factor, that converts from pixels to physical coordinates, can be specified during the image sequence creation. Using the known width of the building floor a camera calibration yields a scale factor of 0.452 mm/pixel.

https://doi.org/10.6084/m9.figshare.14569170 (file size: 132Mb)

11.4.1 Image pre-processing

An example of a raw experimental image is shown in figure 11.3. To the naked eye the blue particles are readily identified. However, the analyst needs to translate what they can see into the particle identification framework provided within *Streams*. All `PID` algorithms are reliant on the particle pixels possessing an intensity that is greater than those in the surrounding image, and that exceeds some specified threshold. Therefore the analyst must devise a threshold test that will effectively identify the particle pixels in the image. Perhaps it is clear that it is not the reflection of blue light from the particles that makes them stand out in the image, but the predominance of blue light over other light components. Much of the image background in figure 11.3 is close to white, and the light reflecting from these surfaces also contains a strong blue component. However, this white light also includes strong signals of red and green, not present in the particle pixels.

This is illustrated in figure 11.4a where the blue light component from each pixel has been extracted using an `extract filter`. In this image the particles lose their differentiability from the background, and a particle identification algorithm using the blue light intensity would perform poorly. Consider, instead, figure 11.4b where a `mathematical formula filter` has been used to compute the difference between the blue and red intensities at each pixel. Under this filter the white background pixels become almost black due to the similar intensities of the red, green and blue light components. The particles on the other hand contrast vividly with the background. It is worth noting that the `mathematical formula filter` computes a real number for each pixel, and it is most convenient to convert that real number back into an RGB grayscale value using a `convert type filter`. It is the resulting monochrome image, obtained from the sequential application of these two `filters`, that is shown in figure 11.4b.

While other image processing options may provide suitable images for particle identification, we choose the combination of a `mathematical formula filter`, computing blue-red intensities, followed by a `convert type filter`, converting from real to greyscale (RGB), to pre-process the experimental images.

To summarise, the `filter pipeline` is as follows:

`Mathematical formula filter` – Blue – red.
`Convert type filter` – Converts from real to greyscale (RGB).

11.4.2 Particle identification

Particle identification requires the selection of a suitable `particle identifier` and the setting of its associated parameters. We utilise a `single threshold monochrome PID` for this problem due to its universality. The settings available to the analyst for this `PID` include the following:

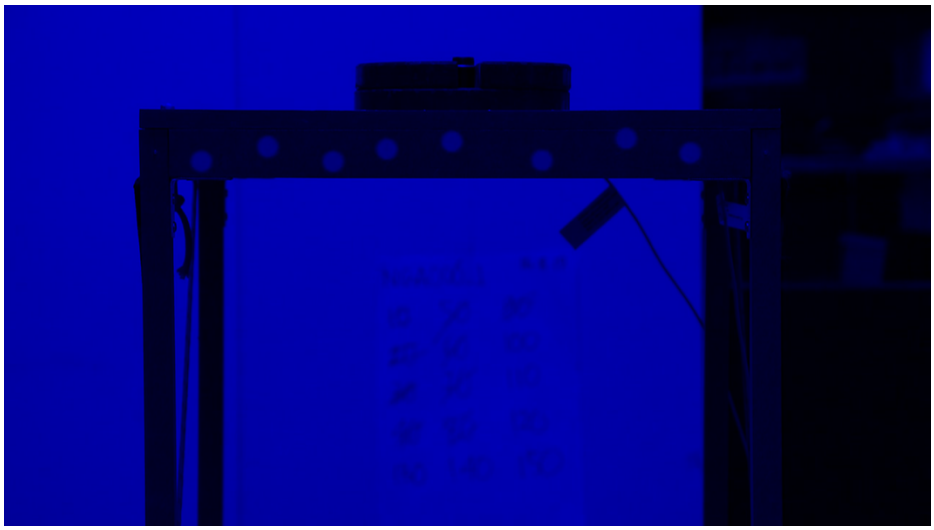

(a)

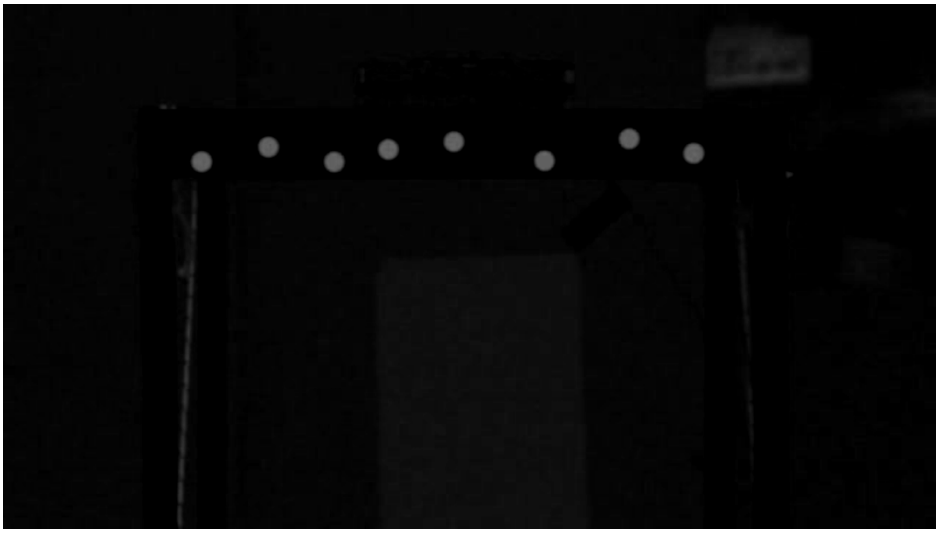

(b)

Figure 11.4. The result of applying a `filter pipeline` *to an experimental image. (a) The pipeline includes a single* `extract filter` *that extracts the blue channel. (b) The pipeline contains two filters, first a* `mathematical formula filter` *followed by a* `convert type filter`*. The* `mathematical formula filter` *calculates the blue-red intensity at each pixel. The result of this* `filter` *is a real number that is then converted back to an 8 bit grayscale value using the* `convert type filter`*. This enables easy visualisation.*

- *Intensity calculation* – specifies how the intensity is to be computed at each pixel. It could use an individual colour channel or an average (greyscale). The image pre-processing has generated greyscale images, so an average of all guns or one of the colour channels could be used. They are equivalent.
- *Threshold* – specifies the intensity that determines whether the pixel is part of a particle. The choice of this parameter is based on an inspection of the pre-processed images. Some experimentation is almost always required in order to deduce its optimal value.

- *Minimum diameter* – specifies the minimum diameter of a particle for it to be treated as valid. The blue stick-on dots have a diameter of 15mm, so a minimum somewhat less than this value is appropriate. It is worth noting that, depending on the threshold chosen, the particle size will vary due to the fall-off in intensity towards the edges of the particle.
- *Maximum diameter* – specifies the maximum diameter of a particle for it to be treated as valid. A value of approximately 15mm is appropriate.
- *Maximum aspect ratio* – specifies the maximum aspect ratio of a particle for it to be treated as valid. As the particles are circular a maximum aspect ratio a little larger than 1 would be suitable. If an aspect ratio of 1 is too strictly enforced particles are likely to be left unidentified, so some experimentation with this parameter is wise.
- *Frames for analysis* – enables the analyst to restrict the particle identification to a subset of the frames in the image sequence so that fast processing times can be achieved while appropriate parameters are being deduced.

The highly irregular nature of the shake table motion will lead to significant variability in particle motion during the measurement period. This variability can have an appreciable impact on the particle images due to the inability of the camera to freeze particles when they are travelling at high speed. If the experimenter has set the camera shutter speed manually, and has an estimate of the maximum particle speed that is likely to occur, then they should be able to calculate the distance a particle is likely to move while the shutter is open under these high velocity conditions.

It is wise, therefore, to compare the image frames obtained during periods of low particle velocity – when the particles will be frozen by the camera – with those captured during periods of maximum velocity – when the particles will suffer the greatest blurring. The maximum intensity of the particle pixels in the latter case is likely to be somewhat lower due to the blurring, and this variability in intensity needs to be considered when selecting the threshold parameter.

Figures 11.5a and 11.5b show the filtered images at two different times – times of zero velocity and maximum velocity. To emphasize the differences between the two frames, false colour images of two small rectangular regions surrounding one of the particles in each frame are provided in figures 11.5c and 11.5d. The slight blurring of the particle image is evident in figure 11.5d through both the increased horizontal extent of the pixels that comprise the particle, and their reduced intensity.

Selecting an intensity threshold at the upper end of the range of pixel intensities and/or placing strong constraints on the allowable particle size variation and maximum aspect ratio may lead to the `PID` identifying particles when they are slow moving, but failing to identify them when they are moving rapidly.

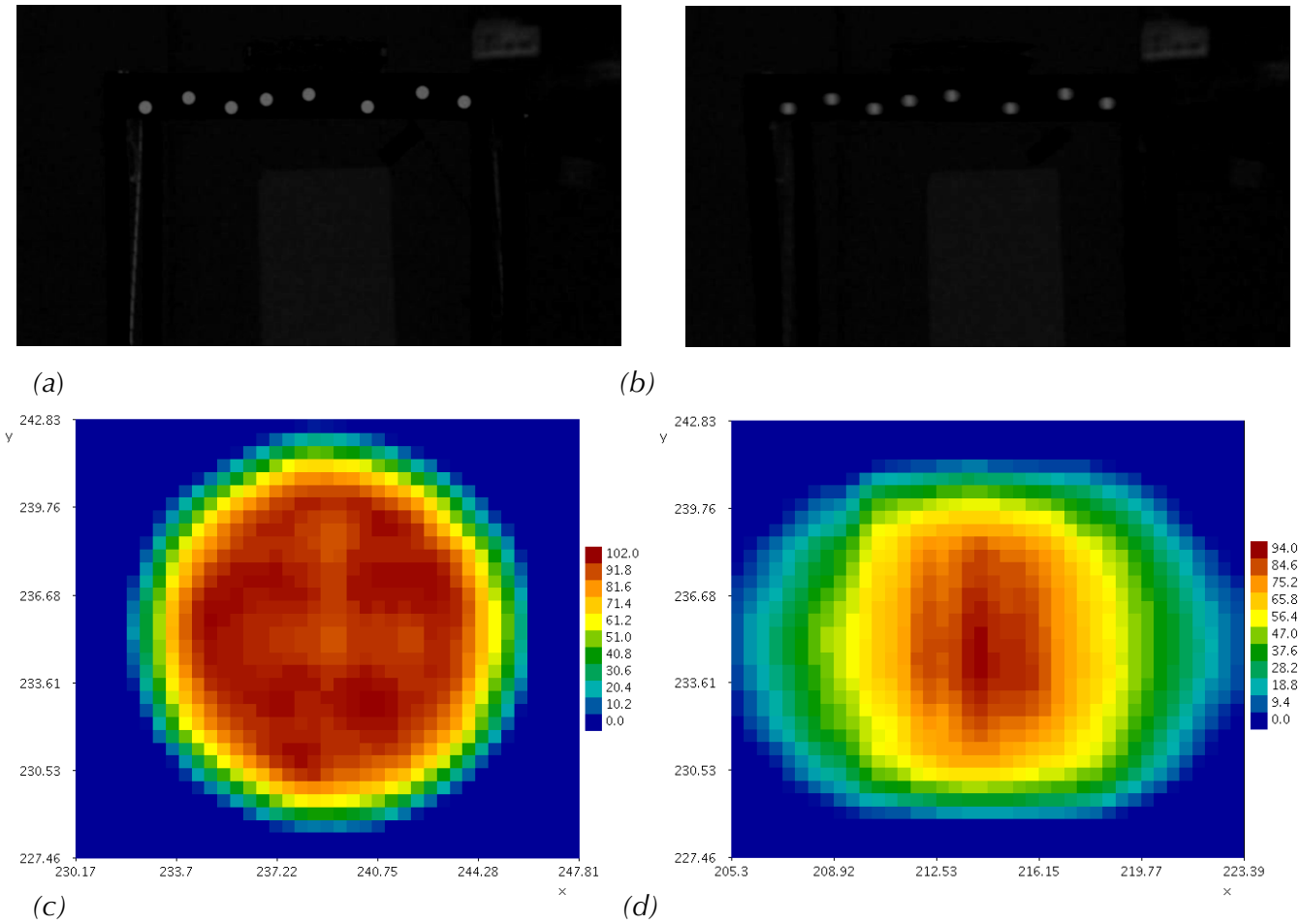

Figure 11.5. (a) The filtered image of frame 0 in the image sequence at which time the particle motion is negligible. (b) The filtered image of frame 375 in the image sequence at which time the particle is moving at close to maximum speed. (c) A false colour image of the greyscale intensity of the pixels surrounding the 4th particle from the left in (a). (d) A false colour image of the greyscale intensity of the pixels surrounding the 4th particle from the left in (b).

The observant reader will have noticed a thin strip of pixels visible on the left hand side of figure 11.4b. This region corresponds to the strut visible in figure 11.3. In determining the particle identification parameters the analyst must be conscious of the need to exclude particles being incorrectly identified in this region. A number of mechanisms are available to achieve this goal. The first is the setting of the threshold. In this particular case the maximum intensity in this region is less than the threshold selected and so these pixels are automatically excluded from consideration. The second would be to utilise the limits on particle size, and the third to take advantage of the fact that this region of pixels has a very high aspect ratio compared to the particle pixel clusters. Thus the maximum aspect ratio test could be employed to ensure that long narrow particles are rejected.

Through simple experimentation the following PID parameters are found to be effective – finding all 8 particles in all 2751 frames:

Intensity calculation – Average of all colour guns (greyscale).
Threshold – 60.
Minimum diameter – 5mm.
Maximum diameter – 15mm.
Maximum aspect ratio – 1.5.

With these settings no spurious particles are identified and therefore the auxiliary step of removing such particles proved to be unnecessary in this particular analysis.

11.4.3 Particle tracking

Particle tracking is the next critical step in the analysis pipeline. In this step suitable `PTV analyses` must be built by the analyst that, through their collective application, lead to a high quality set of particle matches or tracks. The performance of each `PTV analysis` rests firmly on the shoulders of the `costing`, or `costings`, that it employs. Their selection, and calibration, are of paramount importance.

We will follow the guidelines provided in chapter 9. The initial `PTV analysis` will comprise a single state-based `costing`. The first question that the analyst might ask, is whether the `distance costing` is suitable for this initial analysis. The performance of this `costing` was discussed in chapter 9 and it was stated, without proof, that the `distance costing` is effective provided the particle displacement between frames is much less than the inter-particle spacing.

Figure 11.6 provides an instructive illustration of the particle displacement relative to the inter-particle spacing. Two frames, selected to be at the time of maximum particle velocity or displacement, are overlaid in the `particle view` of the `particle record`. The left-most particles of each pair are from frame 374, and the right-most particles are from frame 375 – the particles are moving from left to right. It is apparent, even during this period of maximum velocity, that the particles move only a fraction of the distance between them and their neighbours. Therefore, based on the performance guidelines, the `distance costing` should be an ideal choice for this dataset. This fortuitous circumstance is largely due to the fact that the number of particles present in each frame is small. If, for example, the experimenter had employed hundreds of particles on the face of the building floor instead of eight, those particles would have been, of necessity, very much closer together, and the particle movement would have likely exceeded the inter-particle spacing.

The `search window` is an important parameter in the optimisation process. This window limits the number of particles considered for matching to those within a constrained rectangular region. It is critical that the correct match always lies within this window. Using the particle displacements illustrated in figure 11.6 we can deduce that the maximum particle displacement between frames is approximately 13-14mm in the *x* direction, with very little movement in the *y* direction.

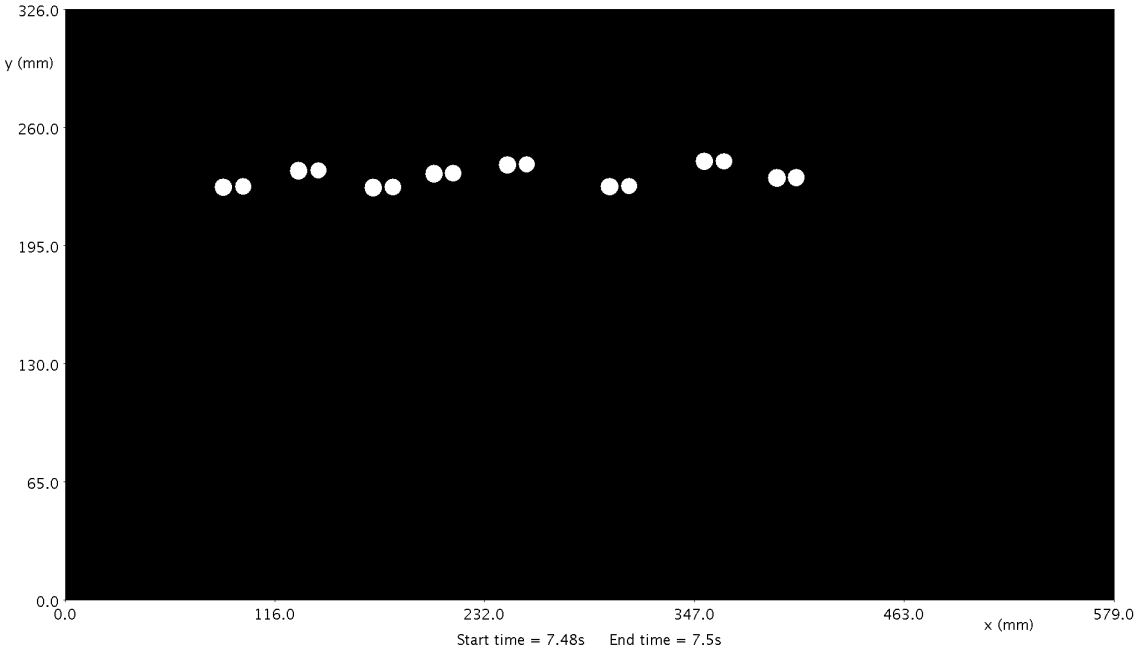

Figure 11.6. Frames 374 and 375 overlaid in the **`particle view`** *of the* **`particle record`**. *The left-most particle in each pair is from frame 374 and the right-most particle is from frame 375. The particles are moving at close to maximum speed.*

Based on this analysis, and the associated arguments, the following parameters are selected:

PTV analysis 1:

Process	global optimisation.
MMC	1.0.
Search window	40mm wide and 5mm high, centred on the particle.
Costing	**`distance costing`** with a reference length of 20mm.

All other parameters for both the **`PTV analysis`** object and the **`distance costing`** are set to their defaults.

The application of this analysis to the **`particle record`** yields a perfect set of particle matches. A total of 8 particle paths are generated, each with a length of 2751 frames. Figure 11.7 provides an illustration of the particle tracks and the particle matches. Ten frames are overlaid and the red lines indicate the particle matches.

This level of performance is typical of particle tracking systems that incorporate a modest number of particles, and in which the particles are identifiable in every frame. As will be seen in the next case study systems with hundreds, or thousands, of particles, and with particles appearing and disappearing throughout the sequence of images, pose a considerably greater challenge to the analyst.

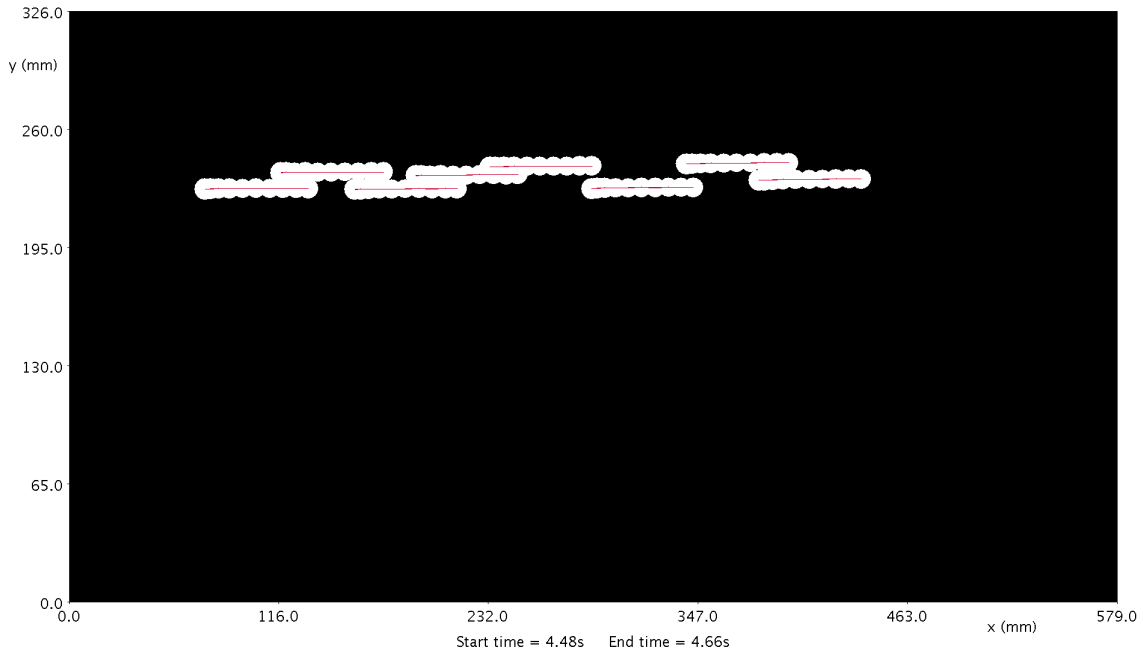

Figure 11.7. Frames 224-233 are overlaid in the ***particle view*** *of the* ***particle record****. The red lines indicate the particle matches generated by the* ***PTV analysis****.*

The reader may reflect on how a more sophisticated state-based **costing**, such as the **pseudo-correlation costing**, would have performed in these circumstances. With sensible **costing** parameters it, too, generates a perfect set of matches. The sole parameter of concern in the **pseudo-correlation costing** is the size of the window employed by the **costing** itself. This window is unrelated to the **search window** of the optimisation process. The **costing** window is designed to ensure that other particles in the frame are available to construct a particle pattern around the particle of interest, while the **search window** is designed to guide the optimisation process in seeking possible matches. Thus the size of the **costing** window is related to the inter-particle distance, while the size of the **search window** is related to the maximum particle displacement between frames. Clearly, for this problem the **costing** window will need to be considerably larger than the **search window**, although this is not a general rule.

An alternative **PTV analysis** that utilised the **pseudo-correlation costing** has the following settings.

PTV analysis 1:

Process	global optimisation.
MMC	1.0.
Search window	40mm wide and 5mm high centred on the particle.
Costing	**pseudo-correlation costing** with a window 140mm wide and 30mm high.

11.4.4 Field generation

The ultimate goal of this experiment is the measurement of the temporal variation of the floor displacement. Thus, we are interested in the displacement and velocities of the dots themselves, and these data are most readily available through a `Lagrangian path field`. This field will comprise eight particle paths, for each of which the displacement, and derived quantities such as velocity, can be computed.

The `create Lagrangian 2D path field` process, operating on a `particle record`, is the tool by which the `Lagrangian path field` can be constructed. This process provides the analyst with a number of options that impact on the paths present in the final `Lagrangian path field` – these are explained in the *Streams* manuals. For this simple application none of these options need be utilised. The only setting that might concern the analyst is the imposition that only displacements that can be generated through a central difference approximation (double estimate in *Streams* terminology) can be incorporated into the final paths. The effect of this is to remove the initial and final particle locations from every path as these particles do not possess previous or subsequent particle matches respectively.

The `calculators` contained in the `Lagrangian path field` provide the analyst with the tools necessary to extract specific motion data in the form of a scalar, or vector, `field`. In fact, the analyst is at liberty to define their own calculators based on the measured variables such as displacement or velocity. Illustrative results from these fields are provided in section 11.5.

11.4.5 Field transformation

A field transformation, is entirely optional, and depends on whether the raw data extracted by the `calculators` is in the required form, or whether that raw data is best exported to a separate software tool for further manipulation.

Transformations can occur via two mechanisms. The first mechanism is via a `transform pipeline` for the particular field time series. Such a pipeline is available for `displacement` and `velocity field time series`, and the `Lagrangian path field`. The second mechanism is via the suite of tools for manipulating `fields` available in a `tablet`.

11.5 Illustrative results

This final section is not primarily instructional. The material is presented solely to satisfy the curiosity of the reader, who, beyond their interest in the tools and techniques discussed in previous sections, may be intrigued to see some of the results that particle tracking makes available. The results that we present are simply a selection of possibilities, and are not intended as a definitive set of experimental outputs. They do, however, provide us with an opportunity to illustrate some of the

visualisation tools available to the user in *Streams*, and to explore some aspects of the system performance.

The output of primary importance from this particle tracking system is the displacement of the building floor. The `x` and `y calculators` in the `Lagrangian path field` extract the particle locations, and figures 11.8a and 11.8b present the *x* and *y* coordinates of the particles as functions of time. Each particle location history is indicated in a different colour. If the assumption of negligible internal floor deformations is valid then each of these curves should be identical barring the relative initial offset.

Note that the ordering of the curves in each plot has no particular significance. It is dependent on the ordering of the particles in the original `particle record`, which in turn is dependent on the peculiarities of the particle identification algorithm.

The `fields` plotted in these figures have two independent variables, the particle number and time, consistent with the Lagrangian field expressed in equation 2.2. Thus these fields are two-dimensional scalar fields – referred to as `scalar 2D fields` in *Streams*.

Figure 11.9a collapses the curves in figure 11.8a by computing the position of the particles relative to their starting locations. These relative displacements are generated by the `xrel calculator`. To the accuracy of the naked eye these displacement curves are indistinguishable.

To explore the variability of the curves in more detail figure 11.9b presents an expanded view of the first few seconds of particle motion utilising a stretched vertical scale. This figure possesses two interesting features. Firstly, it is clear that the system was not initially at rest when the image recording began. A very weak harmonic motion, with a period of approximately 0.4 seconds and an amplitude of roughly 0.1mm, was present. All particle tracks capture this motion. Secondly, the noise present during this initial period provides some sense of the accuracy of the measurement system. The reader will remember from the discussion in section 11.3 that the expected accuracy is better than ±0.11mm based on the physical size of each pixel. The actual accuracy is, in fact, somewhat better than this estimate. Variability between curves suggests an accuracy better than ±0.05mm.

The reason for deploying eight particles, instead of one, is to increase the system's accuracy by averaging the motion of all particles. The black dots in figure 11.9b trace the average particle displacement through time. The irregularity of this average curve is appreciably less than that of the individual curves, and its uncertainty is less than the estimate of ±0.05mm for the individual particle time histories.

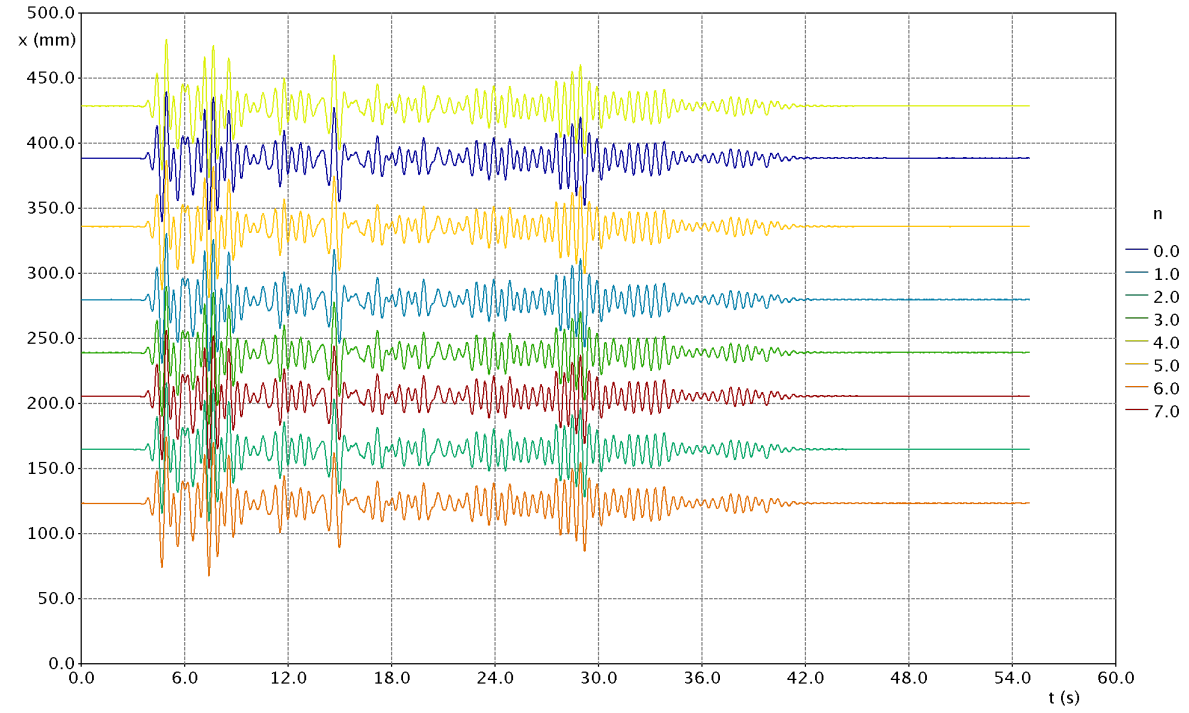

(a)

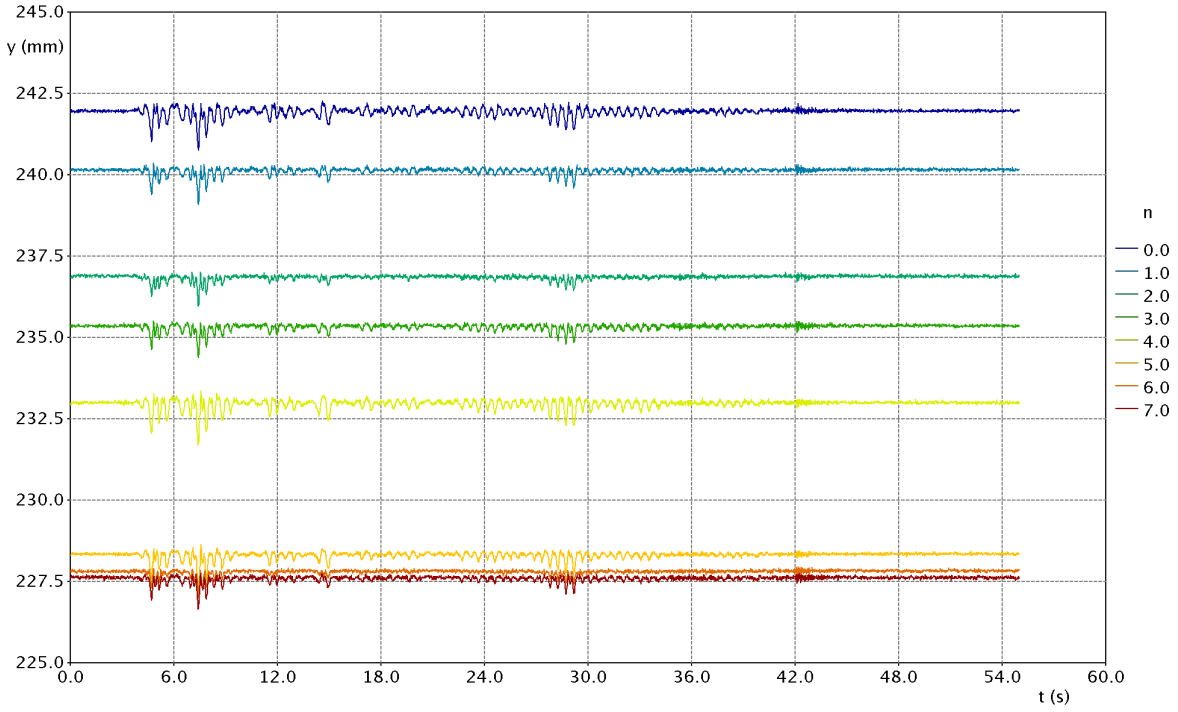

(b)

Figure 11.8. (a) The x location of the 8 particles as functions of time. The legend labels the particles by number. If the building floor suffers no internal deformation all of these displacements curves should be identical, with the exception of their starting location. (b) The y location of the 8 particles as functions of time. The legend labels the particles by number. Note the different vertical scales. The vertical displacements are more than an order of magnitude smaller than their horizontal counterparts. The graphs presented are illustrative of the `multi-graph` *view of a* `scalar 2D field`*.*

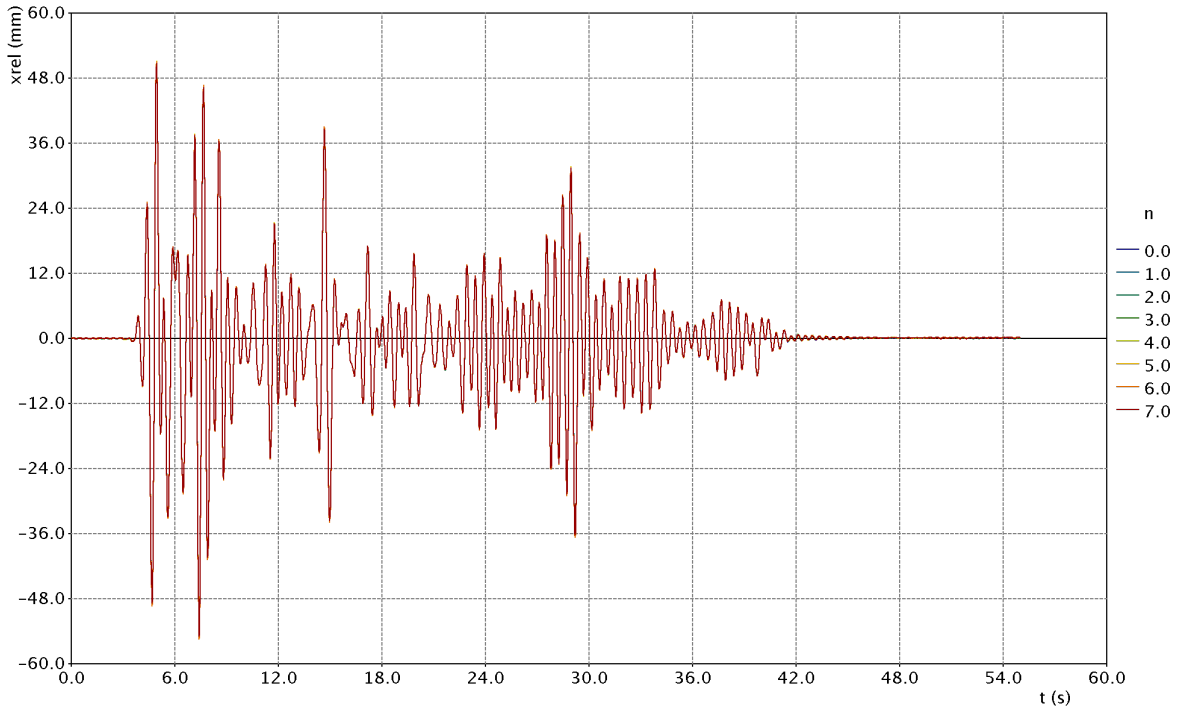

(a)

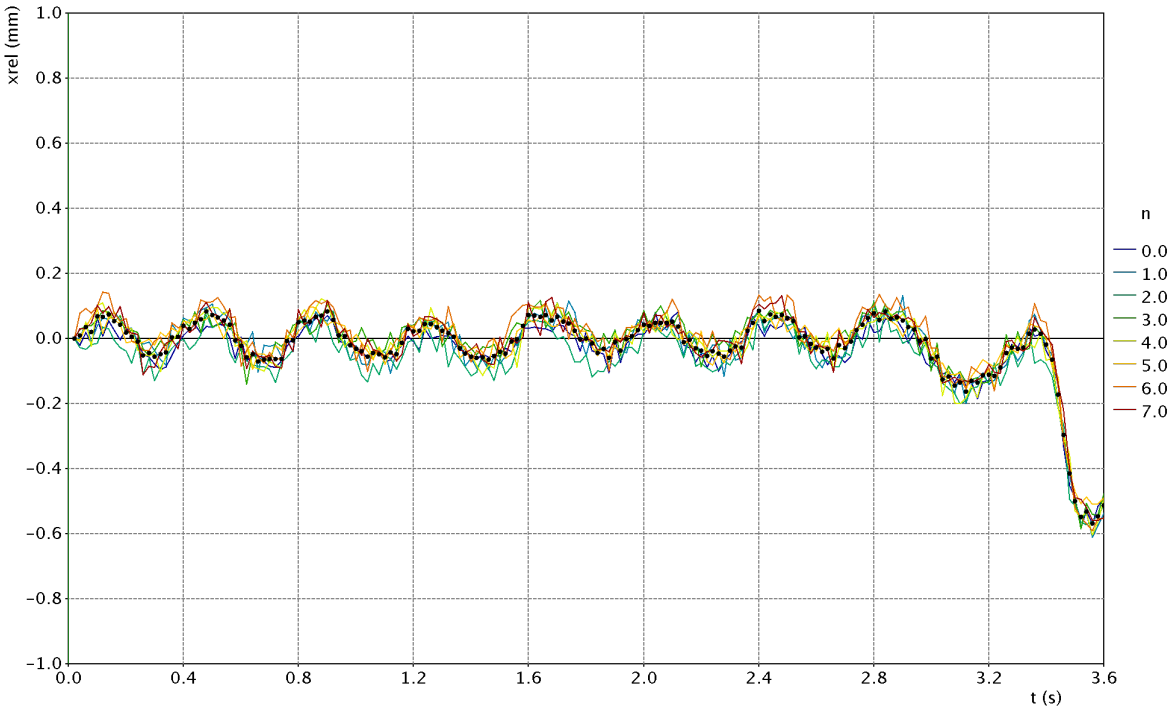

(b)

Figure 11.9. (a) An overlay of the relative x displacement as a function of time for all 8 particles. The legend labels the particles by number. The curves are indistinguishable to the naked eye. (b) An enhanced view of the first 3.6 seconds of the displacements displayed in (a). Note the vertical scale has been stretched compared to (a). The black dots indicate the average displacement of all 8 particles. A very weak, approximately, harmonic motion is identifiable. The figure also provides evidence of the system's accuracy.

Figure 11.10 provides information about the spectral content of the floor displacement, extracted from a fast Fourier transform (FFT) of the average displacement of the particles. Two aspects of the graph are worthy of attention.

Firstly, the maximum frequency resolvable is half the capture frequency of 50Hz. This is indicated by the cut-off at the upper end of the frequency range in the figure. It can also be seen that the relative noise level at these higher frequencies is substantially higher than for lower frequencies and, as discussed in chapter 2, the analyst should not expect to seriously resolve temporal content for frequencies greater than approximately $1/10^{th}$ of the capture frequency. Certainly the data for frequencies above 5 Hz seems noisy and unreliable, although it must be noted that the energy content of these frequencies is very low in any case.

Secondly, the spectrum in figure 11.10 shows a strong peak in energy at 2.2 Hz. This is consistent with both the energy peak of the forcing (see figure 11.2), and the weak initial motion identified in figure 11.9b. That motion is likely to be residual motion still present from a previous experiment, and it would suggest that a natural mode of the structure has a similar frequency.

To provide a simple illustration of the application of the analysis tools available within `tablets` figure 11.11 shows the x velocity of the floor. This velocity has been computed by differentiating the displacement field in a `tablet`. A second order polynomial, computed as a least squares best fit to the five points surrounding each data point, was used to fit the displacement field before differentiation.

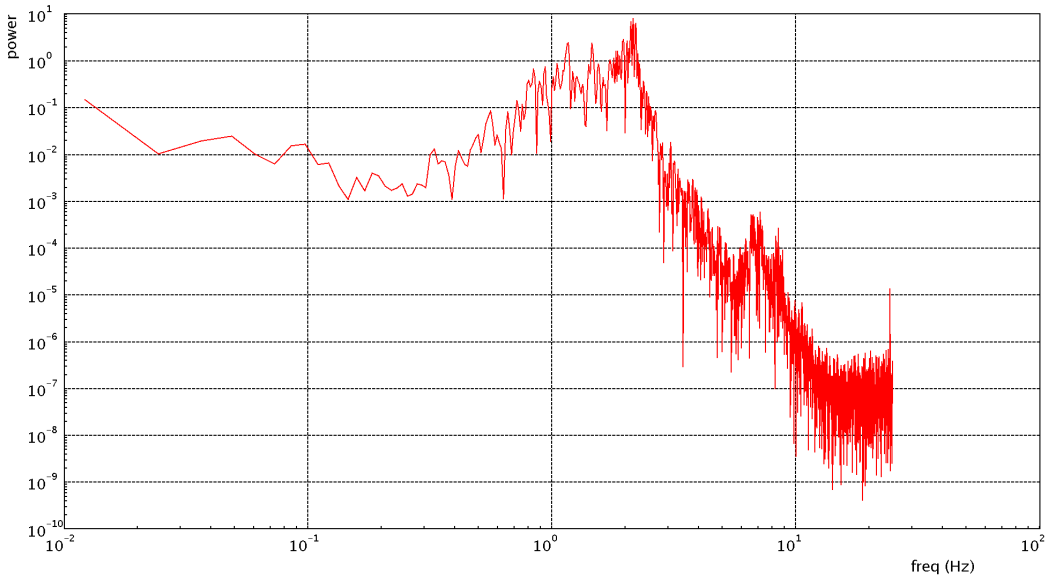

Figure 11.10. The spectral decomposition of the x displacement based on the average of the motion of all 8 particles and computed using a fast Fourier transform. The graph presented is illustrative of the ***`spectral`*** *view of a* ***`scalar 1D field`****.*

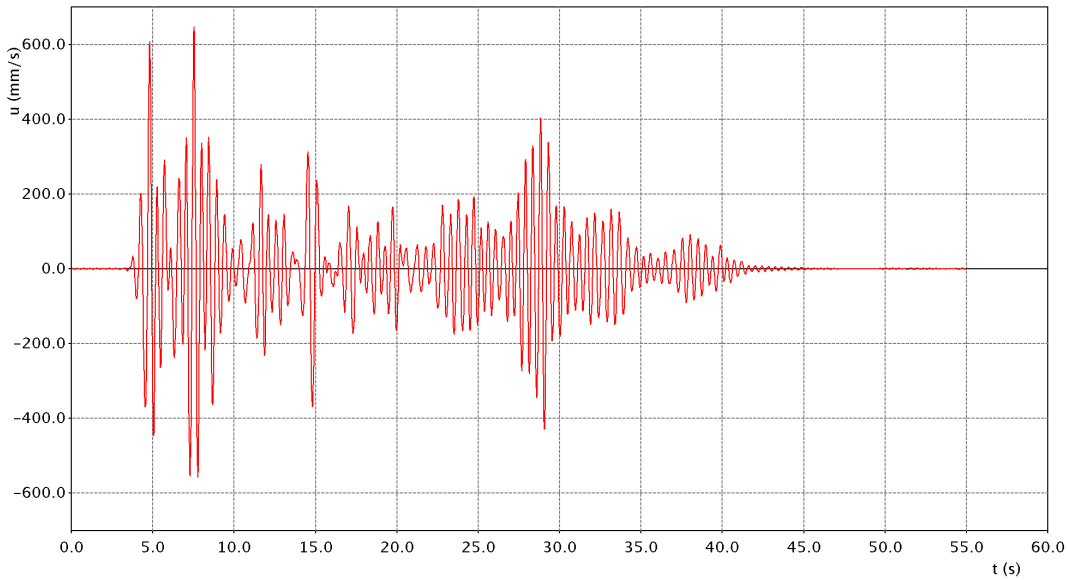

Figure 11.11. The x velocity field obtained by differentiating the x displacement field in a ***`tablet`*** *using the* ***`Differentiate`****() function. The displacement field was approximated locally by a quadratic function fitted in a least squares sense using the 5 points surrounding each data point.*

11.6 Summary

The first case study has illustrated the particle tracking analysis process for a simple problem of measuring the bulk motion of a single mass. Any internal deformations have been neglected. Appropriate tools have been introduced, rationalised and applied. The result has been an impeccable set of particle matches and a displacement time history with an accuracy better than ±0.05mm. The system accuracy has exceeded the baseline expectations reasoned in chapter 2.

12. Case Study 2: Lock exchange gravity currents

12.1 Introduction

The second case study contrasts markedly with the first. It arises from an experimental programme in fluid mechanics aimed at measuring the internal velocity field of a gravity current propagating along a smooth, horizontal boundary. Instead of the very small number of particles deployed in case study 1, this experimental system requires hundreds, or thousands, of particles in order to be able to capture a velocity field for which spatial gradients, in certain regions, are very strong. In case study 1 the particles remained visible throughout the experiment, and it was a modest task to produce flawless particle tracks. In this fluid flow particles will enter and exit the light-sheet as they move, and many will only remain within the camera's viewing window for a short period of time. Therefore, in this case study we encounter sterner challenges in the particle tracking process.

Before considering the analysis in detail let us first provide the reader with a brief introduction to **gravity currents**. These flows occur in natural environments, driven by small differences in density between two fluid bodies. One could imagine a fluid region that is at a lower temperature, or perhaps contains more dissolved or suspended material, than an adjacent fluid body. These variations in heat content or material composition cause the densities of the two fluids to differ, and when these fluid bodies are horizontally adjacent to one another this variation in density will lead to pressure gradients that cause the fluids to move. These flows are termed gravity currents. The well-known sea-breeze that occurs in the summer months, is an example of a gravity current. Here the air above the land is less dense than that above the adjacent sea due to the fact that the land heats more rapidly than the sea due to the incident solar radiation. Thus a gravity current occurs as the denser sea air moves onshore beneath the lighter landward air.

Gravity current experiments in the laboratory often employ the **lock exchange** configuration for current generation. The detailed experimental setup will be explained in section 12.3, but here we will provide a brief qualitative explanation and introduce the flow regime in which we are primarily interested. Consider a long narrow flume (tank) that has a short portion at one end partitioned from the rest of the flume with a vertical barrier (gate). This short section is known as the lock. The long section of the flume is filled with fresh water while the short section, behind the gate, is filled with salt water whose density exceeds that of the fresh water by an amount $\Delta\rho$. The experiment is initiated by the rapid withdrawal of the gate. The salt water experiences a buoyancy force that drives the fluid beneath the lighter fresh water in the form of a gravity current propagating along the smooth, bottom boundary. This gravity current initially propagates in what is referred to as the slumping regime, until it has travelled a distance of approximately ten lock lengths. During this regime the front of the current travels at a constant speed and, in the frame of reference of the front, it

appears to be in a quasi-steady state. The current possesses a characteristic flow structure with an identifiable leading head and a following tail. The head is deeper than the tail and exhibits strong interfacial disturbances known as Kelvin-Helmholtz instabilities or billows. It is the current behaviour in this moving frame of reference that is of interest to us in this study.

12.2 Analysis overview

This case study, due to its complexity, will provide us the opportunity to employ a greater variety of analysis tools. During the analysis process the following tools are covered:

1. *Image pre-processing*: The `Bayer`, `remove background`, `and amplify filters` will be used.
2. *Particle identification*: The `single threshold monochrome PID` will be employed for particle identification.
3. *Particle tracking*: Particles will be tracked using `PTV analyses` based on the `distance`, `pseudo-correlation`, `local velocity` and `recent velocity costings`. Both global optimisation and residual optimisations will be employed.
4. *Field creation*: A `velocity field time series` will be created.
5. *Field transformation*: The `velocity field time series` will be transformed into the moving frame of reference of the current front, and suitably non-dimensionalised.
6. *Field analysis*: `Tablet` functionality will be exploited to interpolate the time-averaged velocity field onto a more suitable grid, and to extrapolate it to the flow boundaries, thus yielding a velocity field that is valid throughout the entire flow domain.

12.3 Experimental setup

The experimental lock exchange setup is illustrated in figure 12.1. A 520cm long Perspex flume, with a horizontal bed, was installed in an experimental darkroom. The flume was partitioned in the manner described in section 12.1, with a vertical, stainless steel gate located 100cm from the right hand end of the flume. The lock region, to the right of the gate, was filled with salt water, while the longer partition was filled with a fresh water/ethanol solution, both to a depth, H, of 20cm. The quantities of salt and ethanol were selected to provide a density difference between the two fluids of approximately 0.5%, while at the same time ensuring that the refractive indices of the two fluids were matched.

The densities of the two fluids were measured accurately using an Anton Parr DMA5000 density meter. For the experiment described here the density difference was 0.00516 g/cm^3.

Cenedese, Nokes and Hyatt (2016) provides further details of the experiments.

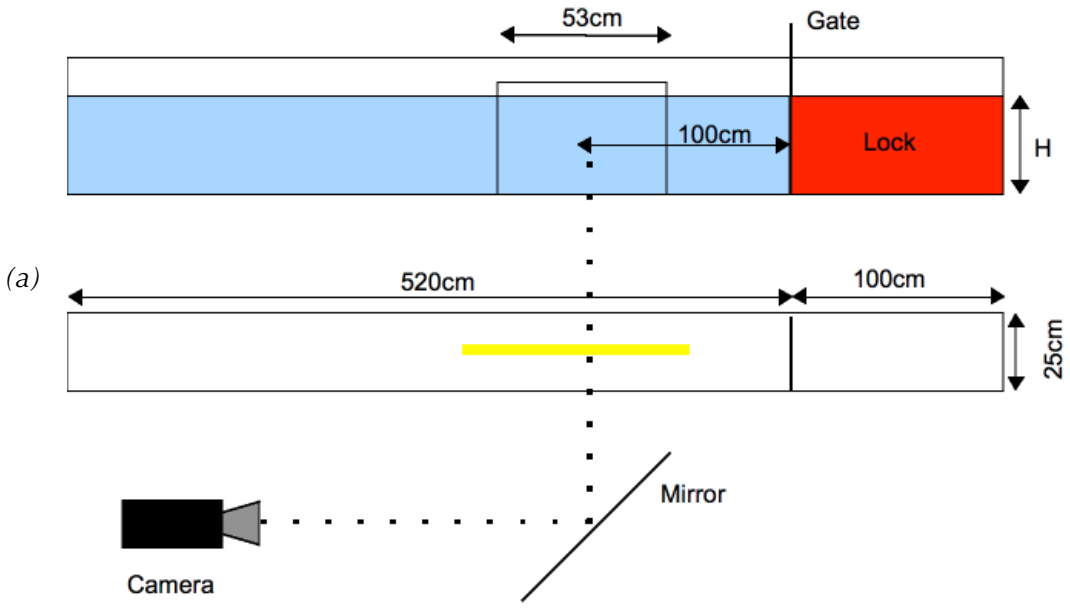

Figure 12.1. A schematic of the experimental setup. (a) An elevation view of the experimental flume showing the location of the gate 100cm from the right hand end of the flume. The blue shaded region corresponds to fresh water with added ethanol to ensure the refractive index of the fresh water matched that of the salt water, shaded in red. The two regions were filled to a depth of H (20cm). The camera viewing window is the rectangular region centred 100cm to the left of the gate. (b) A plan view of the flume. The camera is mounted in such a way as to view the flume through a mirror mounted at 45° to the flume wall. This increased the effective distance from the viewing window, and hence avoided issues associated with non-linear mapping between pixel and physical coordinates (see section 4.1.5). The yellow band indicates the light-sheet generated by a linear array of LEDs mounted above the flume (not shown).

12.3.1 Particle tracking system

Fine pliolite particles were added to both the ambient fluid to the left of the gate, and to the dense fluid within the lock. The volume of particles chosen was based on the expectation that approximately 2000 particles would be visible in the light-sheet. They were introduced to the two fluids using the slurry technique described in section 3.2.1.3.

A JAI BB141GE video camera with a zoom lens, and capturing images at 30.13 Hz, was used to record the particle motion. The 1392x1040 pixel images were transferred directly to a solid state drive on a PC during image capture. Each colour image was in raw Bayer format. The camera was mounted approximately 800cm from the flume in order to avoid lens distortion that could arise if the lens angle of view was too large. Because of the physical dimensions of the darkroom the camera needed to be mounted alongside the flume such that it viewed the flow via a vertical mirror mounted near, and at 45° to, the flume wall. The mirror was located so that the camera's viewing window was centred 100cm to the left of the gate, and the zoom lens was adjusted so that the viewing window was approximately 50cm wide. This arrangement is illustrated in figure 12.1.

Lighting was provided by a light-sheet generator comprising a 1.5m long linear array of LEDs mounted above the flume. The light-sheet generator created a vertical sheet of light, approximately 1cm wide, along the centreline of the flume. As the length of the light-sheet was significantly longer than the viewing window, the light intensity was acceptably uniform along its length. Temporal variations in intensity were negligible.

Before an experiment began the camera was calibrated by capturing an image of a stainless steel ruler placed along the centre of the light-sheet. From this image a scale factor from pixel to physical coordinates was obtained. For the experiment analysed here this factor was 0.382 mm/pixel.

An experiment was initiated once all ambient motion in the flume, produced by the filling process, had decayed to an acceptable level. The room lights were extinguished, the light sheet turned on, the gate was rapidly removed and image capture commenced.

12.4 Analysis guide

Following the approach taken in chapter 11 we will now take the reader through the various steps of the analysis pipeline, explaining the strategies employed and the results obtained. The experimental images can be downloaded from figshare© using the following DOI.

https://doi.org/10.6084/m9.figshare.14569227 (file size: 368Mb)

12.4.1 Image pre-processing

Figure 12.2 shows a raw image captured by the JAI camera. As the image is primarily monochrome the impact of the Bayer format is somewhat obscured. If the image were a single colour, such as green, then the image would look like a fine chequerboard as only every second pixel would have a measurable intensity. The pixel intensities have been amplified by a factor of two to enable the particles to be more clearly seen.

The light intensity is relatively uniform across the image, although there is some variability in background intensity – highlighted by the visibility of the current. While it may be possible to minimise the degree of pre-processing and work with the raw images we will illustrate some of the tools available by utilising the `remove background filter`. The aim of this `filter` is to reduce the background intensity to near zero everywhere in the image, thus leaving the particles distinct from their surrounding pixels. To be strictly correct, the image must first be converted into a true colour image using a `Bayer filter`. This `filter` performs the colour interpolation described in section 4.1.1. A `filter pipeline` incorporating firstly a `Bayer filter` and secondly a `remove background filter` using a 5 pixel region to compute the average intensity of the background for each pixel, produces an image that is hard to discern with the naked eye. Therefore an `amplify filter` is added to the `filter pipeline` to enable the particles to be more clearly seen. An image showing the results of this `filter pipeline` is displayed in figure 12.3.

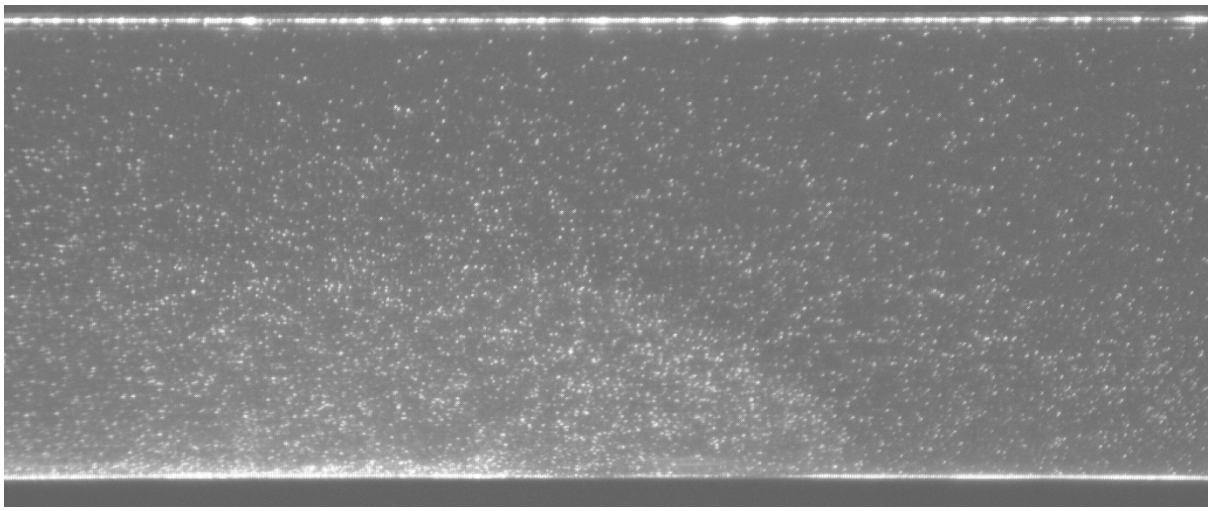

Figure 12.2. A raw image of the gravity current passing through the camera window – apparently travelling left to right due to the mirror. The image has been trimmed top and bottom to remove extraneous regions and the pixel intensities have been amplified by a factor of 2 to improve clarity.

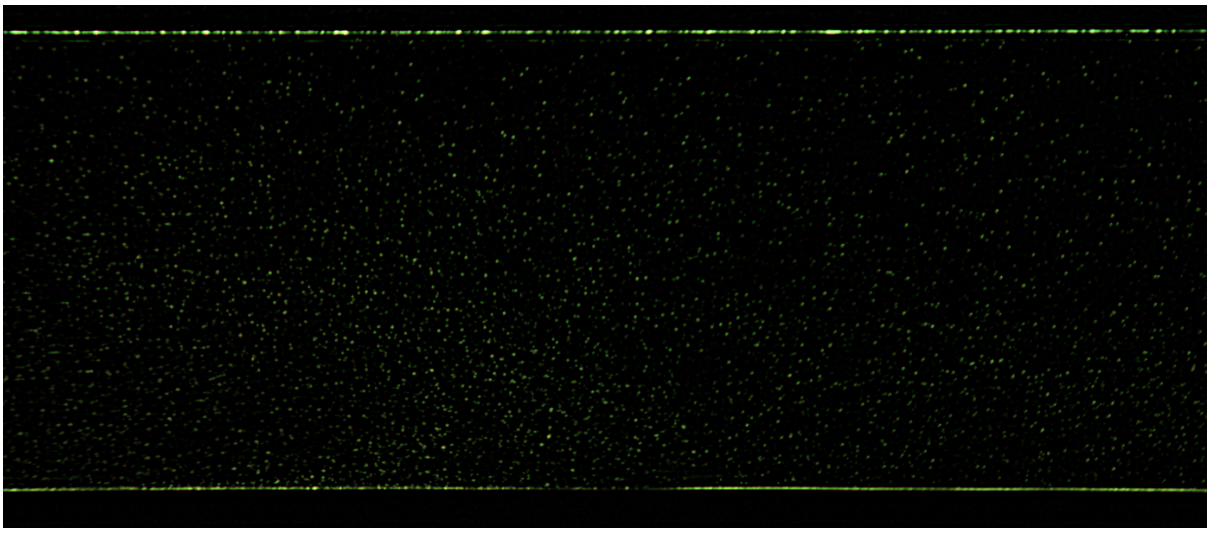

Figure 12.3. A filtered image using the **`Bayer filter`**, **`remove background filter`** *and* **`amplify filter`**. *The purpose of the* **`Bayer filter`** *is to convert the image to true colour. As it has not been calibrated for white balance the combination of the red, green and blue intensities is arbitrary. Hence the greenish tinge. This could be eliminated by varying the gains applied to each colour channel until a monochrome image is obtained. The* **`remove background filter`** *averages the intensity in a 5x5 pixel square centred on each pixel and subtracts this intensity (colour by colour) from the intensity of the pixel itself. Due to the small size of the particles this process results in background pixels having an intensity close to zero, while the particle pixel intensities remain measurably above zero. Finally, the* **`amplify filter`**, *with an amplification factor of 5 (note, only a factor of 3 was used in the actual pre-processing – the factor of 5 is used here simply for visualisation purposes), increases the particle pixel intensities so that they are visible to the naked eye. Note that this image is not of the same frame as that displayed in figure 12.2.*

To summarise, the `filter pipeline` is as follows:

`Bayer filter`
`Remove background filter` – solid square of 5x5 pixels used for averaging.
`Amplify filter` – amplification factor of 3 (5 is used in figure 12.3).

12.4.2 Particle identification

Particle identification for fluid flows of this nature is inherently less certain when compared to the simple system analysed in case study 1. These uncertainties arise from the fact that the analyst has no benchmark against which to test the resulting `particle records`. In case study 1 each frame in the image sequence included eight particles, and a check on the correctness of the identification of those particles was a simple matter using the `particle record match summary` and `particle views`. In this fluid flow the particles number in the hundreds, or thousands, and the exact number in each frame is unknown. In addition, as is clear in figures 12.2 and 12.3, the particles are not uniform in intensity or size, even after the image pre-processing. The reasons for this are manifold, including different particles lying within different regions of the light-sheet and particles having a range of sizes. The impact of this variability is that the sets of particles identified by the particle identification algorithms will be dependent on the choice of `PID` parameters.

This uncertainty requires the analyst to adopt a different mindset when undertaking the particle identification phase, and use of the various quality assurance measures discussed in section 8.3.1 becomes imperative. The key principle here is that there is no "correct" outcome from the particle identification process. Different parameter choices will lead to different `particle records`, and the validity of a particular `particle record` should be judged solely on the quality assurance metrics previously discussed – small variability of particle numbers between frames, clear particle tracks, and strong temporal coherence. While different particle identification algorithms may lead to different `particle records`, if the parameter selections have been made wisely, it is possible, in fact it is likely, that all of these `particle records` will be of high quality. At times there is an argument for verifying the robustness of the particle identification and tracking processes by analysing a number of different `particle records` through to the generation of the final field data. In theory, the final field should be independent of these preliminary processes. A failure to find a congruence between the final field data generated from the different `particle records` should lead the analyst to question the reliability of the previous steps for one or more of these records.

A `monochrome single threshold PID` is used to identify the particles in the pre-processed images. Its parameters have been discussed in detail in section 8.3.2.1. For this experiment the following parameters are used:

Intensity calculation – Average of all colour guns (greyscale).
Threshold – 50.
Minimum diameter – 0.5mm.
Maximum diameter – 2.5mm.
Maximum aspect ratio – 2.0.

The quality of the resulting `particle record` can be qualitatively appraised by considering figures 12.4 and 12.5. In the first, the number of particles identified in each frame is plotted against the frame number. Two important features of the graph are noteworthy. Firstly, the variability of particle numbers between consecutive frames lies within the general guidelines of no more than a few percent. Secondly, the number of particles in each frame shows an increasing trend up until frame 500. This behaviour is consistent with the observation that the current fluid is particle rich compared with the ambient fluid – an artefact of the initial seeding process. Once the current has propagated across the viewing window, at around frame 400, the particle numbers stabilise and then gradually drop once again as the current tail, shallower than the current head, begins to pass through the viewing window.

The second figure, figure 12.5, is taken from the `particle view` of the `particle record`. It simultaneously displays the particles from five frames, beginning at frame 239 (t = 7.93s) when the front of the current is a little over halfway across the viewing window. The display of multiple frames provides the user with a strong sense of the coherence of the particle motion. A careful inspection of the figure indicates many tracks comprising five particles following a smooth trajectory. Gaps within such tracks would indicate particles appearing and disappearing, but this, in general, appears to be relatively uncommon.

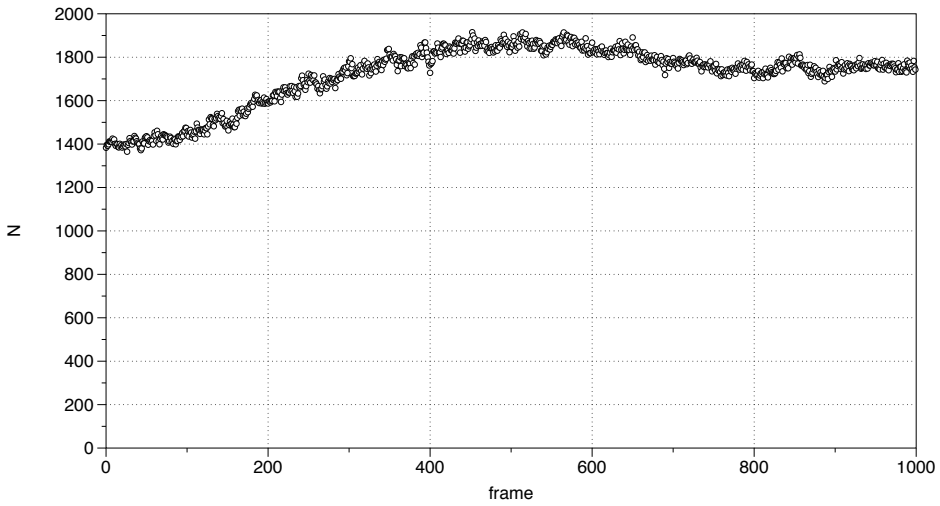

Figure 12.4. The number of particles identified in each frame, N, plotted against the frame number. There were 1000 frames in the particle record. Small variations in N are seen from frame to frame, with a slow variation of N with time that is consistent with the fact that the current fluid possessed a higher particle density than the ambient fluid. Note spurious particles were eliminated before producing this figure.

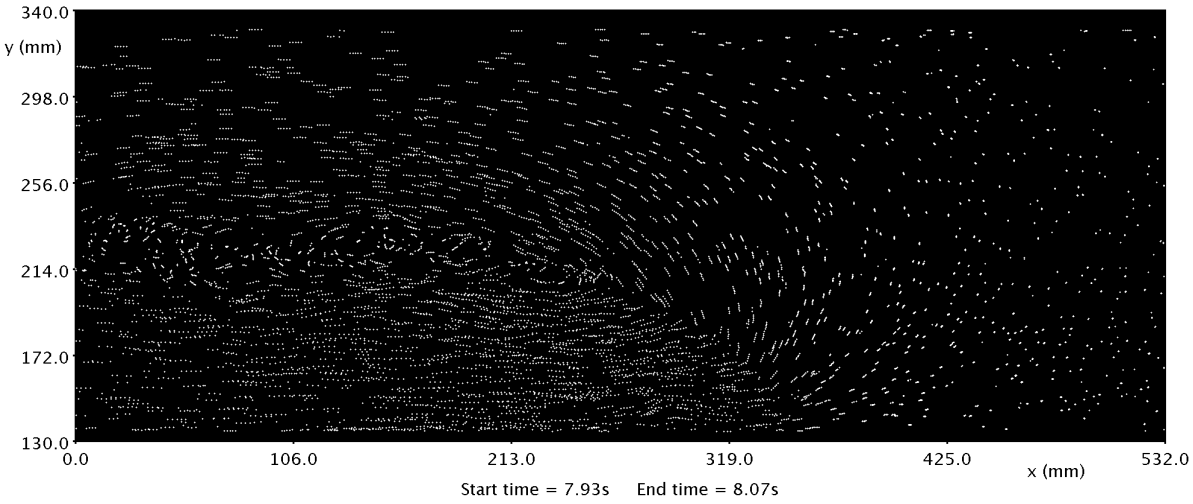

Figure 12.5. The particles in frames 239-243 overlaid in the ***`particle view`*** *of the* ***`particle record`****. The quality of the identification process can be judged by the large number of particle tracks containing 5 particles – one from each of the frames.*

It is reasonable to conclude, based on the evidence presented in figures 12.4 and 12.5, that the particle identification process yields a `particle record` suitable for particle tracking. However, let us reiterate. A different set of `PID` parameters, or even a different `PID` altogether, could generate a `particle record` with different numbers of particles, that still demonstrates a comparable level of quality, and the reader is encouraged to experiment with the data to satisfy themselves that this is, in fact, the case.

12.4.3 Spurious particle removal

The identification of spurious particles is almost inevitable considering the strong light reflections from the free surface and flume bed seen in figure 12.2. These boundary regions are easily isolated using the manual tools available. In the `particle view` of the `particle record` the analyst can use the drawing tools to select the spurious particles for elimination and choose the appropriate editing command from the available popup menu. By displaying all of the frames simultaneously the spurious particles for the entire `particle record` can be removed at one stroke.

12.4.4 Particle tracking

Particle tracking for this flow is not trivial. Particles are densely arrayed across the physical domain and the data presented in section 12.4.2 makes it clear that particles are appearing and disappearing between frames. This is reinforced by a perusal of figure 12.5 in which there are regions where particles do not form smooth trajectories comprising one particle from each of the five frames on view. All of these elements are inherent in systems designed to measure internal fluid velocities.

However, a strategy for approaching complex problems of this nature has been laid out in section 9.4, and illustrated in figure 9.5. This strategy constitutes an iterative process whereby a series of particle tracking algorithms are applied, in each case followed by a quality assurance assessment to determine whether the latest set of matches is accurate and complete. In this way the analyst is not required to design a definitive analysis strategy at the start of the process, but instead they are at liberty to adapt their approach depending on the outcome of the previous iteration. We adopt this approach here. Ultimately four different `PTV analyses`, each within its own `PTV analysis pipeline`, are employed and the result is a set of particle matches in which the analyst can have a high level of confidence.

Before embarking on these analyses the analyst needs to extract two important quantities from their data. The first is the largest particle displacement between frames, Δ_{max}, as this guides the choice of dimensions for the `search window`. The second is the typical inter-particle distance, d_p, or alternatively, the particle density, ρ_p (number/mm^2). This second measure is helpful in defining parameters for `costings` that use neighbouring particles to compute the cost. We have discussed two of these previously, the `pseudo-correlation costing` and the `local velocity costing`, and both of these will be employed here.

The largest particle displacement can be found from the `particle record particle view`. Two frames can be displayed simultaneously and the region and time of maximum particle displacement can be found visually. An inspection of this `particle record` suggests a maximum particle displacement between frames of approximately 2.5mm in the horizontal, and a somewhat smaller value in the vertical. It is also noted that both positive and negative velocities in the *x* and *y* directions are present, so the `search window` needs to be centred on the particle. From these observations it is possible to select a `search window`, including a factor for uncertainty, that is 7mm wide, 4mm high, and centred on the particle.

The typical inter-particle spacing, and particle density, can be estimated from the number of particles in a frame and the physical size of the fluid region under observation. From figure 12.4 we can deduce an average particle number of 1600. The area of the region under observation, *A*, is given by

$$A = W \times H = 520 \text{ mm} \times 200 \text{ mm} = 106{,}400 \text{ mm}^2 \tag{12.1}$$

Thus, the particle density is

$$\rho_p = \frac{N}{A} \approx \frac{1600}{106{,}400} = 0.015 \text{ mm}^{-2} \tag{12.2}$$

and the typical particle spacing is given by

$$d_p = \sqrt{\frac{1}{\rho_d}} = \sqrt{\frac{1}{0.015}} = 8.2 \text{ mm} \tag{12.3}$$

The first `PTV analysis` must include a state-based costing. Our candidates are the `distance` and `pseudo-correlation costings`. The performance of the first, and simpler, of the two costings is dependent on the ratio of Δ_{max} and d_p, which for this `particle record` is

$$\frac{\Delta_{max}}{d_p} = \frac{2.5}{8.2} = 0.30 \qquad (12.4)$$

This ratio is less than one, but not greatly so. Therefore we expect the `distance costing` to perform moderately well, but still likely to produce a noticeable number of incorrect matches. The `pseudo-correlation costing` is expected to perform more robustly than the `distance costing` provided a suitable window is chosen. This window, which determines the surrounding particles that contribute to the particle pattern used in the correlation calculation, needs to be large enough to include roughly ten particles. Given the inter-particle spacing a window of dimensions 40 mm x 15 mm seems reasonable, although this is certainly a parameter the analyst may wish to modify and test. An explanation for why this window should be rectangular, and not square, is left until later in this section.

We trial both the `distance costing` and `pseudo-correlation costing` and compare their performances. To summarise we have:

PTV analysis 1:

Process	Global optimisation.
MMC	1.0.
Search window	7mm wide and 4mm high centred on the particle.
Costing	`distance costing` with a reference length of 5mm.

or

PTV analysis 1:

Process	Global optimisation.
MMC	0.5.
Search window	7mm wide and 4mm high centred on the particle.
Costing	`pseudo-correlation costing` with a window 40mm wide and 15mm high and radius factor of 3.

In order to compare the relative performances of the two costings we extract two bulk statistics, the percentage of particles matched in each frame, averaged over the entire record, and the average path length. Both of these statistics can be found in the `match summary view` of the `particle record`. Table 12.1 presents these statistics. The figures indicate that both `costings` were successful in matching the vast majority of the particles, and the matches led, in general, to long particle paths. By these statistics alone the `distance costing` would appear to slightly outperform the `pseudo-correlation costing`.

Table 12.1. A comparison of the bulk matching statistics for the ***distance*** *and* ***pseudo-correlation costings****. The average % matched is the percentage of particles in each frame that have been matched, averaged over the entire* ***particle record****. The average path length is the weighted average of all particle paths created by the particle matches. The weight for each path is the number of particles in the path. For example, imagine a particle record with 10 frames with each frame containing 2 particles. If one particle is matched through all 10 frames and the other particles are left unmatched, the particle record will contain 10 paths of length 1 and 1 path of length 10. Calculating the weighted average produces an average path length of 5.5.*

Statistic	Distance	Pseudo-correlation
Average % matched	89.5	83.8
Average path length	87.5	66.5

Table 12.2. Detailed matching statistics for the ***distance*** *and* ***pseudo-correlation costings*** *obtained from the* ***diagnostic view*** *of the* ***particle record*** *that has been analysed using the* ***pseudo-correlation costing****. The statistics, that are averages over all frames, are defined in the following way:*

# of matches using `pseudo-correlation costing` – *the average number of matches, per frame, for this* ***particle record*** *using the* `pseudo-correlation costing`.

# of matches using `distance costing` – *the average number of matches for the* `particle record`*, per frame, using the* ***distance costing***.

# of common matches – the average number of matches that are common to both `particle records`.

# of matches in conflict – the average number of matches, per frame, that differ for the same particle.

# of matches only using `pseudo-correlation costing` – the average number of matches, per frame, that appear only in the `particle record` using the `pseudo-correlation costing`.

# of matches only using `distance costing` – the average number of matches, per frame, that appear only in the `particle record` using the `distance costing`.

Statistic	
# of matches using `pseudo-correlation costing`	1439
# of matches using `distance costing`	1536
# of common matches	1404
# of matches in conflict	25
# of matches only using `pseudo-correlation costing`	10
# of matches only using `distance costing`	107

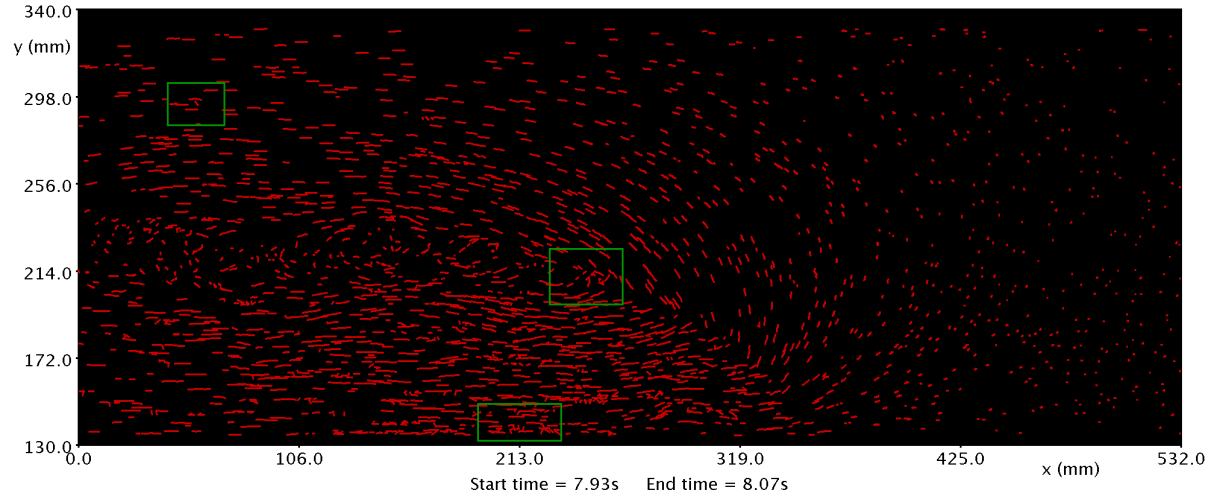

(a)

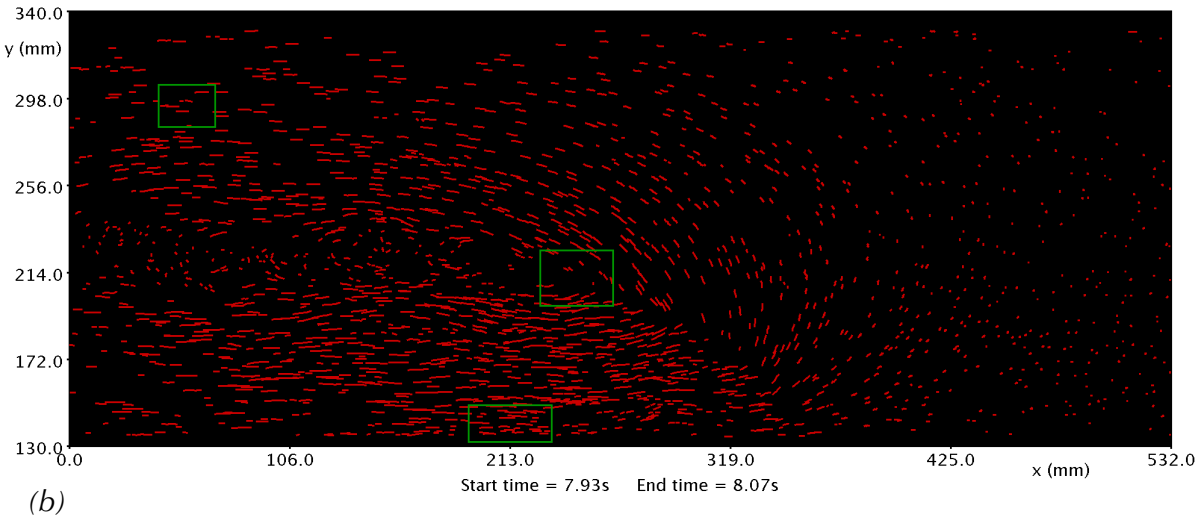

(b)

Figure 12.6. A comparison of the particle matches produced by (a) the ***`distance costing`*** *and (b) the* ***`pseudo-correlation costing`****. Particle tracks for 5 frames, beginning at frame 239, are displayed. A close inspection of the green rectangular regions will reveal discrepancies between the two* ***`costings`****, with the* ***`distance costing`*** *producing clearly incorrect matches.*

However, these statistics alone are insufficient, as they do not give an indication of the quality of the matches themselves. Thus, a more important comparison involves an inspection of the particle tracks. Figures 12.6a and 12.6b display the particle matches over five frames starting at frame 239 for the two `costings` respectively. Unmatched particles are removed to lessen the congestion in the figure. The two figures are broadly similar, and the particle matches are consistent with the particle tracks visible in figure 12.5. However, on closer inspection the reader can see clear differences between the two sets of matches. Three exemplar regions have been highlighted. These focus attention on some of the areas where the particle matches differ between the `costings` and, most importantly, they show that some matches produced by the `distance costing` are poor.

A more quantitative comparison between the two sets of matches can be acquired through the `diagnostic view` of the `particle record`. This view enables the analyst to generate a range of statistics regarding the commonality of the matches, broken down frame by frame. Table 12.2 provides a summary of these statistics averaged over all frames in the two `particle records`. The statistics demonstrate that, in fact, the performance of the two `costings` is comparable, with a very high percentage of the matches common to both. A very small number, approximately 2%, of the matches are in conflict, while the `distance costing` generates a significant number of additional matches, undetected by the `pseudo-correlation costing`.

Our intuition, based on our understanding of these two costings, informs us that the matches produced by the `pseudo-correlation costing` are likely to be more reliable than those produced by the `distance costing` given the ratio of the pertinent length scales in equation 12.3. However, the fact that this ratio is significantly less than one encourages us to expect that the matches produced by the `distance costing` will be generally good, and the statistics in table 12.2, and the particle tracks illustrated in figure 12.6, support this view.

We can proceed, confident that the particle matches generated by the `pseudo-correlation costing` provide a strong base upon which to build with further matching-based costings. As has been discussed in chapter 9, the `local velocity costing` is the most powerful of the matching-based costings available. It relies on the matches of particles surrounding a particular particle to predict where that particle will lie in the following frame. Being a matching-based costing its performance may be enhanced by its repeated application.

The second `PTV analysis` object selected uses the `local velocity costing`. The window for this costing is the same as for the `pseudo-correlation costing` used in the first analysis. It is worth explaining why the particular dimensions of 40mm x 15mm are chosen for this window. This window needs to include a significant number of neighbouring particles – we have suggested around ten. However, it also needs to be chosen to include particles whose velocities, or displacements, are similar to the particle at its centre. Thus, some knowledge of the flow structure can be helpful in choosing the dimensions of this window. Except at the front of the gravity current, the primary velocity gradients lie in the vertical direction, particularly near the interface between the two fluids. This is apparent in figure 12.6. Therefore a wise window choice will possess a larger horizontal than vertical dimension.

Through the application of the `local velocity costing` it is hoped that the number of particle matches is increased and poor matches are eliminated. These two outcomes are both dependent on the chosen `MMC`. By decreasing `MMC` a stronger requirement is placed on a potential match. Therefore as `MMC` is decreased one expects that gradually all erroneous matches will be eliminated and only correct matches remain. Decreasing `MMC` further beyond this point will not improve the quality of matches, but will reduce their number. Therefore the analyst seeks a value of `MMC` that is sufficient to remove all, or nearly all, of the spurious matches without unnecessarily reducing the total number of matches. We find that an `MMC` of

Table 12.3. The impact of `MMC` *on the performance of the* `local velocity costing`*. The two statistics are the same as those listed in table 12.1.*

MMC	Average % matched	Average path length
0.1	49	8
0.3	78	63
0.5	86	86
0.7	84	72
0.9	85	73

0.5 strikes a good balance between the number and quality of matches, although we find that the `local velocity costing` is relatively insensitive to the choice of `MMC` and performs very well over a range of settings. To illustrate the point, table 12.3 summarises the average number of matches, and the average path length, obtained from the application of the `local velocity costing` (following the `pseudo-correlation costing` already discussed) with a range of `MMCs`. We note that in all cases the quality of matches is high.

These performance results are for a particular flow so we would always encourage the analyst to explore the impact of this parameter, along with the window dimensions, in their own data analysis.

To summarise:

PTV analysis 2:

Process	Global optimisation.
MMC	0.5.
Search window	7mm wide and 4mm high centred on the particle.
Iterations	2, in alternating directions.
Costing	`local velocity costing` with a window 40mm wide and 15mm high.

In truth, the analyst might look at the results of their analysis at this point and conclude that the outcomes are perfectly satisfactory, allowing progress to the next step of field generation. The percentage of matches is high, the path length is excellent, and a visual inspection of the particle tracks indicates particle matches of very high quality. No regions, or periods, in the flow exhibit low numbers of matches, or matches of poor quality that might be a cause for concern. However, we will continue with two further analyses in order to demonstrate their use. Their impact is minimal but still beneficial to the final outcome.

The goal of further `PTV analyses` is to increase the number of particle matches without compromising their quality. As the matches produced by the `local velocity costing` are perceived as being of very high quality the application of a `recent velocity costing` might enable some particle tracks to be extended. Thus the third `PTV analysis` utilises a `recent velocity costing`.

To summarise:

PTV analysis 3:

Process	Global optimisation.
MMC	0.5.
Search window	7mm wide and 4mm high centred on the particle.
Iterations:	3, in alternating directions.
Costing	`recent velocity costing`

A final `PTV analysis` is likely to be one of two types – either a clean-up process designed to eliminate false matches, or a residual optimisation designed to extract additional matches from the particles currently unmatched. The quality of the matches in the current analysis precludes the need for a clean-up, so instead we attempt to increase the matches by applying a residual optimisation based on the same `local velocity costing` employed in the second `PTV analysis` – the reasoning being that the particle track extensions generated by the `recent velocity costing` might facilitate additional matches using the `local velocity costing`. These two costings in some ways complement one another as one, the `recent velocity costing`, is temporally based, while the other, the `local velocity costing`, is spatially based.

To summarise:

PTV analysis 4:

Process	Residual optimisation.
MMC	0.5.
Search window	7mm wide and 4mm high centred on the particle.
Iterations:	2, in alternating directions.
Costing	`local velocity costing` with a window 40mm wide and 15mm high.

Table 12.4 provides a summary of the high level matching statistics after the application of each of these `PTV analyses`. Each step brings an incremental improvement to the percentage of particles matched and the lengths of the particle tracks, but it clear that the improvements beyond the second `PTV analysis` are of marginal value.

Table 12.4. The high level matching statistics, defined in table 12.1, resulting from the application of each step in the complete particle tracking process.

Analysis – Costing – Process	Average % matched	Average path length
PTV 1 – Pseudo correlation (Global)	83.8	66.5
PTV 2 – Local velocity (Global)	85.8	87.5
PTV 3 – Recent velocity (Global)	87.5	90.3
PTV 4 – Local velocity (Residual)	87.7	90.4

12.4.5 Field generation

The Eulerian velocity field, and fields derived from it, are the ultimate objective of the experimental programme. The `create velocity 2D field` process, acting on a `particle record` in which particles have been matched, provides the tool to create this field. This process requires the specification of a number of key parameters. These are summarised here.

- *Grid* – a uniform rectangular grid, overlaid on the flow domain. The velocity field is interpolated onto the nodes of this grid using the particle-based velocities.
- *Velocity* – specifies the method by which the velocity is computed. The analyst can specify whether a central difference approximation for the velocity is required – i.e. a particle must possess matches in both the previous and subsequent frames if it is to be used in the velocity interpolation.
- *Interpolation schemes* – specifies the interpolation schemes used to interpolate the velocity and its derivative onto the grid. A number of options are available for both. These are best understood through reading the *Streams* manuals. The default options are generally adequate. For the velocity field the default invokes the triangulation-based scheme discussed in section 10.2. For the derivative field a finite difference scheme based on the grid values of the velocity is the default.
- *Excluded regions* – lists regions within the flow domain where flow velocities are not present – for example where there is an obstacle in the flow. The velocity field at grid points that lie within any of these regions will be left undefined by the interpolation process.

For all except the grid, the default settings are adopted for all parameters in the `create velocity 2D field` process. Two considerations are taken into account when choosing the grid location and resolution. Firstly, the grid origin and dimensions are selected so that all grid points lie within the flow domain. Secondly, the grid resolution is chosen so that it is consistent with the spatial resolution of the measurement system, as determined by d_p. A grid spacing of 4mm in both the horizontal and vertical directions is selected.

Illustrations of the resulting velocity field will be left until section 12.5.

12.4.6 Field transformation

Unsteady turbulent flows, like gravity currents, pose significant challenges for the analyst. Due to the turbulent fluctuations within the flow instantaneous velocity profiles are hard to interpret. Ideally, the analyst would wish to undertake a temporal averaging process in order to eliminate the fluctuations and produce mean flow statistics. However, such a temporal average is only meaningful in steady flows where flow statistics are invariant with time. In the slumping regime of a lock exchange gravity current the flow is most certainly not in steady state in the laboratory frame of reference. However, due to the constant front speed, the flow can be considered to be

in a quasi-steady state in a frame of reference moving with the front. Therefore, the velocity data computed in the previous step will be most informative if transformed into a moving frame of reference, whilst at the same time non-dimensionalising both the independent and dependent variables.

These two transformations are undertaken, sequentially, in this final step of the analysis process. However, before discussing how to implement these transformations in *Streams*, it is first necessary to compute the speed of the front. A number of possible approaches could be adopted for this calculation. All involve ascertaining some parameter that acts as a surrogate for the front location, and tracking that parameter through time. While this is most easily done using the density field (which was measured separately in the actual experimental programme – see Cenedese et al. 2016) there are characteristics of the velocity field that are suitable for the task. At the nose of the current the ambient fluid is driven rapidly upward as the current displaces the ambient fluid in front of it. Therefore, a sharp increase in vertical velocity, near the bed of the flume, is a marker of the passing front.

Figure 12.7 displays a false colour plot of the vertical velocity as a function of time and distance along the flume, at a height approximately 20mm above the flume bed. The arrival of the front appears starkly as the bright, high intensity, band. An arbitrary value of 10mm /s is chosen as a suitable contour (displayed in dark blue) to act as a surrogate for the front. A linear least squares best fit to this contour is computed and the slope of this contour is used to determine a front speed of 47.5 mm/s.

This front speed can be compared to the results of previous studies (see Cenedese et al. 2016). The non-dimensional front speed, or **Froude number**, Fr, is defined as

$$Fr = \frac{u_f}{\sqrt{g' H}} \tag{12.4}$$

where

u_f is the front speed,
H is the fluid depth, and
g' is the **reduced gravity** defined as

$$g' = g\frac{\Delta\rho}{\rho_0} \tag{12.5}$$

where

g is the gravitational acceleration,
$\Delta\rho$ is the density difference between the fluids, and
ρ_0 is a reference density, typically that of the lighter fluid.

The Fr typically lies within the range 0.44-0.47. For this experiment it is 0.47.

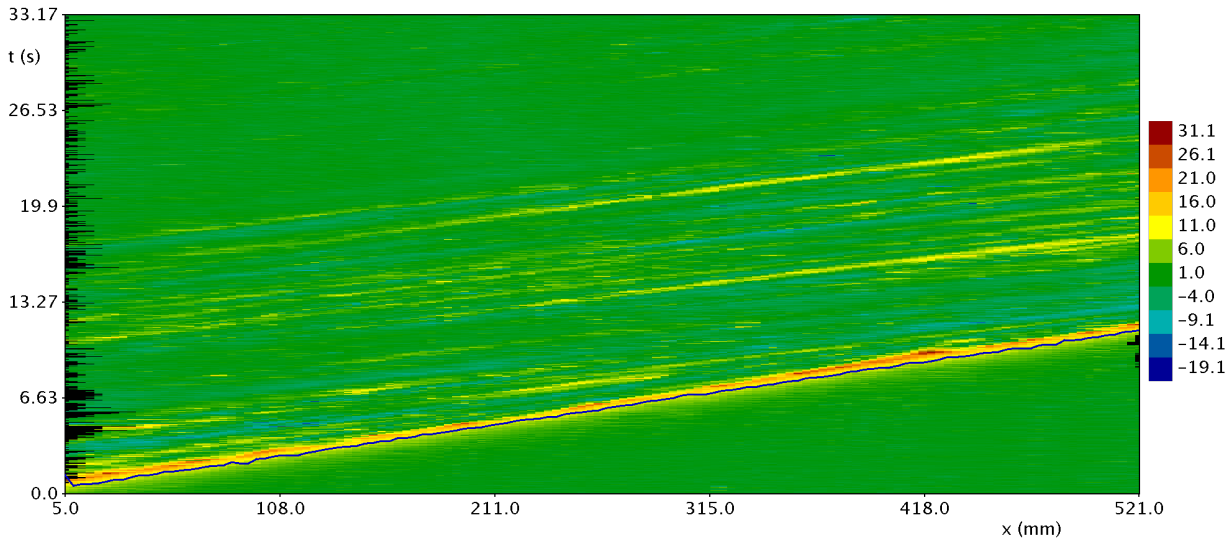

Figure 12.7. The vertical velocity, v, measured approximately 20mm above the flume bed as a function of x and t. The dark blue line is a contour corresponding to v = 10 mm/s.

With this speed in hand a `transform velocity 2D field pipeline` can be created to effect the two transformations described above. The first transform effectively moves the camera with a speed of 47.5 mm/s, thus mimicking a moving frame of reference. The second transform non-dimensionalises all variables, using the following transformations

$$x^*, y^* = \frac{x}{H}, \frac{y}{H} \qquad u^*, v^* = \frac{u}{u_f}, \frac{v}{u_f} \qquad t^* = t\sqrt{\frac{g'}{H}} \tag{12.6}$$

where all asterisked variables are dimensionless. The asterisks will be dropped in all future references. In addition, it adds -1 to all horizontal velocities to ensure they are consistent with the moving reference frame, and the vertical coordinate is shifted so that the bed of the flume lies at $y = 0$.

To summarise, the two transformations and their associated parameters are:

Constant velocity transform

x velocity	47.5	
y velocity	0.0	

Linear transform

Field scaling	0.02105	($1/u_f$)
Constant vector x comp	-1.0	
Constant vector y comp	0.0	
Spatial scaling	0.005	($1/H$)
x offset	0.0	
y offset	-0.659	
Temporal scaling	0.503	
t offset	0.0	

We propose taking the manipulation of the velocity field a step further. The reason for this is threefold. Firstly, it provides an opportunity to demonstrate some of the tools available within a `tablet`. Secondly, it is desirable to have all velocity fields computed on a standard grid with the current nose located at $x = 0$. Thirdly, the velocity data is not suitable for an extensive analysis of fluxes. As the particle field did not extend to the flow boundaries the velocity field is not defined across the entire flow domain. Therefore, if the analyst is interested in fluxes, the current velocity field is deficient.

All analysis is performed on the time-averaged velocity field. This field is computed via the `(u,v) calculator` in the steady state, non-dimensional `velocity field time series`. Once this time-averaged field is loaded into a `tablet`, three transformations are exploited.

`LTVectorField()` – this linear transformation enables the velocity field to be translated in x so that the stagnation point at the front of the current lies at $x = 0$. In addition, a subset of the velocity field is extracted as the field values on the edge of the computed domain tend to be less reliable.

`Regrid()` – this transformation interpolates the velocity field onto a standard grid, defined within the `tablet`.

`ExtrapolateVectorField()` – this transformation extrapolates the velocity field to the flume bed and the free surface. A no-slip boundary condition is imposed at the bed, while no condition is imposed at the free surface. Least squares extrapolation functions are defined for use at the two boundaries.

The final result is a velocity field that is defined on a standard grid, is valid throughout the flow domain, and has the stagnation point at the front located at $x = 0$.

12.5 Illustrative results

The results presented here will be extracted from both the steady state, non-dimensional velocity field, via its numerous `calculators`, and the standardised time-averaged velocity field computed within the `tablet`. In each case the data source will be noted.

Figure 12.8 illustrates the horizontal velocity extracted from the non-dimensional, steady state velocity field before its manipulation within the `tablet`. The top panel displays the time-averaged velocity field, possible because of the transformation into the frame of reference moving with the current front. The remaining panels, (b)-(h), provide instantaneous velocity fields at a series of different times. The turbulent nature of the flow, that is not apparent in the time-averaged field, is clear in these instantaneous snapshots. What is also clear is the impact of the shift to the moving reference frame. The observation window of the camera moves steadily left as time progresses so that only a short section of the current, roughly 2.5 units long in dimensionless coordinates, is visible at any one time. The imperfect smoothness of the

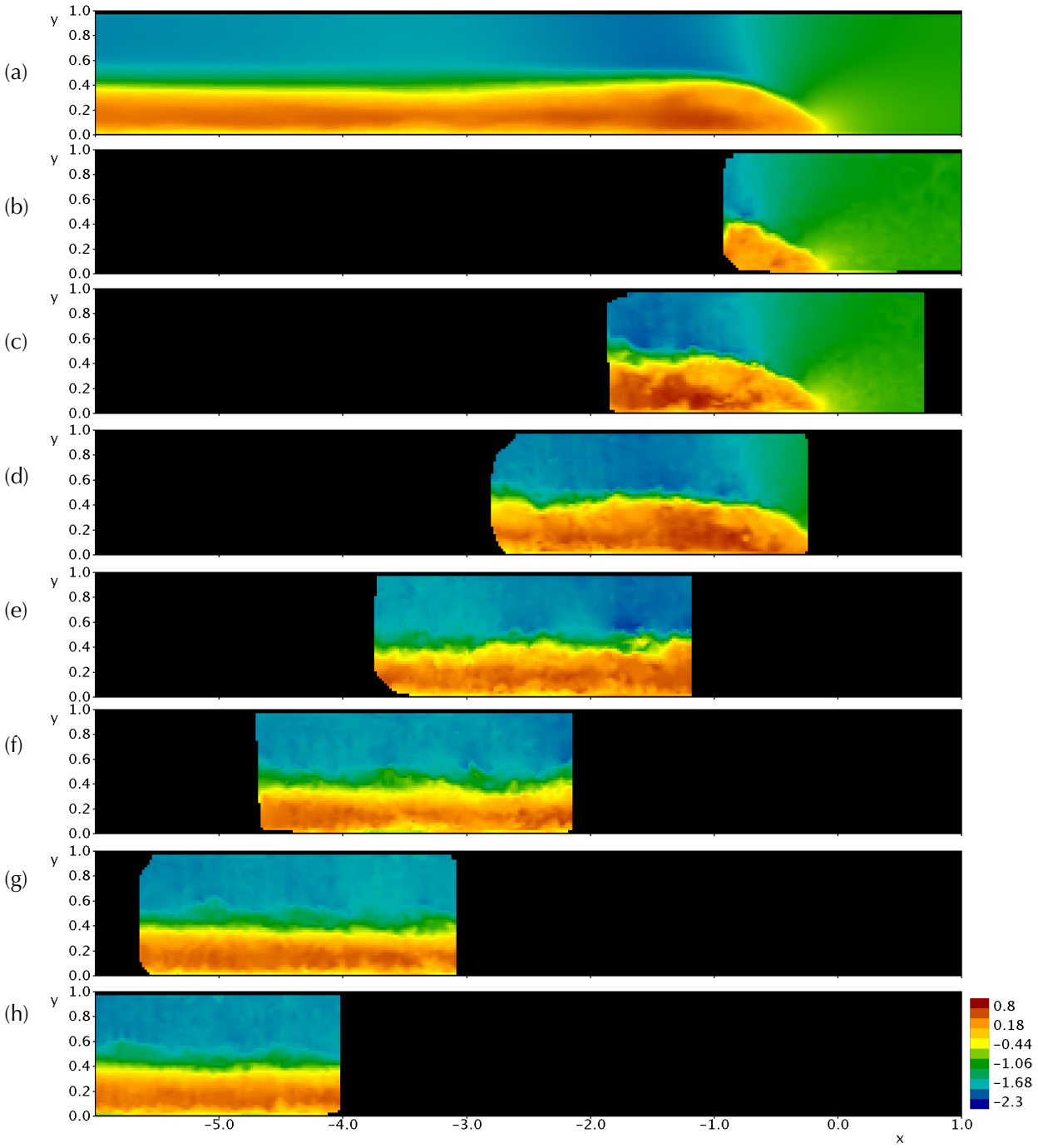

Figure 12.8. False colour images of the non-dimensional, steady state, horizontal velocity field. (a) Time averaged (b) t = 2 (c) t = 4 (d) t = 6 (e) t = 8 (f) t = 10 (g) t = 12 (h) t = 14. Because of the transformation into a moving frame of reference the camera appears to move to the left with time, leaving the current front fixed in space. The colours are defined in the legend adjacent to panel (h). Note that the current appears to move left to right instead of right to left because of the use of the mirror during image capture.

time-averaged velocity field can be partly blamed on the limited time that any section of the current is visible. Robust turbulent averages require averaging times that are long compared to the timescale, or turnover time, of the dominant eddies. In this flow, an averaging time of approximately 6 time units is insufficient, as it corresponds to only 6 eddy turnover times based on a rough estimate of the timescale of the eddies in the shear layer between the two fluids. Despite these limitations, which are due primarily to the design of the measurement system – this is an example of an experiment where multiple cameras positioned along the flume would have provided valuable additional data – the velocity field provides excellent insights into the flow structure.

Figures 12.9 and 12.10 present two further time-averaged fields extracted from the non-dimensional, steady state velocity field.

Figure 12.9 presents the vertical velocity component. The very strong uplift of fluid at the front of the current, as it advances into the ambient fluid, can be identified near the origin. The magnitude of this vertical velocity is similar to the horizontal velocity of the fluid within the current. Behind the head of the current, from x = -3 to -1.5, a weak downflow can be detected, consistent with the elevated head and the entrainment of fluid from the ambient into the current in this strong mixing region.

Figure 12.10 displays the time-averaged vorticity in the flow. Two regions of strong vorticity, or rotation, are to be expected. The first lies along the interface where the two fluids, travelling in opposite directions, generate the Kelvin-Helmholtz instabilities that drive the mixing referred to above. The vorticity in this shear layer is particularly pronounced near the head, decaying to significantly reduced levels in the tail. The second is in the boundary layer at the base of the flume. This shear region is much narrower than that at the interface, and suffers from the difficulty of resolving velocities very close to the flume bed. Even so it can be identified in the figure.

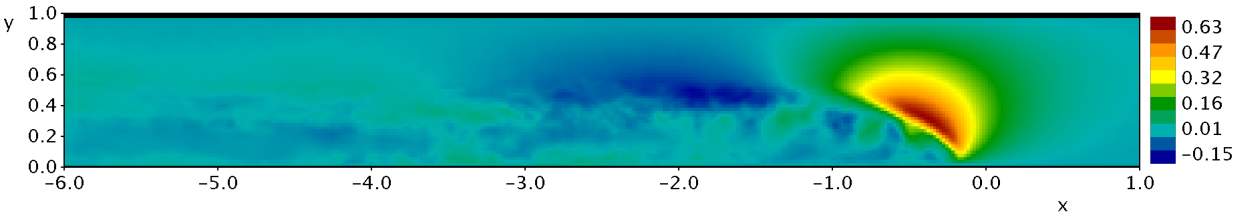

Figure 12.9. False colour image of the time-averaged vertical velocity field extracted from the non-dimensional, steady state velocity field. The averaging time is insufficient to produce a smooth mean field.

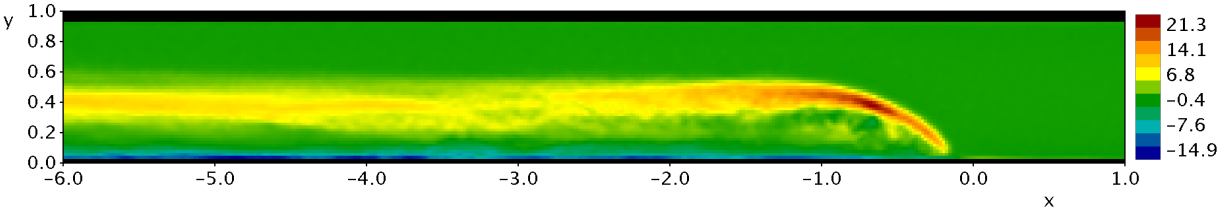

Figure 12.10. False colour imag of the time-averaged vorticity field extracted from the non-dimensional, steady state velocity field. The averaging time is insufficient to produce a smooth mean field.

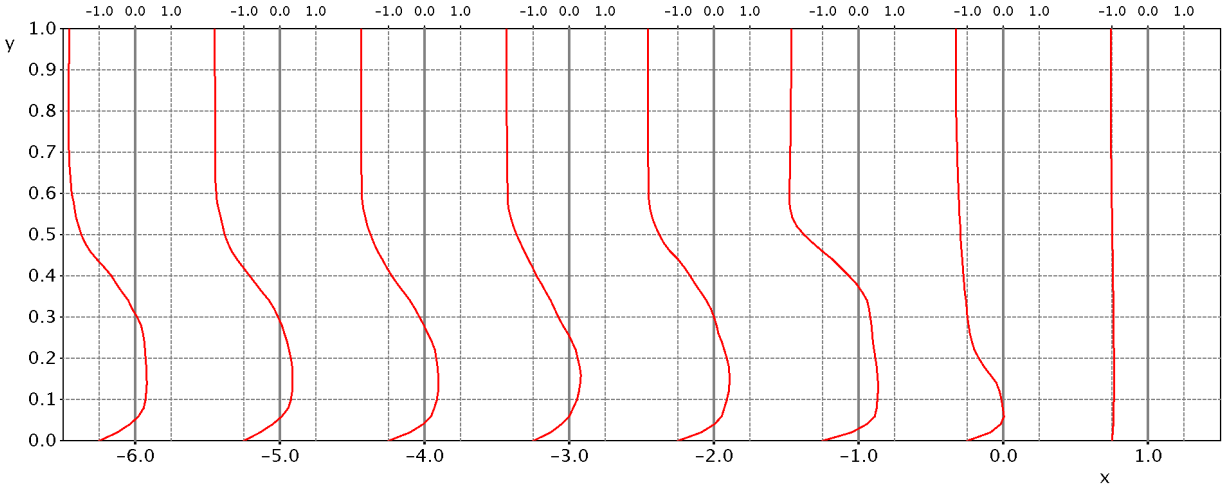

Figure 12.11. Vertical profiles of the time-averaged horizontal velocity field extracted from the transformed velocity field. The value on the x axis indicates the location of the profile, while the scales at the top of the figure indicate the value of the velocity in the profile.

Finally, an example of the output from the field resulting from the tablet transformations is illustrated in figure 12.11. Profiles of the time-averaged horizontal velocity are presented at a number of locations along the *x* axis – remembering that the stagnation point at the front of the current lies at $x = 0$. These profiles can be viewed as vertical slices through the time-averaged velocity field, similar to that presented in figure 12.8a. The difference is that the velocity field in figure 12.11 has been extrapolated to the flow boundaries so that fluxes can be computed. The no-slip boundary condition in the moving frame of reference corresponds to a velocity of -1 at the flume bed, while the linear extrapolation used at the upper boundary extends the approximately constant ambient velocity to the free surface. The profiles are surprisingly smooth considering the limitations of the time averaging previously discussed.

12.6 Summary

This second case study has exposed the reader to a considerably more complex measurement system than that discussed in chapter 11. A full, two-dimensional, internal velocity field has been measured by a particle tracking system employing nearly 2000 particles. The analysis process has been guided by the general advice provided in chapters 8-10 and the result is a set of high quality matches with approximately 90% of all particles matched, and with an average path length of over 90.

Despite the complexity of the flow, and the challenges presented by the appearance and disappearance of particles between frames, a sound analysis strategy, combined with an eye to high quality assurance standards, has delivered reliable and accurate velocity fields. The computation of higher order quantities such as vorticity is generally challenging, and often the quality of the velocity fields can be judged by the reliability of these derived fields – as evidenced by figure 12.10. The primary limitation in the

dataset analysed in this case study is the inadequate time scale over which turbulent averaging can take place – the result being fields that still exhibit a lack of spatial smoothness.

The unsteady nature of this gravity current flow in the laboratory frame of reference has offered the opportunity to demonstrate a number of specialised transformations that enable the velocity field to be transformed into non-dimensional form in a frame of reference moving with the current front. These transformations have been extended through a variety of `tablet` tools that have enabled the extrapolation of the measured field to the flow boundaries and its interpolation onto a standard spatial grid.

13. Case Study 3: Performance of floor panels under seismic loading

13.1 Introduction

The third case study returns us to the domain of structural engineering. It considers the detailed measurement of displacement and strain within concrete floor panels, mounted in a reinforced concrete frame, subject to quasi-static loading. While the loading pattern did not precisely mimic a specific earthquake record it was designed to replicate much of the direction and magnitude content of the Kaikoura earthquake experienced in New Zealand in 2016.

This experimental programme was highly ambitious and placed serious demands on the design of the particle tracking system. A number of these demands are listed below.

- Multiple cameras were required – 18 in total – and the data from each of these cameras needed to be integrated into a global dataset.
- The cameras were, of necessity, mounted above the floor panels. This requirement presented a number of challenges including the need to ensure minimal camera movement during testing. In addition, the cameras could not be mounted far from the specimen and therefore the difficulties that arise when the cameras are relatively close to the particles being tracked were unavoidable.
- The particle tracking system was to be integrated with traditional potentiometer measurement devices. Thus these artefacts were present in the images captured by the particle tracking system.
- The quasi-static loading protocol allowed regular inspection of the panels for cracking. Cracks were highlighted with marker pen and these drawn lines also appeared in the captured images.

It is not our intent to present the full dataset from this study – it is simply too large and complex to do so. Instead our intent is to take the images from just two cameras (cameras 7 and 8) and to demonstrate the methods used to extract relevant information from them. We will also provide a commentary on a range of issues associated with the experimental design that we believe could be improved if the experiment were to be repeated.

The author acknowledges M. Parr who kindly provided some of his data for this case study.

13.2 Analysis overview

This case study, due to its complexity, will provide us with the opportunity to explore a number of analysis techniques that have not been employed in either of the previous two case studies. In particular, this case study will require the integration of particle

data from more than one camera. This integration has two components. Firstly, the mapping of data from both cameras onto a global coordinate system. Secondly the identification and handling of any relative camera movement. As will be seen, the integration process presents a number of challenges to the analyst.

During the analysis process the following tools will be covered:

1. *Image pre-processing*: A `mathematical formula filter` will be used to pre-process the experimental images.
2. *Particle identification*: The `single threshold monochrome PID` will be employed for particle identification.
3. *Calibration*: Mapping functions that will enable the data from each camera to be integrated into a global coordinate system will be computed using a specialised `tablet` function.
4. *Particle tracking*: Particles will be tracked using `PTV analyses` based on the `distance, shape`, and `local velocity costings`.
5. *Lagrangian path field creation*: `Lagrangian path fields` will be generated from the `particle records` for each camera.
6. *Relative camera motion*: Motion of the particles in the overlapping region between the two cameras will be used to determine whether relative camera movement has occurred during the experiment. A transformation will be computed for one camera and the associated `Lagrangian path field` will be transformed to remove the identified camera movement.
7. *Field creation*: A material-based `displacement field time series` will be generated from each of the `Lagrangian path fields`.
8. *Field integration*: An integrated `displacement field time series` will be created by merging the `two displacement time series` into a single time series.

13.3 Experimental setup

A full description of the experimental setup will not be provided as it is of minimal value in elucidating the design and operation of the particle tracking system. Instead, our primary focus will be on the technical demands of the particle tracking system.

Figure 13.1 provides a plan view of the specimen consisting of a two-bay, two-storey reinforced concrete structural frame. The frame consisted of six, 850mm x 850mm, columns with eight embedded hollow core reinforced concrete floor panels, four in each bay, comprising the first floor flooring system. Each column was 4580mm high with the bottom of each floor panel located 2040mm above the base of each column. The hollow core floor panels were 240mm thick with a 75mm topping. The beams connecting the columns measured 750mm deep and 450mm wide. Each bay had dimensions of 4850mm wide (east-west) and 7300mm deep (north-south), measured from the centre of the columns. Thus the total floor area was approximately 70.8 m^2.

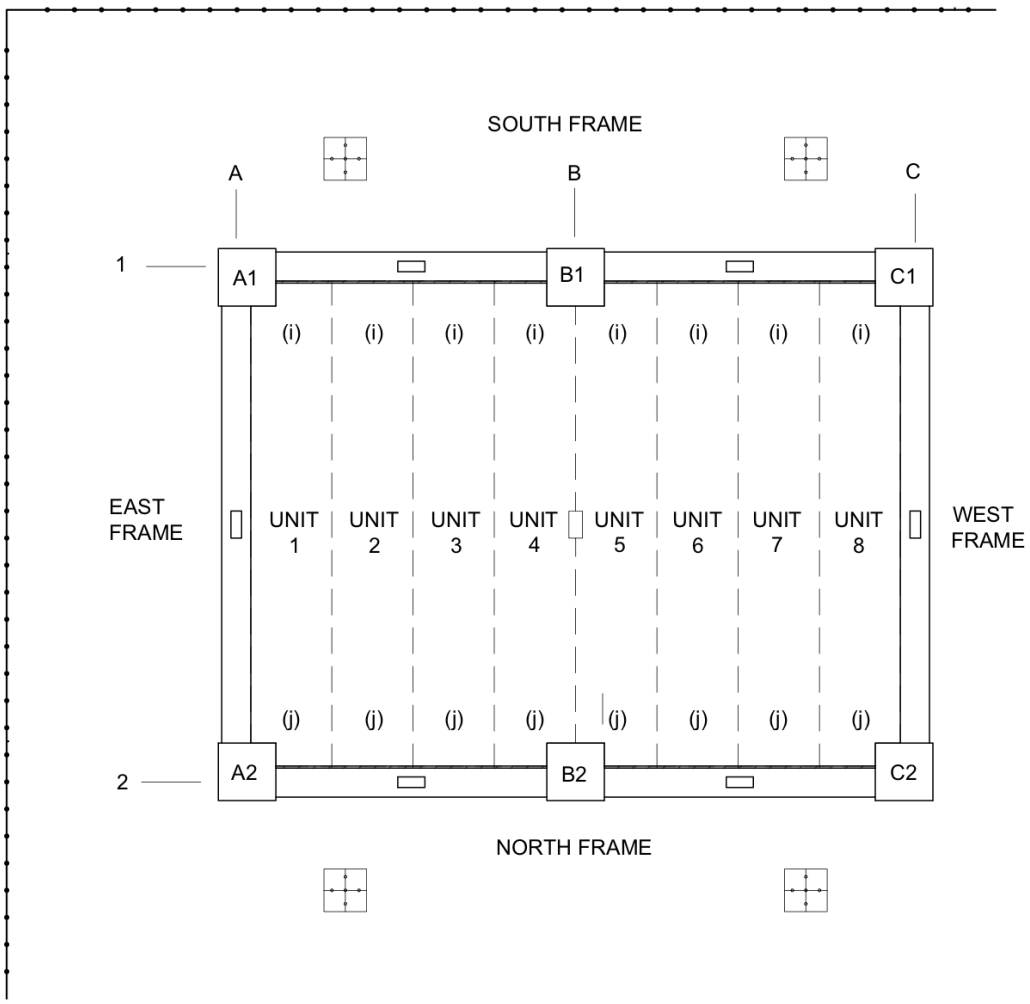

Figure 13.1. A schematic plan view of the eight hollow core floor panels mounted in a two bay, two storey reinforced concrete frame. The perimeter line corresponds to the strong wall to which the rams were connected.

A suite of static rams were connected to columns A1, A2, B1 and C1 allowing for a range of two dimensional motions. The reaction end of each ram was bolted to a strong wall indicated by the L shaped perimeter in the figure. The strong wall was assumed to exhibit minimal motion during the loading cycles.

A global coordinate system was selected such that x increased from left to right, with the origin at column A1, while y increased top to bottom (in the figure) starting at column A1. The result is a coordinate system where the z axis is downwards. This should be borne in mind when viewing the experimental results as by convention x-y plots are viewed in the negative z direction and thus the data will appear as if it is being viewed from below.

13.3.1 Particle tracking system

The objective of the PTS was to provide full coverage of the floor regions adjacent to the south and north walls of the building, together with complete coverage of the four

floor panels contained within one bay, those lying between columns A1, A2, B1 and B2. In order to meet reasonable accuracy expectations, and due to the limited height that was available for the camera mounts, 18 cameras were required to achieve this coverage. The camera coverage is illustrated in figure 13.2. Note the significant overlap (shaded regions) between the viewing areas of adjacent cameras. The value provided by these overlap regions will be discussed in the analysis section.

Fujifilm X-T2 digital cameras operating in still mode with pixel resolutions of 6000 x 4000 were selected for image capture. Each camera was connected to a triggering system that generated a pulse shortly after each loading increment had been applied. Thus, all cameras were synchronised during the loading process. All cameras operated in manual mode and were permanently connected to a mains power supply. This was necessary as the experiment lasted for a number of days.

Cameras were mounted on timber beams located above the structural assembly. It was hoped that significant camera movement would be avoided during the testing period but unfortunately no effective mechanism for measuring the absolute camera motion, and testing this hypothesis, could be devised. This issue is addressed in the analysis section to follow.

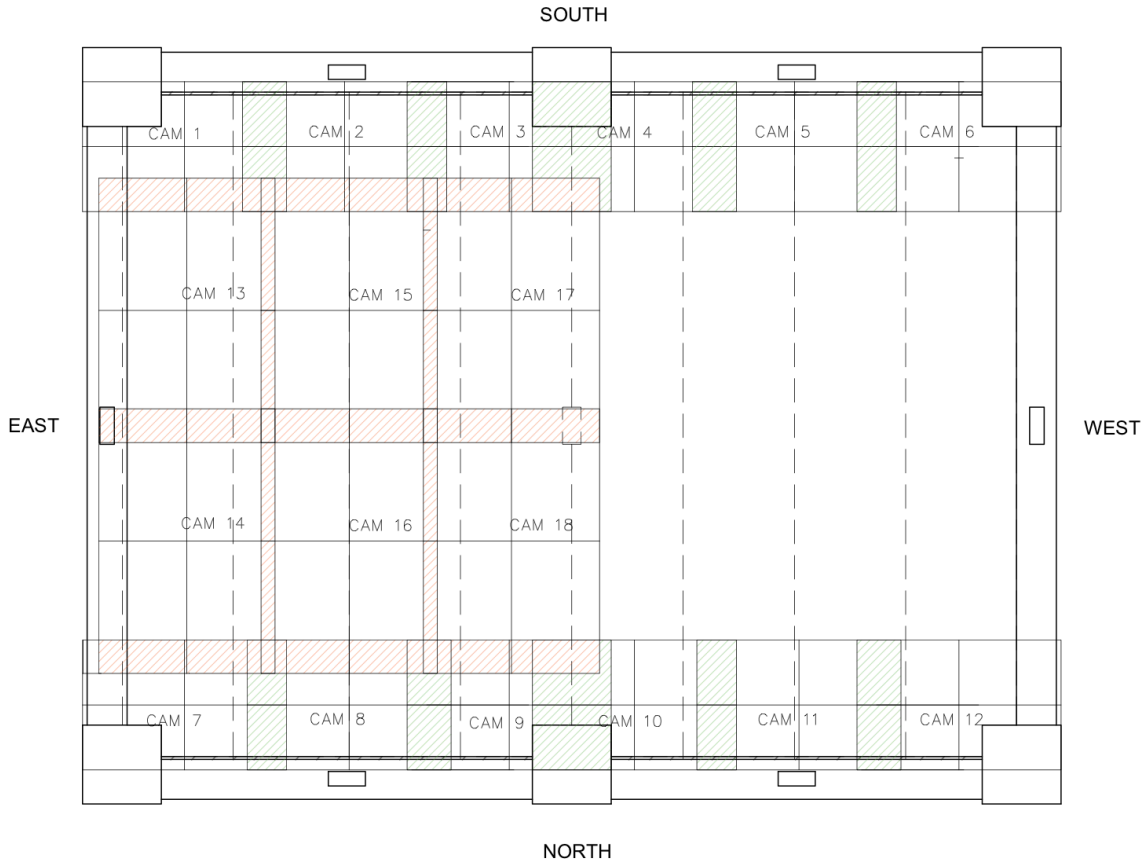

Figure 13.2. A schematic illustrating the layout and coverage of the cameras.

Calibration of a multi-camera PT system is a significant challenge. Simply using the image of a ruler in the view of each camera is insufficient for two reasons. Firstly, the particle data from all of the cameras must be integrated into a global coordinate system. Secondly, due to the limited distance between the cameras and the surface of the floor panels it was likely that a simple linear scaling from pixel to physical coordinates would be insufficient, and a more sophisticated non-linear mapping would be required.

To facilitate a suitable camera calibration a rectangular grid of lines was drawn on the surface of the floor panels – see figure 13.3. The physical coordinates of the grid line intersections (grid points) were measured using a laser range finder, and this information, together with calibration images from each camera, enabled mapping functions from pixel coordinates to physical coordinates to be deduced. The method by which this was achieved is left until the analysis section.

It is perhaps worth mentioning that if the experiment were to be repeated, improvements in two aspects of the calibration system would be sought. The first improvement would be to substantially increase the number of grid points. The purpose of this would be two-fold . Firstly a larger number of grid points would allow more highly resolved calibration mapping functions to be computed. Secondly, additional grid points could be placed closer to the extremities of each camera's image, thus reducing edge effects in the mapping functions.

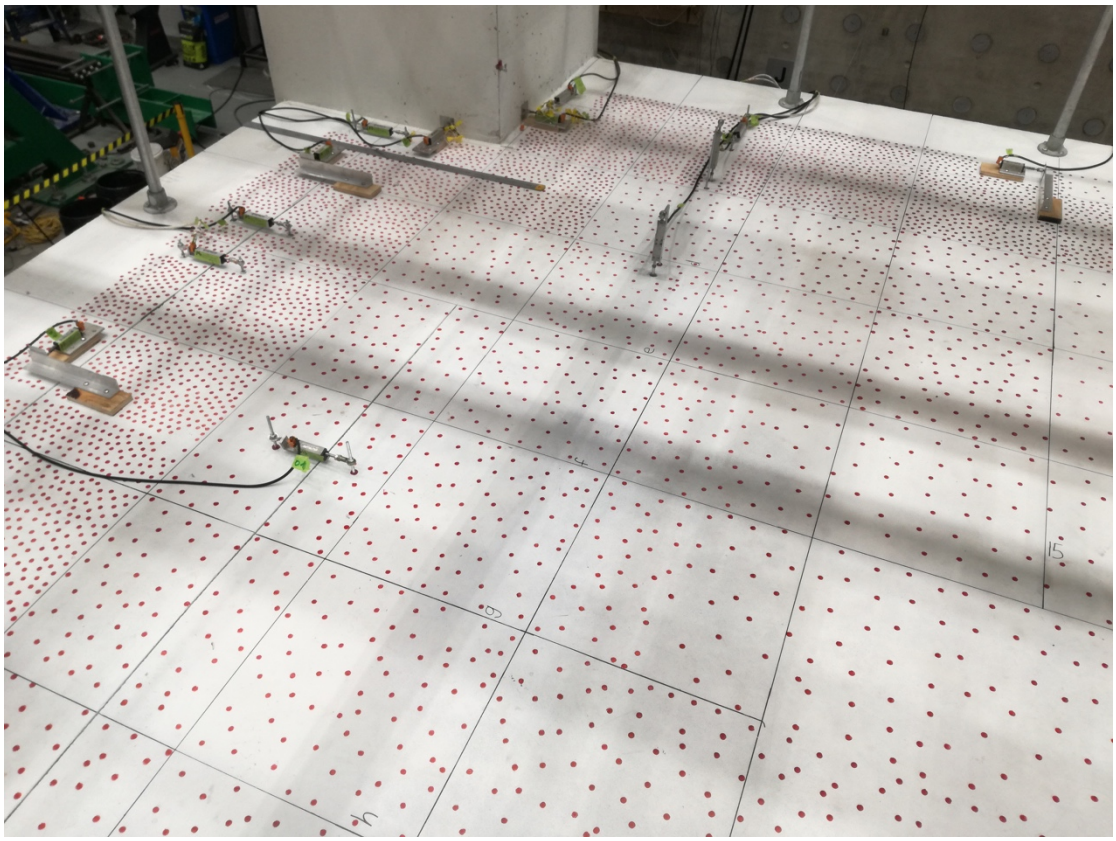

Figure 13.3. An image taken in the vicinity of column A2. The calibration grid lines are clearly seen along with the physical instrumentation.

The second improvement would be to develop procedures and tools that would increase the measurement accuracy of the physical coordinates of each grid point. There is no doubt that experiments on this scale present significant challenges when accuracy levels, comparable with the PTS itself, are desired. As will be seen, in this case, the PTS boasted spatial accuracy of approximately ±0.1mm while the calibration system exhibited uncertainties of a few millimetres.

Particles were manually applied to the surfaces of the floor panels. This was achieved through the use of red marker pens. The number of particles was very large – tens of thousands – so that the application was a time consuming process. Particle density was variable across the floor, as seen in figure 13.3. In regions where high strains were expected particle spacing was two to three times smaller than in regions away from these high strain areas.

Particle tracking for this application faced a number of challenges due to the presence of the physical measurement devices – potentiometers – and their associated cabling. In addition, the calibration grid lines and highlighted crack lines drawn by the experimenters during the course of the experiment, added extra contamination to the captured images. It was hoped that with appropriate pre-processing of the images these unwanted artefacts could be largely eliminated. For this reason the following decisions were made:

- the surface of the floor panels were painted white,
- red was the chosen colour of the particles,
- cracks were highlighted in blue,
- the calibration lines were drawn in black,
- all cabling was black or white in colour, and
- any components of the potentiometers that exhibited a reddish colour, of which there were a number, were covered with green tape.

Each one of these decisions ensured that an appropriate `image filter`, that emphasised the excess red light intensity over the green and/or blue components, would be able to successfully isolate the red particles from the surrounding background. The results of these decisions can be seen in the image in figure 13.3.

Even with this strategy in place unforeseen difficulties arose during the experiments. As the structure moved, the potentiometer cables moved across the floor. While the cables could be eliminated from the images through appropriate image processing their motion had the unintended effect of sometimes partially obscuring one or more particles. These particles would therefore appear to move because of their apparently changing size and location. Two possible solutions to this problem are discussed in the analysis section.

Lighting also posed a challenge. Due to the infrastructure associated with the camera mounts, as well as the assembly itself, significant shadows were cast across the floor panels when the building's roof lights were the sole light source. No convenient way to include additional lighting to eliminate the shadows was devised and it was ultimately

decided that the effects of the shadows would need to be managed via the image processing. The shadows are easily identified in figure 13.3.

13.4 Analysis guide

Following the approach taken in chapter 11 we will now take the reader through the various steps of the analysis pipeline, explaining the strategies employed and the results obtained. The images from the two cameras – 4500 for each - can be downloaded from figshare© using the following DOIs.

Experimental images: Camera 7
https://doi.org/10.6084/m9.figshare.14582736 (file size: 8.77Gb)

Experimental images: Camera 8
https://doi.org/10.6084/m9.figshare.14582793 (file size: 7.55Gb)

13.4.1 Image pre-processing

Figure 13.4a shows a typical image captured by camera 7. The image composition strategy described in the previous section was adopted to ensure simple pre-processing of the images, based on the assumption that the particles could be extracted using the difference between the red light intensity and the green light intensity.

A `mathematical formula filter`, that computes the difference between the red and green intensities is selected and the result of applying this filter is illustrated in figure 13.4b.

To summarise, the `filter pipeline` is as follows:

`Mathematical formula filter` – Red – green.
`Convert type filter` – Converts from real to greyscale (RGB).

It is worth noting that the positioning of camera 7 was not ideal in that edge of the floor panel, in its initial undisturbed position, extended beyond the top of the camera image. Thus, as the panel moved upwards (in the image) particles were lost from view and hence could not be tracked throughout the entire the time history of the panel motion. This resulted in a region of the panel not being available for analysis. A superior alignment of the panel in the image would correspond to that on the right hand side of the image where a significant portion of the image extends beyond the edge of the panel. In this case, panel movement to the right was captured by the particle tracking system throughout the loading cycles.

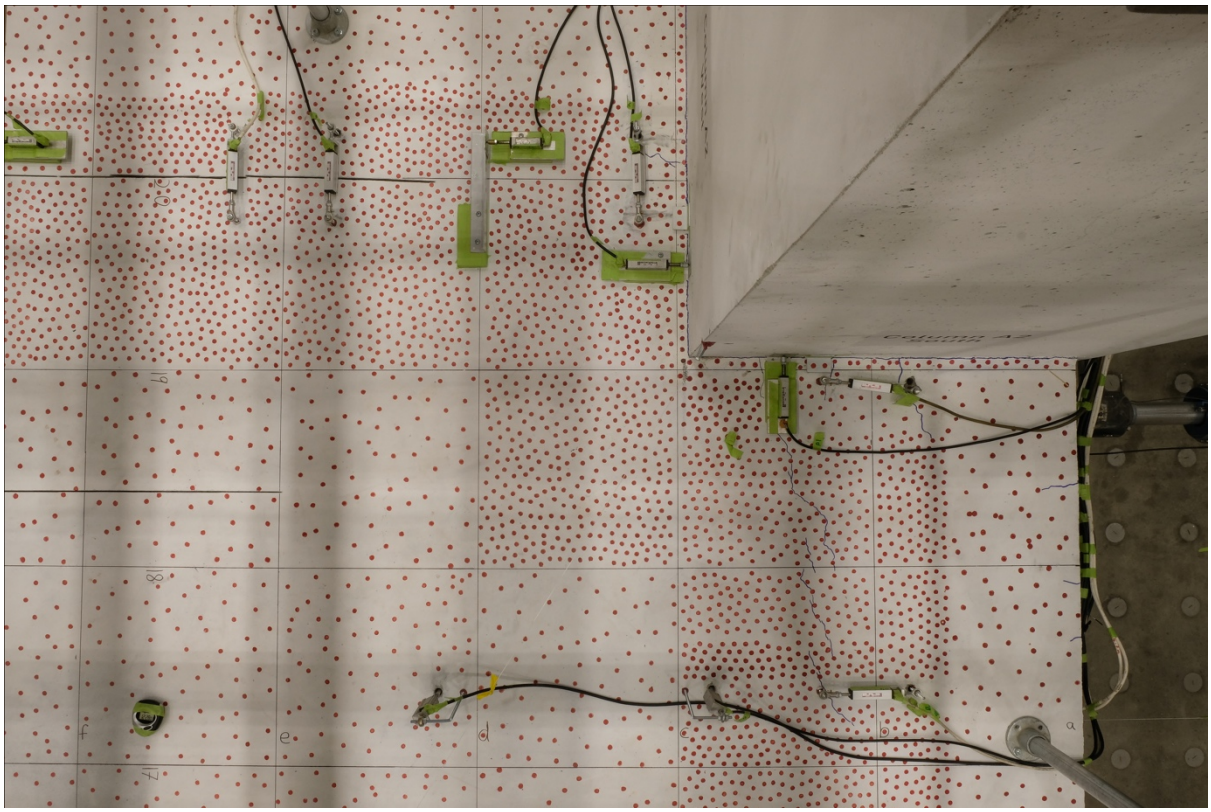

(a)

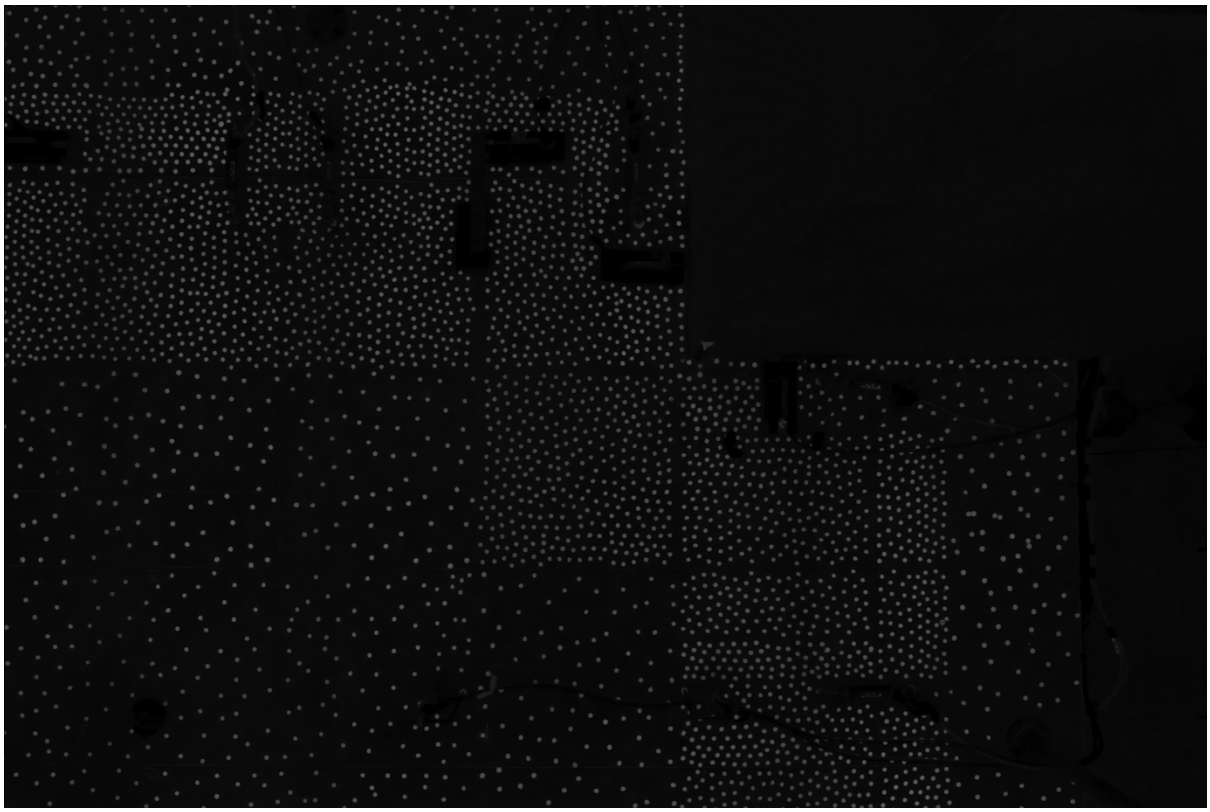

(b)

Figure 13.4 (a) A typical image captured by camera 7. Column A2 is visible. (b) The image in (a) after the application of the `mathematical formula filter`.

13.4.2 Particle identification

A standard `single threshold monochrome PID` is utilised for the particle identification process. As for most structural applications the identification is relatively straightforward as the particles generally remain in the camera's field of view for the entire experiment. In addition, due to the uniformity in size and shape tight constraints could be applied to the `PID` to ensure stray particles were not identified. The `PID` parameters varied somewhat between the cameras due to the slightly varying lighting conditions, but for cameras 7 and 8, those that will be the focus of this exposition, a common set of parameters are used.

The `PID` parameters are:

Intensity calculation – Average of all colour guns (greyscale).
Threshold – 30.
Minimum diameter – 15 mm.
Maximum diameter – 30 mm.
Maximum aspect ratio – 1.5.

Careful examination of figure 13.4(b) reveals that the cables and physical devices are eliminated from the image except where they obscure the particles themselves.

Figures 13.5a and 13.5b plot the number of particles per frame for cameras 7 and 8. It is noticeable that as the test progresses the number of particles exhibits oscillatory behaviour, with a magnitude for camera 7 that is larger than one might expect for a structural test of this nature. The cause of this can be garnered from a careful examination of figure 13.4. As the floor panels move laterally in the image, particles will move in and out of the camera frame along the left hand boundary of the image. However, on the right hand boundary, as the image extends beyond the edge of the floor panels, similar particle behaviour is not observed in this region. The result is that particle numbers rise and fall during the loading cycles depending on the direction of floor displacement. In addition, as the amplitude of the loading cycles increases with time the variation in particle numbers also increases with time.

This effect is significantly less for camera 8. Figure 13.6 shows a typical image captured by this camera. It can be seen that the floor panels extend beyond all four image boundaries. Thus the effect described for camera 7 is not present.

As we have discussed previously the variation in number of particles between frames is by no means sufficient to judge the quality of the particle identification process. An examination of the tracks themselves is essential in order to make an informed judgement. Figure 13.7 displays 200 frames, starting at frame 600 for camera 7. Across the vast majority of the figure the particle tracks are consistent and apparently complete. However, there are a few regions, often in the neighbourhood of the physical devices, where the particle tracks are not continuous.

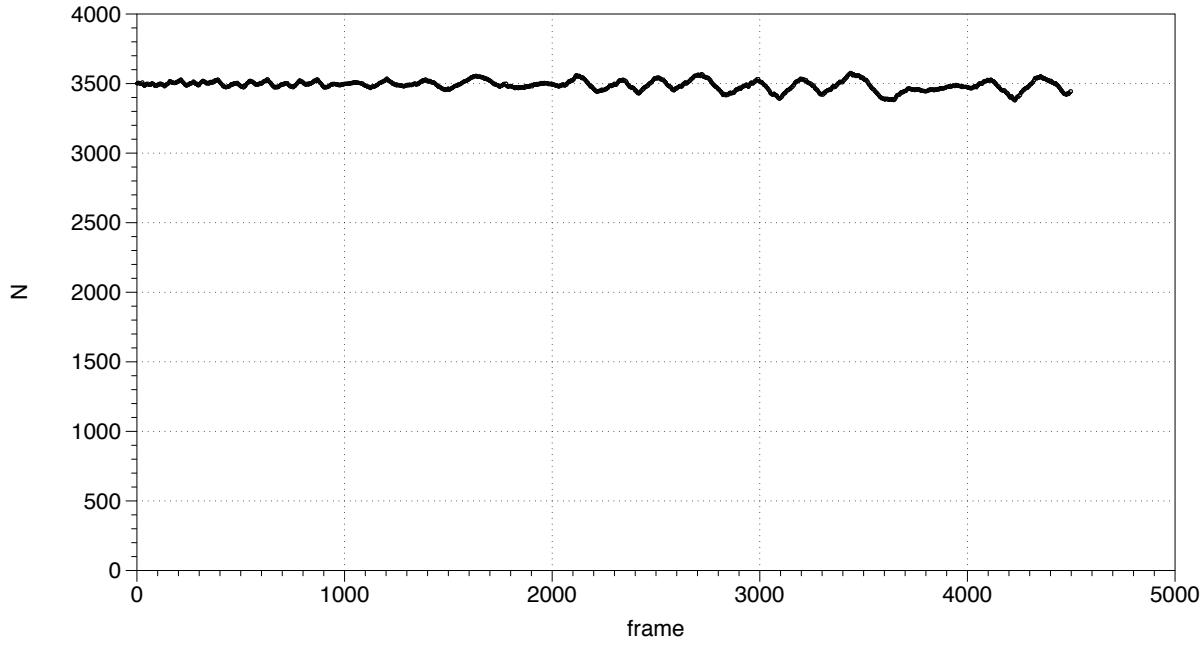

(a)

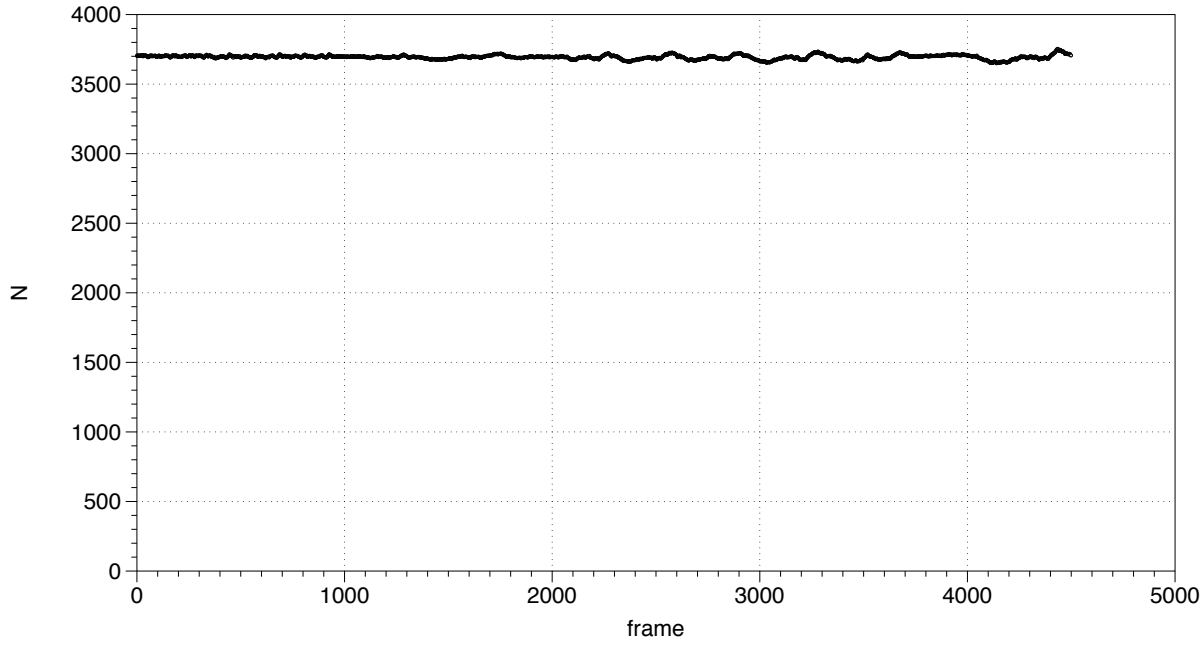

(b)

Figure 13.5 (a) The number of particles identified in each frame for camera 7. (b) The number of particles identified in each frame for camera 8.

Figure 13.6. A typical image captured by camera 8.

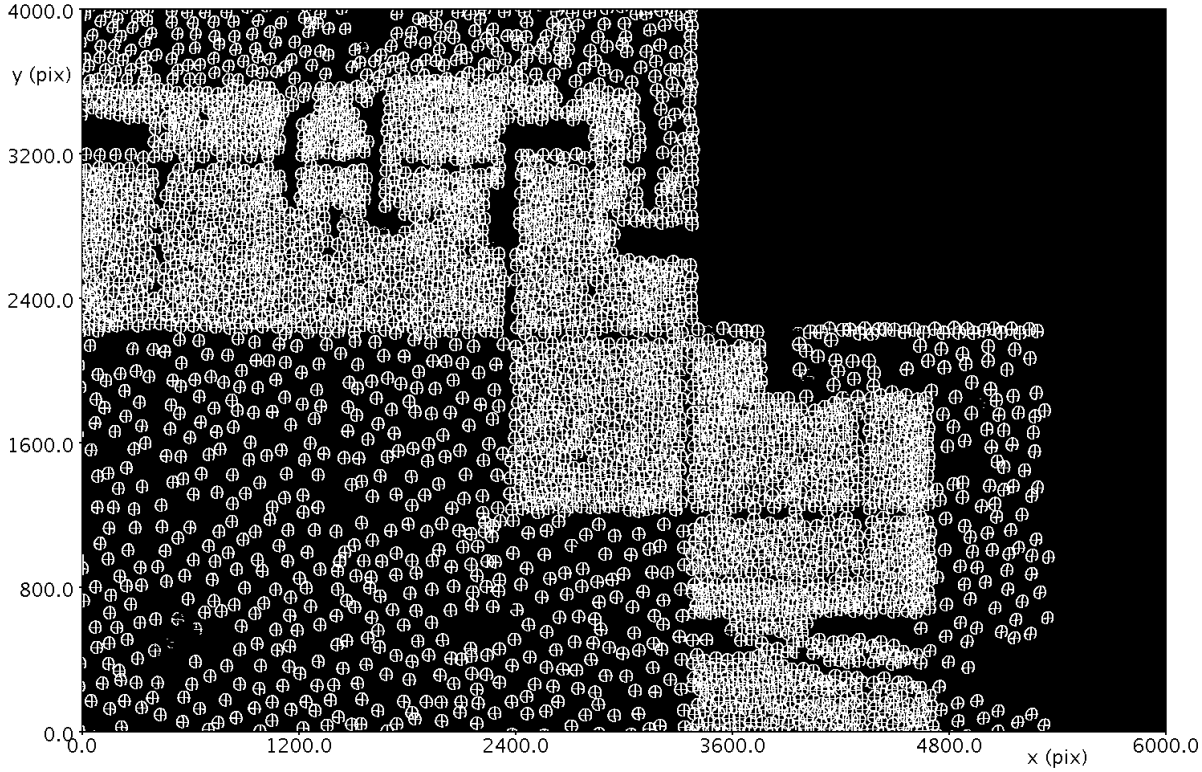

Figure 13.7. An overlay of 200 frames of particles, starting at frame 600, for camera 7. Inspections of figures such as this provide the analyst with confidence that the particle identification process is robust.

13.4.3 Spurious particle removal

Spurious particles can arise in images that capture information beyond the edge of the floor panels. For example, it can be seen in figure 13.4a that a strip along the right hand side of the image has recorded a region of the strong floor upon which the specimen was mounted. During the course of the experiment equipment, with an orange hue, was moved into this region and, not surprisingly, the `particle identifier` started to detect a small number of spurious particles in this region. As all of these particles lay outside of the domain of interest they are easily removed using the manual tools previously described. The number of particles involved is very small and their removal has negligible impact on figure 13.5a.

13.4.4 Camera calibration

Camera calibration is an important component of the analysis pipeline when multiple cameras are present. The calibration grid lines discussed in section 13.3.1, and visible in figure 13.3, provided the basis for the calibration process. Each calibration line running east-west was labelled with a number and those running north-south were labelled with a letter. Tables 13.1 and 13.2 list the physical x, y coordinates of the calibration points (given by a letter and number) relevant to cameras 7 and 8, along with the pixel coordinates of these grid points extracted from the images captured by the two cameras before the experiment began. Between 20 and 30 grid points were visible by each camera. To allow for some non-linearity in the function chosen to map from pixel coordinates to physical coordinates a two-dimensional second order polynomial was selected. Increasing the order of the polynomial to three had little impact on the fitted function.

The mapping functions for the physical x and y coordinates are computed using the `tablet` function, `LeastSquaresSurfaceFitFunction()`. This function computed second order polynomials that provided the best fit, in a least squares sense, to physical x and y coordinates as functions of the x and y pixel coordinates of the grid points. For completeness, these four functions are:

Camera 7:

$$x = 2176.64 - 0.399458x_p + 0.01324y_p - 4.5912\times10^{-7}x_p{}^2 - 4.0264\times10^{-6}x_py_p - 1.563\times10^{-7}y_p{}^2$$
$$y = 6354.1 + 3.026\times10^{-3}x_p + 0.39556y_p - 5.0155\times10^{-7}x_p{}^2 + 9.4475\times10^{-8}x_py_p - 3.3898\times10^{-6}y_p{}^2$$

Camera 8:

$$x = 4002.09 - 0.40666x_p + 0.001627y_p + 1.75283\times10^{-7}x_p{}^2 - 1.19826\times10^{-7}x_py_p - 3.3665\times10^{-7}y_p{}^2$$
$$y = 6265.81 + 0.0036526x_p + 0.40578y_p - 4.87179\times10^{-7}x_p{}^2 - 3.99568\times10^{-7}x_py_p + 2.05993\times10^{-7}y_p{}^2$$

where x_p and y_p are the pixel coordinates and x and y the physical coordinates.

Table 13.1. Camera calibration data for camera 7.

N-S line	E-W line	x (mm)	y (mm)	x (pix)	y (pix)
a	18	10	6838	5364	1208
a	19	8	7236	5344	2180
b	17	427	6438	4354	208
b	18	432	6839	4338	1202
b	19	431	7237	4326	2182
c	17	828	6440	3364	198
c	18	831	6838	3360	1192
c	19	831	7240	3356	2184
c	20	831	7631	3352	3126
d	17	1231	6440	2358	202
d	18	1235	6836	2364	1192
d	19	1232	7237	2370	2182
d	20	1233	7633	2380	3136
e	17	1635	6437	1356	208
e	18	1637	6832	1370	1194
e	19	1636	7234	1384	2182
e	20	1638	7632	1402	3144
f	17	2034	6442	366	218
f	18	2036	6836	390	1202
f	19	2034	7238	416	2182
f	20	2036	7634	442	3144

Table 13.2. Camera calibration data for camera 8.

N-S line	E-W line	x (mm)	y (mm)	x (pix)	y (pix)
e	17	1635	6437	5832	420
e	18	1637	6832	5834	1396
e	19	1636	7234	5830	2386
e	20	1638	7632	5824	3368
f	17	2034	6442	4852	414
f	18	2036	6836	4852	1392
f	19	2034	7238	4850	2380
f	20	2036	7634	4848	3364
g	17	2440	6437	3850	404
g	18	2442	6835	3850	1384
g	19	2440	7234	3852	2378
g	20	2443	7637	3844	3372
h	17	2837	6436	2868	404
h	18	2840	6833	2864	1384
h	19	2838	7232	2864	2378
h	20	2840	7638	2860	3374
i	17	3234	6434	1888	406
i	18	3236	6832	1888	1384
i	19	3234	7231	1886	2372
i	20	3235	7634	1888	3360
j	17	3638	6434	898	408
j	18	3640	6830	900	1384
j	19	3638	7232	898	2370
j	20	3640	7634	899	3356

The errors in the fitted functions are typically less that 2-3mm at each grid point. These errors are consistent with the level of uncertainty associated with the grid point measurements discussed in section 13.3.1. While these errors are small compared to the size of the physical domain they do cause problems when the particle data from multiple cameras are integrated. Particles that are observable by two or more cameras should map to the same physical location in the common coordinate system. However, due to the errors in both the calibration data, and the fitted functions, the same particle will appear in different locations depending on the camera, and these different locations may be some millimetres apart. In regions of small spatial gradients it can be assumed that these discrepancies do not cause serious problems in the computed displacement field, but in regions of high gradient this assumption may be invalid. One approach to handling this problem is discussed in a later section.

Strategies that might be adopted to improve the accuracy of the calibration process have been mentioned in section 13.3.1.

The final step in the calibration process requires the application of these mapping functions to the particle coordinates. This is achieved through the application of a `particle record transform pipeline` containing a single `map coordinates transform`. This transform applies the two mapping functions associated with a particular camera to the `particle record` associated with that camera, producing a second `particle record` whose particle coordinates are referenced to physical space.

The `overlay particle 2D records` process is a convenient method for merging two particle records into one. While the combined particle record is not a required output from the analysis process it is perhaps useful to check the merging of the two cameras as a quality control check. Figure 13.8 Illustrates the merged particle records, displaying the first frame of each.

A number of features are worthy of comment. The blue rectangle highlights the overlap region where the two cameras are observing the same set of particles. The discrepancy between the coordinates of these common particles, due to the inaccuracies of the calibration process discussed above, are not obvious. The domain captured by these two cameras is over 4m long in the x direction and nearly 2m wide in the y direction. Thus, the location errors of two or so millimetres is almost impossible to detect with the naked eye.

The intrusive nature of the physical instruments is clear. The mounting requirements of the potentiometers and other instruments leave a number of regions within the particle domain with no particle coverage. The displacement, and strain, fields will need to be interpolated within these regions.

The large, particle-free, square region in the top left corner corresponds to the column visible in figure 13.4a

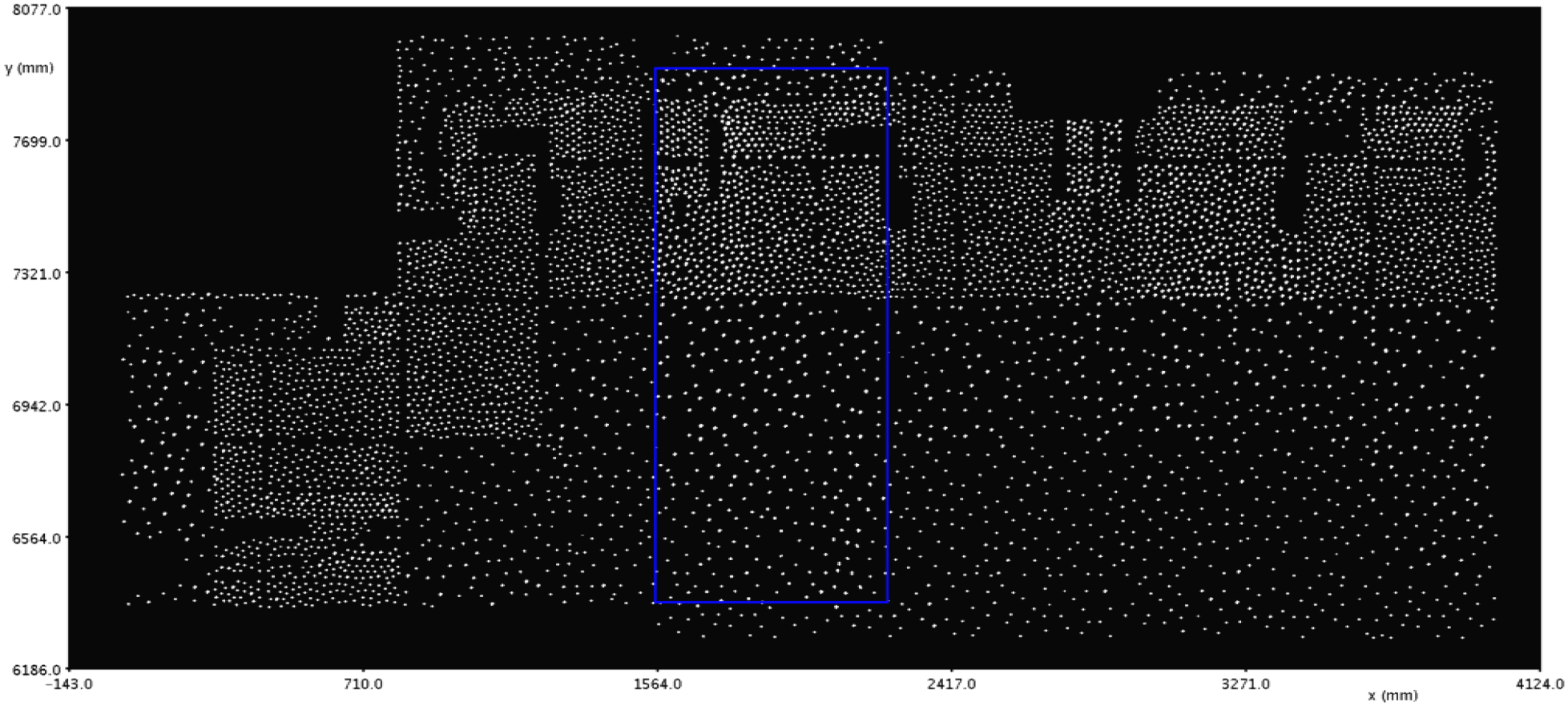

Figure 13.8. An illustration of the combined particle records from cameras 7 and 8 once transformed to the global coordinate system.

13.4.5 Particle tracking

As for most structural applications the particle tracking process is relatively straightforward. The reason for this is twofold. Firstly, the vast majority of particles remain in view throughout the experiment – the exceptions being those particles near the edges of the image that may be displaced sufficiently far that they pass out of the view of the camera – and therefore long coherent particle tracks are expected. Secondly, particle displacements between frames are relatively small even for the particle densities present in this experiment. Maximum particle displacements are of the order of a few millimetres, while inter-particle spacing, in the region of highest particle density, is tens of millimetres. Based on the reasoning provided in chapter 9 the `distance costing` should be an adequate tool for tracking the particles accurately.

In section 13.3.1 the issue of moving cables obscuring particles was raised. To address this during the particle tracking phase two additional `PTV analyses` are included. The first is a `shape costing` executed as a clean-up process. The `shape costing` uses a physical attribute of the particle – in this case the diameter – to compute the cost. The cost is the percentage change in the particle diameter between frames. A change of greater than 5% between frames is deemed to indicate that the particle had been excessively obscured and hence any match that had an associated change in diameter that exceeded 5% is removed. This costing does remove a small number of particle matches, but does not entirely eliminate the problem of the moving cables.

The second strategy employed is a `local velocity costing`. Particles that are partly obscured by an instrumentation cable exhibit erroneous movement due to their fluctuating shape. A strict `local velocity costing,` with an `MMC` of 0.05, is effective at identifying particle motion that is not consistent with that of the surrounding particles.

These features are illustrated in figure 13.9 where a small portion of frames 362 and 363 from camera 8 are displayed. A careful inspection of these images reveals that the black cable has moved to the right during the time period between the capture of these two frames, and the particle roughly in the centre of the blue rectangle, that was partially obscured by the cable in the first of the images, has become unobscured in the second. Figures 13.9(c) and (d) show the sizes of the particles within the blue rectangle for each of the frames. It is clear that the obscured particle's size noticeably changes between frames. Figure 13.9(e) shows the particle matches when the `distance costing` alone is used. The spurious movement of the obscured particle is evident. Figure 13.9f illustrates the effect of applying the `shape` or `local velocity costing`, eliminating the match corresponding to the spurious motion.

In practice, only a small number of particles are affected by the use of the `shape` and `local velocity costings`, but the elimination of local distortions in the strain field are noticeable as a result. Overall, well in excess of 99% of the particles in the `particle records` were matched.

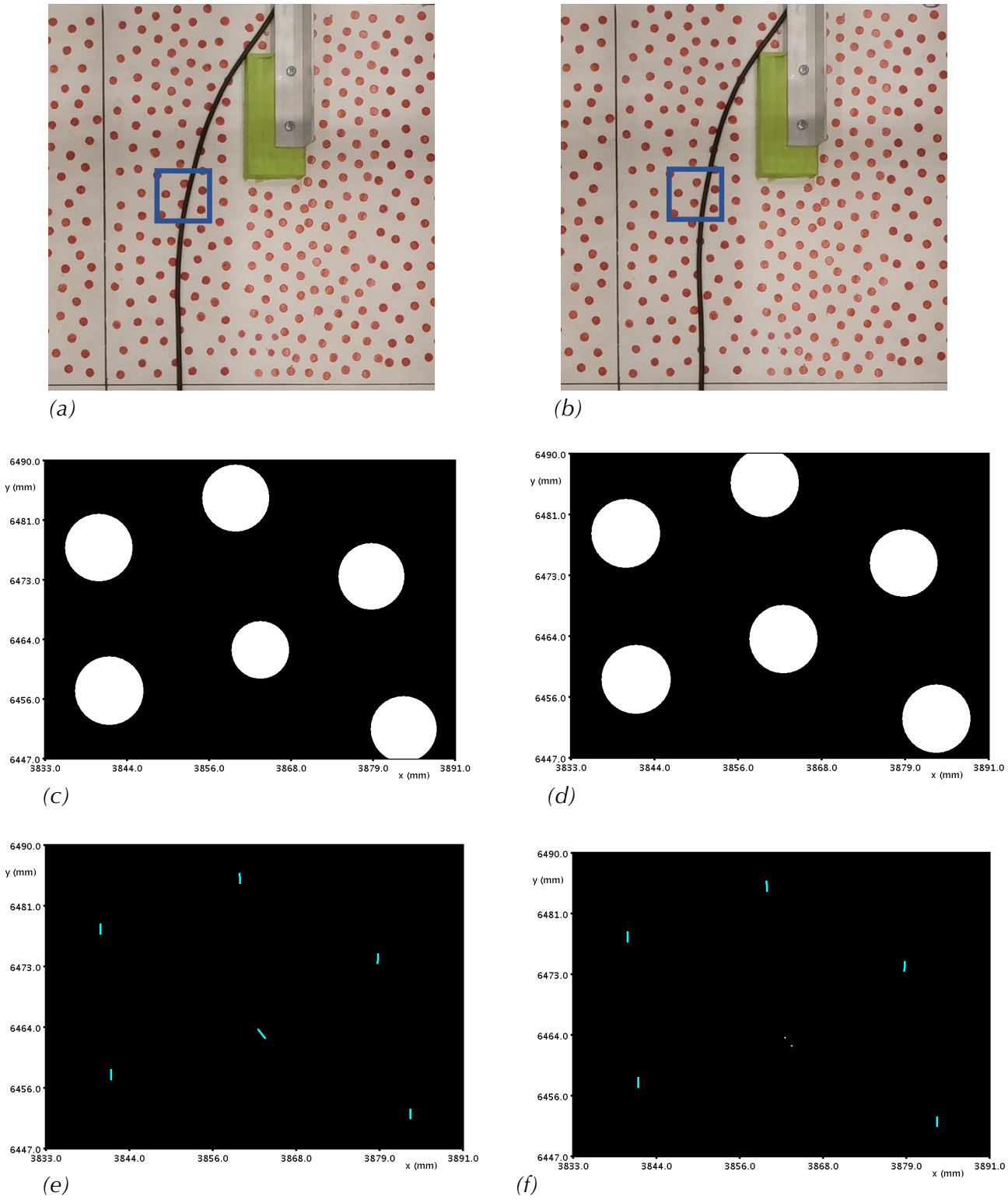

Figure 13.9. An illustration of the impact of cable movement on particle identification and tracking. (a) (b) Cut-outs of frames 362 and 363 captured by camera 8. Note the displacement of the black cable to the right between these two frames. (c) & (d). A blow-up of the blue rectangle in figures (a) and (b). The central particle, partially obscured in frame 362 experiences a size change. Note the coordinate mapping means the x axis is flipped in figures (c)-(f) relative to (a) and (b). (e) Particle matches after the application of the ***`distance costing`****. (f) Particle matches after the application of the* ***`distance costing`*** *and the* ***`local velocity costing`*** *or* ***`shape costing`****.*

To summarise:

PTV analysis 1:

Process	Global optimisation.
MMC	1.0.
Search window	10mm wide and 10mm high centred on the particle.
Costing	`distance costing` with a reference length of 10mm.

PTV analysis 2:

Process	Clean-up.
MMC	0.05.
Costing	`shape costing` with a diameter weight of 1 and all other weights set to 0.

PTV analysis 3:

Process	Global optimisation.
MMC	0.05.
Costing	`local velocity costing` with a window of 200mm x 150mm.

13.4.6 Relative camera movement

When analysing the images from a camera in a particle tracking system it is essential that any camera motion is identified and accounted for. This is particularly important when integrating the outputs from numerous cameras into a consistent global coordinate system. Ideally each camera would record the motion of a set of reference points that are known to remain stationary, relative to the chosen coordinate system, during the course of an experiment, and the motion of these points would enable any camera movement to be identified, and if need be, eliminated. This idea has been touched upon in section 4.4.

Figure 13.4a shows that a small portion of the laboratory strong floor was visible in the images captured by camera 7. The strong floor suffered no motion during the experiment and therefore any movement of camera 7, relative to the strong floor, would provide information about the movement of this camera. No reference particles were expressly placed on the strong floor and during the experiment equipment was moved into this region. However, the mounting points, corresponding to the circular regions visible on the strong floor were sufficiently distinguishable from the surrounding concrete floor to enable them to be identified by a suitable `PID`. Regrettably, due to the presence of equipment moved into this region, and the fact that the contrast between the mounting points and the floor was variable, and modest at best, these particles could not be reliably tracked through time. Even so, what was clear from the `particle record` generated through this particle identification process, was that these mounting points, when clearly visible, underwent minimal movement and it could be concluded, with some confidence, that camera 7 could be treated as stationary relative to the global coordinate system fixed to the laboratory frame of reference.

The same analysis was not possible for most of the other cameras as they included no potential reference points in their images. Therefore an alternative strategy was required. We utilise the fact that images from cameras 7 and 8 had a significant overlap (see figure 13.8). This overlap region enables the motion of particles, common to both cameras, to be compared. While these particles may not lie on top of one another due to the errors in the mapping process, their positions should remain constant, relative to one another, if the cameras suffer no relative motion.

Identification of any relative motion is most easily accomplished by generating the particle paths in the overlap region and comparing the displacements of equivalent particles as measured by the two cameras. `Lagrangian path fields` are most suitable for this purpose. The `create Lagrangian 2D path field` process, already introduced in chapter 11, generates a `Lagrangian path field` from a `particle record`. A number of parameters are available to the user to control the computation of the `Lagrangian path field`. Amongst these are:

- *Velocity* – particle velocities, or displacements, can be computed using `single estimates` – forward or backward differences can be used if central differences are not available – or `double estimates` – central differences only are used.
- *Length* – limits can be placed on the minimum and maximum path lengths that are to be included in the field.
- *Time* – the user can constrain the time at which a path must start and/or end.
- *Space* – paths can be constrained to start, end or lie within certain regions of the domain.

Particle paths, or tracks, that extend throughout the entire time domain of a `particle record` are generally viewed as highly desirable. Therefore, throughout this case study all `Lagrangian path fields` are comprised of only these, so-called, **full paths**. This is achieved by ensuring all particle paths start in frame 0 and have a length of 4500 frames. A corollary to these constraints is the need to ensure that particle displacements are computed using `single estimates` as particles in the first and last frames can never have displacements computed using central differences.

Therefore the parameters for this process are:

Particle velocity:	Single estimate
Lower length limit:	4500
Start time lower limit:	0
Start time upper limit	0
Paths must start in regions	*Rectangle containing the overlapping region*

Figures 13.10a and 13.10b provide two examples of the relative motion of the two cameras. In each case a common particle has been selected at random from the two `Lagrangian path fields` – one towards the top of the overlapping region and one towards the bottom – and its x displacement, relative to its starting position, is

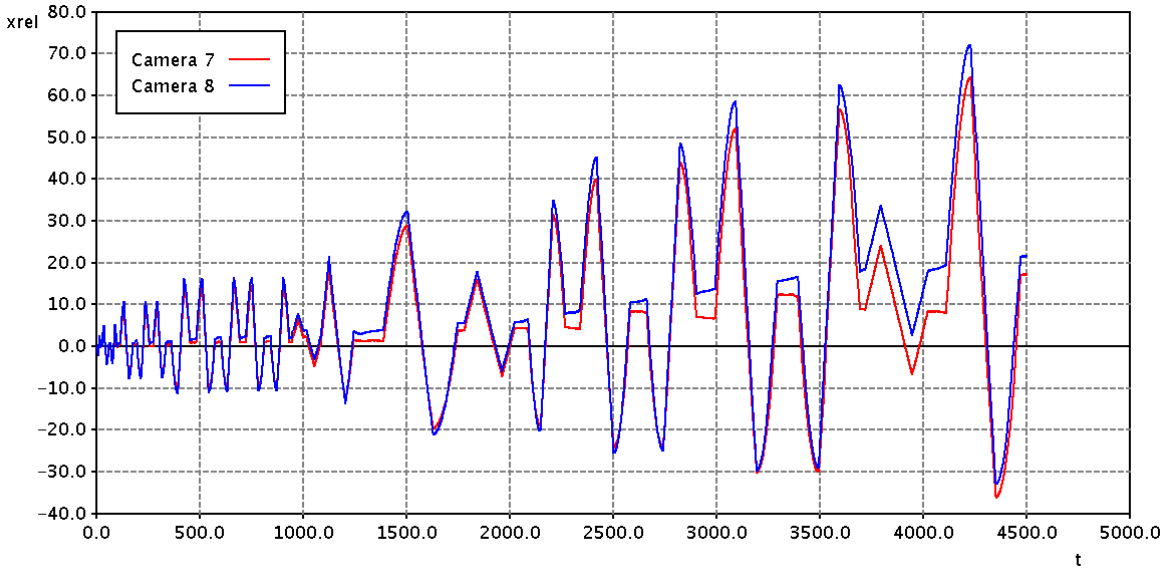

(a)

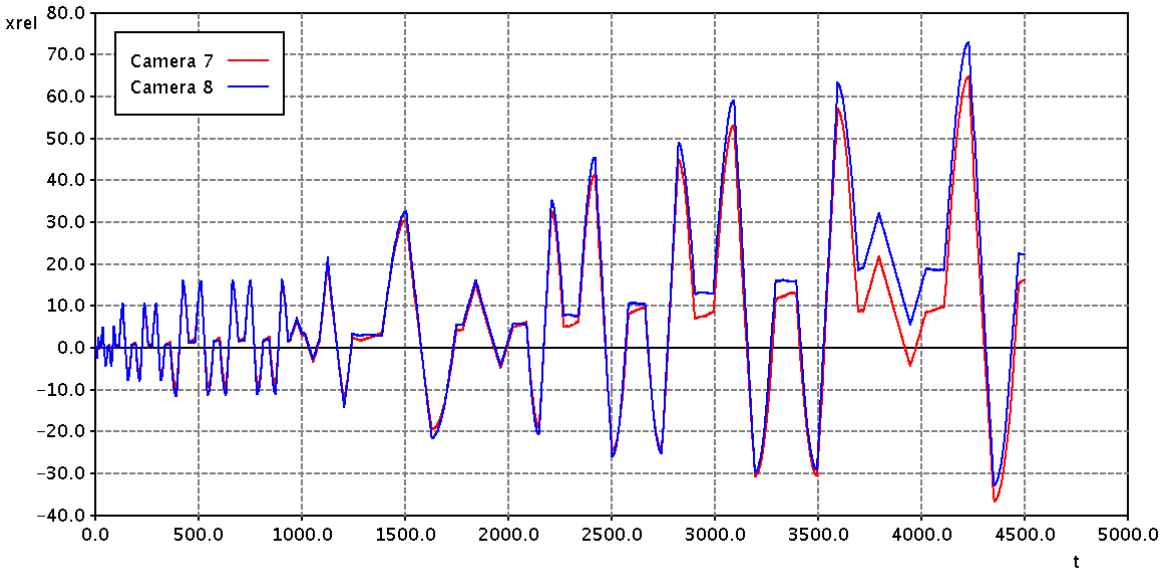

(b)

Figure 13.10. The relative x displacements of two particles in the overlapping region between cameras 7 and 8. The red curves correspond to the x displacement measured by camera 7, while the blue curves correspond to the x displacement measured by camera 8. The differences between the curves indicate that relative motion between the two cameras has occurred during the experiment. These displacements have been extracted from the `Lagrangian path fields` *computed from particles in the overlapping region of the two camera views. The units for all displacements are mm, and those for t are frames.*

plotted against frame number. To reiterate, if the cameras suffer no relative motion the two displacement curves should coincide. As is clear from the figures, this is not the case. Over time the two displacement curves diverge. The data indicate relative motions in the *x* direction of up to 10mm. Relative motion in the *y* direction (not shown) was smaller and of the order of 3-4mm.

Streams provides specific tools to address issues of relative camera motion. The elimination of this motion requires two steps. In the first step a time dependent transformation is computed from the paths of the common particles in the overlapping region. This transformation, comprising a two-dimensional translation and a rotation in the *x*-*y* plane, is calculated so that when the transformation is applied to the particles viewed by the second camera their displacements relative to the equivalent particles as viewed by the first camera, are minimised. Thus, it is assumed that the first camera provides the reference displacements. In the second step this transformation is applied to the particle locations in a `particle record` or `Lagrangian path field` through a `transform coordinates` transform which in turn is part of a `particle record transform pipeline` or a `Lagrangian path field transform pipeline`. The result is a modified `particle record` or `Lagrangian path field` from which the camera movement has been removed from the particle motion.

The second of these steps is straightforward, while the first is rather more complex. For that reason we will provide a more complete description of it here. The determination of the transformation required to remove the relative camera motion involves two steps. In the first, the particles recorded by the two cameras in their first frame must be paired with one another. Thus each particle pair corresponds to the same physical particle viewed by the two different cameras. The pairing is achieved through a simple particle matching process that is very similar to that employed in a `PTV analysis` object. `Costings` can be selected and their parameters set, along with the parameters for the optimisation process. Generally it is expected that equivalent particles from the two cameras lie close to one another in the first frame of their particle paths, and therefore this matching process should be straightforward. In the second step a transformation (translation and rotation), that varies with time, is computed based on the relative motion of all of the particles paired in the first step. The transformation is determined by minimising the relative particle motion for all particle pairs in a least squares sense.

This transformation is generated by a free process called `transform from two path fields 2D`. It requires the specification of the `Lagrangian path fields` corresponding to the paths of the common particles in the overlap region of the two cameras. Note that these two `Lagrangian path fields` need not include the same number of paths. Any paths that have no equivalent in the other path field will be ignored in the analysis. In addition, the user needs to create the particle matching process that will compute the pairs of equivalent particles. The `details view` of this process, once the process has executed, provides statistical information about the paths before and after the transformation has been applied. Figures 13.11 provides examples of this statistical information. In each sub-figure the distance between the

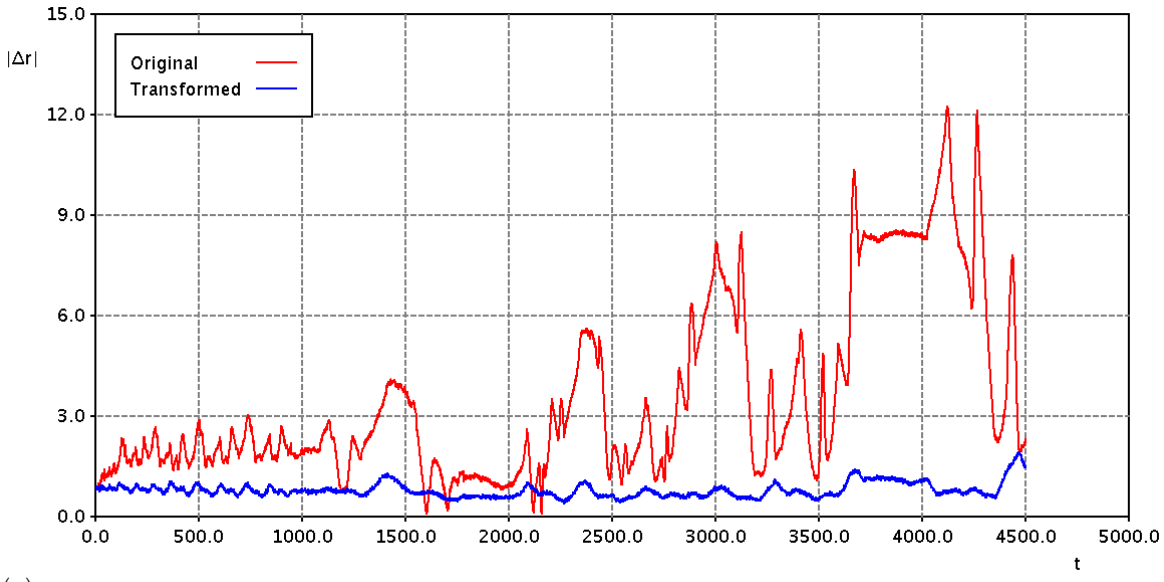

(a)

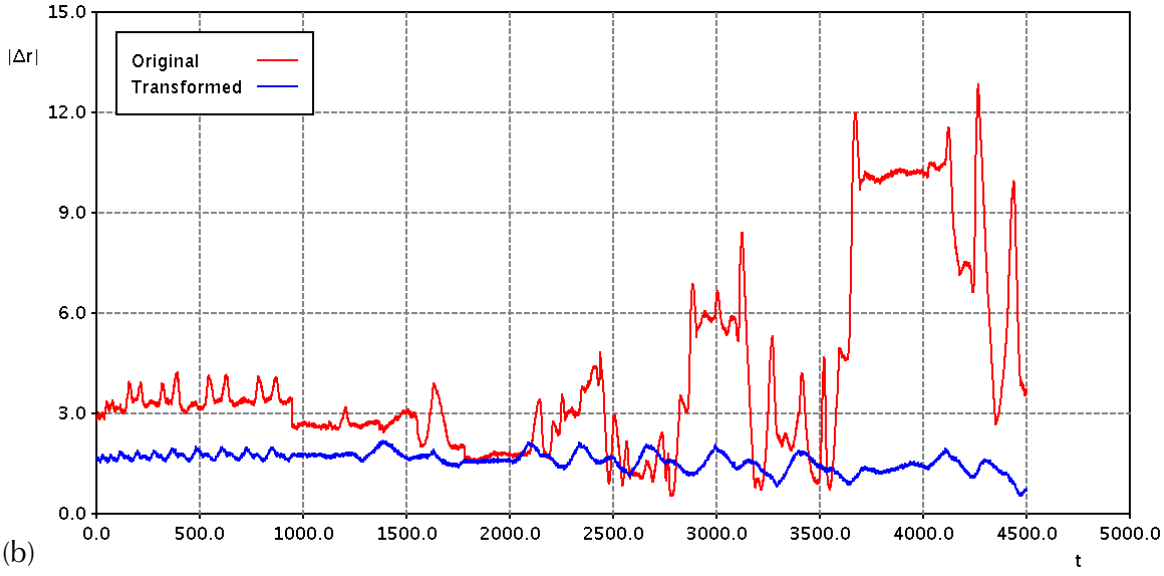

(b)

Figure 13.11. (a) The distance between the particle paths corresponding to particle pair 100 in the overlapping region between cameras 7 and 8. The red curve corresponds to the distance between the paths before the transformation aimed at removing camera movement is applied while the blue curve corresponds to the distance after the application of the transformation. (b) The same information as in (a) but for a different particle pair – in this case pair 400. Note that there is a total of 749 path pairs in the overlapping region.

two particle paths, before and after the transformation has been applied, is plotted for two different path pairs. Separations of up to 13mm can be seen towards the end of the loading cycles. The aim of this transformation is not necessarily to reduce the separation between the paths to zero. Instead its purpose is to remove the time dependency of the path separation. In the two examples provided in the figure this time variation has been reduced to less than ±1mm.

To conclude, the transformation outlined in the preceding paragraphs is computed from the particle paths in the overlapping region between cameras 7 and 8 and applied to the `particle record` produced from camera 8. This final step ensures that the `particle records` for the two cameras were based on a consistent, stationary, global coordinate system, and enabled the data from the two cameras to be integrated into a single displacement field.

13.4.7 Lagrangian path field creation

`Lagrangian path fields` play a fundamental role in structural engineering applications of particle tracking. The reason, as alluded to in previous sections, is that `Lagrangian path fields` naturally capture the cumulative displacement information of material particles that is most useful in the computation of material-based displacement and strain fields. Therefore the first step towards the generation of the final displacement field is the creation of two `Lagrangian path fields` from the camera's `particle records` using the `create Lagrangian 2D path field` process. Only full paths, those extending throughout the record, are included.

13.4.8 Displacement field generation

Displacement fields can be created from the two `Lagrangian path fields` using the `create displacement 2D field from paths` process. This process requires the specification of a number of key parameters, many of which are similar to the velocity field creation process described in the previous chapter. These are summarised here.

- *Field* – the first decision of the analyst is to choose between a material-based displacement field and a space-based field. The first option is almost invariably the preferred choice.
- *Grid* – a uniform rectangular grid, overlaid on the material domain. The displacement field is interpolated onto the nodes of this grid using the particle-based displacements. As this is a material-based grid this grid remains fixed to the material. A grid spacing of 20mm was selected as this is comparable to the inter-particle distance.
- *Interpolation schemes* – specifies the interpolation schemes used to interpolate the displacement and its derivative onto the grid. A number of options are available for both and two options will be discussed in detail.
- *Excluded regions* – lists regions within the material domain that should be excluded from the computation of the displacement field – for example the region occupied by the column in the images from camera 7. As this is a material-based displacement field the excluded regions are always located in the original undisturbed state of the system. The displacement field at grid points that lie within any of these regions will be left undefined by the interpolation process.

We explore two options for the interpolation of the displacement field and its derivatives. This analysis will demonstrate some of the consequences these choices have on the resulting fields and hence provide some insight into which options may be preferable in particular circumstances. The first option uses a standard triangle-based interpolation scheme for the displacement field and a derivative based on linear interpolation over the Delaunay triangulation. The second option uses a least squares estimate of both the displacement and derivative fields. The least squares estimate is based on a quadratic approximation to the displacement field in the neighbourhood of each grid point using the 15 nearest neighbours (particles).

Figures 13.12a and 13.12b provide colour maps of the absolute value of the volumetric strain field for the first frame captured by camera 8 using the triangulation-based interpolation and least squares interpolation schemes respectively. The first frame has been chosen because no significant movement of the system has yet been imposed, and therefore any variations in strain will be due to the noise or errors in the field calculation. The differences between the two figures are best understood by considering the uncertainties in the calculation of the displacement field. The mapping functions cited in section 13.4.4 yield, to first order, a scale factor from pixel to physical coordinates of approximately 0.4 mm/pixel. Thus, using the standard estimate for accuracy of ±1/4 pixel for the location of a particle yields an uncertainty in physical location of approximately ±0.1mm. Now consider a crude estimate of the uncertainty in the strain measurement between two points. This can be computed as the sum of the displacement errors at the two grid points divided by the distance between them as the strain is effectively the gradient in the differential displacement. This distance is somewhat dependent on the region within the domain. In the regions of high particle density the inter-particle spacing is approximately 20mm, while in the remaining regions it is closer to 40mm. Therefore the uncertainty in strain will be ~0.2mm/20mm = 0.01 in the high density regions and ~0.2mm/40mm = 0.005 in the low density regions.

The two interpolation schemes will modify this estimate somewhat. In the first case, where the displacement and its derivative are estimated from the displacement at the three particle locations that form the triangle in which the grid point resides, assuming that the errors are random, we would expect the error to be somewhat less than the crude estimate provided above. Indeed this can be seen to be the case when considering figure 13.12a. The vast majority of grid points in the high density region, near the top of the domain, exhibit a noise level less than 0.003 with only a few points having errors close to 0.01. In the low density region the noise level, as predicted, is less with typical values between 0.001 and 0.002, and maximum values rarely exceeding 0.003.

In the second case, again assuming that the errors are random, the noise level will be substantially less due to the averaging effect of the 15 point least squares fit. Here no errors rise above 0.002 in the high density region and in the low density region the error levels are half that.

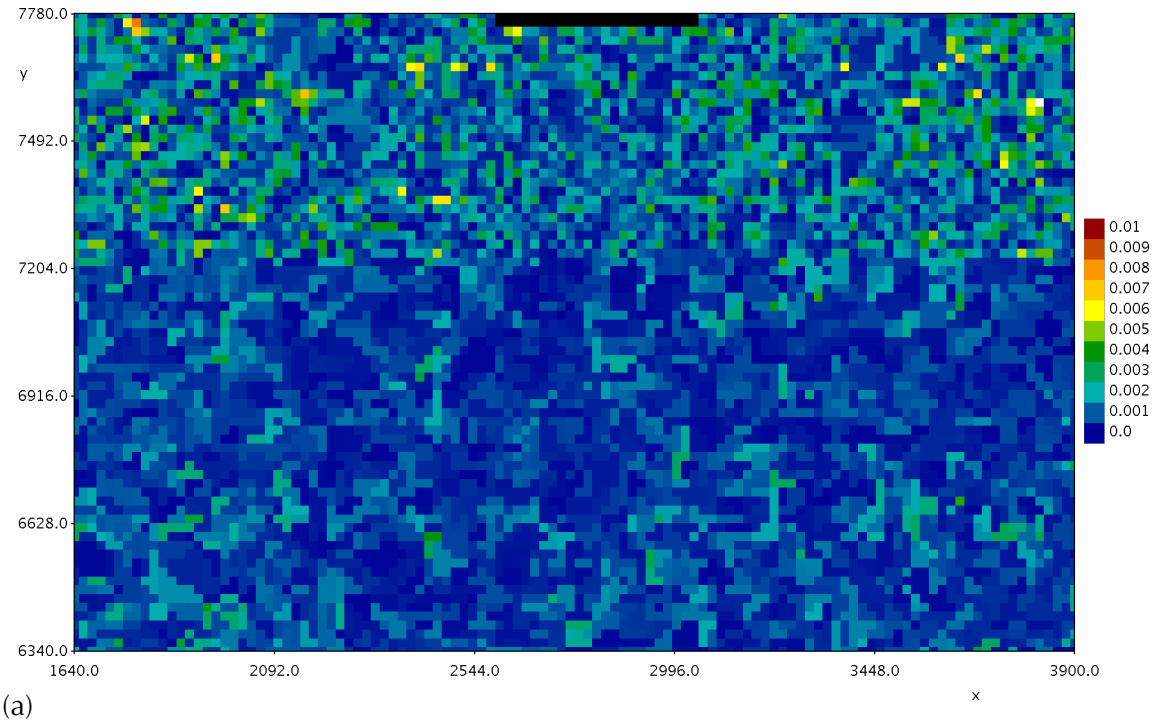

(a)

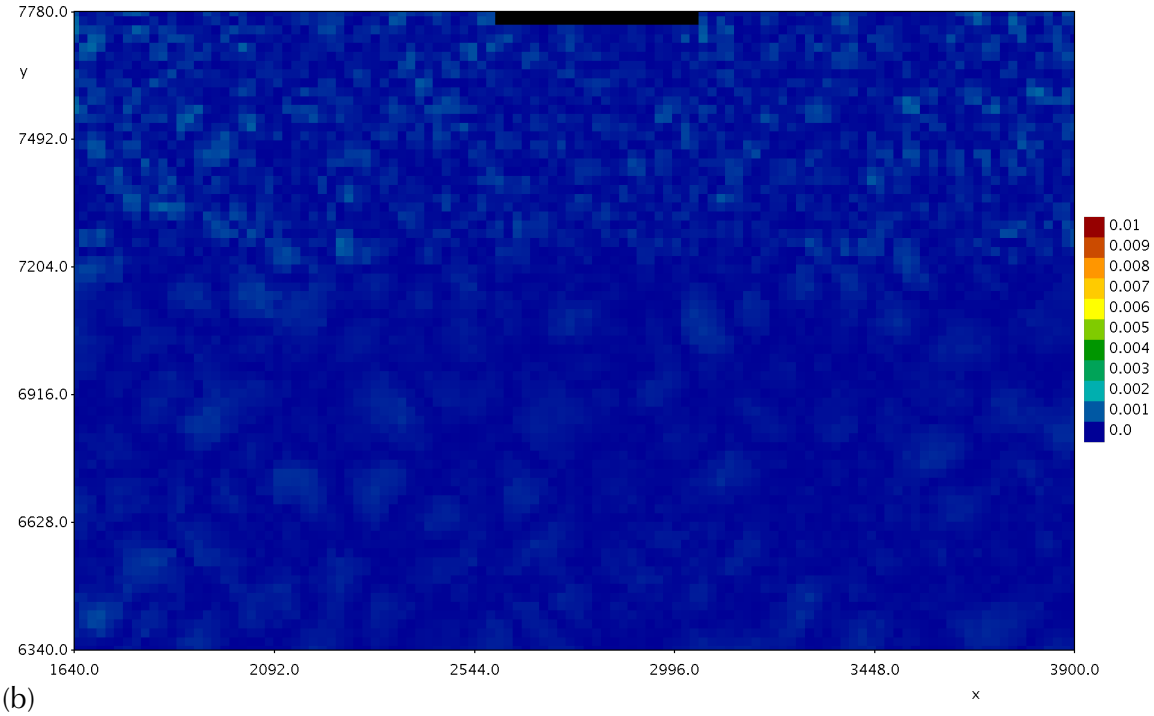

(b)

Figure 13.12. (a) The volumetric strain field for frame 1 captured by camera 8. The interpolation scheme for both the displacement and its derivatives are triangulation-based. (b) The volumetric strain field for frame 1 captured by camera 8. The interpolation scheme for both the displacement and its derivatives are least squares-based.

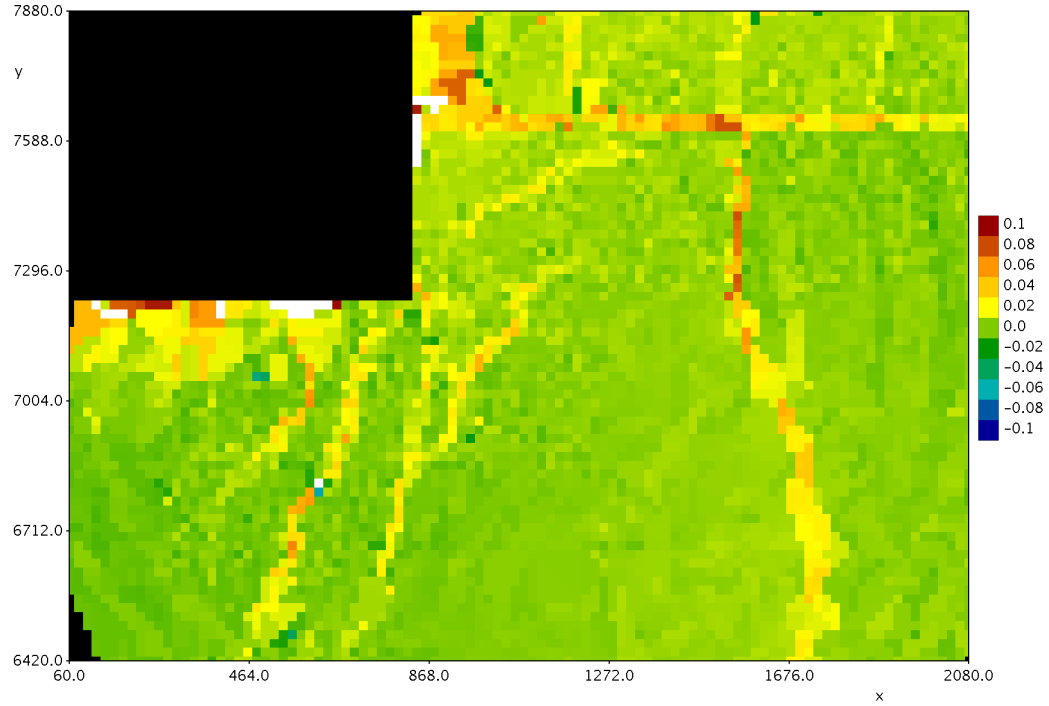

(a)

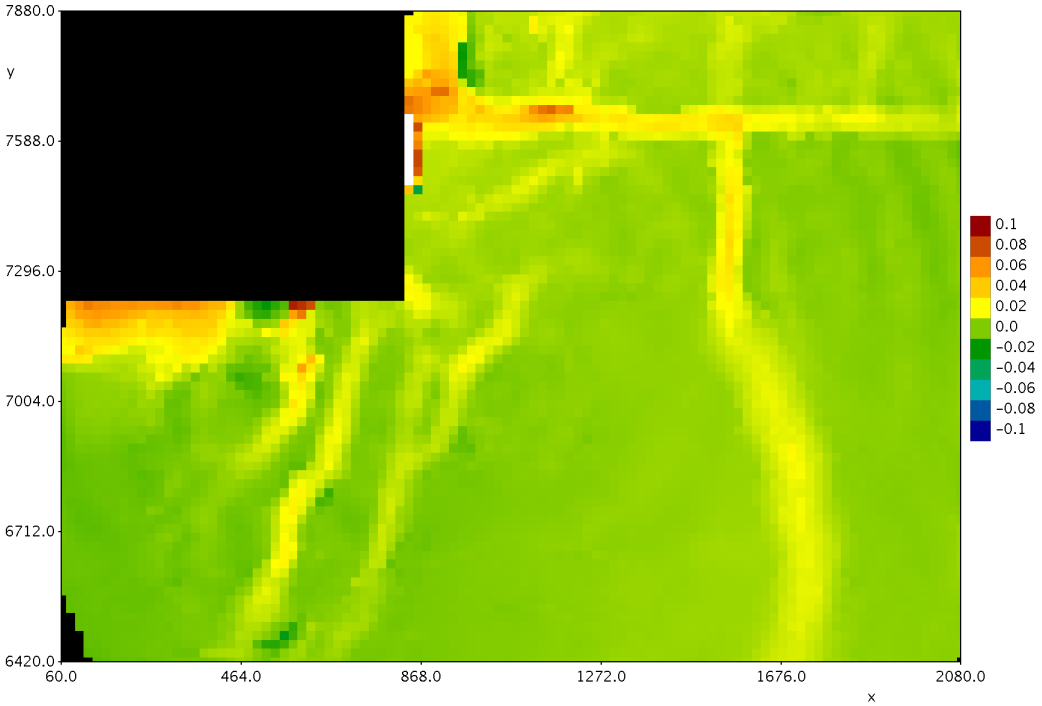

(b)

Figure 13.13. (a) The volumetric strain field for frame 2500 captured by camera 7. The interpolation scheme for both the displacement and its derivatives are triangulation-based. (b) The volumetric strain field for frame 2500 captured by camera 7. The interpolation scheme for both the displacement and its derivatives are least squares-based. Note, the regions coloured white correspond to strain values outside the range specified in the legends.

There are other ramifications that arise due to the choice of interpolation scheme. Not surprisingly the least squares based schemes not only averages the error over the cluster of nearest neighbours, they also average the field itself. Thus one would expect that the least squares strain field would exhibit smeared gradients with smaller amplitudes.

Figures 13.13a and 13.13b display the volumetric strain fields for frame 2500 captured by camera 7 using the two different interpolation schemes. The location of the column corresponds to the blacked out rectangle in the upper left corner of each figure. It is clear from the figures that the regions of high strain are sharper, more noisy and with larger amplitudes when the triangulation-based interpolation scheme is employed, but, the networks of cracks, corresponding to the coherent bands of high strain, are consistent and visible under both schemes. As these cracks are highly localised the triangulation-based interpolation scheme is more effective at determining their location.

13.4.9 Merged displacement field

The final analysis step for a multi-camera experiment of this nature involves the merging of the displacements from each camera. The `overlay displacement 2D field` free process enables the displacement fields from an unlimited number of cameras to be overlaid. The process expects that all displacement fields are based on a common grid and the user must specify the spatial offsets, in terms of number of grid points, of each displacement field in the overlaid field. Typically some regions have displacements defined by more than one camera and the user can specify the overlay rule – in this case we average the two fields in these overlap regions.

To be explicit the grids for the two cameras are listed in table 13.3. Based on these grid parameters the displacement field from camera 8 is overlaid on that from camera 7 with offsets of 79 grid points in the *x* direction and -4 grid points in the *y* direction. The resulting overlaid displacement field has an origin at (60, 6340) with 193 grid points in the horizontal *x* direction and 78 grid points in the vertical.

Table 13.3. The grid parameters for cameras 7 and 8. (x_0, y_0) is the location of the lower, leftmost point in the grid relative to the chosen global coordinate system. n_x and n_y are the number of grid points in the x and y directions and Δx and Δy are the grid spacings in these two directions.

	Camera 7	Camera 8
x_0 (mm)	60	1640
y_0 (mm)	6420	6340
n_x	102	114
n_y	74	73
Δx (mm)	20	20
Δy (mm)	20	20

13.5 Illustrative results

The results presented here will be taken from the overlaid field interpolated using the least squares schemes for displacement and its derivatives. We reiterate that the strain field captured by this scheme generally will be smoother than that computed using the triangulation-based scheme and will have slightly reduced strain magnitudes.

Figure 13.14 illustrates the typical displacements experienced by the floor panels. The displacements are for the point (1300,6800) located in the region captured by camera 7 (see figure 13.13) and well separated from the cracking regions indicated in that figure. Both *x* and *y* displacements are included in the figure. The figure indicates maximum displacements of approximately 70mm in both directions. Figure 13.15 provides an expanded view of the same data between frames 100 and 300. The individual data points are included in order to provide the reader with a sense of the smoothness of the data.

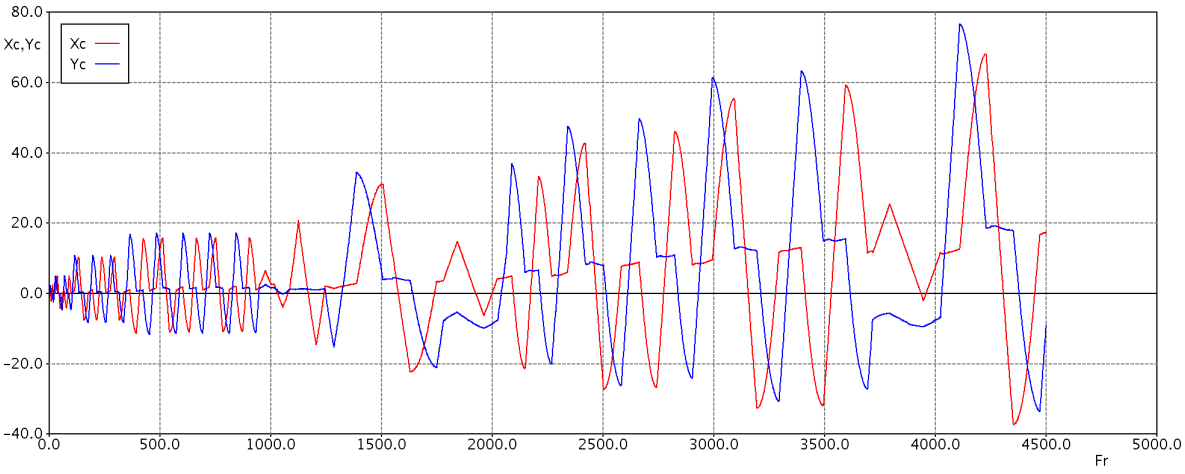

Figure 13.14. The cumulative x and y displacements experienced by the floor panel at the point (1300,6800) – see figure 13.13. The displacements are measured in mm.

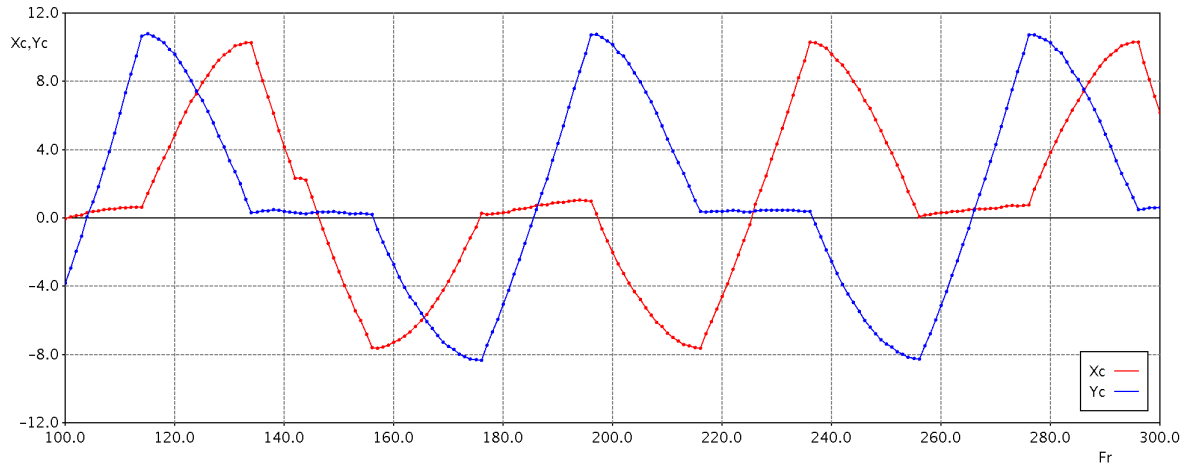

Figure 13.15. An expanded view of frames 100 to 300 from the dataset plotted in figure 13.14. Note the change in vertical scale. Dots, corresponding to each data point, have been included to provide the reader with a sense of the noise within the data.

Before exploring the strain field it is worth a moment to illustrate the importance of removing the relative camera motion as described in section 13.4.6. A separate analysis is undertaken whereby the relative camera motion is disregarded and the combined displacement field from the two cameras computed in the same way as previously explained. Figures 13.16a and 13.16b provide colour maps of the cumulative y displacement field at frame 2500. In figure 13.16a the relative camera motion has been removed – as effectively as it can be given the tools available – while in 13.16b the relative camera motion remains. The differences between the two resulting fields are stark. The removal of the relative camera motion, while not perfect, is essential if physically meaningful results are to be attained.

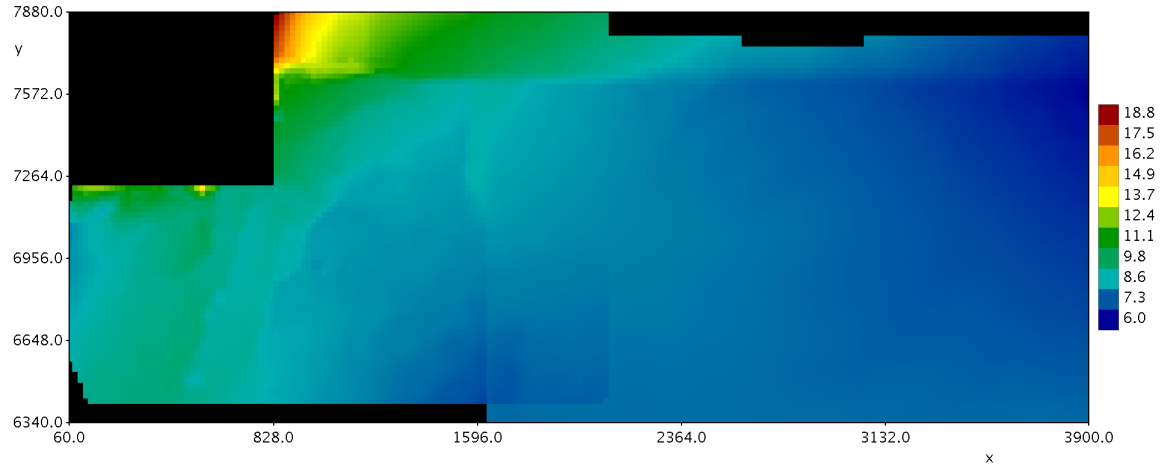

(a)

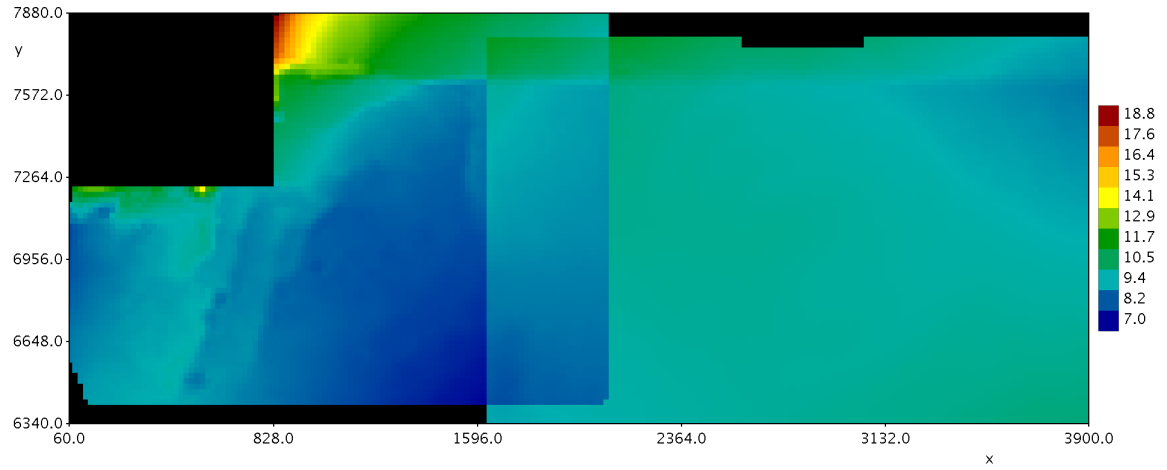

(b)

Figure 13.16. The cumulative y displacement field of the combined cameras at frame 2500. (a) The relative motion between the cameras has been removed using the tools described. The region of transition from camera 7 (on the left) and camera 8 (on the right) is just visible. (b). The relative motion between the cameras remains. In this case the transition region is stark and clearly unacceptable. Note that in the overlap region the average displacement from the two fields is computed.

The impact of the relative camera motion is of considerably less importance when computing the strain field, as this field is based on the derivatives of displacement, largely unaffected by the camera movement.

Figure 13.17 provides a sequence of strain fields for a number of arbitrarily selected frames. The corresponding time history of the displacements can be read from figure 13.14. These strain plots contain a number of interesting features.

The most striking aspect of the figures is the network of high strain regions corresponding to cracks in the panel floors. As indicated earlier, due to the interpolation scheme the crack signatures are somewhat smeared but their locations are still readily identified. The fact that this network of cracks persists throughout the entire time history of the experiment indicates that they are permanent features identified by the particle tracking system. It is also clear that these cracks open and close during the course of the experiment. While the long vertical crack, somewhat to the left of centre, is always visible, the magnitude of the strain along this feature varies substantially during the loading cycles. The strain is strongly positive in frame 2500 (figure 13.17b) with strains of up to 3%, while in frame 4000 (figure 13.17e) the strain is almost zero and, in fact, at some locations along the crack the panel is in weak compression.

Unsurprisingly the most dramatic straining occurs in the regions where the floor panels meet the column – visible in the top left of the figures. The scales on the figures have been chosen to allow the clear identification of the crack network, but limiting the range of strains in this way causes off-scale strains to occur at some locations around the column – as indicated by the white regions in the figures. The analyst would be wise to undertake further analysis if they wish to gain confidence in the strain levels indicated in these regions. `Lagrangian path fields` possess a calculator – the `two path` calculator - that imitates the output of a physical potentiometer. Any two particles can be treated as the two ends of a potentiometer and various outputs from the virtual potentiometer can be computed. Due to the number of particles present the analyst effectively has access to hundreds of virtual potentiometers in these regions of high strain and this provides them with the tools to undertake a detailed forensic examination of these regions.

A particularly intriguing artefact in these figures is the set of apparently concentric circles in the strain field measured by camera 8. These circles are present, to a greater or lesser extent, in all of the figures. One possible interpretation of these features might be that they are optical anomalies, but as they are not present for all cameras (they are not detectable in the camera 7 images) the evidence to support this hypothesis is not totally convincing. They cannot be due to the non-linear mapping of the pixel coordinates to physical coordinates as these mapping functions are only very weakly non-linear and are only quadratic in form. Thus oscillations could not be created by such functions. Their explanation remains an open question, but as the strains associated with them are quite small compared to those elsewhere in the domain, they can be considered to not unduly influence the results.

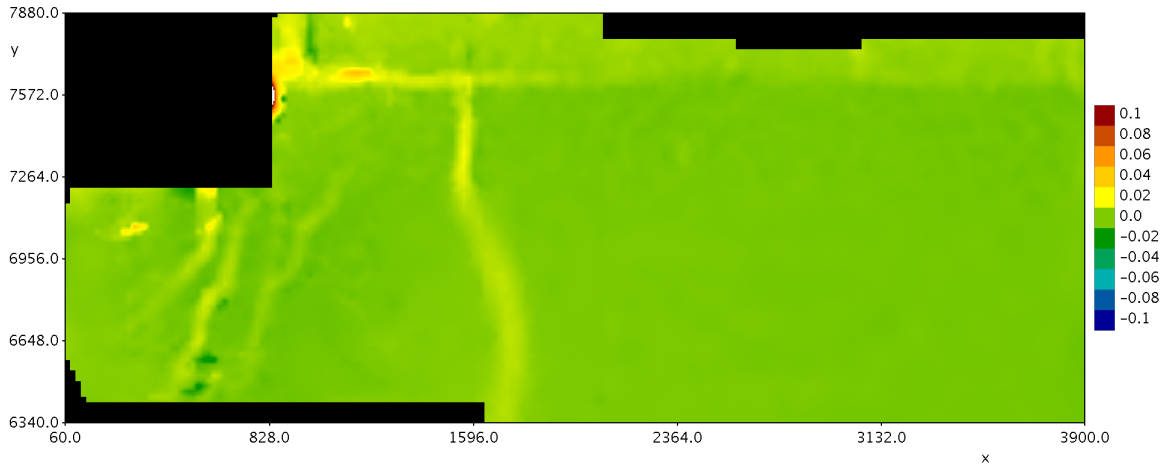
7880.0
y
7572.0
7264.0
6956.0
6648.0
6340.0
60.0
828.0
1596.0
2364.0
3132.0
3900.0
x
0.1
0.08
0.06
0.04
0.02
0.0
-0.02
-0.04
-0.06
-0.08
-0.1

(a)

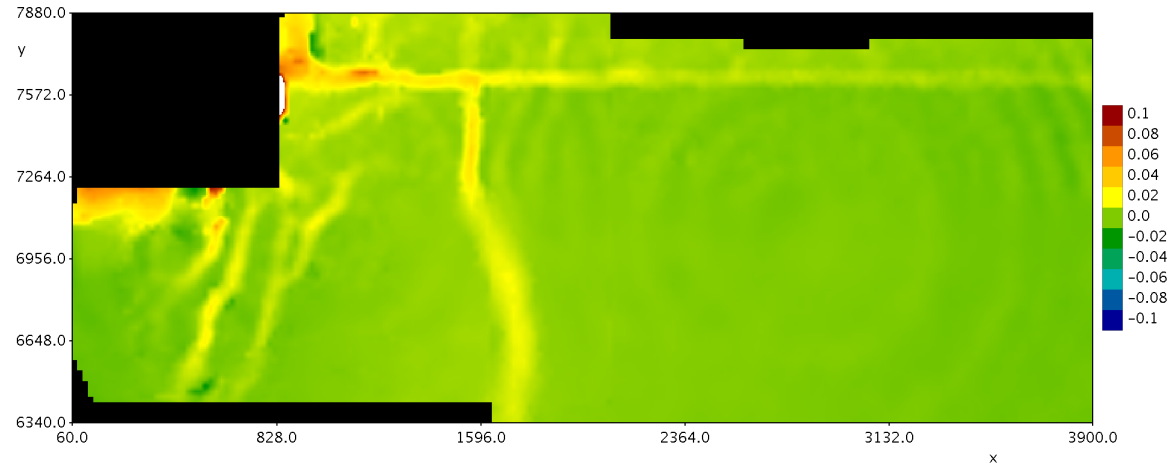
7880.0
y
7572.0
7264.0
6956.0
6648.0
6340.0
60.0
828.0
1596.0
2364.0
3132.0
3900.0
x
0.1
0.08
0.06
0.04
0.02
0.0
-0.02
-0.04
-0.06
-0.08
-0.1

(b)

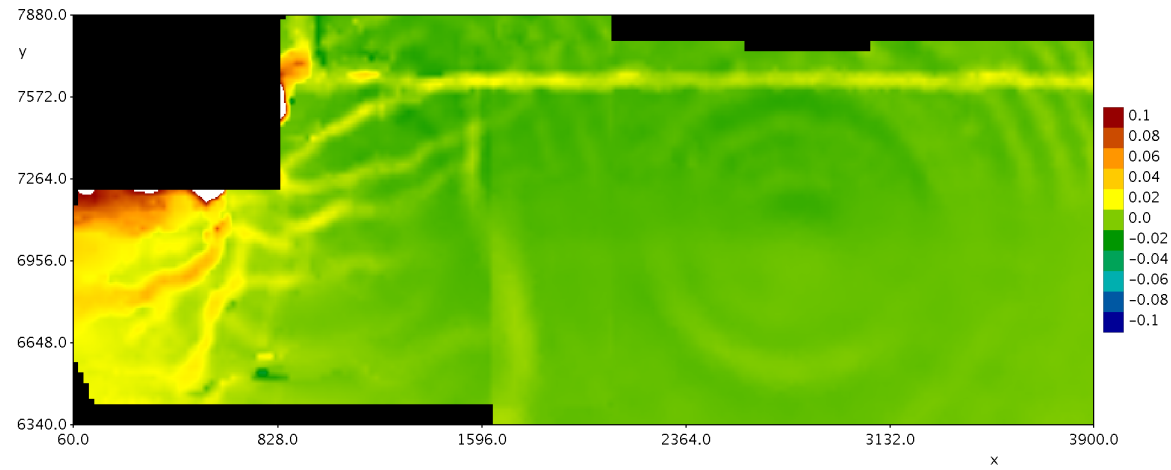
7880.0
y
7572.0
7264.0
6956.0
6648.0
6340.0
60.0
828.0
1596.0
2364.0
3132.0
3900.0
x
0.1
0.08
0.06
0.04
0.02
0.0
-0.02
-0.04
-0.06
-0.08
-0.1

(c)

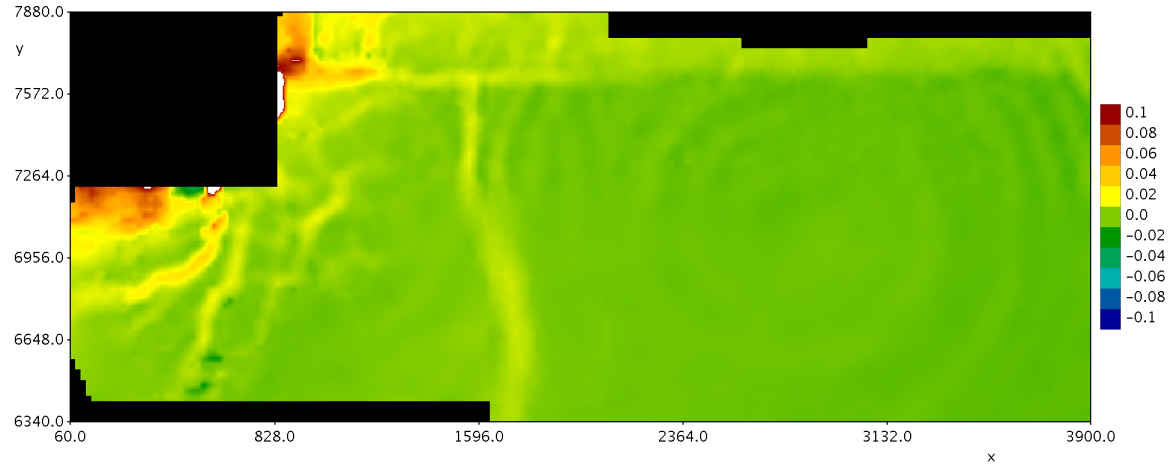

(d)

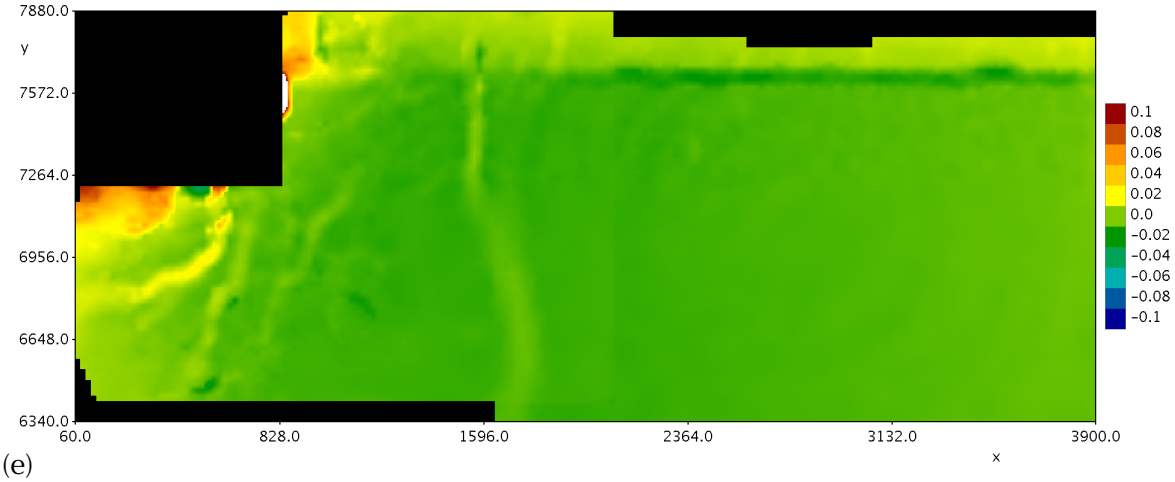

(e)

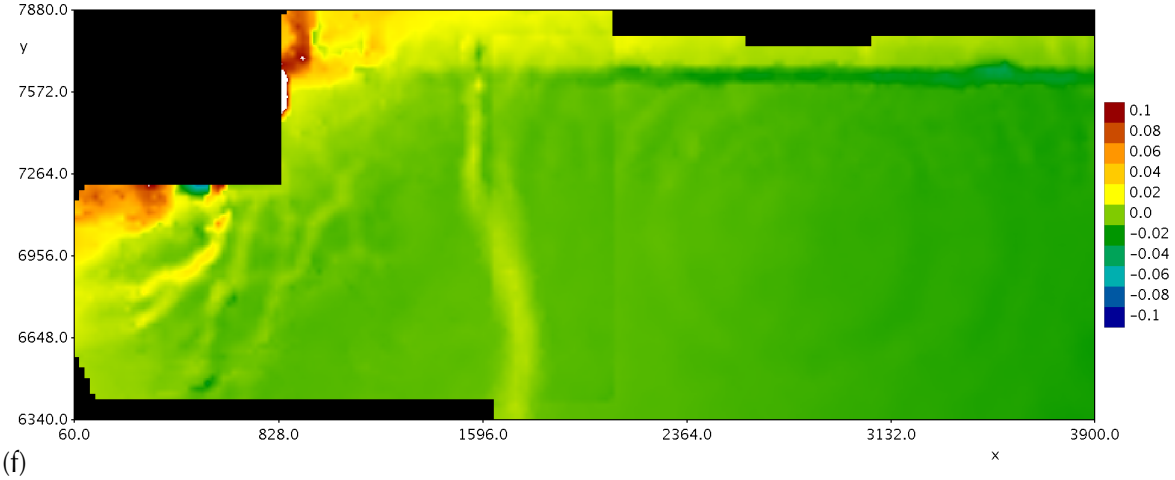

(f)

Figure 13.17. The volumetric strain field for combined cameras 7 and 8. (a) Frame 2000, (b) Frame 2500, (c) Frame 3000, (d) Frame 3500, (e) Frame 4000, (f) Frame 4499. Figure 13.14 provides a guide to the displacements corresponding to each of the strain fields.

13.6 Summary

The third case study has provided the reader with experience in the handling of complex datasets typical of structural applications where multiple cameras are present. These experimental configurations present a number of challenges that we summarise here.

- Mapping functions, that allow the data captured by all cameras to be mapped onto a global coordinate system, are required for any multi-camera system. These mapping functions are generally determined through a calibration process requiring the construction of a set of calibration points whose physical locations are accurately known. We have provided a critique of the calibration grid used in this experiment highlighting the need for a greater number of points, as well as a greater coverage of the camera image. In particular more calibration points near the edges of the observation window is strongly recommended. A principal difficulty with such calibration systems is achieving a comparable error level in the mapping functions to that inherent in the particle tracking system. In general, this is unlikely to be achieved.

- Camera movement during an experiment, and relative camera movement in particular, can cause serious distortions to the measured data if not adequately managed – see figure 13.16. Camera movement is best monitored through the observation of reference particles by each camera, whereby the movement of those particles can be used to interpret the motion of the camera. In this experiment one camera recorded, albeit imperfectly, the motion of elements embedded in the strong floor, thus allowing some understanding of the camera's motion during the experiment to be obtained. The motion of a second camera, relative to this camera, was deduced from the relative motions of particles observed by both cameras in their overlapping region. Whilst not wholly satisfactory, this technique at least enabled the removal of the worst impacts of the camera movement.

- In structural applications of this nature the adoption of both traditional measurement systems, such as potentiometer strain gauges, and a particle tracking system can cause difficulties for the latter. The presence of physical devices and their associated cables cause a number of problems. Firstly, the physical devices prohibit the placement of particles at the locations occupied by the devices, thus causing "blind spots" in the PTS. Secondly, the physical devices may cause spurious particles to be identified unless they are carefully camouflaged. Thirdly, cables attached to these devices can obscure particles if they move during an experiment, and the partial obscuring of particles can lead to incorrect displacement calculations from the particle data. All of these difficulties arose in this experiment and only the second was handled entirely satisfactorily. It would be our advice that, unless there are very good reasons, the experimentalist should choose one or the other of these measurement systems, and not both. Once confidence in the quality of data derived from a PTS grows the setting aside of the more traditional methods should be possible.

Despite the challenges just discussed the particle tracking system employed in this experiment has performed well. Extensive particle fields, comprising approximately 3000 particles for each camera, have been constructed. Using tracking algorithms, specifically adapted to counter the impact of moving cables, a very high percentage of the identified particles have been tracked. Displacement fields were constructed by utilising only particle paths that extended throughout the 4500 frames captured by the cameras. Even under this severe restriction approximately 90% of all particles contributed to the interpolation of the displacement field. Detailed strain fields across a significant region of the floor panels have been obtained, and a clear network of major cracks has been identified. Error levels for strains, when a least squares interpolation scheme was employed, were typically 0.1-0.2% while the maximum strains measured in the vicinity of the column exceeded this by up to two orders of magnitude. A triangulation-based interpolation scheme, while increasing the error levels by a factor of 2 or 3, provided more localised measures of the strain and sharper delineation of the crack lines.

References

Al-Behadili, A. J. M., Sellier, M., Nokes, R., Moyers-Gonzalez, M., Geoghegan, P. H., 2018, "Rheometry based on free surface velocity", *Inverse Problems in Science and Engineering*. doi:10.1080/17415977.2018.1509965

Campagnol, J., Radice A., Nokes, R., Bulankina V., Lescova, A., Ballio, F., 2013, "Lagrangian analysis of bed-load sediment motion: database contribution", Journal of Hydraulic Research, 51, 5, pp 589-596, DOI 10.1080/00221686.2013.812152

Cenedese, C., Nokes, R. I., and Hyatt, J. 2016. Lock-exchange gravity currents over rough bottoms. *Environmental Fluid Mechanics*, *18*(1), 59-73. doi:10.1007/s10652-016-9501-0

Chiou, B., Darragh, R., Gregor, N., Silva, W. 2008, "NGA Project Strong-Motion Database, *Earthquake Spectra*, 24, pp 23-44.

Crowe, A, Davidson, M., Nokes, R. 2016 "Velocity measurements in inclined negatively buoyant jets", Environmental Fluid Mechanics, 16, 3, pp 503-520.

Hendrickson, C., Roper, W., 2019, "Using accelerometers for damage detection: is the accuracy of the device important?", *Proceedings of the CNRE Research Conference 2019*, University of Canterbury, pp 671-678.

Nikora, V., Nokes, R., Veale, W., Davidson, M., Jirka, G, 2007 "Large scale structure of uniform shallow free-surface flows", Environmental Fluid Mechanics, 7, 2, pp 159-172.

Ottenhaus, L. -M., Li, M., Nokes, R., Cammock, P., McInnes, B., 2018, "Use of Particle Tracking Velocimetry in Timber Material and Connection Testing", *European Journal of Wood and Wood Products*. doi:10.1007/s00107-018-1376-y

Raffel, M., Willert, C., Kompenhans, J., 1998, "Particle Image Velocimetry", *Springer-Verlag*, Berlin, Germany, pp 253.